A UNIFIED NUMERICAL MODEL FOR THE SIMULATION OF THE SEISMIC CYCLE IN DIP-SLIP ENVIRONMENTS: EXAMPLES FROM ITALY

M. Albano[1], S. Barba[1], C. Bignami[1], C. Doglioni[1], E. Carminati[2], M. Saroli[3], M. Moro[1], S. Stramondo[1], S. Samsonov[4]

[1] Istituto Nazionale di Geofisica e Vulcanologia, Roma
[2] Dipartimento di Scienze della Terra, 'Sapienza' Università di Roma
[3] Dipartimento di Ingegneria Civile e Meccanica, Università degli Studi di Cassino e del Lazio Meridionale, Cassino, FR
[4] Natural Resources Canada, Ottawa, ON KA E, Canada

Introduction. According to the concept of the seismic cycle, earthquakes are the result of the strain accumulation in the earth's crust over a variable decade to millennial period, i.e., the interseismic stage, followed by a sudden stress release at a crustal discontinuity, i.e., the coseismic stage, finally evolving in a postseismic stage (Scholz, 2019).

Commonly, the seismic cycle is modelled with analytical and numerical approaches. Quasi-static analytical methods simulate the interseismic coupling, the coseismic dislocation and the postseismic relaxation independently and assuming an elastic, viscoelastic or poroelastic half-space. Often, these models impose the slip on single or multiple planar sources to infer fault geometry, slip distribution and regional deformations in order to fit the available geodetic or seismological measurements, often regardless of the magnitude and orientation of the interseismic gravitational and tectonic forces (Anderlini *et al*., 2016; Atzori *et al*., 2009).

Numerical approaches allow simulating complex geometries in heterogeneous media and at different modelling scales, assuming elastic, viscoelastic, or elasto-viscoplastic constitutive laws. However, such models often impose the slip on the fault plane to simulate the observed coseismic dislocation or the propagation of the seismic waves (Trasatti *et al*., 2011), or they adopt ad-hoc boundary conditions to investigate the interseismic stress accumulation or the postseismic relaxation for specific cases (Carminati and Vadacca, 2010).

We contribute to the understanding of the seismic cycle associated to a single fault segment by developing a numerical model to simulate the long-term crustal interseismic deformation, the coseismic brittle episodic dislocation, and the postseismic relaxation of the upper crust within a unified environment for both normal and reverse fault events. This model is developed to simulate typical extensional and compressional earthquakes in Italy (Fig. 1a) and includes the forces acting during the interseismic period, i.e., the lithostatic load and the horizontal stress field (Finocchio *et al*., 2016). We adjusted the setup of our model to simulate the interseismic, coseismic and postseismic phases for two major seismic events in Italy, the 2009, M_w 6.1 L'Aquila normal fault earthquake (Fig.1b) and the 2012, M_w 5.9 Emilia-Romagna reverse fault earthquake (Fig. 1c).

The results of our analysis, compared with geodetic and InSAR data from the literature, show that the proposed numerical model is able to reproduce the seismic cycle associated with the investigated events.

Methods. We developed a first-order model that combines poroelasticity, discrete discontinuities simulating detachments and faults, tectonic forces, and gravity. To this purpose, we built two plane-strain numerical models by exploiting the finite element commercial code MSC Marc 2018 (MSC Software Corporation, 2018). The 2D models (Sections A, and B Fig. 1a and Fig. 2) extend 220 km horizontally and to a depth of 40 km (Fig. 2a, b) (Finocchio *et al*., 2016) and are almost orthogonal to the strike of the earthquake causative faults. Discontinuities in the model's mesh are introduced to simulate a steadily shearing fault in the interseismic phase (segment n°1 in Fig. 2) and the earthquake causative fault in the coseismic phase (segment n°2 in Fig. 2), whose dip and length are defined according to the retrieved fault geometry from previous inversions of geodetic and satellite data (Atzori *et al*., 2009; Pezzo *et al*., 2013). Mesh discontinuities are modelled using a contact interface, where nodes are doubled so that the upper and lower parts of the domain can move relative to each other. Unlike common, quasi-static, analytical and numerical modelisations, no forces or displacements are imposed on the fault's

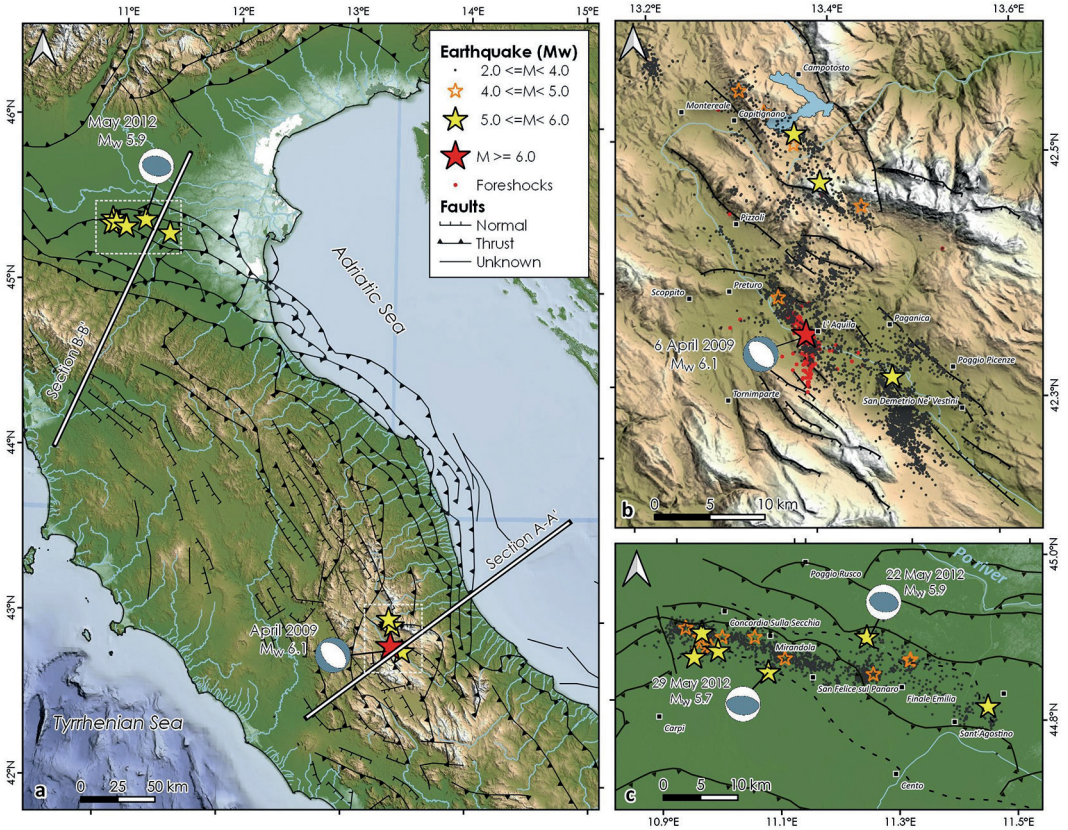

Fig. 1 - A framework of the study area: a) Location of the analysed earthquakes. b) The 2009, L'Aquila seismic sequence. c) The 2012 Emilia seismic sequence.

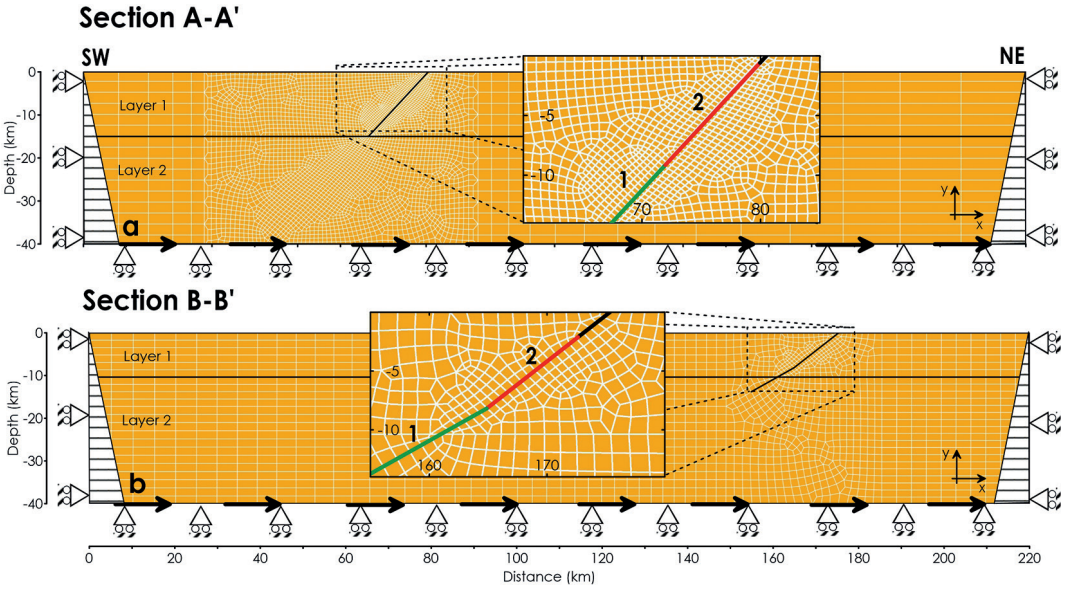

Fig. 2 - First-order finite element model geometries and grid exploited for the simulation of interseismic, coseismic and postseismic phases associated with the L'Aquila 2009 (a) and Emilia Romagna 2012 (b) earthquakes.

edges to induce the slip. Instead, faults are assumed alternatively locked or unlocked in space and time (Doglioni *et al*., 2011). When unlocked, fault's edges move each other according to the applied far-field boundary conditions, loads, and internal stresses. A fully coupled, isotropic, linear poroelastic rheology describes the evolution of stresses and strains inside the medium (Wang, 2000), whose elastic and hydraulic parameters were derived from literature data and geophysical measurements available over the study areas.

The mechanical boundary conditions consist of roller supports, orthogonal to the bottom and the sides of the model (Fig. 2) while the upper boundary is free to move in all directions. Applied forces consist of gravity load, and uniform shear traction applied at the model base (black arrows in Fig. 2) and directed north-eastward. The latter simulates the mantle convection in the Tyrrhenian asthenosphere and the Adriatic slab rollback, and it is intended to explain the present-day contraction-extension pair across the Apennine chain (Barba *et al*., 2008; Carafa *et al*., 2015).

Simulations include an interseismic, coseismic and postseismic phase. In the interseismic phase, the lithostatic load and the interseismic tectonic load are simulated by activating the northeast-oriented basal shear tractions (black arrows in Fig. 2) (Finocchio *et al*., 2016) to simulate the hypothetical crustal deformations and stresses gathered in the time interval between two earthquakes of similar magnitude and happening on the same fault segment. During this phase, the deeper fault segment (segment n°1 in Fig. 2) is assumed unlocked to simulate the effect of a fault segment steadily shearing during the interseismic phase, while the upper segment (segment n°2 in Fig. 2) is locked (Doglioni *et al*., 2011; Scholz, 2019). Drained conditions are assumed for the fluid phase, and excess pore pressures are neglected.

In the coseismic phase, the earthquake nucleation is simulated by instantaneously unlocking the upper part of the fault (segment n°2 Fig. 2), keeping both the mechanical boundary conditions and loads applied in the interseismic phase. Undrained conditions are assumed in this phase to allow for the development of excess pore pressures (hereinafter Δp) caused by the nearly-instantaneous fault dislocation.

In the postseismic phase, the pore pressure excess caused by the earthquake dislocation dissipates over time because of pore fluid diffusion. The calculation time is two years. Boundary conditions and applied loads are kept constant, and the upper part of the fault (segment n°2 Fig. 2) is assumed unlocked. During this phase, the evolution of fluid pore pressures, stresses, and displacements caused by the pore fluid diffusion are monitored over time.

Results. In the interseismic phase, the action of both gravitational and tectonic forces modulates the stress and strain field for normal- and reverse-fault events. The applied shear tractions at the model's base (Fig. 2) cause the elongation of the left part of the model, with a reduction of both stresses and strains, and the compression of the right part of the model, with an increase of both stresses and strains. The assumed interseismic shearing of the deep fault segment at depth (segment n°1 in Fig. 2) modifies locally the displacement, strain and stress field. For the L'Aquila 2009 normal-fault event, the interseismic displacement vectors (white arrows in Fig. 3a) emphasise the shearing of the deep fault segment. Dilation occurs locally at depth in the hangingwall (Fig. 3b), i.e., at the contact between the unlocked and locked portions of the fault segment, while volumetric contraction develops up to two-kilometre depth, because of the interseismic ground subsidence caused by the fault shearing.

For the Emilia 2012 reverse-fault event, the interseismic shearing produces displacements, volumetric strains and stresses opposite to those obtained for the normal-fault event. Displacements are upward oriented (Fig. 3c), causing the volumetric contraction of a wide area of the hangingwall (Fig. 3d), at the contact between the locked and unlocked portions of the fault segment.

In the coseismic phase, the earthquake dislocation is simulated by unlocking the shallow part of the fault segment (segment n°2 in Fig. 2). For the L'Aquila 2009 normal-fault event, the coseismic deformation pattern (Fig. 3e) highlights the collapse of the hanging wall and the

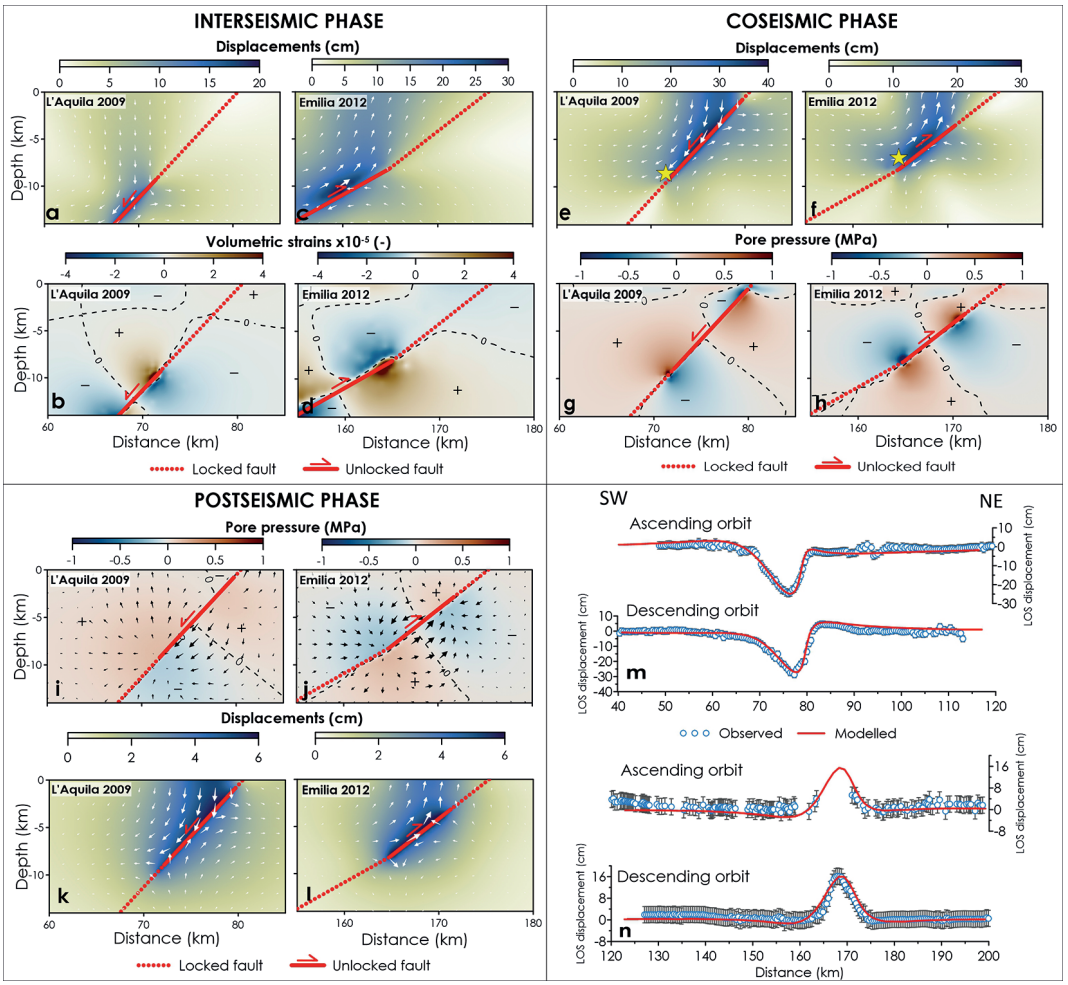

Fig. 3 - Interseismic differential displacements (panels a and c) and volumetric strains (panels b and d) caused by the interseismic shearing of the deeper fault segment (green segment n°1 in Fig. 2), calculated for the L'Aquila 2009 and the Emilia 2012 events. Positive volumetric strains indicate dilation, while negative volumetric strains indicate contraction. Coseismic differential displacements (panels e and f), and pore pressure excess (panels g and h) caused by the unlocking of the shallow fault segments (red segment n°2 in Fig. 2). The yellow stars in panels e and f locate the position of the mainshock. Postseismic Δp pattern after 20 days from the simulated earthquakes (panels I and j) and cumulated postseismic displacements after two years from the simulated earthquakes (panels k and l). Comparison between the InSAR and modelled LOS displacement profiles along sections A and B in Fig. 1a for the L'Aquila 2009 (panel m), and Emilia 2012 (panel n) earthquakes. The vertical bars indicate the uncertainty of the InSAR-derived ground displacements.

mainly rightward movement of the footwall. The coseismic dislocation induces the volumetric contraction of the hangingwall at depth, thus recovering the volume dilation occurred in the interseismic phase, while dilation occurs in the shallower 1-2 km.

For the Emilia 2012 reverse-fault event, the displacement pattern emphasises the hangingwall uplift (Fig. 3f), which induces volume dilation in the hangingwall at depth and contraction in the shallower part. The footwall undergoes extension and compression in its upper and lower parts, respectively, because of its leftward movement. Since the models are fluid saturated, coseismic volumetric changes develop a Δp pattern in excess to the hydrostatic (Fig. 3g and h). In detail, suprahydrostatic pore pressures develop in areas affected by volumetric compression,

whereas subhydrostatic pore pressures develop in areas affected by volumetric dilation.

In the postseismic phase, the Δp values gradually dissipate because of fluid diffusion. After 20 days from the simulated earthquakes, the ongoing fluid diffusion in the medium (black arrows in Fig. 3i and j) gradually mitigates the postseismic pore pressures, which are approximately four times lower than the coseismic ones (Fig. 3g and h). Since pore pressures and stresses are coupled, the gradual dissipation of the coseismic Δp alters the stresses inside the medium, developing further deformations. Indeed, the modelled postseismic deformations two years after the simulated events show further subsidence of the hangingwall for the L'Aquila 2009 normal-fault earthquake (Fig. 3k) and uplift for the Emilia 2012 reverse-fault earthquake (Fig. 3l).

Discussion and concluding remarks. The developed numerical model allowed to reproduce the interseismic, coseismic and postseismic phases for extensional and compressional earthquakes in Italy within a unified framework. The imposed geometrical and boundary conditions resulted in a distribution of stresses and strains in the earth's crust that is compatible with the interseismic, coseismic and postseismic evolution of normal and reverse fault earthquakes. In detail, the simulation results show that the applied basal shear traction appears to be an essential factor to model the large-scale interseismic pattern since it allows for a first-order simulation of the ongoing crustal interseismic extension of the Central Apennines and compression of the Adriatic foreland and the north-eastern part of the Italian territory. The action of shear tractions and lithostatic forces generates a local concentration of stresses and strains in the presence of local heterogeneities or discontinuities, i.e., at the transition between the brittle locked fault and the ductile unlocked slipping fault during the interseismic stage (Fig. 3b and d). Such an interseismic strain partitioning provides maximum horizontal stress sufficient to exceed the friction on the locked brittle part of the fault, with the subsequent collapse of the hangingwall in case of extensional earthquakes (Fig. 3e) or the expulsion of the hangingwall in case of compressional earthquakes (Fig. 3f). The displacement profiles at zero depth in Fig. 3e and f are compared in with the observed displacements profiles form InSAR along the Line of sight of the satellite, taken along the sections A, and B Fig. 1a. The agreement between the modelled (continuous blue line) and measured (blue circles) LoS displacements (Fig. 3 m and n) is satisfactory for both normal and reverse-fault events.

The instantaneous slip of the hangingwall perturbs the crustal pore fluid pressures, triggering groundwater flow in the postseismic phase from regions of higher pore pressures, which further compress, to regions of lower pore pressures, which further dilate. As a result, displacements gradually accumulate in the postseismic phase, according to the dissipation of pore pressure excess. The poroelastic compression/dilation of the medium causes the mainshock causative fault to further slip in the postseismic phase, which contributes to the accumulated ground displacements. Once the postseismic phase terminates, a new cycle of interseismic loading can start again.

References

Anderlini L., Serpelloni E., Belardinelli M.E.; 2016: *Creep and locking of a low-angle normal fault: Insights from the Altotiberina fault in the Northern Apennines (Italy)*. Geophys. Res. Lett. 43, 4321–4329. https://doi.org/10.1002/2016GL068604

Atzori S., Hunstad I., Chini M., Salvi S., Tolomei C., Bignami C., Stramondo S., Trasatti E., Antonioli A.,Boschi E.; 2009: *Finite fault inversion of DInSAR coseismic displacement of the 2009 L'Aquila earthquake (central Italy)*. Geophys. Res. Lett. 36, n/a-n/a. https://doi.org/10.1029/2009GL039293

Barba S., Carafa M.M.C., Boschi E.; 2008: *Experimental evidence for mantle drag in the Mediterranean*. Geophys. Res. Lett. 35, 1–6. https://doi.org/10.1029/2008GL033281

Carafa M.M.C., Barba S., Bird P.; 2015: *Neotectonics and long-term seismicity in Europe and the Mediterranean region*. J. Geophys. Res. Solid Earth 120, 5311–5342. https://doi.org/10.1002/2014JB011751

Carminati E., Vadacca L.; 2010: *Two- and three-dimensional numerical simulations of the stress field at the thrust front of the Northern Apennines, Italy*. J. Geophys. Res. 115, B12425. https://doi.org/10.1029/2010JB007870

Doglioni C., Barba S., Carminati E., Riguzzi F.; 2011: *Role of the brittle-ductile transition on fault activation*. Phys. Earth Planet. Inter. 184, 160–171. https://doi.org/10.1016/j.pepi.2010.11.005

Finocchio D., Barba S., Basili R.; 2016: *Slip rate depth distribution for active faults in Central Italy using numerical models*. Tectonophysics 687, 232–244. https://doi.org/10.1016/j.tecto.2016.07.031

MSC Software Corporation; 2018: *Marc 2018.1 Volume A: Theory and User Information* <http://www.mscsoftware.com/it/product/marc>.

Pezzo G., Merryman Boncori J.P., Tolomei C., Salvi S., Atzori S., Antonioli A., Trasatti E., Novali F., Serpelloni E., Candela L., Giuliani R.; 2013: *Coseismic Deformation and Source Modeling of the May 2012 Emilia (Northern Italy) Earthquakes*. Seismol. Res. Lett. 84, 645–655. https://doi.org/10.1785/0220120171

Scholz C.H.; 2019: *The Mechanics of Earthquakes and Faulting*. Cambridge University Press. https://doi.org/10.1017/9781316681473

Trasatti E., Kyriakopoulos C. and Chini M.; 2011: *Finite element inversion of DInSAR data from the Mw 6.3 L'Aquila earthquake, 2009 (Italy)*. Geophys. Res. Lett. 38. https://doi.org/10.1029/2011GL046714

Wang H.; 2000: *Theory of linear poroelasticity with applications to geomechanics and hydrogeology*. Princeton University Press.

SEISMICITY INDUCED BY THE DYNAMICS OF THE SOUTHERN FLANK OF MT. ETNA (SICILY, ITALY): THE TRECASTAGNI FAULT ACTIVITY IN FEBRUARY 2019

S. Alparone[1], S. Gambino[1], S. Grassi[2], S. Imposa[2], G. Patti[2], A. Ursino[1]

[1] Istituto Nazionale di Geofisica e Vulcanologia - Osservatorio Etneo - Sezione di Catania - Catania

[2] Università degli Studi di Catania - Dipartimento di Scienze Biologiche, Geologiche e Ambientali - Sezione di Scienze della Terra - Catania

Introduction. Mt. Etna is one of the most active volcanoes in the world and is considered one of the most interesting natural laboratories for the understanding of eruptive processes and the ascent of magma. The geodynamic framework of Mt. Etna is located within the collisional process of the Eurasia and Africa plates with a roughly N-S trend and E-W extensional regime.

The volcano edifice is located at the intersection of the two major regional structural lineaments, with NNW-SSE and NE-SW trends, which play a fundamental role in the dynamic processes of the volcano (Bonaccorso *et al*., 1996, Gresta *et al*., 1998).

The complex interaction between regional stress, gravity force and dyke-induced rifting, has caused the slow sliding of the eastern and south-eastern flanks of the volcano (Borgia *et al*., 1992; Lo Giudice and Rasà, 1992; Monaco *et al*., 1997; Borgia *et al*., 2000; Neri *et al*., 2004; Walter *et al*., 2005). Therefore, the dynamics of the eastern flank seems to have a key role in the triggering of volcanic eruptions.

The eastern flank dynamics is controlled by several fault systems; among these, the Provenzana-Pernicana fault represents the northern boundary. The earthquakes occurring along this structure mainly take place in the form of seismic swarms, even of low energy. The main events reach magnitudes of up to 4.3 and sometimes cause damage to existing structures (Alparone *et al*., 2013 and references therein).

From west to east, the Ragalna, Tremestieri Etneo and Trecastagni faults (Azzaro, 1999), which in some places have evident morphological slopes (Gambino *et al*., 2011), make up the southern boundary of the eastern flank. These structural lineaments release energy in the form of aseismic creep and generate earthquakes that are mostly isolated with medium energy. The seismic sources are characterized by extremely superficial foci, which sometimes cause moderate damage to existing structures. Although it has been recognized as a southern boundary, these structural fault systems have not been affected in recent decades by significant seismicity, showing a low rate of occurrence. This characteristic, probably linked to the scarce detection of

microseismicity and to the insufficient constraint of the seismic sources, could represent a limit of the current seismological knowledge in this volcano sector.

The Trecastagni Fault (TF) is a discontinuity that develops in the southern flank of Mt. Etna, between the Trecastagni and San Giovanni la Punta villages. This is an active structure with an approximately NNW-SSE trend (Fig.1a) characterized by morphological escarpments. The seismicity of the TF is characterized by very shallow earthquakes with typical focal depths of 1-2 km below sea level. Also south of TF creep effects are visible along the San Gregorio di Catania fault (Imposa *et al*., 2015). Evident co-seismic surface faulting occurred along the fault scarp of TF in September 1980 and in November 1988 (Azzaro, 1999). Hollows appeared in agricultural land and fractures in buildings, boundary walls and the road 8/III, were observed after the local shocks on September 16 and 20, 1980 and also after the 21 November 1988 earthquake (Azzaro, 1999). Other similar episodes on 26 May 1903, 20 July 1917 and 17 February 1955, have been reconstructed by historical research (Azzaro and D'Amico, 2008). In recent years, some minor shallow earthquakes have been felt by the local residents; in particular, on 15 October 2009, at 00:52 GMT, M=2.1 and on 29 October 2010, at 01:37, M=2.2. (Gambino *et al*., 2011).

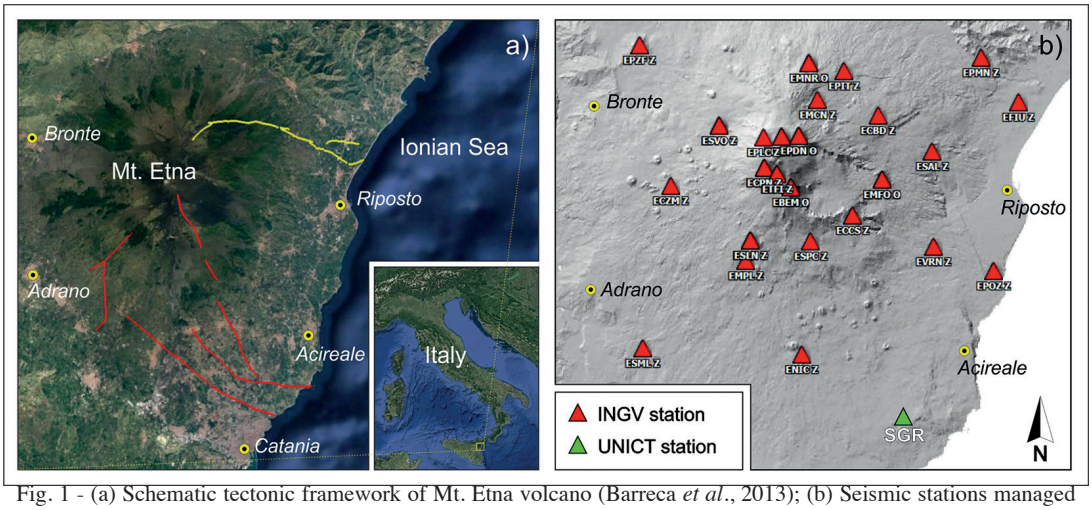

Fig. 1 - (a) Schematic tectonic framework of Mt. Etna volcano (Barreca *et al*., 2013); (b) Seismic stations managed by the Istituto Nazionale di Geofisica e Vulcanologia Osservatorio Etneo – Sezione di Catania (red triangles) and by the University of Catania (green triangle).

Ten years after the last flank eruption of 2008-2009, on December 24, 2018 an intense seismic sequence preceded and accompanied the beginning of a flank eruption at Mt. Etna volcano. In a few days, more than 3000 earthquakes were recorded by the INGV-OE (Istituto Nazionale di Geofisica e Vulcanologia - Osservatorio Etneo) permanent seismic network, most of them in the first 24 hours. The most powerful event (ML=4.8; MW=4.9) was recorded on December 26 at 02:19 UTC and occurred just below sea level between the villages of Fleri and Pennisi. After this event, the seismicity affected the central areas of the volcano and subsequently it involved more peripheral sectors including the southern structures, in particular the Tremestieri Etneo and Trecastagni fault systems (Alparone *et al*., 2009 submitted).

The purpose of this paper is to study three earthquakes and their possible links with ground deformation data recorded by extensometric stations operating in this volcano sector. In particular, we integrated the seismic data of the permanent INGV-OE network with the station managed by the University of Catania and located near the fault under investigation.

Monitoring network. The permanent seismic network, managed by INGV-OE, consists of about 30 stations equipped with broadband 3-component seismometers (Fig.1b). Since the geometry of this network is sparse in the southern sector of volcano, we have added a

station (SGR), managed by an agreement between the Dipartimento di Scienze Biologiche, Geologiche e Ambientali of the University of Catania and the Municipality of S. Gregorio di Catania. This station SGR, located in San Gregorio di Catania territory, near the Trecastagni Fault, is equipped with a short-period 3-component seismometer.

The extensometer stations of the INGV-OE comprise two continuous wire extensometers (Mod Sisgeo D241A20) equipped with a compact data-logger programmed for 48 data/day sampling (Carnazzo *et al.*, 2006; Gambino *et al.*, 2011).

ET1 was installed in May 2005 directly on a fractured concrete structure, while ET2 was set up in 2007 on the ground after the creation of an 8-meter long and 30-cm deep trench. The two stations measure the relative displacements perpendicular to the fracture (the extensional component).

Data. Figure 2a,b shows the seismic activity, in the study area, over the last 19 years and the relative earthquakes daily rate and associated seismic strain release; of note is the scarce seismic activity.

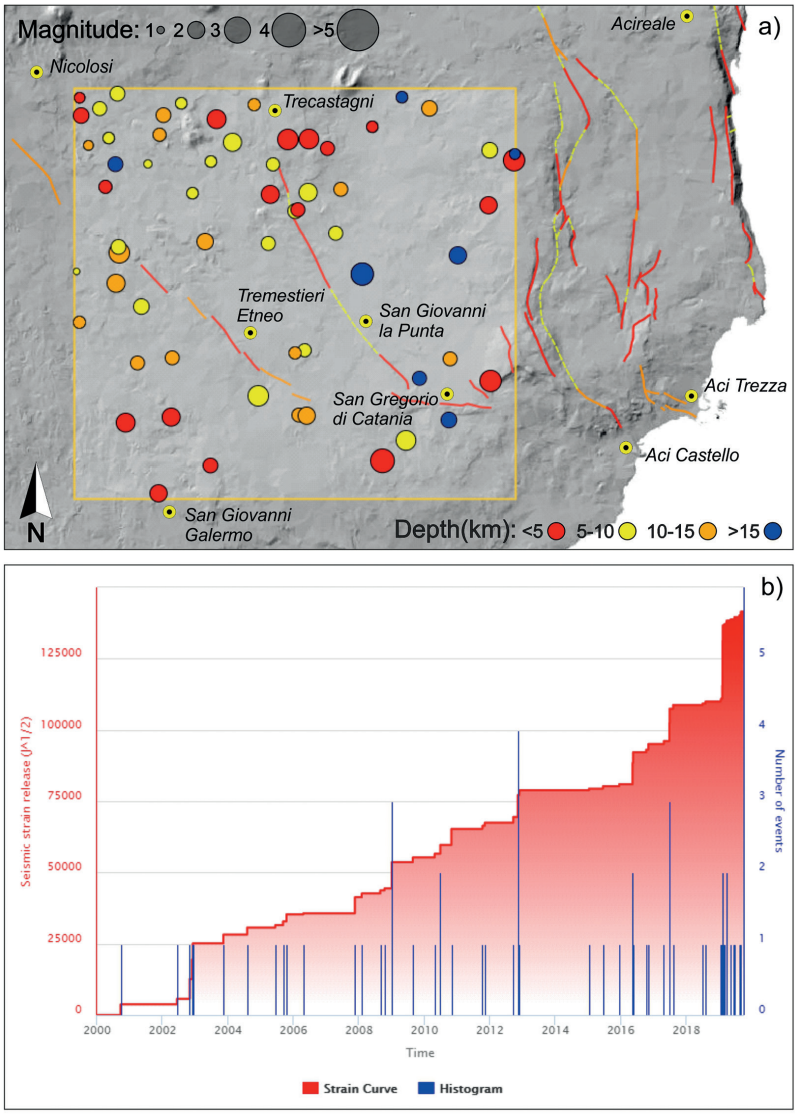

Fig. 2 - (a) Epicentral map of earthquakes located in the study area from 2000 to 2019; (b) Relative earthquakes daily rate and associated seismic strain release in the same period. Circle size indicates magnitude, colours indicate range depth.

We focused on three earthquakes that occurred in the post-eruption December 2018 phase. The earthquakes were located using the Hypoellipse algorithm (Lahr, 1989) and the 1D crustal velocity model proposed for Etna area by Hirn *et al*. (1991) and subsequently modified by Patanè *et al*. (1994). They occurred on February 6th 2019 (23:38 UTC Ml =2.5), on February 9th (06:02 UTC, Ml=2.9) and on February 10th (04:00 UTC, Ml =2.4), and were felt by the local people living near the epicenter area.

We have collected the readings of the P and S-phases recorded by the INGV-OE seismic network with those of the SGR station. This integration has allowed improving the main hypocentral location parameters (GAP; RMS, ERH and ERZ) and to better associate these earthquakes with the geometry of the faults known in the literature. In particular, the earthquakes are ascribable to the seismogenic activity of the main faults system recognized in the study area (Fig.3a,b).

On the same days, extensometer data showed millimetric variations at both stations. In particular, ET2 cumulated an opening of about 11 mm and ET1 2.5 mm.

Fig. 3 - (a) Investigated area; (b) Epicentral map of three earthquakes located in February 2019.

Conclusions. This research is focused on the study of three earthquakes that occurred in the lower southern sector of Mt. Etna. The integration of INGV-OE seismic data with those from the station managed by the University of Catania (SGR) has allowed improving the hypocenter earthquake parameters and consequently the conjunction of seismic sources with the structural lineaments of the survey area. The evidence of activation of southern flank of volcano could be related to extensometers data, which in the same period, recorded some millimetric variations.

This multidisciplinary study will allow to better understand the complex geodynamics of the lower southern slope of the volcano and to link this with the eruptive activity of Mt. Etna volcano.

Acknowledgments. A special thanks to the Municipality of San Gregorio di Catania (CT) which enabled installing the seismic station and provided considerable logistic support. This work was funded by the Dipartimento di Scienze Biologiche, Geologiche e Ambientali, Università degli Studi di Catania, in the frame of "Piano Nazionale della Ricerca 2019". Scientific Supervisor Prof. S. Imposa.

References

Alparone S., Barberi G., Giampiccolo E., Maiolino V., Mostaccio A., Musumeci C., Scaltrito A., Scarfì L., Tuvè T., Ursino A.; 2019: Seismological investigations of the Mt. Etna (Italy) 2018 flank eruption: implications in the dynamics of the eastern flank of the volcano Submitted to Terra Nova.

Alparone S., Cocina O., Ferrari F., Gambino S., Mostaccio A., Spampinato S., Tuvè T., Ursino A.; 2013: Seismological features of the Pernicana - Provenzana Fault System (Mt. Etna, Italy) and implications for the dynamics of the northeastern flank of the volcano. J. Volcanol Geotherm Res. 251, 16-26, doi:10.1016/j.jvolgeores.2012.03.010.

Azzaro, R.; 1999: Earthquake Surface Faulting at Mount Etna Volcano (Sicily) And Implications For Active Tectonics. J. Geodyn., 28, 193-213.

Azzaro R., D'Amico S.; 2008: Catalogo Macrosismico dei Terremoti Etnei dal 1832 al 2005. INGV-CT, http://www.ct.ingv.it/sismologia/macro.

Barreca G., Bonforte A., Neri M.; 2013: A pilot GIS database of active faults of Mt. Etna (Sicily): A tool for integrated hazard evaluation. Journal of volcanology and geothermal research,251, 170-186.

Bonaccorso, A., F. Ferrucci, D. Patanè and L. Villari (1996). Fast deformation processes and eruptive activity at Mount Etna (Italy), Journal of Geophysical Research, 101,17467–17480.

Borgia A., Lanari R., Sansosti E., Tesauro M., Berardino P., Fornaro G., Neri M., Murray J.B.; 2000: Actively growing anticlines beneath Catania from the distal motion of Mount Etna's decollement measured by SAR interferometry and GPS, Geophys. Res. Lett., 27 (20), 3409–3412.

Carnazzo A., Ferro A., Falzone G., Gambino S., Laudani G.; 2006: La rete estensimetrica della Faglia di Trecastagni. INGV Rapporto Tecnico n° 56.

Gambino S., Bonforte A., Carnazzo A., Falzone G., Ferrari F., Ferro A., Guglielmino F., Laudani G., Maiolino V., Puglisi G.; 2011: Displacement across the Trecastagni Fault (Mt. Etna) and induced seismicity: the October 2009–January 2010 episode. Annals of Geophysics, 54, 414-423. doi: 10.4401/ag-4841.

Gresta S., Peruzza L., Slejko D., Distefano., G 1998: Inferences on the main volcanotectonic structures at Mt Etna (Sicily) from a probabilistic seismological approach, J. Seismol., 2, 105–116.

Hirn A., Nercessian A., Sapin M,. Ferrucci F., Wittlinger G.; 1991: Seismic heterogeneity of Mt Etna: structure and activity, Geophys. J. Int., 105, 139-153.

Imposa S., De Guidi G., Grassi S., Scudero S., Patti G., Boso D.; 2015: Applying geophysical techniques to investigate a segment of a creeping fault in the urban area of San Gregorio di Catania, southern flank of Mt. Etna (Sicily-Italy). Journal of Applied Geophysics, 123:153-163.

Lahr J.C., 1989: HYPOELLIPSE/VERSION 2.0*: A computer program for determining local earthquakes hypocentral parameters, magnitude, abd first motion pattern, U.S. Geol. Sur., Open File Rept., 89-116, 81 pp.

Lo Giudice E., Rasà R.; 1992: Very shallow earthquakes and brittle deformation in active volcanic areas: the Etnean region as example, Tectonophysics, 202, 257–268.

Monaco C., Tapponnier P., Tortorici L., Gillot P.Y.; 1997: Late Quaternary slip rates on the Acireale–Piedimonte normal faults and tectonic origin of Mt Etna (Sicily), Earth Planet. Sci. Lett., 147, 125–139.

Neri, M., Acocella V., Behncke B.; 2004: The role of the Pernicana Fault System in the spreading of Mount Etna (Italy) during the 2002–2003 eruption, Bull. Volcanol., 66, 417–430, doi:10.1007/s00445-003-0322-x.

Patanè D., Privitera E., Ferrucci F., Gresta S.; 1994: Seismic activity leading to the 1991–1993 eruption of Mt Etna and its tectonic implications, Acta Vulcanologica, 4, 47–55.

Walter T.R., Acocella V., Neri M., Amelung F.; 2005: Feedback processes between magmatic events and flank movement at Mount Etna (Italy) during the 2002-2003 eruption, J. Geophys. Res., 110(B10), B10205, doi:10.1029/2005jb003688.

ADRIATIC EARTHQUAKES FROM THE MID-LOWER CRUST: POSSIBLE HINTS FOR THE PALEOGEOGRAPHY OF ADRIA

A. Argnani
CNR, ISMAR-Bologna, Italy

The Emilia 2012 seismic sequence, that occurred from the end of May to early June, is characterized by a large numer of earthquakes that range from 16 to 2 km in depth (e.g., Carannante *et al*., 2015), with the epicentres that are located west of the city of Ferrara. However, on the 6th June, towards the end the seismic sequence, an earthquake occurred way to the east, near the city of Ravenna. This event worried the citizenship as it was perceived as a potential eastward propagation of the Emilia fault rupture. The hypocentral depth of this Ravenna earthquake, however, was ca. 30 km, significantly deeper than the earthquakes of the Emilia sequence, and it remained an isolated event. On the 15th January 2019 an earthquake of Mw 4.3 occurred near Ravenna at ca. 21 km depth, suggesting that tectonic stress in the area can be released by earthquake ruptures in the middle-lower crust. Focal mechanisms indicate strike-slip or reverse fault solutions, and the nodal planes suggest the occurrence of ruptures along relatively high angle faults. It is likely that these eathquakes nucleate on pre-existing faults characterized by some inherited weakness (e.g., Middleton and Copley, 2014). The aim of this contribution is to attempt relating the mid-lower crustal earthquakes in the Adria domain to the inherited Mesozoic fault system and to infer a palaeogeography of Adria that still has some control over the current seismicity of the Adriatic foreland.

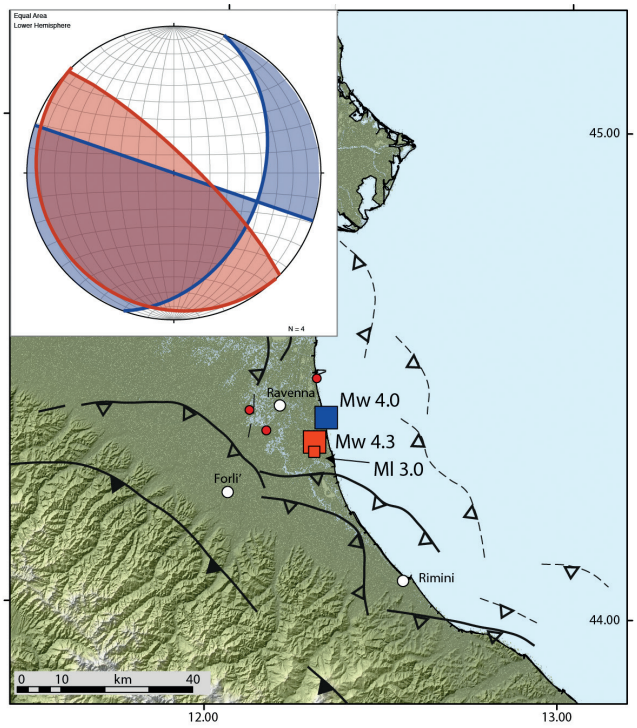

Fig. 1 - Map showing the epicenters of the 6th June 2012 (blue square) and 15th January 2019 (red square) Ravenna earthquakes and the simplified tectonic structures. The small square and circles indicate earthquakes of Ml 3 and around 2, respectively. Dashed lines are thrusts affecting mainly the Pliocene-Quaternary sediments. Continuous lines with open and filled triangles are thrusts involving the Mesozoic succession and the basement, respectively (from Carannante *et al*., 2015). The inset shows the nodal planes of the two larger earthquakes, with the same colour code.

The distribution of instrumental seismicity in Italy shows that several mid-lower crustal earthquakes (deeper than 15 km) occurred in the Adriatic foreland (Chiarabba *et al*., 2005: 2015).Where focal mechanisms are available, the solutions point to reverse or strike.slip faults. In some instances the relationships of these earthquakes with pre-existing extensional faults seem to be convincingly proven (Herak *et al*., 2005). Moreover, several lines of geological evidence indicate that tectonic inversion is rather widespread in the Adriatic foreland (Argnani *et al*., 1993, 2002; Argnani and Frugoni, 1997; Scisciani, 2009; Stanculete *et al*., 2014; Pace, 2018), extending also into the Po Plain foreland (Fantoni *et al*., 2004, 2017).

The large-scale control exerted by the Mesozoic paleogeography of Adria on the evolution of the fold-and-thrust belts that currently

fringe the Adriatic foreland has been suggested for the Northern Apennines, facing the Po Plain foreland (Castellarin *et al*., 1985; Masetti *et al*., 2012; Livati *et al*., 2018) and the Albanides, facing the Southern Adriatic foreland (Argnani, 2013). The Mesozoic paleogeography of the central-northern Adriatic is still less well defined and the structural trends, in particular, are poorly constrained. It will be explored whether the hints offered by the mid-lower crustal earthquakes of the Adriatic domain can help contraining the large-scale Mesozoic structural trends. Furthermore, an interference between seismicity related to the Apennine fold-and-thrust belt and the deeper foreland seismicity can be hypothesized.

Acknowledgements. The data concerning location, hypocentral depth, magnitude, and focal mechanism of the earthquakes mentioned in the text are taken from the INGV website http://cnt.rm.ingv.it/event/, unless otherwise indicated.

References

Argnani, A.; 2013: The influence of Mesozoic palaeogeography on the variations in structural style along the front of the Albanide thrust-and-fold belt. Ital. J. Geosci., 132, 175-185.

Argnani, A., Favali, P., Frugoni, F., Gasperini, M., Ligi, M., Marani, M., Mattietti, G., and Mele, G.; 1993: Foreland deformational pattern in the southern Adriatic Sea: Annali di Geofisica, 36, 229–247.

Argnani, A. and Frugoni F.; 1997: Foreland Deformation in the Central Adriatic and its Bearing on the Evolution of the Northern Apennines. Annali di Geofisica 40, 771-780.

Argnani, A., Bonazzi, C., and Costa Pisani, P.; 2002: Neogene deformation in the central Adriatic Sea: Bollettino di Geofisica Teorica e Applicata, 42, suppl., 135–138.

Carannante, S., Argnani, A., Massa, M., D'Alema, E., Lovati, S., Moretti, M., Cattaneo, M., and Augliera, P.; 2015.: The May 20 (MW 6.1) and 29 (MW 6.0), 2012, Emilia (Po Plain, northern Italy) earthquakes: new seismotectonic implications from subsurface geology and high-quality hypocenter location. Tectonophysics 655, 107–123.

Castellarin, A., Eva, C., Ciglia, G., and Vai, G. B.; 1985: Analisi strutturale del Fronte Appenninico Padano. Giornale di Geologia, 47, 47–75.

Chiarabba, C., Jovane, L., and Di Stefano, R.; 2005: A new look to the Italian seismicity: seismotectonic inference. Tectonophysics 395, 251–268.

Chiarabba, C., De Gori, P., and Mele, F.M.; 2015: Recent seismicity of Italy: Active tectonics of the central Mediterranean region and seismicity rate changes after the Mw 6.3 L'Aquila earthquake. Tectonophysics 638 (2015) 82–93.

Fantoni, R., Bersezio, R. and Forcella F.; 2004: Alpine structure and deformation chronology at the Southern Alps-Po Plain border in Lombardy. Boll. Soc. Geol. It., 123, 463-476.

Fantoni, R., Dal Zotto, O., Fattorini, A., Martinis, S. and Stanculete, A.; 2014: Inversion structure in the Po Plain and Adriatic foreland (Northern Italy). Abstract, Societa' Geologica Italiana, Milano.

Herak, D., Herak, M., Prelogovic, T.E., Markusic, S. and Markulin, Z.; 2003: Jabuka island (Central Adriatic Sea) earthquakes of 2003. Tectonophysics 398 (2005) 167– 180.

Livani, M., Scrocca, D., Arecco, P., and Doglioni, C.; 2018: Structural and stratigraphic control on salient and recess development along a thrust belt front: The Northern Apennines (Po Plain, Italy). JGR, 123, 4360–4387.

Masetti, D., Fantoni, R., Romano, R., Sartorio, D. and Trevisani, E.; 2012: Tectonostratigraphic evolution of the Jurassic extensional basins of the eastern southern Alps and Adriatic foreland based on an integrated study of surface and subsurface data. AAPG, AAPG Bulletin, 96, 2065–2089.

Middleton, T.A. and Copley. A.; 2014: Constraining fault friction by re-examining earthquake nodal plane dips. Geoph. J. Int. 196, 671-680.

Pace, P.; 2018: Emma Inversion Structure, Adriatic Sea, Italy, In: A. A. Misra and S. Mukherjee (eds.), Atlas of Structural Geological Interpretation from Seismic Images, 61-64.

Scisciani, V.; 2009: Styles of positive inversion tectonics in the Central Apennines and in the Adriatic foreland: Implications for the evolution of the Apennine chain (Italy). Journal of Structural Geology 31, 1276–1294.

Stanculete, A., Corrao, A., Cosgrove, J., Ronchi, P., Vandeginste, V., and Fantoni ,R.; 2014: Inversion structure of dinaric age in the Adriatic foreland (Northern Italy). Abstract, Mesozoic and Cenozoic Carbonates of the Neo-Tethys, Naples.

IL TERREMOTO DI FLERI (ETNA) DEL 26 DICEMBRE 2018, M_W 4.9. PARTE I: RILIEVO MACROSISMICO ED EFFETTI DI DANNO

R. Azzaro[1], S. D'Amico[1], T. Tuvè[1], A. Tertulliani[1], F. Bernardini[1], C. Castellano[1], E. Ercolani[1], A. Maramai[1], A. Amantia[1], M.S. Barbano[2], E. Giampiccolo[1], A. Mantovani (QUEST Working Group, Emergenza Etna 2018)

[1] Istituto Nazionale di Geofisica e Vulcanologia (Catania, Roma, Bologna)
[2] Dipartimento di Scienze Biologiche, Geologiche e Ambientali, Università di Catania

Introduzione. Il terremoto del 26 dicembre 2018, ore 02:19 UTC, è localizzato dalla rete sismica dell'INGV – Osservatorio Etneo nel basso versante sud-orientale dell'Etna, ad una profondità inferiore al chilometro (Gruppo Analisi Dati Sismici, 2019). Con una magnitudo M_L 4.8 o M_w 4.9 (dato Regional Centroid Moment Tensors, https://doi.org/10.13127/rcmt/italy), esso costituisce l'evento più energetico registrato a seguito della breve eruzione effusiva che ha interessato il settore sommitale del vulcano due giorni prima. L'area danneggiata comprende una fascia grosso modo estesa tra Acireale e Zafferana, che è attraversata dalla struttura sismogenetica nota in letteratura come Faglia di Fiandaca, appartenente al sistema delle Timpe. L'evento in questione è stato seguito, nell'arco di un mese circa, da una sequenza sismica di circa 50 scosse di bassa magnitudo (M_{max} 3), localizzate lungo la stessa struttura tettonica.

Rilievo macrosismico ed effetti osservati. Il gruppo di emergenza QUEST (QUick Earthquake Survey Team, http://quest.ingv.it/) dell'INGV, in collaborazione con altri ricercatori, ha condotto il rilievo macrosismico secondo le procedure operative consolidate in questi anni, ovvero sopralluoghi nell'area di danno, e indagini telefoniche/raccolta di notizie pubblicate sui media per delimitare l'area di avvertibilità del terremoto. Viste le caratteristiche del territorio densamente urbanizzato, in cui le località rappresentative per l'indagine macrosismica (capoluoghi comunali, frazioni, contrade) si presentano come aggregati senza soluzione di continuità, e la forte attenuazione dell'intensità macrosismica a brevissima distanza dalla zona epicentrale (Azzaro *et al*., 2006), nell'area di massimo risentimento è stato effettuato un rilievo di dettaglio (edificio per edificio). In tal modo è stato possibile ottenere una stima affidabile della intensità macrosismica, basata sulla scala europea EMS (Tertulliani *et al*., 2019). Complessivamente sono state effettuate otto campagne macrosismiche con squadre che si sono alternate sul terreno (per un totale di 28 gg/persona) e stimate le intensità per 48 località (QUEST WG, 2019).

L'area più colpita comprende le località attraversate dal settore di monte della Faglia di Fiandaca, tra Fleri e Pennisi, lungo una fascia con direzione NO-SE estesa circa 4 km. Qui tutti gli edifici rurali e con scarse caratteristiche costruttive (cl. A) hanno subìto il crollo totale (5 grado), mentre le costruzioni in muratura in pietra squadrata (cl. B) sono state gravemente lesionate (3 grado) (Fig. 1), subendo anche alcuni crolli parziali (4 grado).

Fig. 1 - Fleri (sx): crollo di un edificio in pietra grezza (cl. A); Mazzasette (dx): danno grave (lesioni a croce di S. Andrea, grado 3) ad un edificio in muratura (cl. B).

Fig. 2 - Fleri (sx): rottura dei tramezzi in un edificio in c.a. (cl. C); Mazzasette (dx): rottura dei pilastri e crollo delle tramezzature (grado di danno 4) in un edificio in c.a. (cl. C).

Per quanto riguarda le strutture in calcestruzzo armato (c.a.), negli edifici più datati (cl. C) si è osservata la rottura dei tramezzi e tamponature e, in qualche caso, lesioni ai pilastri (Fig. 2), mentre in quelli recenti (cl. D) si sono rilevati solo lievi danni (1-2 grado). Il quadro dei danni osservati in quest'area porta all'assegnazione del grado di intensità 8 EMS.

Uno scenario meno grave ma ancora rilevante, pari ad una intensità 7 EMS, con danni strutturali moderati agli edifici in muratura (cl. B) e non-strutturali a quelli in c.a. (cl. C) ha interessato le frazioni e contrade collocate in posizione più periferica rispetto alla fascia di massimo danneggiamento e lungo il settore centrale della faglia di Fiandaca. In tale area si osservano ancora alcuni crolli parziali (4 grado) di edifici rurali (cl. A).

Infine, danni diffusi ma di lieve entità (intensità 6 EMS) – caduta di intonaci, piccole lesioni, scollamenti tra strutture portanti e tramezzature – sono stati rilevati nelle località circostanti di Zafferana Etnea Monterosso, Linera, e lungo il settore sud della faglia di Fiandaca (per es. a S. Maria la Stella). Complessivamente, sono alcune centinaia gli edifici dichiarati inagibili a causa del terremoto.

Va infine rilevato che la presenza di vistosi effetti di fagliazione superficiale (EMERGEO WG, 2019), ha contribuito ad aggravare lo scenario di danno prodotto dal terremoto, dato che numerose infrastrutture, principalmente reti dei servizi (tubature di acqua e gas) e strade (inclusa l'autostrada A18 Messina-Catania), hanno subìto interruzioni funzionali più o meno lunghe, se non permanenti.

L'areale di risentimento del terremoto è complessivamente ampio, esteso a buona parte della Sicilia orientale fino ad una distanza di circa 70-80 km dall'epicentro, particolarmente verso sud nel settore ibleo) (Fig. 3).

Note conclusive. Il quadro degli effetti macrosismici rilevati conferma, come già noto in letteratura, che il terremoto del 26 dicembre 2018 presenta le caratteristiche macrosismiche tipiche dei terremoti superficiali all'Etna: danni gravi su un'area relativamente poco estesa, alta intensità epicentrale associata a valori di magnitudo moderati (Azzaro *et al*., 2011), elevata attenuazione dell'intensità a brevi distanze epicentrali, soprattutto in direzione ortogonale alla sorgente.

In particolare, i dati raccolti hanno evidenziato che:

- l'area epicentrale del terremoto del 2018 è stata interessata in passato da scenari di danno comparabili, che hanno tuttavia interessato settori meno estesi della Faglia di Fiandaca; le maggiori analogie circa la distribuzione ed estensione del danneggiamento, sono riferibili al terremoto dell'agosto 1894 (I_{max} 8-9 EMS, M_w 4.6);
- tra le località maggiormente colpite, l'abitato di Fleri risulta danneggiato nei fabbricati che furono già riparati o "adeguati sismicamente" dopo il sisma dell'ottobre 1984 (I_{max} 8 EMS,

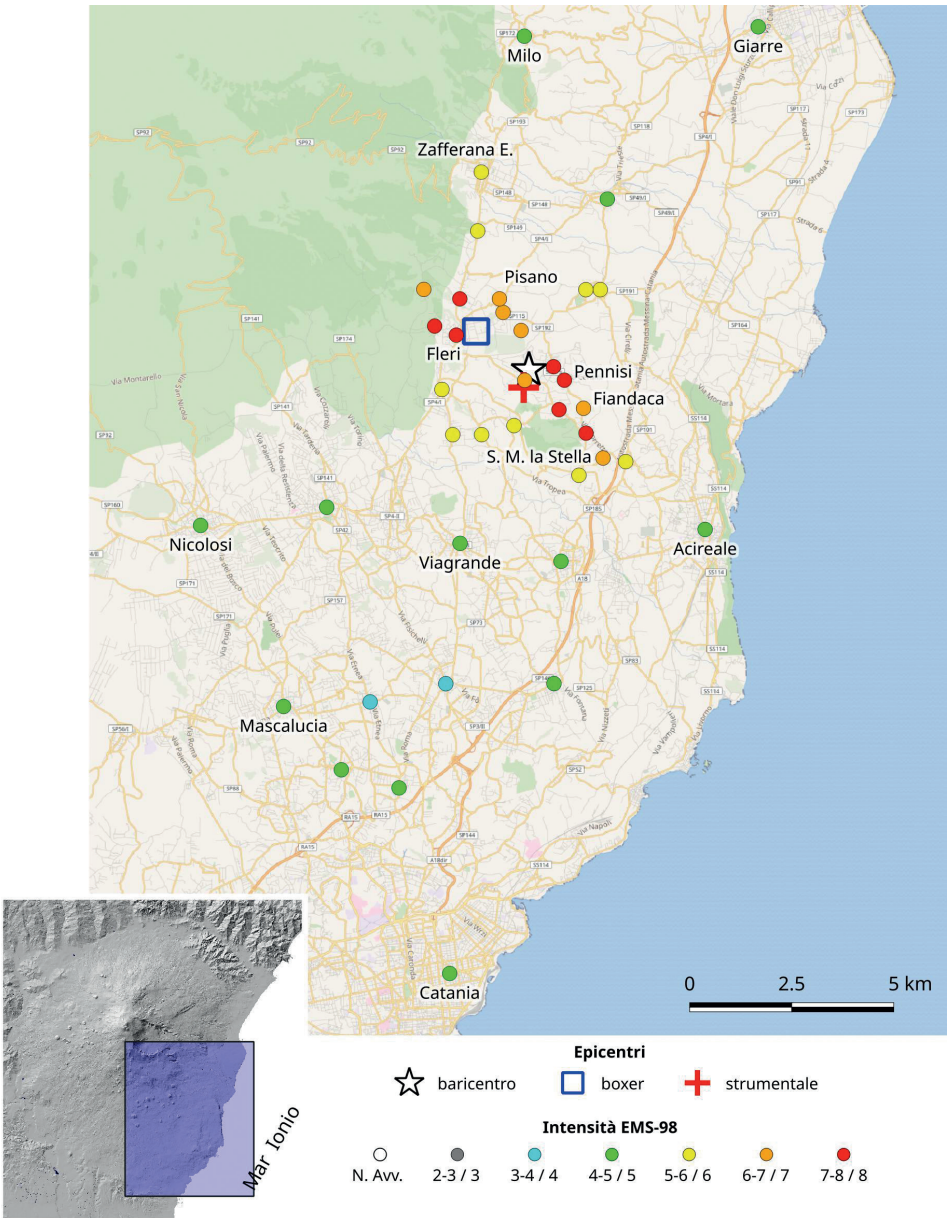

Fig. 3 - Mappa dell'intensità macrosismica del terremoto del 26 dicembre 2018, ore 02:19 UTC (rappresentazione parziale).

M_w 4.4); al contrario, gli edifici recenti costruiti secondo le moderne norme antisismiche (cl. D), non hanno subìto danni degni di nota;

- i parametri del terremoto ricavati dal dato macrosismico tramite il codice BOXER 4.0 (Gasperini *et al*., 2010) sono in accordo con quelli strumentali per quanto riguarda la localizzazione – la distanza tra i due epicentri è 1800 metri – mentre le magnitudo sono sensibilmente differenti, con un +0.5 unità per il dato strumentale (M_{Lmacro} 4.3 vs M_{Lstrum} 4.8; M_{wmacro} 4.4 vs M_{wstrum} 4.9). Questa evidenza indica, per gli eventi storici maggiori riportati nel catalogo etneo CMTE (Azzaro e D'Amico, 2014), una sensibile sottostima della magnitudo ricavata da dati macrosismici.

Bibliografia

Azzaro R., Barbano M.S., D'Amico S., Tuvè, T.; 2006. *The attenuation of the seismic intensity in the Etna region and comparison with other Italian volcanic districts*. Ann. Geophys., **49** (4/5), 1003-1020.

Azzaro R., D'Amico S., Tuvè T.; 2011: *Estimating the magnitude of historical earthquakes from macroseismic intensity data: new relationships for the volcanic region of Mount Etna (Italy)*. Seism. Res. Lett., **82** (4), 533-544.

Azzaro R., D'Amico S.; 2014. *Catalogo Macrosismico dei Terremoti Etnei (CMTE)*. Istituto Nazionale di Geofisica e Vulcanologia (INGV), https://doi.org/10.13127/cmte

EMERGEO WG; 2019. Il terremoto etneo del 26 dicembre 2018, M_w 4.9: rilievo degli effetti di fagliazione cosismica superficiale. Rapporto INGV n. 1 del 21/01/2019, 9 pp., doi 10.5281/zenodo.2545555

Gasperini P., Vannucci G., Tripone D., Boschi E.; 2010. *The location and sizing of historical earthquakes using the attenuation of macroseismic intensity with distance*. Bull. Seism. Soc. Am., 100, 2035–2066.

Gruppo Analisi Dati Sismici; 2019. *Catalogo dei terremoti della Sicilia Orientale - Calabria Meridionale (1999-2019)*. INGV, Catania, http://sismoweb.ct.ingv.it/maps/eq_maps/sicily/catalogue.php

QUEST WG; 2019. *Il terremoto etneo del 26 dicembre 2018, M_w 4.9: rilievo degli effetti macrosismici*. Rapporto INGV n. 1 del 06/02/2019, 9 pp., doi:10.5281/zenodo.2558168

Tertulliani A., Azzaro R., Buffarini G.; 2019. *Scala Macrosismica Europea 1998, edizione italiana*. European Seismological Commission, sub-commission on Engineering Seismology, Working Group Macroseismic Scales. Conseil de l'Europe, Cahiers du Centre Européen de Géodynamique et de Séismologie, Luxembourg, 32, 97 pp., http://media.gfz-potsdam.de/gfz/sec26/resources/documents/PDF/EMS-98_Italian.pdf

IL TERREMOTO DI FLERI (ETNA) DEL 26 DICEMBRE 2018, M_W 4.9. PARTE II: RILIEVO DEGLI EFFETTI DI FAGLIAZIONE COSISMICA SUPERFICIALE

R. Azzaro, S. Pucci, R. Nappi, P.M. De Martini, S. Branca, C.A. Brunori, M. Caciagli, M. Cantarero, F. Cinti, R. Civico, L. Cucci, S. D'amico, E. De Beni, M.T. Mariucci, R. Nave, T. Ricci, A. Smedile, P. Montone, D. Pantosti, L. Pizzimenti, V. Sapia, G. Tarabusi, R. Vallone, A. Venuti, F. Villani
(EMERGEO Working Group, Emergenza Etna 2018)
Istituto Nazionale di Geofisica e Vulcanologia (Catania, Roma, Napoli, Bologna)

Introduzione. Il terremoto del 26 dicembre 2018, ore 02:19 UTC, che ha colpito il basso versante sud-orientale dell'Etna, ha prodotto non solo danni gravi e distruzioni nell'area epicentrale, pari al grado 8 EMS (vedi Azzaro *et al*., questo volume), ma anche vistose rotture superficiali lungo la faglia di Fiandaca, che è la struttura più meridionale del sistema tettonico delle Timpe (Fig. 1a). Gli effetti di fagliazione cosismica in area etnea sono storicamente piuttosto frequenti in occasione di terremoti superficiali (prof. < 2-3 km), anche per valori di magnitudo relativamente modesti (M ≥ 3.5, vedi Azzaro, 1999). Con una magnitudo M_w 4.9 (dato Regional Centroid Moment Tensors, https://doi.org/10.13127/rcmt/italy), il terremoto in questione rappresenta l'evento più significativo, in termini di entità e complessità della fagliazione associata, verificatosi nell'area etnea negli ultimi 70 anni, con una estensione della rottura superiore rispetto a quelle storiche (≤ 6.5 km).

Il gruppo di emergenza per il rilievo degli effetti geologici cosismici EMERGEO (http://emergeo.ingv.it) dell'INGV, si è pertanto attivato effettuando quattro campagne di misura con squadre che si sono alternate sul terreno (per un totale di 60 gg/persona), supportate da personale del proprio Centro Operativo per l'organizzazione dei dati e il popolamento del database del gruppo (43 gg/persona). Il rilievo ha consentito la raccolta e catalogazione di circa 900 punti di misura relativi a posizionamento, geometria, rigetto e cinematica delle fratture cosismiche.

Effetti di fagliazione. La Faglia di Fiandaca è una struttura che si estende per una lunghezza totale di circa 13 km, caratterizzata nel settore più settentrionale (Fleri-Pennisi) da una direzione NO-SE, e nella porzione meridionale (S.M. la Stella-Aci Catena) da una direzione circa N-S (Fig.

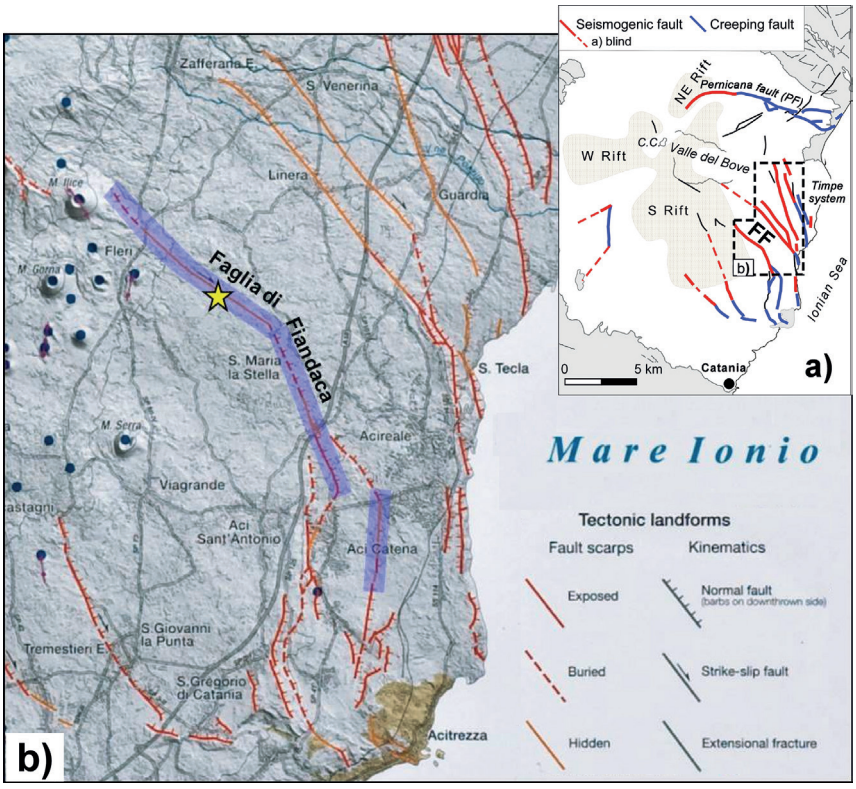

Fig. 1 - a) Modello sismotettonico per l'area etnea, FF indica la Faglia di Fiandaca. b) Dettaglio della carta delle faglie attive nel basso versante sud-orientale, in viola l'estensione della fagliazione cosismica rilevata (modificata da Azzaro *et al*., 2012); la stella rappresenta l'epicentro strumentale del terremoto (Gruppo Analisi Dati Sismici, 2019).

1b). Dal punto di vista morfotettonico, la porzione settentrionale della faglia è prevalentemente nascosta (*hidden fault* in letteratura internazionale) dalle colate laviche del 1000 e 1329, ovvero non mostra una scarpata di faglia chiaramente identificabile senza l'occorrenza della fagliazione (Azzaro *et al*., 2012). Questa struttura tettonica è localmente interessata da *creep* asismico, soprattutto nella sua parte più meridionale, e in passato ha manifestato ripetuti effetti di fagliazione superficiale cosismica, come durante la sequenza sismica del 1984 o il terremoto del 1894, per citare gli eventi maggiori.

Viste le caratteristiche del territorio densamente urbanizzato, e la complessità intrinseca del campo di fratture, è stato condotto un rilievo di estremo dettaglio utilizzando strumentazioni dotate di GPS e bussola elettronica, nonché di un software specifico per la raccolta dei dati di misure geologico-strutturali di terreno (Rocklogger©, www.rockgecko.com). Per la ricostruzione di dettaglio dello scenario deformativo in alcuni punti chiave, sono state inoltre effettuate riprese aree mediante drone per l'utilizzo di tecniche di fotogrammetria ad alta risoluzione (ortofoto e modelli digitali del terreno, risoluzione media di 1 cm/pixel).

Le misure sul terreno sono state integrate da una campagna fotografica che documenta i vari aspetti della fagliazione lungo tutta la struttura attivatasi, non trascurando l'aspetto sostanziale del danno indotto dalle rotture sui manufatti (Cucci *et al*., 2019). I dati raccolti sono stati organizzati in un database, mantenendo l'elevato dettaglio originale, così da poter essere a disposizione della comunità scientifica e delle istituzioni preposte alla gestione del territorio (Villani *et al*., 2020).

Complessivamente il terremoto ha prodotto rotture in superficie per una lunghezza di circa 8.5 km lungo la faglia di Fiandaca (Fig. 2a), che hanno interessato sia terreni di copertura

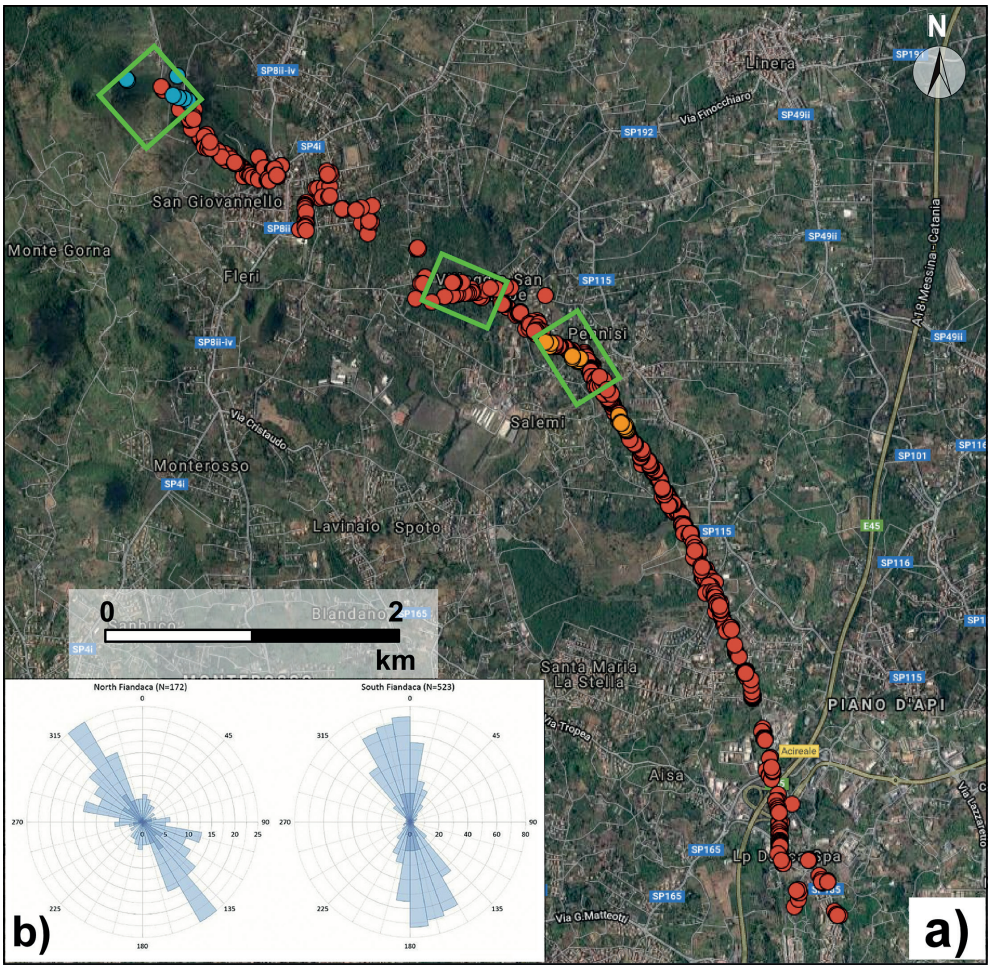

Fig. 2 - a) Distribuzione dei punti di misura effettuati per il rilievo della fagliazione; i rettangoli verdi rappresentano le aree coperte da riprese aeree con droni. b) Diagrammi a rosa delle direzioni delle rotture rilevate lungo la porzione settentrionale (a sinistra) e meridionale (a destra) della Faglia di Fiandaca.

(depositi coerenti e incoerenti) che rilevati stradali e manufatti vari. L'ampiezza della zona di fratturazione è variabile da poche decine fino a 50-60 metri, ed interessa quasi esclusivamente il tetto della faglia; la dislocazione principale è accompagnata da rotture parallele con geometria *en-echelon* sinistra. Notevole la continuità e le caratteristiche della zona di fratturazione sia su suolo agrario che sui manufatti; la direzione prevalente delle fratture ruota da NO-SE a circa N-S spostandosi lungo la faglia (Fig. 2b) e la cinematica è transtensiva destra (Fig. 3a), con spostamenti orizzontali fino a 35 cm e rigetti verticali medi di 10 cm.

Un aspetto ricorrente nel campo di fratture è la presenza di strutture a graben (Fig. 3b) e fessure beanti anche di notevoli dimensioni (Fig. 3c), indice di elevati valori di componente tensionale. In alcuni settori le rotture si sviluppano in coincidenza di una piccola scarpata morfologica, che testimonia il cumularsi di effetti deformativi della faglia nel breve-medio termine (~1000 anni).

Infine, si segnalano anche numerosi effetti secondari, sia nella porzione settentrionale che in quella meridionale della Faglia di Fiandaca, in forma di crolli e deformazioni di muretti a secco e di contenimento sia nelle aree urbanizzate che in quelle di campagna caratterizzate da estesi terrazzamenti.

Fig. 3 - Esempio di tipologie di rotture cosismiche prodotte dal terremoto del 26 dicembre 2018 lungo la Faglia di Fiandaca: a) C.da Testa di Vipera; b) C.da Campanaro; c) Pennisi.

Note conclusive. Il quadro degli effetti rilevati sul terreno conferma, come già noto in letteratura, l'origine primaria della fagliazione del terremoto del 26 dicembre 2018 (M_w 4.9).

In particolare, i dati raccolti hanno evidenziato che:

- la fagliazione cosismica interessa per intero la Faglia di Fiandaca, estendendosi anche al di fuori dell'area di danneggiamento massimo nel settore meridionale in cui l'attività tettonica si esplica in regime di *creep* asismico;
- le Faglie di Acicatena ed Aciplatani mostrano deboli riattivazioni (fagliazione indotta) che, in alcuni casi, hanno portato ad ordinanze di sgombero di edifici già compromessi dagli effetti di *creep* che interessano storicamente queste aree;
- il rilievo di estremo dettaglio effettuato dal gruppo EMERGEO, ha permesso di mappare con precisione lo sviluppo in superficie della Faglia di Fiandaca nel settore nord in cui la morfologia è di tipo *hidden* (tra Pennisi e Fleri, Fig. 1b) (Civico *et al*., 2019). Lo scostamento di circa un centinaio di metri deriva dal fatto che la mappatura di questa parte della faglia in passato (Azzaro *et al*., 2012) era stata definita sulla base di dati storici descrittivi, gli unici in quel momento disponibili;
- la presenza di effetti sismo-geologici secondari quali frane o scoscendimenti è stata del

tutto marginale e limitata a qualche rotolamento di blocchi e alla caduta di muretti a secco.

Va infine rilevato che gli effetti di fagliazione superficiale rappresentano un ulteriore elemento di pericolosità a scala locale, particolarmente quando si sviluppano all'interno di zone fortemente antropizzate, in quanto responsabili di una esaltazione del danno sull'edificato o sulle *life-line* rispetto a quanto prodotto dal semplice scuotimento (i.e. azione sismica).

Bibliografia

Azzaro R.; 1999. *Earthquake surface faulting at Mount Etna volcano (Sicily) and implications for active tectonics*. Journal of Geodynamics, 28, 193-213.

Azzaro R., Branca S., Gwinner K., Coltelli M.; 2012. *The volcano-tectonic map of Etna volcano, 1:100.000 scale: an integrated approach based on a morphotectonic analysis from high-resolution DEM constrained by geologic, active faulting and seismotectonic data*. Italian Journal of Geosciences, 131, 153-170.

Civico R., Pucci S., Nappi R., Azzaro R., Villani F., Pantosti D., Cinti F.R., Pizzimenti L., Branca S., Brunori C.A., Caciagli M., Cantarero M., Cucci L., D'Amico S., De Beni E., De Martini P.M., Mariucci M.T., Montone P., Nave R., Ricci T., Sapia V., Smedile A., Tarabusi G.,Vallone R., Venuti A.; 2019. *Surface ruptures following the 26 December 2018, Mw 4.9, Mt. Etna earthquake, Sicily (Italy)*. J. Maps, 15 (2), 831-837, Doi: 10.1080/17445647.2019.1683476.

Cucci L., D'Amico S., De Martini P.M., Nave R., Pizzimenti L., Azzaro R., Branca S., Brunori C.A., Caciagli M., Cantarero M., Cinti F., Civico R., De Beni E., Mariucci M.T., Messina A., Montone P., Nappi R., Pantosti D., Pucci S., Ricci T., Smedile A., Sapia V., Tarabusi G., Vallone R., Venuti A., Villani F.; 2019. *Photographic collection of the coseismic geological effects originated by the 26th December 2018 Etna (Sicily) earthquake*. Miscellanea INGV, 48, 176 pp., http://editoria.rm.ingv.it/miscellanea/2019/miscellanea48/#

EMERGEO WG; 2019. Il terremoto etneo del 26 dicembre 2018, M_w 4.9: rilievo degli effetti di fagliazione cosismica superficiale. Rapporto INGV n. 1 del 21/01/2019, 9 pp., doi 10.5281/zenodo.2545555

Gruppo Analisi Dati Sismici; 2019. *Catalogo dei terremoti della Sicilia Orientale - Calabria Meridionale (1999-2019)*. INGV, Catania, http://sismoweb.ct.ingv.it/maps/eq_maps/sicily/catalogue.php

QUEST WG; 2019. *Il terremoto etneo del 26 dicembre 2018, M_w 4.9: rilievo degli effetti macrosismici*. Rapporto INGV n. 1 del 06/02/2019, 9 pp., doi:10.5281/zenodo.2558168

Villani F., Pucci S., Azzaro R., Civico R., Cinti F.R., Pizzimenti L., Tarabusi G., Branca S., Brunori C.A., Caciagli M., Cantarero M., Cucci L., D'Amico S., De Beni E., De Martini P.M., Mariucci M.T., Messina A., Montone P., Nappi R., Nave R., Pantosti D., Ricci T., Sapia V., Smedile A., Vallone R., Venuti A.; 2020. *Surface ruptures database related to the 26 December 2018, Mw 4.9, Mt. Etna earthquake, southern Italy*. Sci. Data, 7 (42), 1-9, Doi: https://doi.org/10.1038/s41597-020-0383-0.

A REAPPRAISAL OF THE 1968 VALLE DEL BELÌCE SEISMIC SEQUENCE (WESTERN SICILY): A CASE STUDY OF INTENSITY ASSESSMENT AND EARTHQUAKE PARAMETERS DETERMINATION WITH CUMULATED DAMAGE EFFECTS

R. Azzaro[1], M.S. Barbano[2], A. Tertulliani[1], C. Pirrotta[1]

[1] Istituto Nazionale di Geofisica e Vulcanologia (Catania, Roma), Italy

[2] Dipartimento di Scienze Biologiche, Geologiche e Ambientali, Università di Catania, Italy

Introduction. From 14 to 25 January 1968 six shocks with magnitude M_w 5.0-6.0 hit the *Valle del Belìce* (Fig. 1). An area wide about 2000 km^2 was devastated: over 300 deaths, four towns deemed to be rebuilt in different sites (Gibellina, Montevago, Poggioreale, Salaparuta) and others that were reconstructed in the same locations but greatly modified in their urban layouts.

Since the poor development of the Italian seismic network in 1968, instrumental determinations are affected by large uncertainties but also the macroseismic survey was made difficult because of the continuous shocks modifying the damage scenario. In addition, at that time the macroseismic practice privileged the idea of estimating the intensity of single shocks, without considering the cumulative effects; in other words, intensities reflect the estimation of

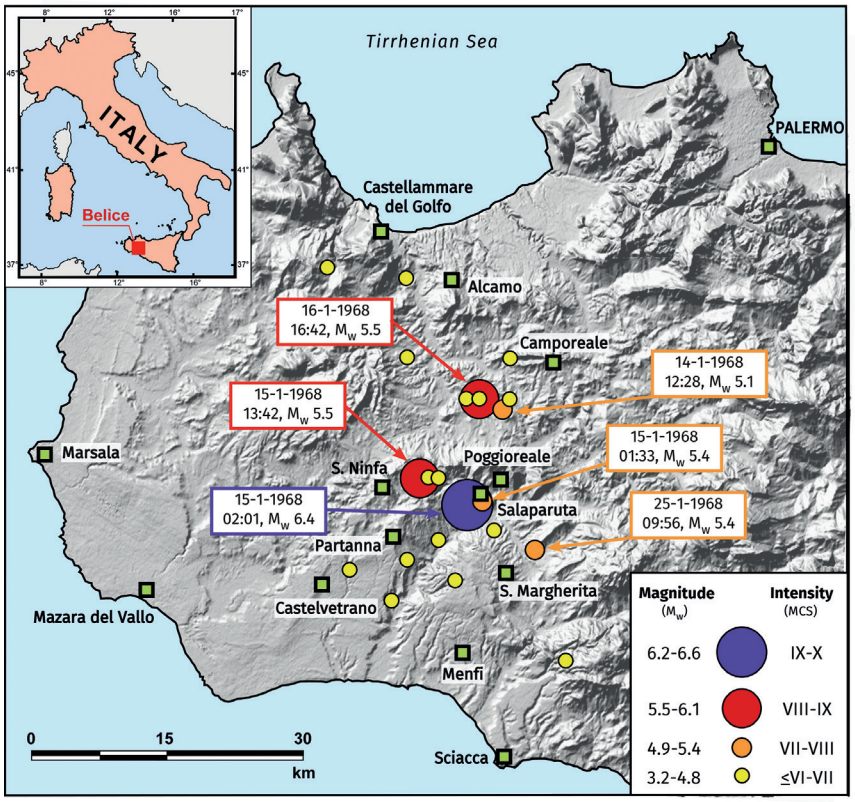

Fig. 1 - Location of the 1968 *Valle del Belìce* earthquakes according to the CPTI15 earthquake catalogue (Rovida *et al.*, 2016).

shaking rather than a real representation of the damage scenario. The recent experience of the 2016-17 seismic sequence in Central Italy proved the importance of this aspect as well as that resulting macroseismic parameters (epicentre, magnitude) are strongly inconsistent with the instrumental ones.

Here we propose a reappraisal, in terms of macroseismic analysis, of the 1968 *Valle del Belìce* earthquakes following the same rationale. The main steps are: (i) re-analysis of primary sources to reconstruct the evolution of damage scenario during the sequence, (ii) intensity assessment, (iii) determination of the macroseismic parameters. For this last point, we propose a procedure for minimizing the magnitude overestimation to be applied in case of seismic sequences, based on "unpacking" the total seismic moment M_0.

Methodological approach. To follow the evolution of damage for as many as possible of shocks and localities, we performed a retrospective analysis of the primary sources with the purpose of simulating a-posteriori survey carried out day-by-day. To this goal, we used a wide spectrum of sources: coeval scientific papers, technical reports, macroseismic questionnaires, archive documents, socio-anthropological and architectural books, local diaries, and newspapers.

The approach can be summarised as follows: (i) unpacking information referred to each single town or village, classifying data day by day and integrating information from different sources; (ii) evaluating the coherence of information; (iii) reconstructing the evolution of damage scenario during the sequence; (iv) assessing intensity and, (v) calculating earthquake parameters.

The 1968 sequence may represent a stimulating laboratory also for applying the European Macroseismic Scale (hereinafter EMS-98, Grünthal, 1998). In fact, the building features can be

clearly recognised by visiting the ruins of the abandoned settlements (especially Poggioreale and S. Margherita) or the deserted neighbourhoods still visible in the reconstructed towns (e.g. Salemi, Menfi, Partanna).

Analysis of the sources. We analysed sources starting from local and national newspapers, which report information on the earthquake effects in both the epicentral and felt areas. The first three days of the sequence are well documented, whereas afterwards the newspapers mostly argue on the slowness of rescue and the hardship conditions of people in the camps. Newspapers usually give an overview of the effects, cumulating the damage due to more shocks in a single day, so that it is impossible to discriminate them individually. As a result, we obtained a daily damage picture referring to the shocks occurred on 14, 15, 16 and 25 January, and a final scenario at the end of the sequence.

Then we used the technical and scientific literature providing a detailed description of damage, along with accurate notes on the building characteristics (Bosi *et al*., 1968; Cannata *et al*., 1968; De Panfilis and Marcelli, 1968; Haas and Ayre, 1969). The authors surveyed the damaged area soon after the sequence, before the bulldozers raised to the ground collapsing buildings and removed ruins; their observations are essential to integrate newspaper information.

Notes on building vulnerability. In our *a-posteriori* survey throughout the epicentral area, we observed the following EMS-98 vulnerability classes associated to relevant building typologies:

- class A: structures built with materials easily available on site, mostly soft calcarenites, made up of coarse masonry with irregular or sometime roughly squared stones, assembled with poor mortar deteriorating over the years (Fig. 2a). Sometimes, old buildings had been modified but without adequate strengthening (Fig. 2b).

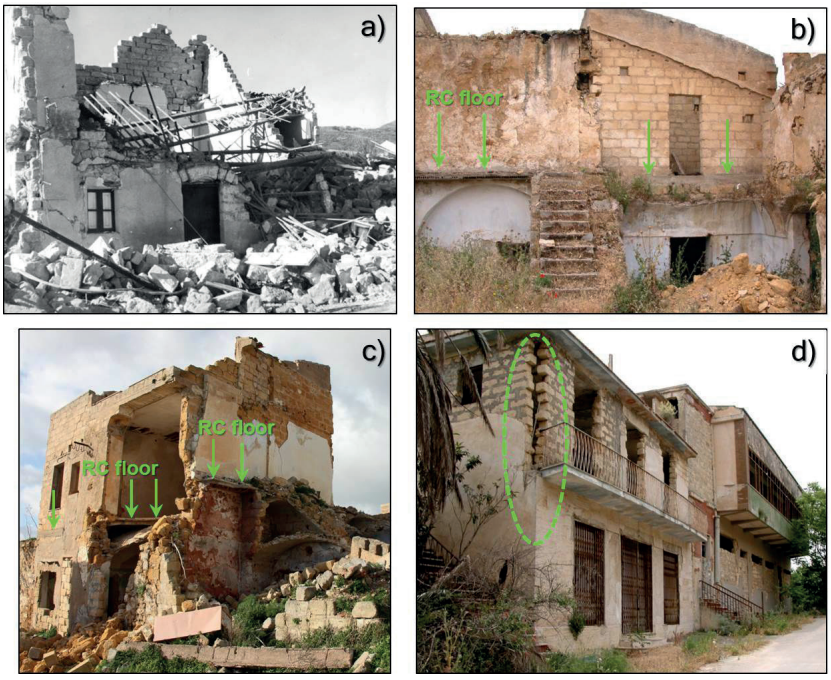

Fig. 2 - Building typologies in the 1968 epicentral area and vulnerability classes according to the EMS-98. a) Class A: Poggioreale, collapse of a structure built with squared blocks of soft calcarenites assembled with little mortar; b) Class A: S. Margherita, interventions of elevation with RC slab floors and heavy blocks of calcarenites above a weak masonry; c) Class B: S. Margherita, structure characterised by numerous interventions that significantly modified masonry over time; note the RC slab floors positioned at different levels; d) Class C: Gibellina, the first floor was added without any structural connection to the underlying RC frame.

- class B: masonry buildings with bearing-walls of good quality, typically roughly dressed calcarenites, one to two stories, with squared stones and generally good mortar, sometime with RC slab floors and tie-rods (Fig. 2c).
- class C: reinforced concrete (RC) buildings, two to four stories, especially in the outskirts built-up since the mid-1960s. These structures were rare and did not include any kind of earthquake-resistant design or reinforcement (Fig. 2d).

Intensity assessment. We interpreted the collected information to produce a scenario in terms of cumulated intensity for every day of the sequence. In all, we evaluated 169 localities.

On 14 January, 3 earthquakes with $4.7 \geq M_w \geq 5.1$ produced substantial damage to class A buildings in Gibellina, Salaparuta and Poggioreale (Tab. 1): large cracks in most walls, failure of non-structural individual elements, a few partial collapse. This scenario is consistent with intensity 7 EMS-98. Very slight damage (I 5-6) occurred in Alcamo, Calatafimi, Camporeale, Menfi, Montevago, S. Margherita, S. Ninfa, Sambuca (Fig. 3a).

On 15 January, a shock with M_w 5.3 (01.33) was followed by the mainshock M_w 5.7 (02.01) and other strong aftershocks ($4.8 \geq Mw \geq 5.4$). Gibellina and Salaparuta suffered the collapse of many of the buildings already damaged (I 9); Poggioreale and Montevago, that the day before

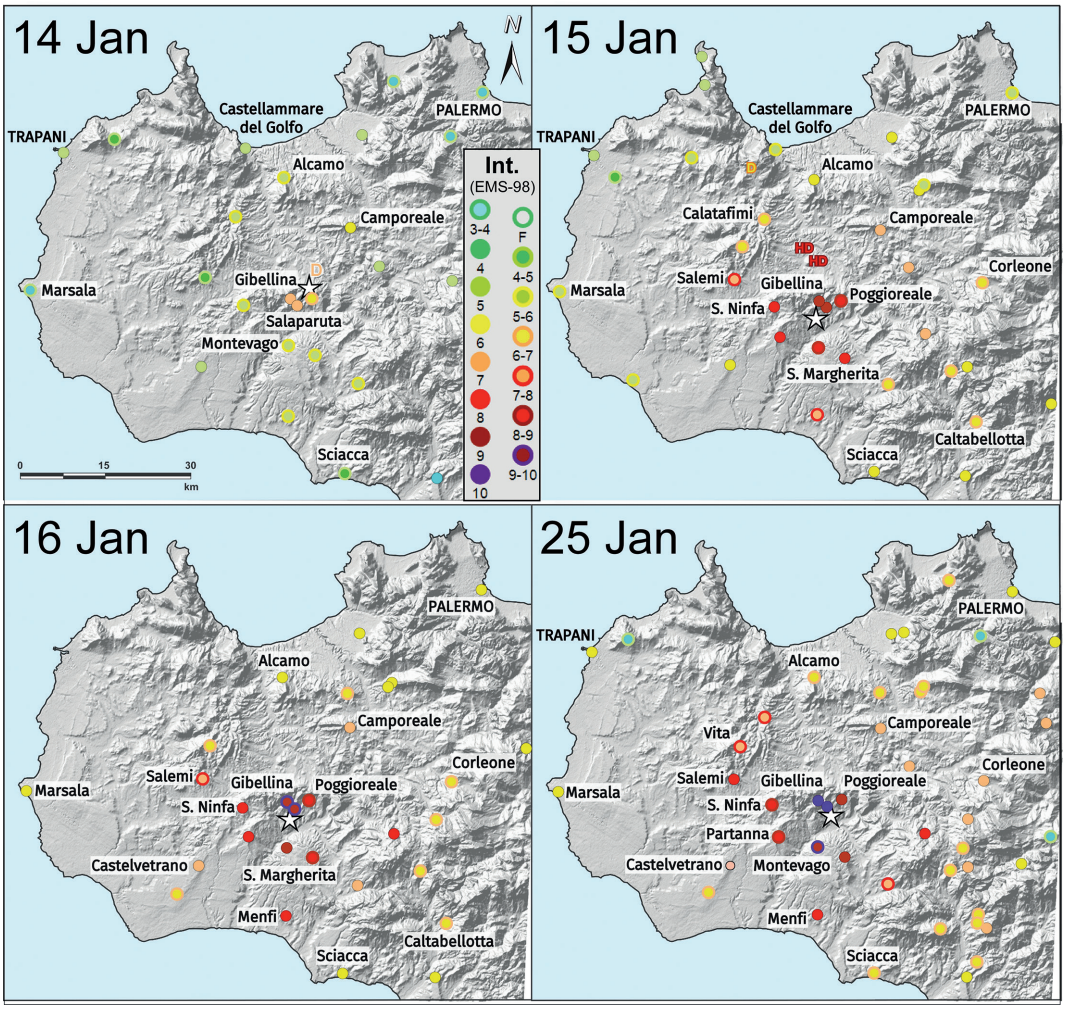

Fig. 3 - Intensity maps referred to the cumulative effects of the strongest earthquakes occurred during the 1968 *Valle del Belice* sequence.

had a few damage, were very heavily damaged (I 8-9). At S. Margherita, S. Ninfa and Partanna heavy damage occurred (I 8); finally, severe damage (I 7-8) also affected Menfi and Salemi (Fig. 3b). Many localities around were moderately or slightly damaged.

On 16 January, another M_w 5.3 shock caused the collapse of the few buildings left standing in Gibellina, Salaparuta and Montevago (I 9-10); very heavy damage (I 8-9) occurred at Poggioreale and S. Margherita, whereas Partanna, Menfi, Santa Ninfa and Contessa had further partial collapses (Class A buildings, I 8). The damage area extended to the North as far as Palermo (I 6) (Fig. 3c).

On 25 January, the last M_w 5.2 event raised to the ground the remains of Gibellina and Salaparuta (I 10) and, partially, Montevago (I 9-10). Poggioreale and S. Margherita remained struck at a lesser degree (I 9) as well as Partanna and S. Ninfa (I 8-9); Menfi did not modify the previous damage scenario (I 8) but moderate damage appeared in several localities little damaged by the previous earthquakes (Fig. 3d).

In conclusion, the intensities in the localities of the epicentral area increased day by day (Tab. 1), reaching the maximum as early as 15 January (Partanna and S. Ninfa), 16 January (Contessa Entellina) and in most of them on 25 January.

Table 1 - Intensity (EMS-98) and damage progression in the most struck towns of the *Valle del Belìce*.

Locality	14 January	15 January	16 January	25 January
Gibellina	7	9	9-10	10
Salaparuta	7	9	9-10	10
Montevago	5-6	8-9	9	9-10
Poggioreale	6-7	8-9	8-9	9
Santa Margherita	5-6	8	8-9	9
Partanna	6	8	8	8-9
Santa Ninfa	5-6	8	8	8-9
Salemi	4-5	7-8	7-8	8
Contessa Entellina		7-8	8	8
Calatafimi	5-6	6-7		7-8

Macroseismic parameters. We calculated epicentres and magnitudes from the macroseismic data points (MDPs) reported in Fig. 2 through the Boxer method (Gasperini *et al*., 2010); the magnitude M_w is obtained by using the last calibration adopted in the CPTI15 catalogue (Rovida *et al*., 2016). Results in Tab. 2 show that macroseismic parameters are increasingly affected by the cumulative effect of damage during the sequence; in practice, epicentre and magnitude of the first earthquake (14 Jan.) can be considered quite reliable, and little less those of the event occurred on the next day (15). This occurs because the epicentres differ significantly each other while those of the following shocks (16, 25 Jan.) vary within the errors. The comparison with the instrumental parameters (ISC data) suggests the same conclusion also for the magnitude values, which diverge considerably from 16 January onwards.

In conclusion, we note that: i) the 14 January shock appears located north of the alignment Gibellina-Poggioreale, near the instrumental epicentre; ii) the following events moved southward, close the most damaged towns of the Valle del Belìce. The epicentre apparent migration along an E-W direction is probably due to the position of the localities (i.e. coverage on the macroseismic map). As a result, though the actual location of the 1968 earthquakes presents wide margins of uncertainty, the epicentres proposed appear closer to the instrumental ones than the previous ones indicated in CPTI15.

Regarding the magnitude overestimation of the earthquakes during the sequence shown by the increasing values of M_w in Tab. 2, we tried to solve the problem through the computation

Table 2 - Macroseismic parameters computed for the four main earthquakes and comparison with the instrumental data by ISC reported in the CPTI15 [Rovida *et al*., 2016]; $\Delta_{Epicentre}$ indicates the distance between macroseismic and instrumental locations.

Date	Epicentre		I_0	M_w (this study)	M_w (instrumental)	ΔEpicentre (km)
	Lat N	Long E				
14 January 1968	37.801	13.000	7.0	5.04 ± 0.35	5.15 ± 0.27	5.7
15 January 1968	37.753	12.970	9.0	5.97 ± 0.18	5.67 ± 0.23	6.0
16 January 1968	37.756	12.981	9.5	6.17 ± 0.27	5.27 ± 0.21	11.5
25 January 1968	37.756	12.995	10	6.34 ± 0.22	5.15 ± 0.21	8.8

of the seismic moment M_0. Assuming that after the last strong shock on 25 January most of the fault displacement associated with the seismic sequence was released, and given that the 25 January MDPs (Fig. 3d) virtually provide the final (cumulative) damage scenario, we supposed that the relevant M_w could represent with a good approximation the total M_0 released at the end of the sequence.

By applying the formula of Hanks and Kanamori (1979), we first calculated the moments (Tab. 3) of each events from the M_w values obtained by the Boxer code, and then we subtracted from the M_0 for a given day those of the previous shocks. For instance, from the 15 January M_0, we subtracted the M_0 calculated for the 14; again, from the M_0 of 16 January, we subtracted the M_0 of 15 and 14 January, etc. Finally, we obtained by the same formula, the "corrected" values of M_w. This procedure minimizes, at least in part, the magnitude overestimation due to cumulative damage during a sequence; while there is not difference in the case of 15 January, the corrected Ms values for 16 and 25 result increasingly smaller than the ones calculated by the Boxer code.

Table 3 - Daily total seismic moment M0 obtained from the macroseismic M_w through the Hanks and Kanamori (1979) formula: M_w=2/3 log M_0 –10.7. The M_w corrected values represent the final estimates proposed in this study.

Date	M_w (from Boxer)	Log M_0	M_0 (dyne-cm)	M_0 (by subtraction)	M_w corrected	M_w (cumulative) Instumental
14 January 1968	5.04	18.260	1.8197E+18		5.04	5,01
15 January 1968	5.97	19.655	4.5186E+19	4.33659E+19	5.96	5,89
16 January 1968	6.17	19.955	9.0157E+19	4.31518E+19	5.96	5,93
25 January 1968	6.34	20.210	1.6218E+20	2.50186E+19	5.80	5.95

We validated these results with the same procedure applied in a reverse way to the instrumental M_w values of all 1968 events listed in CPTI15. By adding the moments of the shocks occurring in the same day, we obtained a cumulative M_0, which was then converted into the M_w. These "cumulative" M_w instrumentally derived are very similar (inside the error) to the "corrected" M_w derived from macroseismic data (Tab. 3), with an evident effect of saturation since 16 January.

References

Bosi C., Cavallo R. and Manfredini M.; 1968: *Il terremoto della Valle del Belice del gennaio 1968*. in "Rassegna dei Lavori Pubblici", n.2, febbraio 1968, Roma.

Cannata D., Costantino M., D'Amore A., Gregorio G., Irti M., Pasta A., Priolo D., Stura V. and Miglietti G.; 1968: *Missione di studio nelle zone terremotate della Sicilia Occidentale*. In "L'industria delle costruzioni". Rivista tecnica dell'ANCE", settembre-ottobre 1968, Roma.

De Panfilis M. and Marcelli L.; 1968: *Il periodo sismico della Sicilia occidentale iniziato il 14 Gennaio 1968*. Ann. Geofis., 21, 79 pp.

Gasperini P., Vannucci G., Tripone D. and Boschi E.; 2010: *The location and sizing of historical earthquakes using the attenuation of macroseismic intensity with distance*. Bull. Seism. Soc. Am., 100, 2035-2066.

Grünthal G. (Ed.); 1998: *European Macroseismic Scale 1998 (EMS-98)*. European Seismological Commission, sub commission on Engineering Seismology, Working Group Macroseismic Scales. Conseil de l'Europe, Cahiers du Centre Européen de Géodynamique et de Séismologie 15. Luxembourg, pp. 99, http://www.ecgs.lu/cahiers-bleus/.

Haas J. E. and Ayre R.S.; 1969: *The western Sicily earthquake of 1968*. Committee on Earthquake Engineering Research, National Academy of Sciences, Washington, D. C., 77 pp.

Hanks T.C., Kanamori H.; 1979: *A moment magnitude scale*. J. Geoph. Res., 84 (B5), 2348–50.

Rovida A., Locati M., Camassi R., Lolli B. and Gasperini P. (Eds); 2016: *CPTI15, the 2015 version of the Parametric Catalogue of Italian Earthquakes*. INGV, doi:http://doi.org/10.6092/INGV.IT-CPTI15.

EARTHQUAKE RUPTURE ON THE FIANDACA FAULT, DEC. 26, 2018, MW 4.9: FAULT FABRIC ANALYSIS, INTENSITY VS. SURFACE FAULTING, AND HISTORICAL SEISMICITY AT MT. ETNA VOLCANO, ITALY

D. Bella[1], G. Tringali[1], R. Pettinato[1], F. Livio[2], M.F. Ferrario[2], A.M. Michetti[2], S. Porfido[3,4], A.M. Blumetti[5], P. Di Manna[5], E. Vittori[5], L. Guerrieri[5], G. Groppelli[6]

[1] Registered Geologist, Acireale, Italy
[2] Università dell'Insubria, Como, Italy
[3] CNR-ISA, Avellino, Italy
[4] INGV-Osservatorio vesuviano, Napoli, Italy.
[5] ISPRA, Roma, Italy
[6] CNR – IGAG, Milano, Italy

Introduction. On December 26, 2018, a Mw 4.9 earthquake hits the eastern flank of Mount Etna volcano (Sicily). The epicenter is located between the Fleri and Pennisi villages, and focal depth is estimated at 0.3 km (http://cnt.rm.ingv.it/event/21285011). This earthquake is part of a seismic sequence begun on December 23, 2018 and a concurrent phase of volcanic eruption, eventually resulting in lava flows and a dyke intrusion (De Novellis *et al*., 2019).

The earthquake is the result of the activation of the Fiandaca Fault; it is accompanied by widespread surface faulting and secondary environmental effects (Emergeo Working Group, 2019; Figs. 1 - 3), and have a maximum intensity of VIII EMS (Quest WG, 2019).

Partial or complete ruptures of the Fiandaca Fault are well-documented in the last 150 years (Fig. 1). The last event that activated the entire structure, as happened in 2018, occurred in 1894 and generated extensive surface faulting and secondary effects (Riccò, 1894; Baratta, 1894; Imbò, 1935).

Despite the abundant documentation of previous events, the Fleri earthquake represents the first opportunity to document coseismic effects of a strong, shallow seismic event at Mt. Etna through modern field techniques, sustained by accurate remote-sensed data, including unprecedented InSar measurements.

Methods. We started mapping ground ruptures in the morning of December 26, 2018, few hours after the earthquake. We collected original structural data on ground break length and orientation, amount of displacement and slip vectors. We compared field data with InSAR imaging, showing coseismic surface rupture and afterslip on some known capable faults on Mt. Etna eastern and southern slopes.

We then compared field measurements with other surface (slope, aspect, elevation) and subsurface (slope and aspect of the basement, thickness of volcanic deposits) data, to evaluate the factors ruling surface faulting occurrence and fabric. We plotted data along the rupture

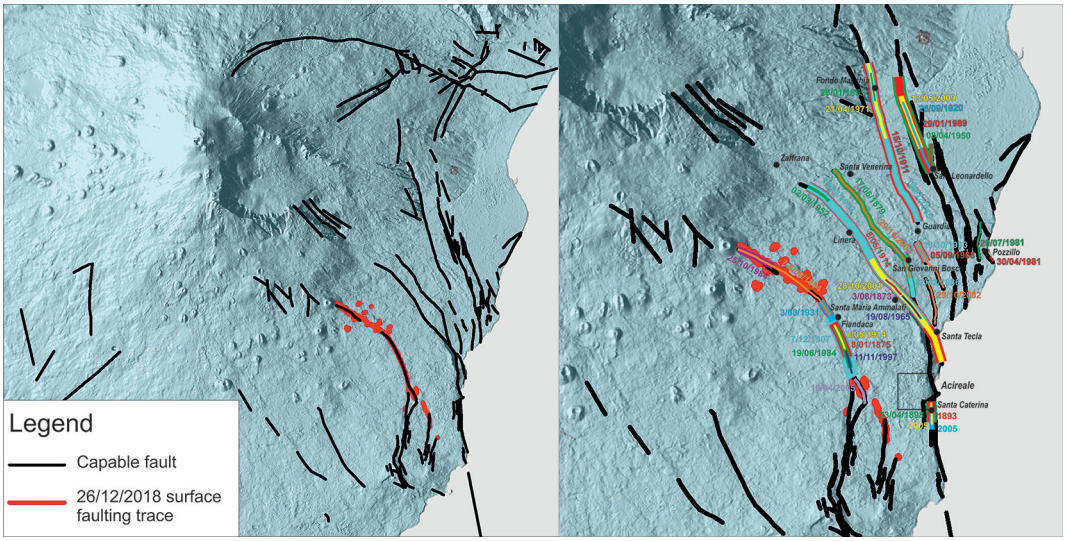

Fig. 1- Left: surface rupture of the December 26, 2018, Mw 4.9 earthquake along the Fiandaca Fault in the southeastern flank of Mt. Etna volcano. Right: recent to historical surface faulting in the same area. The capable faults in the area are also shown, taken from the ITHACA database.

trace, by projecting the data location on a baseline. Fault width was measured across-strike, with a 50-m resolution.

We finally compared our results with macroseismic and surface faulting observations of previous events on Mt. Etna eastern flank.

Results. We map surface faulting for a length of about 5 km, along 3 main sectors, namely the Fleri, Fiandaca and Aci Platani segments. We collected a total of 400 observation points, mainly located along the Fiandaca segment (Fig. 2 and 3). We also documented afterslip during the weeks following the mainshock, in particular affecting the Aci Platani segment.

Fig. 2 - Earthquake surface rupture across the road (right) and a house (left) located a few meters apart in the vicinity of Santa Maria La Stella; notably, the main rupture is located approximately in the middle of a scarp which is the long-term morphological expression of the fault, already censored and mapped with great detail in the Ithaca Database of ISPRA, available since 20 years ago. In spite of this knowledge, the house, built right on the fault trace, was restored and licensed to be widened just before the event. Following the December 26, 2018, earthquake, the house is no longer habitable, being crossed by severe fractures and slightly tilted.

Fig. 3 - Coseismic ground rupture (throw ca. 20 cm) in a field west of Fleri (via Nava), not far from the northwestern tip of the 2018 rupture.

Ground breaks broadly coincide with faults previously included in the database of capable faults (ITHACA database, http://sgi2.isprambiente.it/ithacaweb/viewer/), but in some places the newly formed breaks allowed to better define the fault trace.

Rupture is arranged in several segments, trending N-S to NW-SE. Slip vectors show a dominant dip-slip component, with secondary dextral strike slip motion.

We analyze the across-strike width along the entire rupture: the width can be either very narrow, with ruptures concentrated on a single strand, or distributed in up to 100-m-wide zones, including several en-echelon segments.

Maximum vertical displacements reach 30 cm and right-lateral displacement 15 cm. We estimate the maximum intensity as IX on the ESI-07 scale (Michetti *et al*., 2007).

The comparison with topographic and subsurface factors allowed to evaluate the role of gravity and geological setting in driving shallow deformation. We found an influence of topography (elevation and slope) in the northernmost sector, whereas the overall pattern of deformation is controlled by slope and aspect of the top of basement lying below the volcanic deposits.

Discussion and comparison with previous events. Typically, surface ruptures and environmental effects accompanying strong (Mw 4 to 5) earthquakes at Mt. Etna are clearly confined in a narrow belt around the causative fault. The 2018 earthquake is no exception, as testified by our original results and by macroseismic surveys (Quest WG, 2019).

We compare the macroseismic field of the 2018 event with previous earthquakes that hit the Etnean region, in particular the 2002 Santa Venerina earthquake. In both cases, the very shallow focal depth favors a strong attenuation of intensity with distance.

We argue that in such settings, surface faulting and other environmental effects can tightly define the trace of the causative fault and thus provide complementary information with respect to traditional macroseismic investigations: an integrated approach can foster a more comprehensive understanding of the extremely active volcano-tectonic settings of the Etnean region, and of similar areas affected by very shallow-focus earthquake ruptures, such as the Casamicciola sector at Ischia volcano (Nappi *et al*., 2018).

References

Baratta M. (1894). Intorno ai recenti fenomeni endogeni avvenuti nella regione etnea agosto 1894. Boll. Soc. Geografica Italiana, Ottobre 1894.

De Novellis, V., Atzori, S., De Luca, C., Manzo, M., Valerio, E., Bonano, M., *et al*. (2019), DInSAR analysis and analytical modeling of Mount Etna displacements: The December 2018 volcano-tectonic crisis. Geophysical Research Letters, 46, 5817–5827. https:// doi.org/10.1029/2019GL082467.

Emergeo Working Group, (2019). Photographic collection of the coseismic geological effects originated by the 26th December 2018 Etna (Sicily) earthquake. Misc. INGV, 48: 1-176.

Imbo' G., (1935). I terremoti della Regione Etnea. Reale Acc. Dei Lincei, Pubbl. della Commissione It. per lo studio delle grandi calamità, 5, part. 1, Firenze.

Michetti A.M., E. Esposito, L. Guerrieri, S. Porfido, L. Serva, R. Tatevossian, E. Vittori, F. Audemard, T. Azuma, J. Clague, V. Comerci, A. Gürpinar, J. McCalpin, B. Mohammadioun, N.A. Mörner, Y. Ota, E. Roghozin (2007). Environmental Seismic Intensity Scale 2007 - ESI 2007. Memorie Descrittive della Carta Geologica d'Italia, 74, 7-54, Servizio Geologico d'Italia – Dipartimento Difesa del Suolo, APAT, Roma, Italy.

Nappi, R., Alessio, G., Gaudiosi, G., Nave, R., Marotta, E., Siniscalchi, V., Civico, R., Pizzimenti, L., Peluso, R., Belviso, P., and Porfido, S. (2018). The 21 August 2017 M d 4.0 Casamicciola earthquake: First evidence of coseismic normal surface faulting at the Ischia volcanic island. Seismological Research Letters, 89(4), 1323-1334.

QUEST WG (2019). Il terremoto etneo del 26 dicembre 2018, Mw4.9: rilievo degli effetti macrosismici. Rapporto INGV n. 1 del 06/02/2019, 9 pp., doi:10.5281/zenodo.2558168

Riccò A. (1894). Breve relazione sui terremoti del 7 e 8 agosto 1894 avvenuti nelle contrade etnee. Boll. Soc. Meteor. Ital., 14, 145-148.

EVIDENZE GEOLOGICHE DI LIQUEFAZIONE DURANTE FORTI TERREMOTI IN SEDIMENTI LACUSTRI A GRANA FINA (FUCINO, ITALIA CENTRALE)

P. Boncio[1], S. Amoroso[2,3], F. Galadini[3], A. Galderisi[2,4], G. Iezzi[2,3], F. Liberi[1]

[1] CRUST-DiSPuTer, Università "G. d'Annunzio" di Chieti - Pescara, Italy

[2] InGeo, Università "G. d'Annunzio" di Chieti - Pescara

[3] Istituto Nazionale di Geofisica e Vulcanologia, Roma, Italy

[4] Istituto di Geologia Ambientale e Geoingegneria, CNR, Roma

Introduzione. La liquefazione di terreni a grana fina (particelle di diametro nelle classi del silt e dell'argilla) è un argomento di particolare interesse con implicazioni sia per la pericolosità sismica locale (normativa tecnica, microzonazione sismica, pratica professionale) che per la geologia dei terremoti in generale, cioè per il riconoscimento e l'interpretazione di strutture geologiche sismo-indotte. La liquefazione di sedimenti fini è stata documentata a seguito di vari terremoti forti nel mondo. Tuttavia, la percezione che la liquefazione sismo-indotta avvenga esclusivamente, o quasi, in sedimenti sabbiosi sciolti è molto diffusa. Certamente lo studio di casi reali di liquefazione di sedimenti fini può contribuire ad una migliore comprensione del fenomeno e al trasferimento delle conoscenze.

Nel presente lavoro sono illustrati i risultati di un lavoro svolto in una località situata nel bacino del Fucino, alla periferia di Avezzano (Borgo Via Nuova, Fig. 1), dove un canale di drenaggio ha messo alla luce una serie di dicchi di materiale sedimentario fino all'interno della successione lacustre, interpretati come dovuti a liquefazione sismo-indotta.

Metodi. Il sito è stato studiato con approccio multidisciplinare, al fine di caratterizzare in dettaglio la successione stratigrafica, i meccanismi di messa in posto dei dicchi e la probabile sorgente del materiale fino liquefatto. A questo scopo, sono stati realizzati: 1) uno studio di terreno dettagliato, con approccio paleosismologico; 2) un sondaggio a carotaggio continuo fino a 20 m di profondità; 3) una serie di indagini geotecniche e geofisiche in situ (CPTU, SPT, SDMT); 4) analisi di laboratorio su campioni derivanti dai dicchi e dalla successione stratigrafica ospite per definirne granulometria, limiti di Atterberg e composizione mineralogica tramite diffrazione a raggi X (XRPD); e 5) stima della suscettibilità a liquefazione mediante analisi CRR/CSR sulle indagini in situ.

Risultati. Lo studio svolto indica che i dicchi sono formati prevalentemente da silt, liquefatto e trasportato verso l'alto da forze idrauliche improvvise, di breve durata, come nel caso

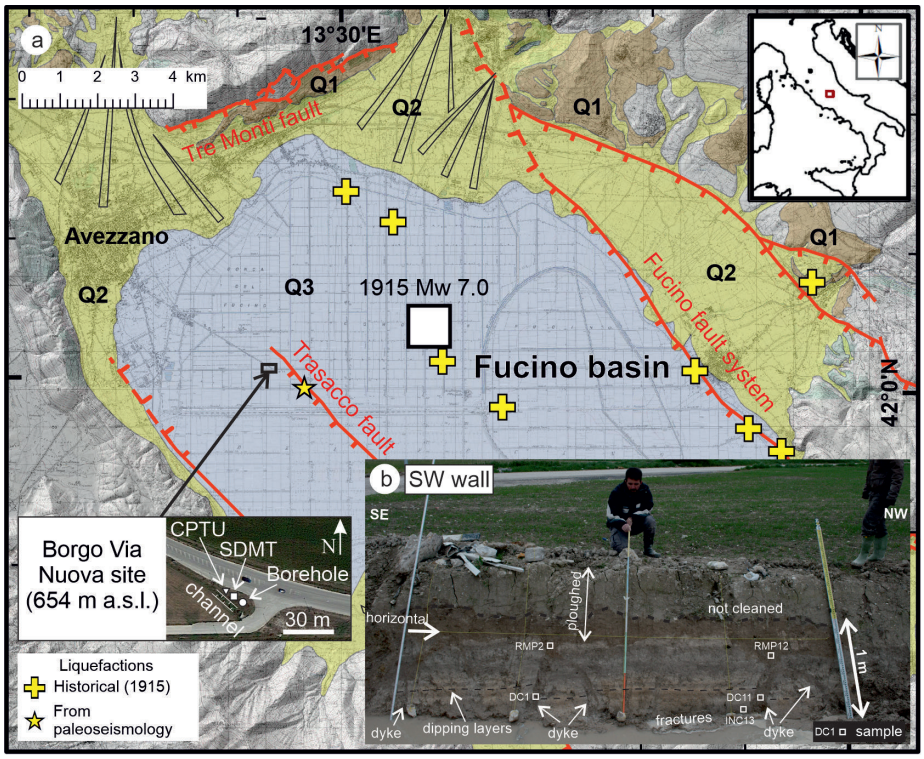

Fig. 1 - a) Carta del Fucino con ubicazione dell'area di studio (Borgo Via Nuova), le aree colorate indicano i depositi continentali del Pleistocene inferiore-medio (Q1), Pleistocene superiore (Q2) e tardo-Pleistocene-Olocene (Q3); b) parete sud del canale di drenaggio su cui sono stati osservati i dicchi di liquefazione.

di liquefazione sismo-indotta (Fig. 2). Tilting della successione sedimentaria ed espandimento laterale (*lateral spreading*) hanno accompagnato il fenomeno. Considerazioni tettono-stratigrafiche ci portano ad associare la formazione dei dicchi ad un terremoto successivo alla formazione di un suolo, cioè successivo al drenaggio dell'antico lago del Fucino, e quindi molto probabilmente al terremoto della Marsica del 1915 (Mw 7.0). Tuttavia non è possibile escludere un'associazione ad un evento precedente al 1915, come ad esempio il terremoto del V-VI secolo AD (Galadini e Galli, 1999).

La stratigrafia fino a 20 m di profondità è fatta da terreni a grana fina del Pleistocene superiore – Olocene (più giovane di 170-180.000 anni; Giaccio et al., 2017), prevalentemente limo e miscele di limo e argilla a bassa plasticità, con rare sottili intercalazioni sabbioso-limose. La suscettibilità a liquefazione deducibile dalle indagini geotecniche in situ è elevata. Il confronto fra la mineralogia XRPD dei campioni prelevati in sondaggio e quella dei campioni prelevati nei dicchi ha consentito di identificare lo strato che più probabilmente ha liquefatto durante il terremoto, alimentando i dicchi in superficie. Si tratta di uno strato di silt ubicato a 7-8 m di profondità. Sia questo strato, sia i dicchi hanno la peculiarità di non contenere i minerali argillosi illite e montmorillonite e di non contenere albite. Solo un altro strato, ubicato a circa 16 m di profondità, ha una composizione analoga. Tuttavia, un suo ruolo di orizzonte sorgente della liquefazione è ritenuto poco probabile, sia per le profondità elevate, sia perché il suo indice di plasticità lo colloca nei terreni a comportamento *clay-like*, e quindi difficilmente liquefacibile, secondo l'abaco di suscettibilità a liquefazione di Idriss and Boulanger (2008).

I risultati ottenuti ampliano la casistica di liquefazioni in terreni fini ed hanno alcune implicazioni importanti. Infatti, la maggior parte dei campioni hanno curve granulometriche che cadono al di fuori, o sono *border-line*, rispetto ai fusi granulometrici utilizzati per individuare le

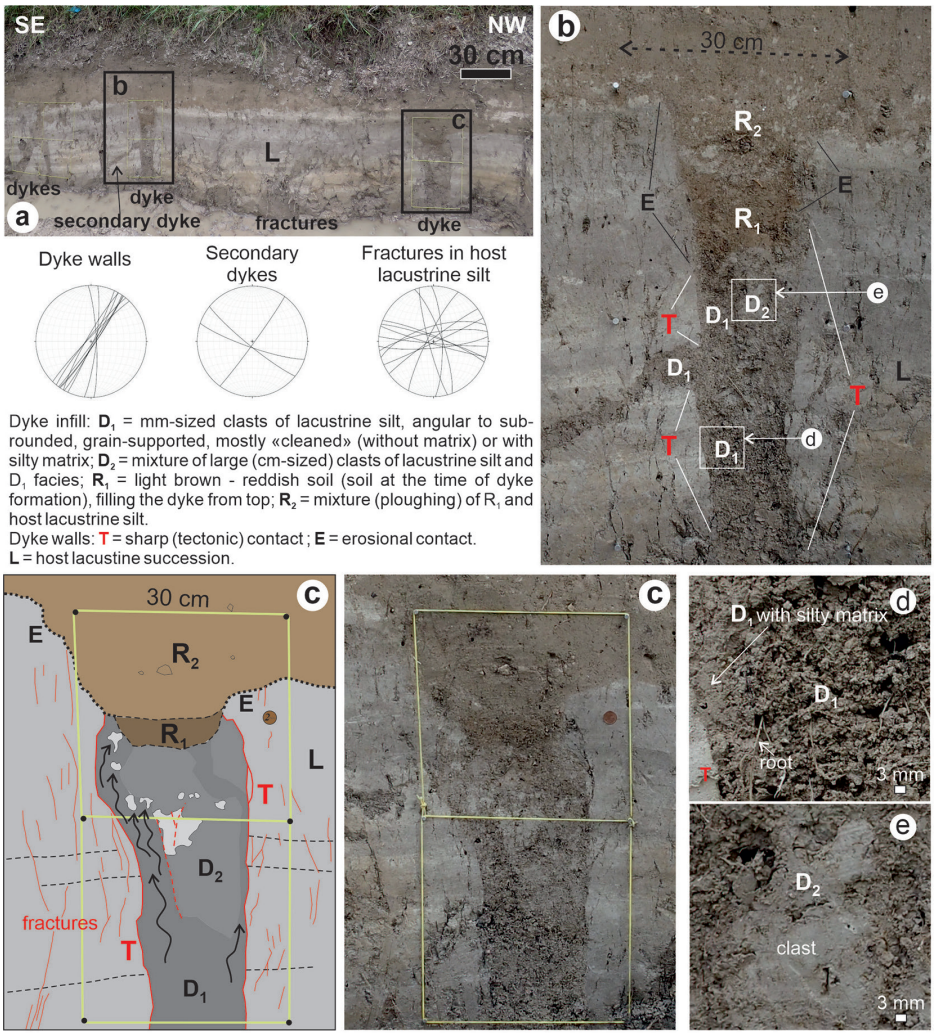

Fig. 2 - Particolare della parete sud del canale (a), dettaglio dei dicchi (b) e (c) e stereonet con giacitura delle pareti dei dicchi principali (a sinistra), dei dicchi secondari (al centro) e delle fratture (a destra). In (c), notare il brusco contatto fra le facies D1 e D2 del riempimento, che suggerisce un flusso all'interno del dicco. Notare anche i frammenti di silt biancastro "dispersi" verso l'alto, che suggeriscono una forza idraulica diretta verso l'alto. Le foto (d) e (c) sono dettagli delle facies D1 e D2.

classi granulometriche maggiormente o potenzialmente suscettibili a liquefazione. Quindi, criteri di esclusione basati sulle curve granulometriche non sono affidabili in successioni lacustri del Pleistocene superiore – Olocene come quella studiata. Al contrario, si rendono necessarie analisi multi-metodo.

Bibliografia

Idriss I.M., Boulanger R.W.; 2008: *Soil liquefaction during earthquakes*. ERI Report, Publ. No.MNO-12, Earthquake Engineering Research Institute, 2008.

Galadini F., Galli P.; 1999: *The Holocene paleoearthquakes on the 1915 Avezzano earthquake faults (central Italy): implications for active tectonics in the central Apennines*. Tectonophysics. 308:143–170.

Giaccio B., Niespolo E., Pereira A., Nomade S., Renne P., Albert P., Arienzo I., Regattieri E., Wagner B., Zanchetta G., Gaeta M., Galli P., Mannella G., Peronace E., Sottili G., Fabio F., Leicher N., Marra F., Tomlinson E.; 2017: *First integrated tephrochronological record for the last ~190 kyr from the Fucino Quaternary lacustrine succession, central Italy*. Quaternary Science Reviews. 158. 211-234. https://doi.org/10.1016/j.quascirev.2017.01.004.

SEISMOTECTONIC MODEL OF THE MONTELLO AREA (NORTHEAST ITALY) DERIVED FROM SEISMIC REFLECTION DATA

L. Bonini[1,2], N. Bertone[1], A. Del Ben[1], G. Areggi[1], M. Ponton[1], G.A. Pini[1]
[1] *Dipartimento di Matematica e Geoscienze, Università di Trieste, Italy*
[2] *Istituto Nazionale di Geofisica e Vulcanologia, Italy*

Reconstructing the architecture of active faults at depth is central to understand their earthquake potential. Among others, the geometry of the fault systems and the involved rocks are primary factors affecting the nature of the slip behavior, i.e. seismic or aseismic. In Northern Italy several active faults are hidden by Plio-Quaternary sediments of the alluvial planes bordering the Alps and the Apennines. Over the past 70 years extensive hydrocarbon exploration in these areas has shed light on a number of thrust-faults belonging to the external parts of the Northern Apennines and Southern Alps. Some of these structures produce anticlines well-visible at the topographic surface, such as the Montello hill in Northeast Italy or the San Colombano hill in the Central Po Plain. Others active faults and folds produce weaker effects at surface and their activity can be imaged through morphotectonic studies (e.g. Burrato *et al*., 2003).

In this study we used seismic reflection data to reconstruct the architectures of the active faults in the Montello area. Then, applying kinematic modelling we calculate their slip rate. Finally, we propose a seismotectonic model speculating on the slip behavior of these faults based on the distribution of the rocks at depth.

The Montello hill is an outcropping anticline located at the front of the Neogene- Quaternary Venetian Alps. Three different kind of data suggest that this structure is still tectonically active: 1) Middle and Upper Pleistocene warped river terraces in the western sector (e.g. Benedetti *et al*., 2000); 2) a geodetic shortening rate of 1-1.5 mm/yr (e.g. Cheloni *et al*., 2014); 3) seismicity (e.g. Romano *et al*., 2019).

As data to reconstruct active faults in the Montello area, we used seismic reflection profiles and deep wells: some of them are publicly available at the VIDEPI database (http://unmig.

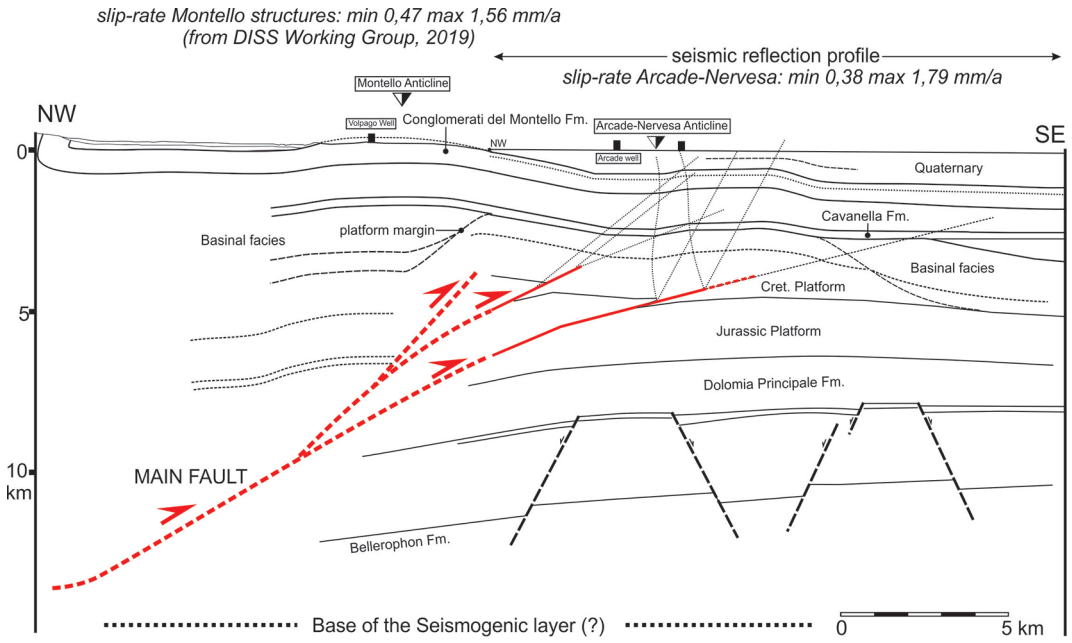

Fig. 1 - Tectonic sketch of the Montello and Arcade-Nervesa anticlines and their associated faults (thick red lines).

sviluppoeconomico.gov.it/videpi/en/), others have been kindly provided by ENI S.P.A in the framework of a research project leaded by Regione Friuli Venezia Giulia – Servizio Geologico (Project: "Mappature delle Faglie Attive").

During the first step we mapped the main seismic facies and we interpreted the main reflectors along 2D seismic reflection profiles displayed in TWT. Then we depth-converted the interpretations obtaining ad preliminary geological model. In the second step we tested different kinematic models to reconstruct the main faults. This procedure allowed to produce balanced models and to calculate the slip rate of the faults (Fig. 1).

Our interpretation in the Montello region displays two main anticlines: the larger one corresponds to the Montello hill, the second one is hidden by Quaternary sediments and is located near the village of Arcade and Nervesa. These two anticlines are generated by a reverse fault system, the lower part of which consists of a main fault rooted in the Permian deposits and dissecting the lower part of the Mesozoic carbonate platform. Three secondary splays characterize the upper part and are directly connected with the anticlines. The kinematic model selected to solve the relationship between faults and folds is the fault-propagation folds for all the structures. As both structures, namely the Montello and the Archade-Nervesa faults, cross carbonate sequences that are well known to be seismogenic (e.g. Bonini *et al*., 2014), we propose that the slip along this fault system is seismogenic.

Acknowledgements. Petroleum Expert Ltd is acknowledged for making available the Move software to the to the University of Trieste.

References

Bonini L., Toscani G. and Seno S.; (2014): Three-dimensional segmentation and different rupture behavior during the 2012 Emilia seismic sequence (Northern Italy). Tectonophysics, http://dx.doi.org/10.1016/j.tecto.2014.05.006.

Burrato P., F. Ciucci F. and Valensise G.; 2003: An inventory of river anomalies in the Po Plain, Northern Italy: evidence for active blind thrust faulting. Annals of Geophysics, 46 (5)

Benedetti L., Tapponnier P. and King G.C.P.; 2000: Growth folding and active thrusting in the Montello region, Veneto, northern Italy. Journal of Geophysical Research, 105, pp. 739-766.

Cheloni D., D'Agostino N. and Selvaggi G.; 2014: Interseismic coupling, seismic potential, and earthquake recurrence on the southern front of the Eastern Alps (NE Italy), Journal of Geophysical Research, 10.1002/2014JB010954.

DISS Working Group; 2019. Database of Individual Seismogenic Sources (DISS), Version 3.2.1: A compilation of potential sources for earthquakes larger than M 5.5 in Italy and surrounding areas. http://diss.rm.ingv.it/diss/, Istituto Nazionale di Geofisica e Vulcanologia; DOI:10.6092/INGV.IT-DISS3.2.1.

Romano, M. A., Peruzza, L., Garbin, M., Priolo, E. and Picotti V.; 2019: Microseismic Portrait of the Montello Thrust (Southeastern Alps, Italy) from a Dense High-Quality Seismic Network. Seismological Research Letter, doi: 10.1785/0220180387.

ARCHAEOSEISMOLOGICAL AND GEOPHYSICAL SURVEYS TO STUDY THE 847 AD EARTHQUAKE EVIDENCE IN CENTRAL-SOUTHERN ITALY

C. Bottari[1,4], L. Ferranti[2], R. Di Maio[2], A. Frisetti[3], C. De Paola[2], M. La Manna[2], E. Piegari[2], F. Marazzi[3]

[1] Istituto Nazionale di Geofisica e Vulcanologia, Roma 2, Italy

[2] CRUST-DiSTAR, Dipartimento di Scienze della Terra, dell'Ambiente e delle Risorse, Università di Napoli Federico II, Napoli, Italy

[3] Facoltà di Lettere, Università degli Studi Suor Orsola Benincasa, Napoli, Italy

[4] Istituto Nazionale di Geofisica e Vulcanologia, Roma 1, Italy

This study provides deeper insights on our knowledge of the 847 AD earthquake that struck a large area in Central-Southern Italy causing diffuse damages in northern Campania, Molise, and Latium. Through the integration of archaeoseismic observations, geological and geophysical surveys together with a critical review of historical written sources, it was possible

to identify evidence of seismic effects on ancient Medieval buildings or structures uncovered during archaeological excavations.

Archaeoseismic evidence of the 847 earthquake comes from two archaeological sites located along the Volturno Valley, namely San Vincenzo al Volturno Abbey near Isernia in northern Molise and the Basilica of Santa Maria at Alvignano in northern Campania (Fig.1). San Vincenzo Abbey showed structural modifications shortly after the earthquake documented by English excavations in 1990's (Hodges, 1993), as well as some still visible evidence of deformation and collapse. The most significant evidence is the collapse of a large wall in a ~NNE-SSW direction, which connected the workshops area with the eastern corridor in the Abbey, in addition to minor damages as cracking in walls (Marazzi, 2014). In the Basilica of Santa Maria (High Volturno Plain) we surveyed deformed arches, pillars tilted along a NE-SW axis, and partial rebuilding of the apsidal area. Furthermore, at this site we performed an integrated geophysical survey, consisting of ERT and GPR measurements, to explore the subsoil and to study local site conditions, which could have influenced co-seismic ground motion. The integrated survey was specifically designed to acquire information on the physical and geometrical features of the shallow subsurface beneath the Basilica of Santa Maria and to explain the tilt of the pillars and collapse of the apse. The integrated interpretation of the acquired data, calibrated by the stratigraphy of available boreholes, documents the presence of altered pyroclastic deposits, which could have certainly enhanced site effects at Alvignano. Indeed, the lateral and vertical variations in resistivity values observed down to the maximum exploration depth (~ 10 m b.g.l.) suggest a significant inhomogeneity of the investigated deposits, which is compatible with different degrees of argillification. This inhomogeneity could have amplified the site effect during seismic shaking and caused the vertical crashing of the left aisle arches.

Analysis of damage descriptions and archaeological reports indicates that the 847 seismic event documented by historical sources damaged a wide area between Latium, Campania and Molise, with destruction of the town of Isernia and damages in Rome (CFTI5Med, Guidoboni *et al*. 2018). For the Isernia settlement, unfortunately, archaeological data relative to destruction and following reconstruction of buildings have not been found. Conversely, historical sources report total destruction of the town. Although historical sources did not explicitly mention damage in Rome, the traces of the 847 AD earthquake have been largely documented in the archaeological excavations and seismological literature (Galli and Molin 2014, Galadini *et al*. 2018). Starting from the documented effects of earthquake shaking, a wide area of damage

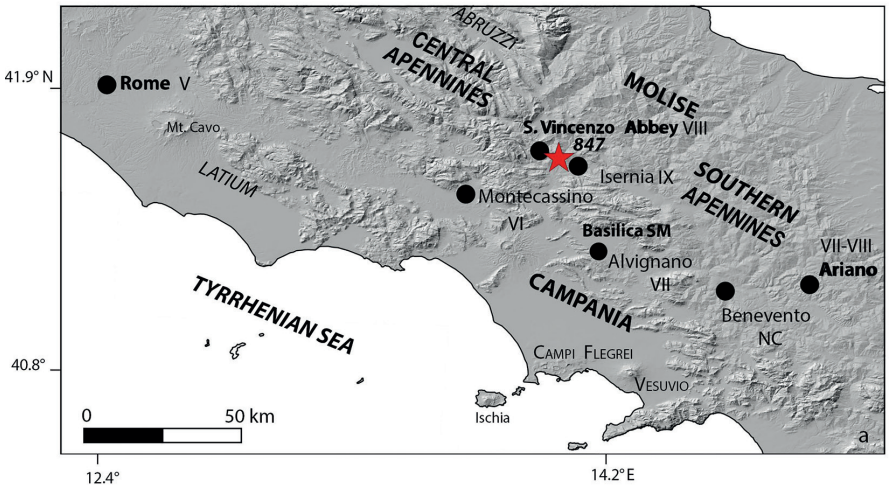

Fig. 1 - a) Map of damaging effects area of the 847 earthquake: the black dots indicate the localities damaged by the seismic event, the Roman numbers report the intensities in MCS (after CFTI5Med 2018).

has been defined in northern Campania, Molise, and Latium, and includes the localities of Benevento, Ariano Irpino, Isernia, San Vincenzo al Volturno, Cassino and Rome. Because the damaged area for this medieval earthquake is loosely defined in literature, the present study represents a contribution to better define the shaking area and provide new hints on the extent and location of the possible seismogenic source.

References

Galadini F, Ricci G, Falcucci E, Panzieri C (2018) Archaesoeismological evidence of past earthquakes in Rome (fifth to ninth century A.D.) used to quantify dating uncertainties and coseismic damage. Natural Hazards 94: 319–348.

Galli P, Molin D (2014) Beyond the damage threshold: the historic earthquakes of Rome. Bullettin of Earthquake Engineering 12:1277–1306.

Guidoboni E, Ferrari G, Mariotti D, Comastri A, Tarabusi G, Sgattoni G, Valensise G (2018) CFTI5Med, Catalogo dei Forti Terremoti in Italia (461 a.C.-1997) e nell'area Mediterranea (760 a.C.-1500), Istituto Nazionale di Geofisica e Vulcanologia (INGV). http://storing.ingv.it/cfti/cfti5.

Hodges R (1993) San Vincenzo al Volturno: The 1980-1986 Excavation, Part I. Archaeological Monographs of the British School at Rome, Rome

Marazzi F (2014) La Basilica Maior di San Vincenzo al Volturno. Scavi 2000-2007, Volturnia, 376 pp.

LA SEQUENZA SISMICA DELL'ISOLA DI SALINA DEL DICEMBRE 1954

C.H. Caracciolo

Istituto Nazionale di Geofisica e Vulcanologia (INGV), sezione di Bologna

I terremoti che sconvolsero l'isola di Salina verso la fine del 1954 non compaiono nel CPTI (Rovida et al, 2016), benché la sequenza sia stata registrata nel Catalogo del Progetto Finalizzato Geodinamica (Postpischl, 1985) con più di 23 segnalazioni e sia stata precedentemente descritta da M. De Panfilis (1959). Quindi, questo lavoro è il "recupero" o il "ritrovamento" di un terremoto, piuttosto che una "scoperta". In realtà, questo "recupero" è il prodotto di un lavoro su di un'altra area geografica, che però nondimeno contribuisce alla revisione della sismicità italiana di una epoca che merita particolare attenzione, come quella del dopoguerra e della ricostruzione postbellica. Come si evince dal tipo di fonti consultate, si tratta di un lavoro preliminare che merita ulteriori approfondimenti.

Sismicità storica di Salina. La storia sismica delle isole Eolie non abbonda di eventi prima del 1954. Solo Lipari conserva una storia di risentimenti che risale fino ai grandi terremoti siciliani del 1693 e calabresi del 1783, con danni rispettivi del 6° e del 7° Mercalli. Il primo evento con epicentro locale di cui si conserva memoria è un terremoto con intensità massima del 5° grado a Lipari, successo nel 1841. Per quanto riguarda l'isola di Salina, l'evento significativo più antico risale al 1892 Barbano *et al*., 2017, però quello di maggiori ripercussioni è quello del 17 agosto 1926, in cui i danni raggiunsero, secondo Cavasino (1935), una intensità non precisata tra il 7° e il 8° grado a Pollara (sessanta case danneggiate e metà di esse rese inabitabili), e a Malfa (quattrocento case danneggiate e due feriti). Danni minori risultano in altre due località dell'isola: a Rinella parecchie case lesionate oltre alla chiesa parrocchiale e anche nel paese di Leni sarebbe crollata qualche casa. Riguardo alle altre isole, si ha la sola segnalazione di leggeri danni per il porto di Filicudi e di Lipari e la caduta di qualche frana. Dopo il terremoto di Filicudi del 1930, un altro terremoto accadde il 27 gennaio 1939, per il quale risultarono danni minori rispetto al precedente e che colpì principalmente la parte occidentale di Salina e il porto di Filicudi. Si può ricordare, infine il terremoto del 13 giugno 1963, che provocò solo lievi danni a Pollara (tra il 6° e il 7° grado, e a Leni, Malfa e Rinella (6°) (Cfr. CPTI15, Rovida *et al*., 2016).

La sequenza sismica del dicembre 1954. Secondo De Panfilis (1959), i primi terremoti avvertiti dalla popolazione sono accaduti l'11 e il 14 dicembre 1954. Il *Corriere della Sera* informò sulle tre scosse del 14 dicembre, che spaventarono la popolazione isolana. Dopo qualche giorno di relativa calma, forti scosse sono state avvertite il pomeriggio del 23 dicembre. In particolare, il pomeriggio alle 16:41, una scossa fece danni ai soffitti e provocò la caduta di calcinacci, almeno a Pollara (Tab.1). Le scosse continuarono, in particolare verso la mezzanotte fino alle prime ore del mattino del 24 dicembre, apparentemente senza danni materiali. I quotidiani dell'epoca raccontano che da quel momento in poi la popolazione dell'isola ha vissuto in permanente allarme, perché si avvertivano tre o quattro scosse al giorno.

Secondo De Panfilis (1959), all'alba del 27 dicembre la popolazione dell'isola fu svegliata da una forte scossa accompagnata da intensi boati. Poco dopo, alle ore 8:59, si sentì una "scossa fortissima", che è risultata quella principale, seguita da un'altra forte scossa avvenuta una ventina di minuti dopo. Poi, secondo le cronache giornalistiche, le scosse si sarebbero ripetute ogni 10-15 minuti. Alla fine della giornata se ne sarebbero contate una trentina e circa ottanta al 30 dicembre, avvertite soprattutto a Pollara, il paese più colpito. Vista la frequenza delle scosse, né De Panfilis (1959), né i quotidiani offrono un resoconto dettagliato, pur accennando ai danni che continuano a verificarsi. Solo la scossa delle 8:45 della mattina del 28 dicembre è menzionata dalle cronache giornalistiche.

Con l'inizio del nuovo anno, si registrano meno scosse: solo i giorni 1, 2, 3, 6 e 10 gennaio, che provocano comunque forte apprensione nella popolazione.

Tabella 1 - Piano Quotato del terremoto del 23 dicembre 1954, nell'isola di Salina.

1954 12 23 15:49 (GMT) Pollara				
Località		Lat	Lon	I
Pollara		38.577	14.809	6

La descrizione dei danni. La maggior parte delle notizie sono state tratte dal *Corriere della Sera*, e sono stati aggiunti alcuni dettagli pubblicati su *La Stampa* e su *L'Unità*. Fondamentale, però, è il resoconto di De Panfilis (1959), il quale non indica in modo preciso quali siano le sue fonti. La prima corrispondenza giornalistica in cui si da conto dei danni è datata la sera del 27 dicembre, per poi susseguirsi con una o due corrispondenze giornaliere fino alla fine dell'anno, con le quali si aggiungevano particolari e si aggiornavano sulle nuove scosse. Purtroppo, la cadenza delle notizie e lo stile narrativo giornalistico non permette di distinguere gli effetti delle diverse scosse avvenute a partire dalla mattina del 27 dicembre. Per questo motivo, i danni devono essere considerati come il risultato cumulato dell'intera sequenza. In linea generale si dice che "quasi tutte le casette dell'isola, di vecchia e primitiva costruzione, sono rimaste lesionate o fortemente danneggiate". Un'altra interessante testimonianza del terremoto viene offerto da due cinegiornali delle serie "*Mondo Libero*" e "*La Settimana Incom*" dell'Istituto Luce, datati 7 gennaio 1955. Questi filmanti non aggiungono informazione dettagliata degli effetti del terremoto, però permettono di osservare i danni maggiori in alcune costruzioni della zona colpita. Ad ogni modo, è importante distinguere tra le diverse località, in ordine alfabetico:

Leni. Non è chiaro se dopo la prima scossa le case di Leni abbiano subito danni. Tuttavia, le notizie successive sostengono che la situazione era drammatica, con tutte le abitazioni più o meno seriamente danneggiate e in qualche caso con danno grave. Buona parte della popolazione rimasta in paese era stata sistemata provvisoriamente nella nuova scuola (che si presume non fosse stata danneggiata).

Lingua. Si afferma che in questo porto, frazione del comune di Santa Marina Salina, risultano danneggiate numerose case di abitazioni. La parrocchia avrebbe patito gravi danni e il campanile sarebbe crollato. Anche il personale della stazione della Guardia di Finanza era stato trasferito per i danni nella caserma. Secondo De Panfilis (1959), anche in questa località (come

a S. Marina Salina), si verificarono lesioni più o meno gravi in molti edifici.

Malfa. Oltre ai danni più o meno significativi segnalati per le abitazioni di tutto il comune, nel paese di Malfa sono rimasti gravemente danneggiati alcuni edifici, tra i quali la caserma della Guardia di Finanza e la chiesa parrocchiale.

Pollara. Dall'inizio si ebbe la percezione che i danni maggiori si riscontrassero nel paese di Pollara (frazione del comune di Malfa), dove erano crollate alcune vecchie case e numerose altre rimassero gravemente danneggiate. Si dice che avevano patito gravi danni quasi tutte le case d'abitazione e che erano crollati alcuni soffitti. In particolare, si dice che tutte le circa ottanta case di Pollara sono rimaste danneggiate, ma che solo una cinquantina di esse era effettivamente abitata al momento del terremoto, mentre le altre erano state abbandonate per causa della forte emigrazione della popolazione verso le Americhe e l'Australia. Un resoconto di *L'Unità* dice che solo undici case erano rimaste lievemente danneggiate, mentre la maggioranza doveva essere demolita. Inoltre, si verificò la caduta di grossi massi dal sovrastante Monte de Porri, i quali, franando, distrussero vecchi casolari di campagna.

Rinella. Poche notizie si hanno sugli effetti del terremoto nel porto di Rinella. Oltre alle note generiche sui danni generalizzati nelle abitazioni dell'isola, le cronache accennano soltanto a danni nella parrocchia e nella stazione della Guardia di Finanza, senza definirne la gravità.

Santa Marina Salina. Poche notizie forniscono le cronache su questo paese, il principale porto dell'isola. Oltre ai danni più o meno generalizzati nelle abitazioni di tutta l'isola, si dice solo che ha sofferto danni minori rispetto a Pollara; tuttavia si sarebbe verificato qualche crollo. Secondo De Panfilis (1959), anche in questa località (come a Lingua), si verificarono lesioni più o meno gravi in molti edifici.

Altre isole. Le cronache consultate non segnalano con precisione gli eventuali effetti nelle altre isole dell'arcipelago o in Sicilia. Solo una corrispondenza della sera del 30 dicembre riferisce che le scosse più violente sono state avvertite anche nelle isole di Filicudi, Lipari e Stromboli, senza però offrire altri dettagli. Invece De Panfilis (1959), pur avvertendo sulle poche notizie possedute sugli effetti del terremoto nelle altre isole, afferma che a Lipari il movimento tellurico fu generalmente avvertito, ma senza destare alcuna apprensione, mentre è stato più leggermente avvertito nelle isole di Panarea, di Filicudi e di Vulcano.

Effetti ambientali. Oltre alla caduta di massi dal Monte de Porri, accennata per la zona di Pollara, gli unici effetti ambientali accennati dalle corrispondenze giornalistiche sono le fenditure "nelle piccole vie dei centri di Malfa, Leni, Pollara e Santa Marina" che si sono aperte con le successive sosse. A differenza del terremoto del 1926, per il quale si riferisce un maremoto, in questo caso non si accenna a nessun effetto di questo tipo, escludendo la preoccupazione suscitata per un effetto di "alta marea".

Le notizie concordano che non si dovette lamentare nessuna vittima e che la maggior parte della popolazione, dopo la forte scossa del 27 mattina, cominciò a cercare rifugio fuori dall'isola. Si dice che dei 1672 abitanti dell'isola, ne siano riamasti circa 400.

Le cronache aggiungono che lo stato di apprensione della popolazione dell'arcipelago si era aggravata con la ripresa, la mattina del 29 dicembre, dell'attività dello Stromboli, con colate laviche dalle tre bocche che dalla sciara del fuoco arrivavano fino al mare.

All'ultimo dell'anno, con il diradarsi delle scosse, era tornata una certa calma nell'isola, la quale permise agli esperti di fare le prime ricognizione degli effetti.

L'attribuzione dell'intensità. Attraverso la mappa isosismica, De Panfilis (1959) divide l'isola in tre livelli d'intensità macrosismica. All'estremo nord-occidentale dell'isola, corrispondente a Pollara, attribuisce il 7° grado Mercalli. Alla regione centrale, che comprende i paesi di Malfa, Leni e Rinella (e il Monte dei Porri), attribuisce un'intensità indeterminata tra il 6° e il 7° grado. Alla frangia orientale, che comprende le località di S. Marina Salina e di Lingua (e la cima del monte Fosse delle Felci), attribuisce un'intensità del 6° grado. Tuttavia, solo per Pollara esplicita i motivi della scelta, sostenendo che attribuisce a questo paese il 7° grado "anche se gli effetti dinamici sulle abitazioni possono indurre a giudicarla più alta". La

scelta è basata sulla constatazione che le case di Pollara, come del resto dell'isola, sono "in generale poco solide sia perché di costruzione assai difettosa sia perché ormai molto vecchie e indebolite da precedenti fenomeni sismici". Nel caso di Malfa e di Leni, l'attribuzione di una intensità indeterminata tra il 6°-7° grado deve essere collegata al riferimento alla violenza della scossa avvertita in quei luoghi che causò "gravi lesioni in molte abitazioni". Tuttavia, per Rinella, ovvero la terza località compresa in questa area, non abbiamo una simile descrizione di danni. Per quanto riguarda la zona orientale dell'isola, che comprende i porti di S. Marina Salina e il porto di Lingua, De Panfilis (1959) attribuisce una intensità del 6° grado.

In questo lavoro si propone una revisione del quadro macrosismico di De Panfilis (1959), il quale appare leggermente sottostimato. Infatti, Cavasino (1935) assegna a Pollara un'intensità del 7°-8° nel caso del terremoto del 17 agosto 1926, con una simile descrizione dei danni nei due casi; come sono certamente simili le condizioni abitative nel 1926 e nel 1954. Inoltre, si preferisce riconsiderare l'intensità attribuita al porto di Rinella. Si presenta il riassunto del quadro macrosismico risultante della scossa del 23 (Tab. 1) e del 27 dicembre (Tab. 2), cumulativo per quest'ultima fase:

Tabella 2 - Piano Quotato del terremoto del 27 dicembre 1954, nell'isola di Salina.

1954 12 27 7:59 (GMT) Isola di Salina				
Località		Lat	Lon	I
Pollara		38.577	14.809	7-8
Leni		38.556	14.827	7
Malfa		38.580	14.835	7
Lingua		38.540	14.870	6-7
S. Marina Salina		38.562	14.873	6-7
Rinella		38.550	14.828	6
Lipari		38.468	14.958	3
Filicudi Porto	IS	38.562	14.582	2
Panarea	IS	38.637	15.077	2
Vulcano		38.416	14.959	2

Conclusioni. Lo scopo di questo lavoro è stato quello di recuperare questa sequenza "dimenticata" e di proporre una valutazione leggermente diversa da quella stimata qualche anno dopo da parte di De Panfilis (1959). Si considera che la nuova stima sia in linea con le attribuzioni d'intensità date in occasione degli altri eventi che provocarono danni più o meno documentati nell'isola. Questa sequenza risulta la seconda in importanza per l'isola di Salina, dopo il terremoto del 17 agosto 1926, per il quale erano stati registrati danni, benché leggeri, nelle isole vicine e che fu avvertito anche nella costa siciliana e calabra con un eventuale effetto di maremoto: conseguenze non registrate durante la sequenza del dicembre 1954. Tuttavia, appare più forte rispetto agli altri eventi conosciuti.

Bibliografia

Barbano M.S., Castelli V., Pirrotta C.; 2017: *Materiali per un catalogo di eruzioni di Vulcano e di terremoti delle Isole Eolie e della Sicilia nordorientale (secc. XV-XX)*. Quaderni di Geofisica, 143.

Bollettino sismico mensile, 1917-1980: Istituto Nazionale di Geofisica.

Carozzo M.T., Cosentino M., Ferlito A., Giorgetti F., Patane G., Riuscetti M.; 1975: *Earthquakes catalogue of Calabria and Sicily (1783-1973)*. Quaderni della Ricerca Scientifica, CNR, 93.

Cavasino A.; 1935: *I terremoti d'Italia nel trentacinquennio 1899-1933*. Mem. R. Uff. Centr. Meteor. e Geof., Appendice, s.3, v.4.

De Panfilis M., 1959: *Attività sismica in Italia dal 1953 al 1957*. Annali di Geofisica, 12, 1, 21-148.

Ingrao G.; 1930: *Bollettino Sismico. Macrosismi. Anno 1926*. R. Uff. Centr. Meteor. e Geofisica, Roma.
Postpischl D.; 1985: *Catalogo Progetto Finalizzato Geodinamica*, Consiglio Nazionale delle Ricerche, Roma.

Quotidiani
Corriere della Sera, 28, 29, 30, 31 dicembre 1954, 1, 4, 7, 8, 11 gennaio 1955.
L'Unità, 28, 30 dicembre 1954, 1 gennaio 1955.
La Stampa, 28, 30, 31 dicembre 1954.

Cinegiornali
La terra ha tremato a Salina, Mondo Libero / M178, 7.01.1955.
Eolie inquiete - Eruzione a Stromboli e terremoto a Salina, La Settimana Incom / 01194, 7.01.1955.

REVISIONE DELLA SISMICITÀ MODERATA ITALIANA DEGLI ANNI '30 DEL XX SECOLO. IPOTESI DI LAVORO E PRIMI RISULTATI

C.H. Caracciolo
Istituto Nazionale di Geofisica e Vulcanologia (INGV), sezione di Bologna

Premessa. Chiunque abbia sommariamente analizzato il CPTI15 (Rovida *et al*., 2016), per gli eventi dello scorso secolo, può avere notato che gli anni centrali mostrano una significativa diminuzione dell'attività sismica. È chiaro che durante gli anni della II Guerra Mondiale la rete di raccolta di dati è stata frantumata e che sono pochi gli eventi sismici accaduti in quelli anni che hanno lasciato significative tracce. Pure negli anni della ricostruzione post-bellica è comprensibile la perdita di informazioni. Tuttavia, anche durante gli anni che precedettero la II Guerra Mondiale si registra un tasso di attività molto minore. A un certo punto degli anni '30, il numero di eventi diminuisce in modo significativo, molto prima che gli eventi bellici abbiano direttamente colpito il territorio italiano. Come possiamo spiegare questo calo nel numero di terremoti registrati? Di certo, non si può escludere *a priori* una diminuzione naturale della sismicità, benché sia noto che in altri periodi storici questo tipo di variazioni siano state dovute a circostanze sociali e politiche che avevano fortemente condizionato la produzione, la diffusione e la conservazione d'informazioni.

È noto che durante gli anni della dittatura fascista la circolazione di informazioni era soggetto a uno stretto controllo, il quale mirava a eliminare o a diminuire l'impatto nella società di certo tipo di notizie, in particolare politiche, ma anche quelle riguardanti le calamità naturali (Cannistraro, 1975; Tranfaglia, 2005). Da parte dell'Ufficio Stampa del governo e poi da parte di un Ministero creato ad hoc (il Ministero di Cultura Popolare), si emanavo ogni giorno le direttive che dovevano essere seguite dai quotidiani, con la minaccia di sanzioni se le "raccomandazioni" non fossero state rispettate:

> "Rapporto del 26 settembre XI. Il conte Ciano ha raccomandato di non drammatizzare in merito al terremoto avvenuto negli Abruzzi. Sarà diramato dalla «Stefani» un comunicato in proposito in base al quale dovranno essere orientati i commenti." *Agenzia Stefani* (1933).

Non è detto che tale controllo sia stato esercitato anche sulle informazioni che arrivavano al (Reale) Ufficio Centrale di Meteorologia e Geodinamica (UCMG), incaricato di pubblicare il *Bollettino* (Cavasino, 1928-1936), con le informazioni macrosismiche, e poi al novello Istituto Nazionale di Geofisica. Nonostante ciò, è plausibile che nel tentativo totalitario di modellare l'immagine del paese, il regime abbia esercitato pressioni anche sul personale (i "relatori") che forniva i dati all'Ufficio, oltreché su altri funzionari (come i podestà), da cui ci si attendevano notizie. Dietro le lamentele più volte espresse da Cavasino (1928-1936) sui "relatori" che

spedivano le informazioni con cui si redigevano i bollettini (di cui ne parla come di "poco pratici" e che realizzavano i rilievi con "incuria"), forse si trova anche la volontà di disinformazione da parte del regime, sebbene al momento questa sia solo un'ipotesi. Ad ogni modo, la dipendenza dell'UCMG da fonti esterne sicuramente non ha giovato alla precisione dei dati raccolti, resa particolarmente vulnerabile a interferenze politiche che allora si esperimentavano in ogni settore della società.

Metodologia e obiettivi. Lo scopo principale della revisione che qui si presenta è di arricchire la Base di Dati (Locati *et al*., 2016) disponibile per il periodo in considerazione, con eventuali eventi "nuovi"; e poi l'aggiornamento della stessa con terremoti noti ma non inseriti nelle precedenti versioni del CPTI15 (Rovida *et al*., 2016), che avevano una soglia d'intensità e di magnitudo più alta.

Altro obiettivo della revisione è quello di fornire, quando possibile, descrizioni macrosismiche di eventi considerati dal CPTI15 (Rovida *et al*., 2016), ma basati solo sugli scarni dati del *Bollettino* (Cavasino, 1928-1936), o su di mappe isosismiche. In alcuni casi, le informazioni raccolte modificano il quadro macrosismico finora noto; in altri, l'evento registrato nel CPTI15 (Rovida *et al*., 2016) manca assolutamente di dati macrosismici, in particolare quando si tratta di eventi con epicentro calcolato fuori dai confini italiani.

Il lavoro di revisione per gli anni '30 parte dalla raccolta sistematica di notizie su eventi sismici in due dei principali quotidiani italiani, *Corriere della Sera*, *La Stampa* e in alcuni giornali austriaci. Inoltre, sono stati consultati altri quotidiani (altoatesini, friulani e bolognesi), con lo scopo di confrontare informazioni di eventi in qualche modo già individuati. Per un arco temporale limitato e in modo puntuale è stata controllata la documentazione del Ministero dell'Interno conservata nell'Archivio di Stato Nazionale, a Roma.

Malgrado la consapevolezza del controllo esercitato da parte del regime, sono stati consultati i quotidiani perché, ad ogni modo, essi costituiscono una fonte alternativa rispetto al *Bollettino* (Cavasino, 1928-1936); infatti, il suo curatore per il periodo che ci riguarda ne fa un uso sporadico e comunque di complemento alle informazioni ricevute dai "relatori".

Inoltre, con lo scopo di evitare in qualche modo la censura, si è fatto ricorso a quotidiani stranieri, in particolare austriaci, per la vicinanza geografica e per la estrema facilità della loro consultazione on-line, nelle pagine della Biblioteca Nazionale Austriaca (ÖNB).

Fino all'anno 1936 risultano fondamentali le più volte menzionate notizie del *Bollettino* macrosismico (Cavasino, 1928-1936). Dal loro confronto con le informazioni giornalistiche non di rado emerge un quadro macrosismico di grande interesse: ben inteso, di solito nella cornice della sismicità moderata del territorio italiano.

Tra le notizie raccolte, si trovano eventi totalmente nuovi, non inseriti nel CPTI15 (Rovida *et al*., 2016), né considerati dal *Bollettino* macrosismico dell'UCMG (Cavasino, 1928-1936) e neppure dal Catalogo del Progetto Finalizzato Geodinamica (PFG) (Postpischl, 1985). Oppure, si trova informazione di terremoti registrati dal *Bollettino* (Cavasino, 1928-1936) come "sotto soglia", i quali però possono essere rivalutati con le descrizioni macrosismiche desunte dalle informazioni giornalistiche.

Degli eventi "nuovi" che non raggiungono la soglia minima del CPTI15 (Rovida *et al*., 2016), si compila comunque una scheda. Non sono stati considerati, invece, i terremoti di cui il DBMI (Locati et al, 2016) conserva studi di riferimento robusti o dei quali le notizie raccolte sono note o non aggiungono nuovi dati.

Alcuni risultati. Come esempio dei risultati finora ottenuti, si presenta in primo luogo la sintesi delle schede riguardanti i terremoti dell'anno 1932 e poi un paio di eventi "nuovi".

Per il 1932, nel CPTI15 (Rovida *et al*., 2016) si registrano 11 eventi, dei quali 8 in territorio italiano e 3 con epicentro al di là dei confini: uno in Carinzia (Austria) e due in Slovenia. Questi ultimi non hanno dati macrosismici. Durante il processo di raccolta di notizie, sono state elaborate schede per 27 eventi sismici, i quali possono distinguersi secondo la seguente tabella (Tab 1):

Tabella 1 - Riassunto delle schede di terremoti per l'anno 1932, secondo il tipo di risultato.

Nuovo, senza danni, di presunta origine vulcanica	1
Nuovi, apparentemente senza danni, sopra la soglia del CPTI15	3
Nuovi, stimati sopra la soglia del danno	5
Noto in CPTI 15, senza alcun dato macrosismico	1
Noti a CPTI15, ai quali si aggiunge informazione significativa	4
Non raggiungono (con i dati per ora disponibili), la soglia del CPTI15.	11

In sintesi, agli 11 eventi elencati in CPTI15 (Rovida *et al*., 2016), si possono aggiornare i dati di base di 5 terremoti e si possono aggiungere altri 9 eventi, 5 dei quali sarebbero sopra la soglia del danno. Uno dei terremoti "nuovi" di questo anno è il seguente:

1932 08 14 11:36 Messinese

> "**Lieve scossa di terremoto a Messina.** Messina, 16 agosto, notte. Poco dopo mezzogiorno è stata avvertita oggi una scossa di terremoto della durata di dieci secondi. Si è avuto molto panico ma nessun danno e nessuna vittima. La scossa è stata avvertita anche in provincia. Nel comune di Floresta, il più alto di tutta la Sicilia, si è verificata qualche lesione a vecchie case. Nessun danno alle persone. *Corriere della Sera*, 17 agosto 1932".

Questo evento non si trova nel CPTI15. Si tratta probabilmente della scossa che nel *Bollettino* (Cavasino 1934) è indicata nel giorno 14 agosto, alle ore 12:36, per la quale segnala altre località nel Messinese. Trattandosi d'informazione giornalistica, non deve stupire che le date siano state modificate per rendere sempre "attuale" l'informazione. Infatti, pressoché lo stesso testo lo si trova in un quotidiano austriaco, secondo il quale l'evento sarebbe accaduto addirittura il 19 gennaio. Tuttavia, questo ultimo periodico descrive meglio il tipo di danni a Floresta: "In der Gemeinde Foresta, der höchstgelegenen von ganz Sizilien, erlitten durch den Erdstoss einige Häuser Sprünge und Risse." (trad:"*Nel comune Foresta, la più alta di tutta la Sicilia, alcune vecchie case hanno subito alcune fessure e crepe"*), *Salzburger Volksblatt*, 22 agosto 1932.

Con l'integrazione delle fonti giornalistiche e le indicazioni del *Bollettino* (Cavasino 1934) risulta la seguente tabella (Tab. 2):

Tabella 2 - Piano Quotato per l'evento del 14 agosto 1932, nel Messinese.

Località	Lat.	Lon.	Int. MCS
Floresta	37.985	14.897	6
Messina	38.187	15.549	5
Naso	38.122	14.788	5
Galati Mamertino	38.032	14.772	4
Tortorici	38.029	14.825	3

1938 03 23 18:00 Crotonese

Come altro esempio dei risultati del lavoro di revisione, si propone un terremoto accaduto in Calabria, nel 1938. Si deve notare che per detto anno, il CPTI15 (Rovida *et al*., 2016) elenca soltanto 10 eventi, quattro dei quali fuori dai confini italiani e solo uno supera la soglia del danno, ovvero quello del 12 agosto nell'Appennino laziale-abruzzese (I max 6, M 4.56). Si osserva che nessun evento era stato registrato per la prima metà dell'anno sul territorio italiano.

Questo terremoto è sconosciuto alla letteratura sismologica e non si trova nel Catalogo del Progetto Finalizzato Geodinamica [Postpisch, 1985]. Una notizia del *Corriere della Sera* ci informa invece di un evento sismico in Calabria:

> "**Scosse di terremoto in Calabria. Due case crollate e tre feriti.** Napoli, 24 marzo. Ieri sera alle ore 19 in alcune località del Crotonese è stata avvertita una scossa di terremoto in senso ondulatorio della durata di pochi secondi. La scossa si è manifestata sensibilmente nei Comuni di San Mauro Marchesato, Mesoraca e Scandale, ove si è provocato un certo panico fra le popolazioni. Nel Comune di Mesoraca sono crollate due case nel centro del paese e si hanno a lamentare tre feriti di cui uno con prognosi riservata. Altre cinque abitazioni sono pericolanti, per cui sono state fatte sgomberare. Sul posto si sono recati il prefetto, che ha disposto i primi soccorsi alle popolazioni danneggiate, e i funzionari del Genio Civile. *Corriere della Sera*, 25 marzo 1938".

Pressoché la stessa notizia comparve su *La Stampa*. Invece, più dettagliata appare la notizia pubblicata sul *Neues Wiener Tagblatt*; il quotidiano viennese aggiungeva un accenno a danni rilevanti in diversi luoghi, all'ordine della polizia di sgomberare un gran numero di abitazioni che minacciavano il crollo e finiva con i commenti del sismologo autodidatta Raffaele Bendandi. Dal testo delle notizie si può ricostruire un primo quadro macrosismico dell'evento (Tab. 3).

Tabella 3 - Piano Quotato per l'evento del 23 agosto 1938, in provincia di Crotone.

Località	Lat	Lon	Int
Mesoraca	39.077	16.789	7-8
San Mauro Marchesato	39.103	16.925	5
Scandale	39.121	16.960	5

Considerazioni finali. In questo lavoro sono state esposte in modo sintetico le linee di ricerca e qualche risultato della revisione sistematica della sismicità minore e moderata degli anni '30 del XX secolo, la quale si presenta assai lacunosa nel CPTI15 (Rovida *et al*., 2016). Gli eventi nuovi o rivalutati, come quelli presenti nel *Bollettino* macrosismico (Cavasino, 1928-1936), appartengono, infatti, alla fascia della sismicità moderata, la cui conoscenza non è di secondaria importanza per lo studio della sismicità del territorio italiano.

Gli eventi che risultano dalla presente revisione, sebbene si propongono di offrire una base sufficientemente solida per contribuire alla Base di Dati Macrosismica Italiana (DBMI15, Locati *et al*., 2016), possono essere certamente oggetto di ulteriori ricerche. Infatti, le informazioni macrosismiche che sono desunte dai quotidiani sono di solito più ridotte, in quanto al numero di località menzionate, di quelle contenute sul *Bollettino* (Cavasino, 1928-1936) o su altre fonti sismologiche. Inoltre, quando è stato possibile il confronto, si è osservato che dagli studi su specifici terremoti, risultano scenari più estesi e di maggiori entità di quanto non esprimano i giornali.

Bibliografia

Cannistraro Ph. V.; 1975: *La fabbrica del consenso. Fascismo e mass media*. Laterza, Roma-Bari.

Cavasino A.; 1928-1939: *Bollettino Sismico. Macrosismi*. (1927 al 1936). R. Uff. Centr. Meteor. e Geofisica, Roma.

Locati M., Camassi R., Rovida A., Ercolani E., Bernardini F., Castelli V., Caracciolo C.H., Tertulliani A., Rossi A., Azzaro R., D'Amico S., Conte S., Rocchetti E.; 2016: *Database Macrosismico Italiano (DBMI15)*. Istituto Nazionale di Geofisica e Vulcanologia (INGV). https://doi.org/10.6092/INGV.IT-DBMI15

Postpischl D.; 1985: *Catalogo dei terremoti italiani dall'anno 1000 al 1980*. Progetto Finalizzato Geodinamica. Quaderni de «La Ricerca Scientifica», 114, 2B.

Rovida A., Locati M., Camassi R., Lolli B., Gasperini P. (eds); 2016: *Catalogo Parametrico dei Terremoti Italiani* (CPTI15). Istituto Nazionale di Geofisica e Vulcanologia (INGV). https://doi.org/10.6092/INGV.IT-CPTI15

Tranfaglia N.; 2005: *La stampa di regime. 1932-1943*. Bompiani, Milano.

Manoscritto citato

Agenzia Stefani; 1933: Ministero dell'Interno-Fondo Morgagni-Agenzia Stefani, b. 69, c. 341, conservato nell'Archivio Centrale dello Stato, Roma.

Quotidiani citati
Corriere della Sera, 17.08.1932.
Corriere della Sera, 25 marzo 1938.
La Stampa, 25 marzo 1938.
Neues Wiener Tagblatt, 25.03.1938.
Salzburger Volksblatt, 22.08.1932.

SLIP BEHAVIOR OF THE CAMPOTOSTO NORMAL FAULT (CENTRAL ITALY) IMAGED BY GEODETIC AND SEISMOLOGICAL DATA: INSIGHTS FROM THE 18 JANUARY 2017, M>5 EVENTS

D. Cheloni[1], N. D'Agostino[1], L. Scognamiglio[1], E. Tinti[1], C. Bignami[1], A. Avallone[1], R. Giuliani[2], S. Calcaterra[3], P. Gambino[3], M. Mattone[3]
[1] Istituto Nazionale di Geofisica e Vulcanologia, Rome, Italy
[2] Dipartimento della Protezione Civile, Roma, Italy
[3] Istituto Superiore per la Protezione e la Ricerca Ambientale, Rome, Italy

On 18 January 2017, the 2016-2017 Amatrice-Visso-Norcia earthquakes sequence in Central Italy reached the Campotosto area with four M>5 events occurring in three hours. This fault remained as the last, 2009-2016 unruptured part of the central Apennines fault system from L'Aquila to Visso. On-going debate is focused on the vertical continuity of the surface trace of the Campotosto fault with the seismogenic structure beneath, and its relevance for the dam sustaining the Campotosto lake. In this work, we use geodetic and seismological observations to document the coseismic and aseismic deformation associated with these multiple moderate seismic events (main event Mw 5.5). In particular, to study the slip behavior of the causative fault we followed two different approaches: 1) we use InSAR and GPS static displacements to retrieve the fault geometry and the ~1-month cumulative slip distribution; 2) we invert strong-motion, high-rate GPS waveforms and high-rate GPS-derived static offsets to constrain the kinematic source models of the two major events (Mw 5.5 and 5.4) of the 18 January 2017.

The geodetic inversion shows that the deformation due to the four M>5 earthquakes is due to the ~50° SW-dipping and ~150° striking Campotosto normal fault, with an average slip of about 40 cm, mainly concentrated in the shallower part of the fault. This fault is well known by geological and paleoseismological studies (e.g. Galadini and Galli, 2003; Boncio *et al*., 2004; Galli *et al*., 2008), being the fault plane well exposed in the central-southern portion of the structure where the fault scarps are evident at the base of the western flank of the Laga Mts. Rupture histories of the two largest events of the sequence show that the two shocks ruptured two distinct and adjacent portions of the Campotosto fault, with significant slip up-dip from the hypocenters. Both geodetic and seismological observations required significant slip extending at shallow depths (< 1-2 km), challenging the hypothesis supporting lack of vertical continuity of the Campotosto fault (e.g. Buttinelli *et al*. 2018).

The cumulative seismic moment release calculated using the geodetic dataset is 9.29×10^{17} Nm, corresponding to an Mw ~6 earthquake. This estimate is larger than the cumulative seismic moment of all the seismic events with M>4 occurred in the corresponding time period (6.01×10^{17} Nm), suggesting that a fraction (~35%) of the overall deformation occurring during and after the 18 January 2017 Campotosto seismic sequence can be associated to aseismic processes. Our results show also that the inferred slip distribution is complementary with respect to the previous L'Aquila 2009 seismic sequence affecting the southern half of the Campotosto fault (Cheloni *et al*., 2014), suggesting the activation of different portions of the seismogenic fault

during the two recent seismic sequences and the presence of an unruptured area between these two portions.

In this context, we use the Coulomb stress changes to examine the interaction between the recent earthquakes that struck central Italy and the potential state of stress of the unruptured portions of the Campotosto fault. We find that the occurrence of the January 18 earthquakes caused an increase of stress in the upper central portion of the fault, just below the Campotosto lake, and on the deeper portions of the fault. The areas of the Campotosto fault positively stressed by the previous seismic sequences may be characterized by velocity strengthening behaviour (e.g., Boatwright and Cocco, 1996) releasing stress increases with aseismic slow deformation. On the other hand, these parts of the fault may be velocity weakening and represent an area that remained locked and acted as a barrier during the recent earthquake sequences.

Finally, while the recent moderate seismic events occurring from 2009 to 2017 released accumulated strain through a series of moderate M~5 events, there is paleoseismological evidence of large surface-rupturing events (M >6.5; e.g., Galadini and Galli, 2003). We suggest, therefore, that the Campotosto fault releases accumulated tectonic strain through a wide range of magnitudes, and a heterogeneous behaviour.

References

Boatwright J., Cocco M.; 1996: *Frictional constraints on crustal faulting*. J. Geophys. Res., **101**, 13895-13909.

Boncio P., Lavecchia G., Milana G., Rozzi B.; 2004: *Seismogenesis in Central Apennines, Italy: An integrated analysis of minor earthquake sequences and structural data in the Amatrice-Campotosto area*. Ann. Geophys., **47**, 1723-1742.

Buttinelli M., Pezzo G., Valoroso L., De Gori P., Chiarabba C.; 2018: *Tectonic Inversions, Fault Segmentations, and Triggering Mechanisms in the Central Apennines Normal Fault System: Insights from High-Resolution Velocity Models*. Tectonics, **37**, 4135-4149.

Cheloni D., Giuliani R., D'Anastasio E., Atzori S., Walters R.J., Bonci L., D'Agostino N., Mattone M., Calcaterra S., Gambino P.; 2014: *Coseismic and post-seismic slip of the 2009 L'Aquila (central Italy) Mw 6.3 earthquake and implications for seismic potential along the Campotosto fault from joint inversion of high-precision levelling, InSAR and GPS data*. Tectonophysics, **622**, 168-185.

Galadini F., Galli P.; 2003: *Paleoseismology of silent faults in Central Apennines (Italy): The Mt. Vettore and Laga Mts. faults*. Ann. Geophys., 815-836.

Galli P., Galadini F., Pantosti D.; 2008: *Twenty years of paleoseismology in Italy*. Earth-Sci. Rev., **88**, 89-117.

CATALOGO COMPLETO DELLA SEQUENZA SISMICA DI AMATRICE-VISSO-NORCIA (ITALIA CENTRALE, BOLLETTINO SISMICO ITALIANO 2016-2018)

M.G. Ciaccio, L. Margheriti, D. Latorre, B. Castello, A. Nardi, F.M. Mele, P. Baccheschi, A. Lisi, A. Marchetti, A.M. Lombardi, L. Improta, M. Moretti, M. Quintiliani, V. Lauciani, A. Bono, S. Pintore, Bollettino Sismico Italiano Working Group http://terremoti.ingv.it/en/bsi

INGV National Institute of Geophysics and Volcanology, Roma, Italy

In questo lavoro presentiamo il catalogo completo delle localizzazioni dei terremoti appartenenti alla più importante sequenza sismica avvenuta in Italia negli ultimi 30 anni, ovvero la sequenza sismica di Amatrice-Visso-Norcia (AVN) iniziata il 24 Agosto del 2016 in Appennino centrale.

Si tratta di 102,582 eventi sismici registrati dalle 129 stazioni della Rete Sismica Nazionale (RSN, http://doi.org/10.13127/SD/X0FXNH7QFY) e della rete temporanea installata nella regione epicentrale (Moretti *et al*., 2016), dal 14 agosto 2016 al 31 agosto 2018 e analizzati manualmente dagli analisti del Bollettino Sismico Italiano (BSI, http://cnt.rm.ingv.it/bsi). Le

fasi P ed S e le magnitudo di questi terremoti, stimate in tempo reale nella sala di sorveglianza dell'Istituto Nazionale di Geofisica e Vulcanologia (INGV) di Roma, sono state successivamente riviste in dettaglio, per tutti gli eventi di $M_L \geq 2.3$, con l'intento di migliorare la qualità dei parametri di localizzazione e della stima della magnitudo. Gli analisti hanno inoltre inserito le fasi P ed S osservate a quelle stazioni che il sistema di acquisizione non aveva eventualmente incluso nelle soluzioni automatiche in real-time. Per i primi mesi della sequenza l'analisi ha riguardato anche l'integrazione delle registrazioni di 9 stazioni temporanee *stand-alone* che non entravano automaticamente nelle localizzazioni della sala sismica; per i giorni nei quali si sono verificati gli eventi di M > 5.5 la revisione è stata particolarmente accurata anche per eventi di magnitudo inferiore a 2.3 (Improta *et al*. 2019)

Il dataset così costruito consiste in 25,496 terremoti rivisti dagli analisti del bollettino (versione della localizzazione 1000) e 77,426 eventi elaborati dai turnisti in sala sismica (versione della localizzazione 100).

Le 1705,987 fasi P che ne sono derivate, e le 1271,757 fasi S, sono disponibili nel database ISIDe (DOI: 10.13127/ISIDe).

Tutte le letture dei tempi di arrivo sono state utilizzate per localizzare gli ipocentri della sequenza utilizzando il codice di inversione non lineare NonLinLoc (NLL, Lomax *et al*., 2001) (Fig. 1 e Fig. 2). L'utilizzo di questa tecnica ha migliorato, rispetto ai lavori precedenti, la stima dei parametri ipocentrali fornendo delle soluzioni più robuste ai fini della ricostruzione sismotettonica dell'area interessata dalla sequenza sismica AVN. Rispetto ai dati forniti in tempo reale dal personale in servizio di sorveglianza sismica dell'INGV, questo nuovo catalogo

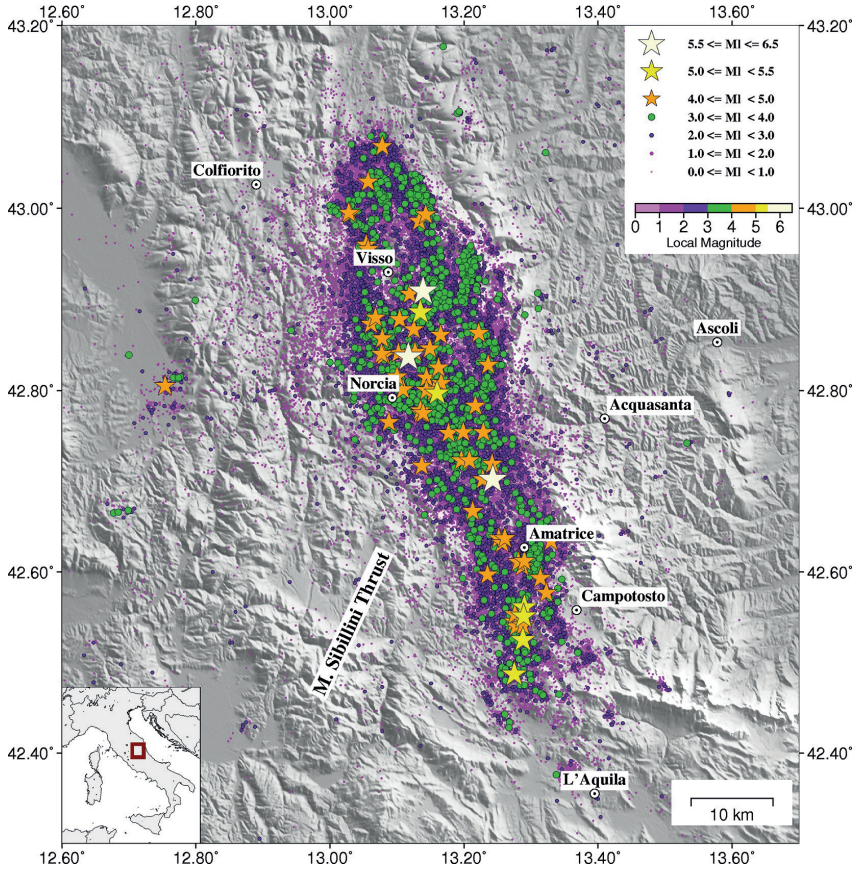

Fig. 1 - Localizzazioni epicentrali in mappa dei terremoti della sequenza del centro Italia 2016-2018.

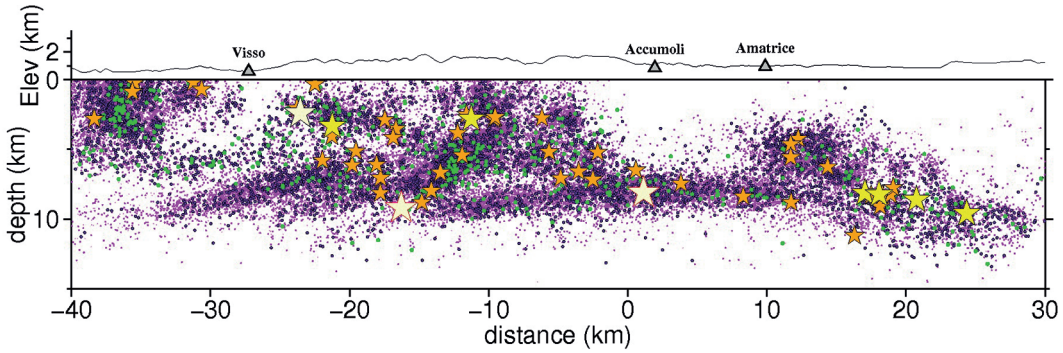

Fig. 2 - Localizzazioni epicentrali in sezione dei terremoti della sequenza del centro Italia 2016-2018.

presenta un notevole miglioramento in termini di omogeneità della stima della M_L, almeno nell'intervallo definito dalla soglia inferiore di revisione pari a $M_L \geq 2.3$. Questa maggiore omogeneità del catalogo permetterà ulteriori analisi per la stima della magnitudo di completezza Mc.

Inoltre, all'interno del catalogo sono presenti 75 terremoti con $M_L \geq 4.0$: per 47 di questi eventi sismici abbiamo calcolato il meccanismo focale a partire dalle prime polarità utilizzando il codice FPFIT (Reasenberg and Oppenheimer, 1985).

Un catalogo di questo tipo, di alta qualità, basato quindi su un imponente numero di fasi e ampiezze riviste manualmente, ha una particolare importanza e può essere un valido riferimento per l'applicazione per esempio di tecniche di *detection* basate sulla cross-correlazione di registrazioni di terremoti *templates*, per la validazione di cataloghi composti da letture automatiche dei tempi di arrivo, o anche per l'ottimizzazione di algoritmi di *picking* automatico.

La qualità delle localizzazioni dei *mainshocks* e degli *aftershocks* della sequenza sismica AVN diventa fondamentale per capire l'analisi dell'evoluzione spazio-temporale della sismicità, anche di bassa magnitudo, e le complesse geometrie delle faglie attivate durante la sequenza sismica, contestualmente alle relazioni tra esse esistenti.

Bibliografia

Improta L., Latorre D., Margheriti L., Nardi A., Marchetti A., Lombardi A.M., Castello B., Villani F., Ciaccio M.G., Mele F.M., Moretti M.; Bollettino sismico Italiano Working Group; 2019: *Multi-segment rupture of the 2016 Amatrice-Visso-Norcia seismic sequence (central Italy) constrained by the first high-quality catalog of early Aftershocks*

Scientific RepoRts, https://doi.org/10.1038/s41598-019-43393-2

Lomax A., Virieux J., Volant P., Berge, C.; 2000: *Probabilistic earthquake location in 3D and layered models: Introduction of a Metropolis-Gibbs method and comparison with linear locations*. In Advances in Seismic Event Location (eds Kluwer) 101–134 (Thurber, C. H. and Rabinowitz, N.).

Moretti M., Baptie B., Segou M.; 2016: SISMIKO: *Emergency network deployment and data sharing for the 2016 central Italy seismic sequence*. Annales de Geophysique, 59(5), https://doi.org/10.4401/ag-7212.

Reasenberg P., Oppenheimer D.; 1985: *FPFIT, FPPLOT and FPPAGE: FORTRAN computer programs for calculating and displying earthquake fault-plane solutions*, U.S. Geol. Surv. O.File Rep. 85-739.

SLIP IMAGING OF THE MAY 20, 2012, MW 5.8, PO PLAIN (NORTHERN ITALY) EARTHQUAKE FROM THE INVERSION OF THE SOURCE TIME FUNCTIONS

V. Convertito, N.A. Pino
Istituto Nazionale di Geofisica e Vulcanologia, Sezione di Napoli - Osservatorio Vesuviano

Introduction. The May 2012 seismic sequence occurred in the Po Plain (Northern Italy) and started on May 19, 2012, at 23:13:27 GMT with a Mw 3.8 earthquake. On 20 May a Mw 5.8 event was recorded, followed by a second Mw 5.6 main shock on 29 May (http://cnt.rm.ingv.it/tdmt) and thousands of aftershocks, six of them with magnitude larger than 5.0 (Govoni *et al*., 2014). The sequence caused 27 fatalities and widespread severe damage to dwellings forcing the closure of several factories.

This seismic sequence took place on a south dipping blind thrust fault system (Ferrara arc) in the Emilia-Romagna region, covered by the quaternary sediment of the Po Plain.

The aim of this study is to analyse the rupture properties of the largest event, occurred on May 20. In particular, we analysed rupture kinematics and image the slip distribution from the analysis of the apparent source time functions by using two different modelling.

Method. We applied an Empirical Green's Function (EGF) approach (see, for instance, Mori (2003) and reference therein) to obtain relative Source Time Functions (STFs) as seen at different azimuths. In order to gain information about the source directivity and the slip distribution we analysed the obtained STFs by using a forward modelling illustrated in Convertito *et al*. (2016) and a Bayesian inversion modelling described below. In particular, for this latter, the direct problem is solved by assigning the slip at a set of a given points (control points) distributed on the fault plane and then interpolated on a finer grid. The number of control points defines the size of the subfaults and is selected on the basis of the magnitude of the EGF. Each subfault is described by: the slip value, the rise-time and the onset time.

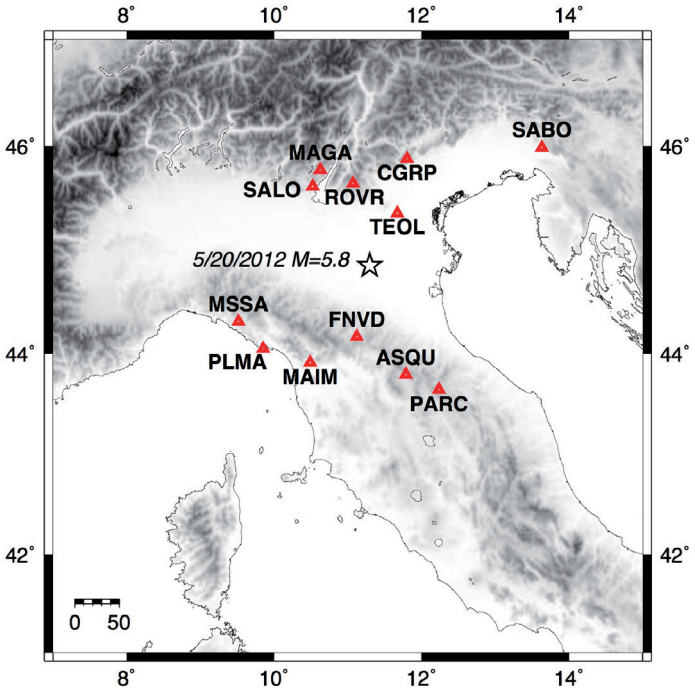

Fig. 1 - Geographic map showing the location of the May 20, 2012, Mw 5.8, Po Plain (Northern Italy) earthquake along with the stations used in the present study.

Slip distribution is mapped on a finer grid by means of a bilinear interpolation and by using a Gaussian bidimensional filter (e.g., Király-Proag *et al*., 2019). The size of the finer grid is selected according to the coherent rupture condition of six source points per wavelength (Archuleta and Hartzell, 1981). The nucleation point is located at fault center and the rupture propagates at a constant rupture velocity.

At each source depth we evaluate the v_p value (i.e., the propagation velocity of the selected seismic phase) using the crustal model proposed by Govoni *et al*. (2014) and compute the Mach number $a=v_r/v_p$, being v_r the rupture velocity. Each sub-fault is allowed to slip only once

with a triangular slip-rate function whose activation time from the origin time will depend on the source position with respect to the specific receiver according to the directivity function Cd (Ben-Menahem, 1961).

As for the inverse problem we implemented the Metropolis-Hastings sampler approach to investigate the model space parameter. For a given model **m**, the next candidate point is generated as $\mathbf{m}_t=\mathbf{m}_{t-1}+\mathbf{z}$ where **z** is an increment random variable from a proposal distribution. The components of **m** are the rupture velocity v_r, the rise-time t and slip distribution at the given control points. The best model parameter corresponds to the model that maximize the posterior distribution of the model space parameters, which is given by

$$f(m|d) = \frac{f(d|m)\rho(m)}{\int_{\Omega} (d|m)\rho(m)dm} \quad (1)$$

Where **d** is data vector and **m** is the model vector selected in the model space Ω, r(m) is the priori distribution and *f(d|m)* is the likelihood function given by

$$f(d|m) = ke^{-Misfit} \quad (2)$$

and,

$$Misfit = \frac{\sum_{i=1}^{Nstaz}\sum_{j=1}^{Nt}(S_{ij}^{cal} - S_{ij}^{obs})^2}{\sum_{i=1}^{Nstaz}\sum_{j=1}^{Nt} S_{ij}^{obs2}} \quad (3)$$

Where *Nstaz* is the number of available stations and *Nt* is number of points of the source time functions S_i.

Results and conclusions. The preferred EGF is the foreshock occurred on May 19, 2012, at 23:13:27 GMT with a Mw 3.8 earthquake.

The STFs display the largest amplitudes and frequencies, between N200° and N230°, at stations located toward SW of the epicentre. Smoother functions are observed to the N-NE (Fig. 2). However, the complexity of the STFs as observed at various azimuths suggests a complex style of rupture propagation. We performed a direct modelling of the retrieved moment rates by trial-and-error approach. The best results are characterized by two main rupture propagation directions, along N225° and N103°, respectively.

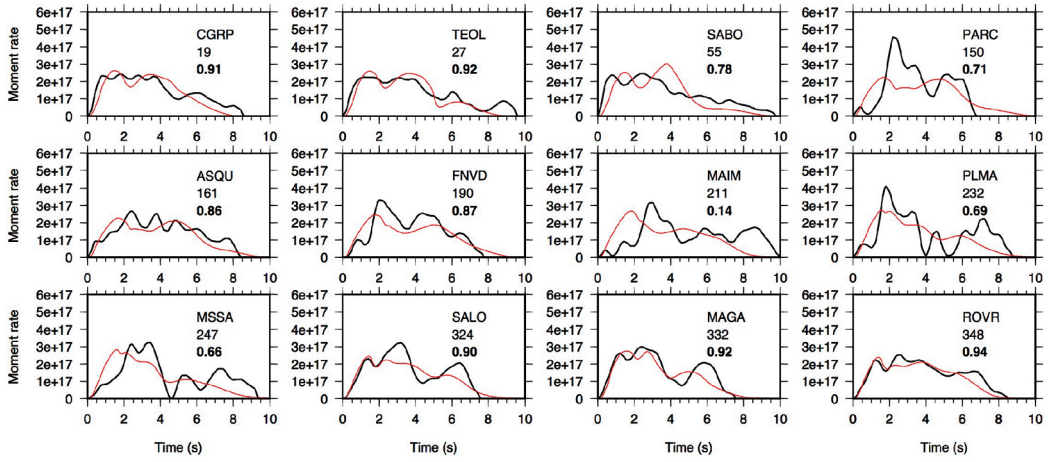

Fig. 2 - Observed STFs (black lines) and synthetics (red line) corresponding to the best solution obtained from the Bayesian approach. In each frame the station code, the source-to-station azimuth, and the correlation coefficient (bold) are reported.

As for the Bayesian inversion modelling, the fault length is assumed 26 km while the width is 13 km. We found that the optimal number of control points is 7x6 (see Fig. 3) and that stable results are obtained if the rise-time is set to the value expected by using the relationship proposed by Somerville *et al*. (1999) and equal to 0.4 s. The spacing of the finer grid is 0.06 km along both the strike and the dip of the fault.

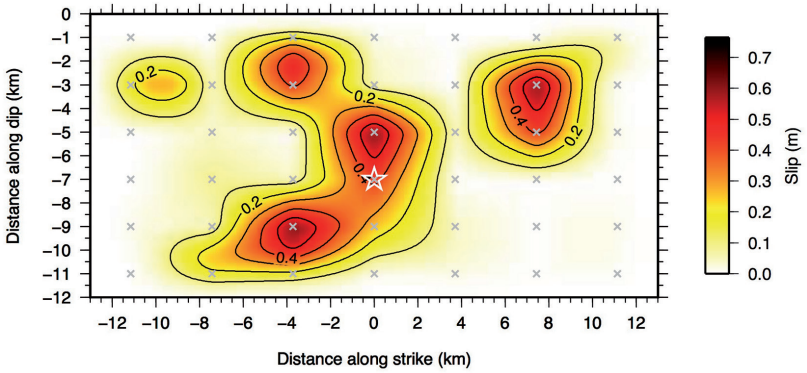

Fig. 3 - Final slip map for the May 20, 2012, Mw 5.8, Po Plain (Northern Italy) earthquake corresponding to the synthetic STFs shown in Fig. 2.

The obtained best model corresponds to a rupture velocity of 1.7 km/s and to the slip map depicted in Fig. 3, which suggests a bilateral rupture with a peak slip value is 0.6 m.

The fit between the observed and synthetic source time functions is shown in Fig. 2 and indicates that all but two the stations have a correlation coefficient larger than 0.7, with only one station lower than 0.6.

Based on the crustal model proposed by Govoni *et al*. (2014), the obtained rupture velocity provides a relatively low Mach number of 0.4. A similar slow rupture velocity was observed also for the close 29 May, Mw 5.6, event (Causse *et al*., 2017).

References

Archuleta, R. J., and S. H. Hartzell (1981). Effects of fault finiteness on near-source ground motion, Bull. Seism. Soc. Am., 71,939–957.

Ben-Menahem, A. (1961). Radiation of seismic surface waves from finite moving sources, Bull. seism. Soc. Am., 51(3), 401–435.

Causse, M., G. Cultrera, L. Moreau, A. Herrero, E. Schiappapietra, and F. Courboulex (2017). Bayesian rupture imaging in a complex medium: The 29 May 2012 Emilia, Northern Italy, earthquake, Geophys. Res. Lett., 44, 7783–7792, doi:10.1002/2017GL074698.

Convertito V., N.A. Pino, and F. Di Luccio (2016). Investigating source directivity of moderate earthquakes by multiple approach: the 2013 Matese (southern Italy) Mw = 5.0 event, Geophys. J. Int., 207, 1513–1528, doi: 10.1093/gji/ggw360.

Govoni, A., A. Marchetti, P. De Gori, M. Di Bona, F.P. Lucente, L. Improta, C. Chiarabba, A. Nardi, L. Margheriti, N.P. Agostinetti, R. Di Giovambattista, D. Latorre, M. Anselmi, M.G. Ciaccio, M. Moretti, C. Castellano, and D. Piccinini (2014). The 2012 Emilia seismic sequence (Northern Italy): imaging the thrust fault system by accurate aftershock location, Tectonophysics, 622, 44-55, 10.1016/j.tecto.2014.02.013.

Király-Proag, E., C. Satriano, P. Bernard, and S. Wiemer (2019). Rupture process of the Mw 3.3 earthquake in the St. Gallen 2013 geothermal reservoir, Switzerland, Geophysical Research Letters, 46. https://doi.org/10.1029/2019GL082911.

Mori, J.J., R.E. Abercrombie, and H. Kanamori (2003). Stress drops and radiated energies of the Northridge aftershocks, J. Geophys. Res., 108 (B11), 2545; doi:10.1029/200JB000474.

Somerville, P. G., K. Irikura, R. Graves, S. Sawada, D. Wald, N. Abrahamson, Y. Iwasaki, T. Kagawa, N. Smith, and A. Kowada (1999). Characterizing crustal earthquake slip models for the predictionof strong ground motion, Seismol. Res. Lett., 70, 59–80.

FAULT ROUGHNESS ASSESSMENT OF THE MONTE VETTORE FAULT SYSTEM AFTER THE MASSIVE 2016 SEISMIC SEQUENCE OF CENTRAL APENNINES, ITALY

A. Corradetti[1], M. Zambrano[2], S. Tavani[3], A. Pitts[2], T. Seers[1], E. Tondi[2]
[1] Department of Petroleum Engineering, Texas A&M University at Qatar, Qatar
[2] School of Science and Technology, Geology Division, University of Camerino, Italy
[3] DiSTAR, Università di Napoli Federico II, Italy

Introduction. After the major seismic events that struck the Northern Apennines (Central Italy) in 2016, a considerable surface rupture exposed fresh fault surfaces in the Monte Vettore-Castelluccio di Norcia area. The seismic sequence comprised three mainshocks: i) Amatrice Mw 6.0, August 24, ii) Visso Mw 5.9, October 26, and iii) Norcia Mw 6.5, October 30, the strongest earthquake of the sequence (e.g. Chiaraluce *et al*., 2017). The surface rupture caused by this seismic sequence has been well-document by the Open EMERGEO Working Group (Civico *et al*., 2018; Villani *et al*., 2018). These authors reported that the coseismic ruptures are generally organized in a systematic pattern of dominantly synthetic (N135°-160° striking, SW-dipping) and subordinately antithetic (N320°–345° striking, NE-dipping) components. In most cases, the ground ruptures follow the trace of mapped faults (e.g. Pierantoni *et al*., 2013 and references therein), and sometimes along fault splays previously unrecognized (Civico *et al*., 2018). The average coseismic throw of the entire sequence is ~0.3 m. However, more than 2 km of the ruptures were characterized by an average coseismic throw higher than 1 m, with a maximum of near 2.5 m along the so-called Cordone del Vettore fault scarp (Civico *et al*., 2018; Villani *et al*., 2018).

The assessment of the surface ruptures is useful for supporting studies on the mechanics of earthquake faulting and adjusting seismic sources modelling for joint inversion of geophysical datasets. In particular, the study of fault topography (e.g. exposed due to coseismic surface deformation) can provide insight into the direction (current or ancient) of slip and the relative exposure time of the surface to atmospheric elements altering the pristine fault morphology at several scales. Various approaches have been reported in the literature for mapping the surface of fractures and faults in the field or laboratory involving the use of Lidar (Candela *et al*., 2009; 2012), laboratory profilometers (Renard *et al*., 2006; 2012; 2013), and Structure from Motion-MultiView Stereo (SfM-MVS) photogrammetry (e.g., Kim *et al*., 2013, Corradetti *et al*., 2017; Zambrano *et al*., 2019). Among these methods, the latter is better suited for rough terrain conditions (e.g. seismically modified terrain, mountainous areas, or generally physically inaccessible outcrops) when compared to Lidar and does not require rock sampling. The method is also cost-efficient since it only requires consumer-grade photography equipment. Thanks to this versatility, SfM-MVS photogrammetry has been successfully used as an analytical tool to gather geologic data from outcrops at several scales. For instance, it has been applied to gather data from >100 meters outcrops by means of drones (e.g. Corradetti *et al*., 2018; Pitts *et al*., 2017), down to the scale of sub-mm fault asperities like in this work.

This study presents preliminary results of a topography (i.e. roughness) assessment of the exposed coseismic fault surfaces using SfM-MVS photogrammetry. The quantitative analysis of fault surface roughness is achieved by implementing the power spectral density (PSD), which provides an objective description of the roughness based on the frequency distribution of the asperities in the Fourier domain. This approach has been successfully applied by previous authors for describing the roughness of fractures (e.g., Ogilvie *et al*., 2006) and fault surfaces (Candela *et al*., 2009; 2012; Renard *et al*., 2013; Corradetti *et al*., 2017). The Monte Vettore fault system was analysed in two localities: Forca di Presta and Colli Alti e Bassi (see map of Pierantoni *et al*. 2013, Fig. 1). The studied fault surfaces are well-cemented and polished, and the surface coseismic displacement is recognisable at a simple view.

Methods. In this work, we present a multiphase integrated methodology for characterizing fracture surfaces. This approach combines fracture surface scanning using SfM-MVS photogrammetry, and spectral description of individual natural fault surfaces.

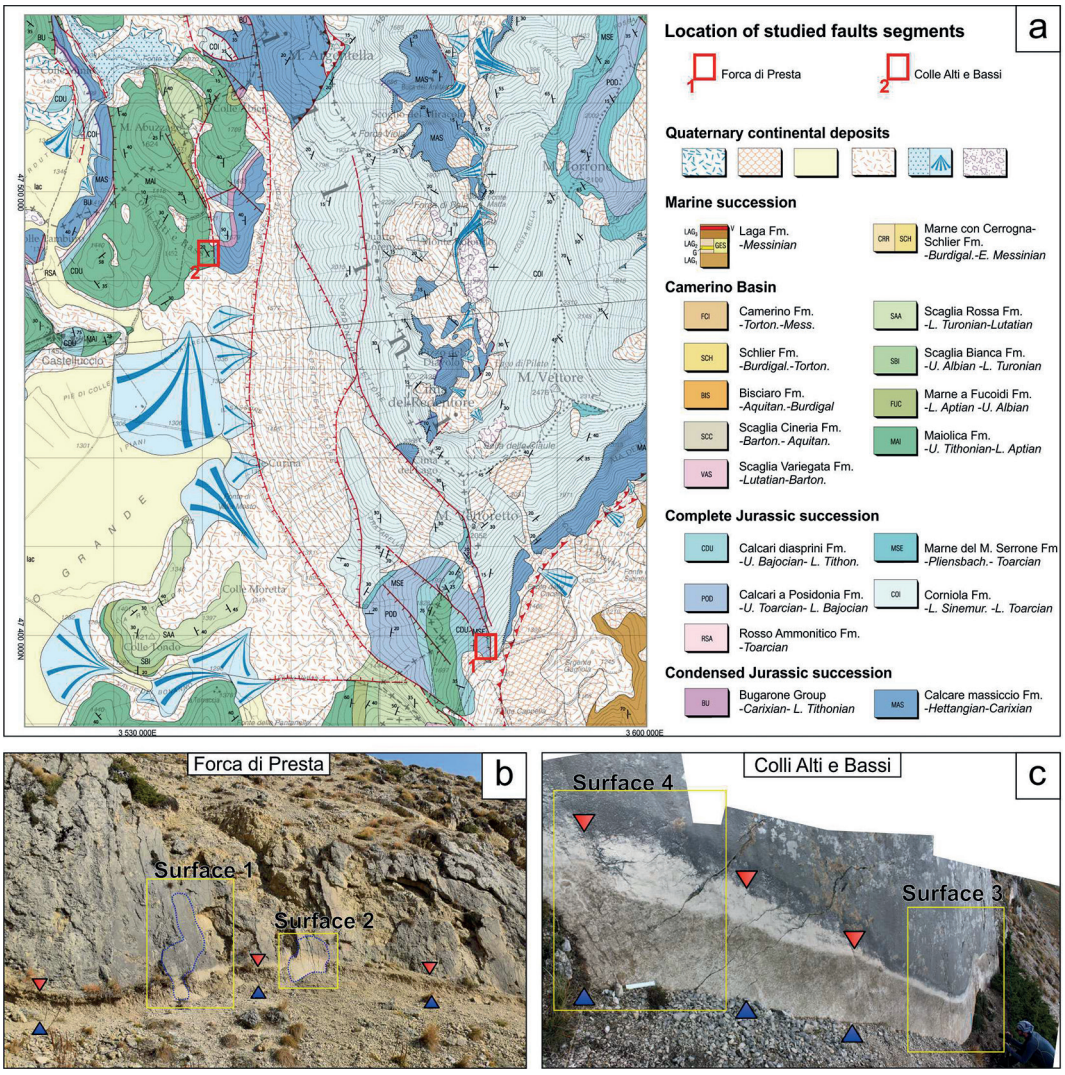

Fig. 1 - Location of the study areas: a) Geological map of the Monte Vettore area (after Pierantoni *et al*., 2013), exposed fault surfaces at b) Forca di Presta, and c) Colli Alti e Bassi.

The field-collected data consist of a series of photographs taken at different heights and positions using a tripod. Photos are acquired using a reflex camera set with low ISOs, high f/ stops (small apertures and long acquisition time) that help to sharpen the background increasing the depth of field. Photo alignment and three-dimensional model creation was achieved using the software Agisoft Photo Scan Pro (http://www.agisoft.com). For each fault surface, around 200 photos were used as input data to create the digital point cloud model. Before Power Spectral Density (PSD) analysis, trimmed patches of the point clouds were processed using an in-house MATLAB script for (i) re-orienting the surface, (ii) interpolation, and (iii) resampling in a regular grid.

For the analysis of the resampled surface topography, the PSD was used both along and perpendicular to slip direction. This provides an objective description of the roughness based on the distribution of the asperities in the Fourier domain (see Ogilvie *et al*., 2006; Corradetti *et al*., 2017; Zambrano *et al*., 2019). The PSD is a function of (wave number) k in a bi-logarithmic scale graph of a self-affine function which exhibits an apparent linear slope, defined by the

following power law equation:

$G(k) \propto a \cdot k^{-\beta}$

where the exponent of the power law β is related with the fractal dimension, D, and the Hurst number (H):

$D = (7 - \beta / 2 \quad ; \quad H = (\beta - 1) / 2$

Results and discussion. Four 3D surface models from two localities (Forca di Presta and Colli Alti e Bassi; Fig. 1) were built and analysed. Surface models contained several heterogeneities, such as fractures and striations (Fig. 1a and 1b). Faults are expected to show an anisotropic self-affine behaviour, that is, they scale differently in the slip and perpendicularly to slip directions. In agreement with Scholz (2019), this is likely to be the direct result of wear produced by friction resulting in striated surfaces (Fig. 1b). Consequently, the linear interpolation of the power spectra in a log/log graph should indicate this anisotropy in the form of a different Hurst number (Fig. 2c). Our results show that the analysed surfaces are only slightly anisotropic roughness ratio ($|H_{perpendicular}/H_{parallel}| < 1.1$). However, previous works (Candela *et al.*, 2012) considering data from kilometre to micrometre scale indicated higher roughness ratio values (near 1.33) with Hurst values equal to 0.6 and 0.8, respectively along and perpendicular to slip. From a visual inspection of the surfaces, it is possible that the low value of roughness ratio is a consequence of weathering (un-related to faulting).

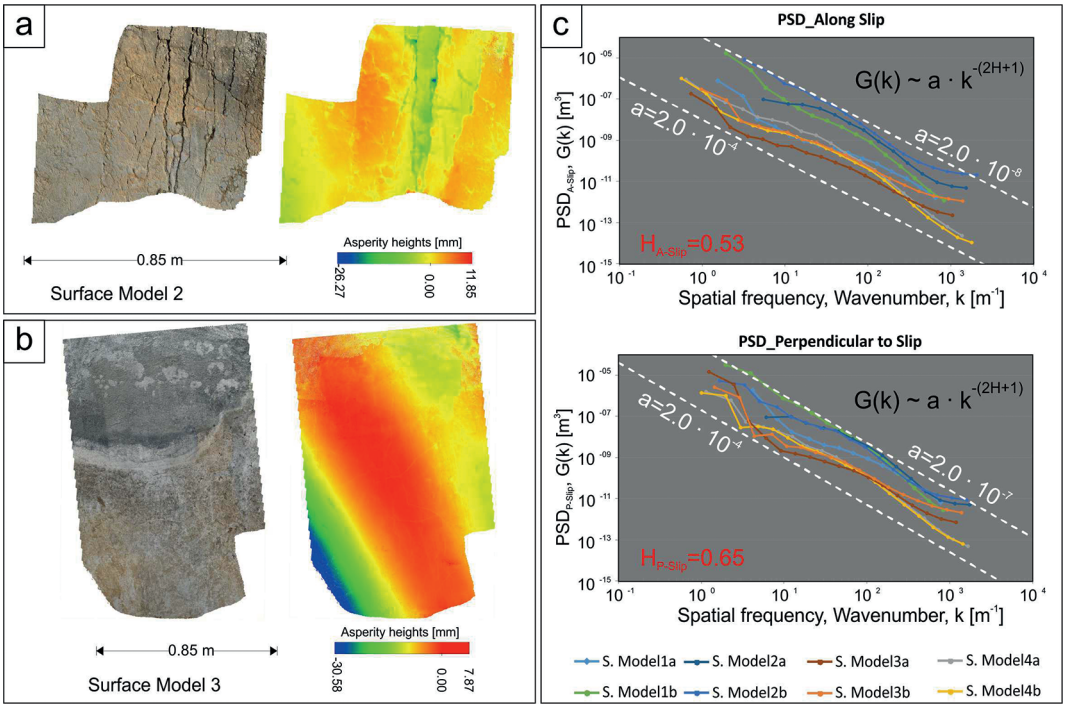

Fig. 2 - a) and b) Surface models showing different heterogeneities such as fractures and slip marks indicators, c) Power Spectral Density analysis along and perpendicular to fault slip.

A detailed evaluation of the fault roughness (avoiding fractures) indicates that roughness varies along dip. This variation could be quantified in terms of wavelength, Hurst values. A similar trend is followed by the pre-factor, a, and other indicators of the roughness based on the distance to the best fitting plane (indicating also asperity height changes). This also maybe be related to weathering of the surfaces. At the cm-scale, the roughness seems very isotropic. Therefore, the features creating anisotropy are likely to have a wide wavelength. These results

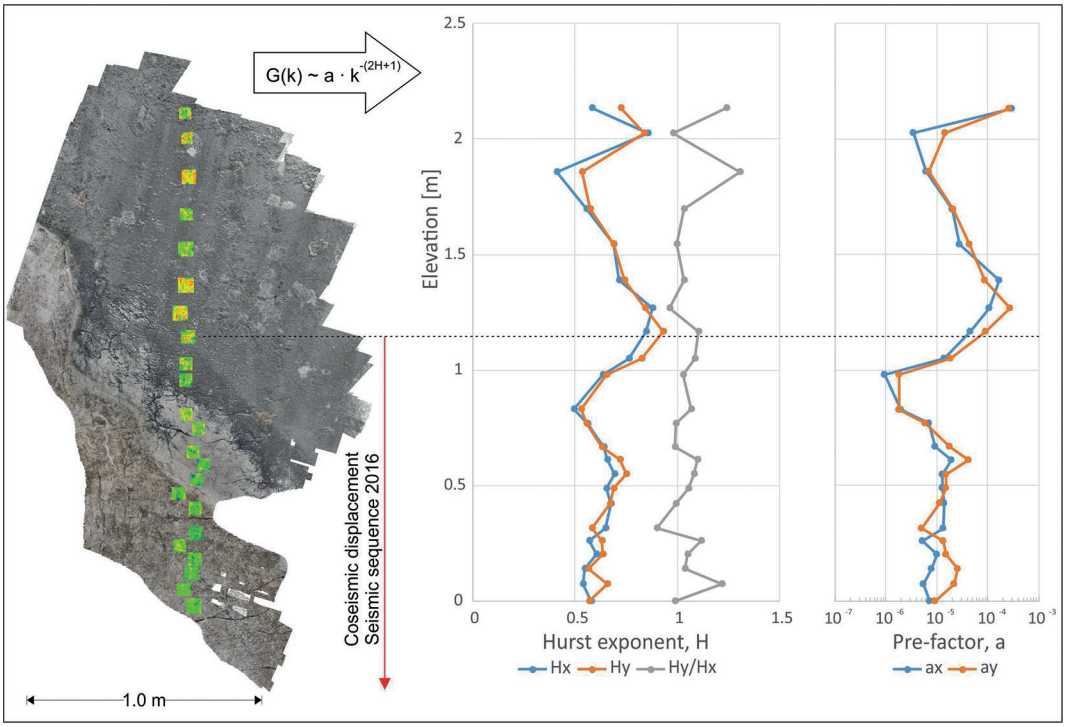

Fig. 3 - Detailed analysis of fracture roughness variation along the slip. Both parameters controlling the Power Spectral Density, Hurst exponent (H) and pre-factor (a) are varying along the slip.

open the way to the application of this method for estimating patches of faults with same exposure time (paleo-seismology).

Preliminary conclusions. Field-based SfM-MVS photogrammetry, and spectral surface analysis have been used to describe and investigate the roughness of fault surfaces recently exposed in the Monte Vettore area after the seismic sequence that hit Central Italy during 2016. Despite the preliminary nature of our investigation, results allowed us to provide the following key conclusions:

- The field-based Structure from Motion-MultiView Stereo (SfM-MVS) photogrammetry provides high quality data of the fault surface topography adapted to rough terrain conditions.
- Fracture roughness varies along dip in terms of wavelength and amplitude, likely indicating an interplay of different processes, such as wearing and weathering.
- Fault roughness is slightly anisotropic due to the presence of smooth and wide undulations (slip indicators).

References

Candela, T., Renard, F., Bouchon, M., Brouste, A., Marsan, D., Schmittbuhl, J., and Voisin, C. ; 2009: *Characterization of fault roughness at various scales: Implications of three-dimensional high resolution topography measurements*. In *Mechanics, structure and evolution of fault zones* (pp. 1817-1851). Birkhäuser Basel.

Candela, T., Renard, F., Klinger, Y., Mair, K., Schmittbuhl, J., and Brodsky, E. E.; 2012: *Roughness of fault surfaces over nine decades of length scales*. Journal of Geophysical Research: Solid Earth, 117(B8).

Corradetti, A., McCaffrey, K.J.W., De Paola, N. and Tavani, S.; 2017: *Evaluating roughness scaling properties of natural active fault surfaces by means of multi-view photogrammetry*. Tectonophysics 717, 599–606.

Corradetti, A., Tavani, S., Parente, M., Iannace, A., Vinci, F., Pirmez, C., Torrieri, S., Giorgioni, M., Pignalosa, A., Mazzoli, S.; 2018: *Distribution and arrest of vertical through-going joints in a seismic-scale carbonate platform exposure (Sorrento peninsula, Italy): insights from integrating field survey and digital outcrop model*. J. Struct. Geol. 108, 121–136. https://doi.org/10.1016/j.jsg.2017.09.009

Pierantoni, P., Deiana, G. and Galdenzi, S.; 2013: *Stratigraphic and structural features of the Sibillini Mountains (Umbria-Marche Apennines, Italy)*. Italian Journal of Geosciences 132(3), 497–520.

Pitts, A. D., Casciano, C. I., Patacci, M., Longhitano, S. G., Di Celma, C., and McCaffrey, W. D.; 2017: *Integrating traditional field methods with emerging digital techniques for enhanced outcrop analysis of deep water channel-fill deposits*. Marine and Petroleum Geology, 87, 2-13.

Renard, F., Voisin, C., Marsan, D., and Schmittbuhl, J.; 2006: *High resolution 3D laser scanner measurements of a strike-slip fault quantify its morphological anisotropy at all scales*. Geophysical Research Letters, 33(4).

Renard, F., Mair, K., and Gundersen, O.; 2012: *Surface roughness evolution on experimentally simulated faults*. Journal of Structural Geology, 45, 101-112.

Renard, F., Candela, T., and Bouchaud, E.; 2013: *Constant dimensionality of fault roughness from the scale of micro-fractures to the scale of continents*. Geophysical Research Letters, *40*(1), 83-87.

Scholz, C. H.; 2019: *The mechanics of earthquakes and faulting*. Cambridge university press. Villani, F., and Open EMERGEO Working Group; 2018: *A database of the coseismic effects following the 30 October 2016 Norcia earthquake in Central Italy*. Science Data. 5, 180049. Zambrano, M., Pitts, A.D., Salama, A., Volatili, T., Giorgioni, M. and Tondi, E.; 2019: *Analysis of Fracture Roughness Control on Permeability Using SfM and Fluid Flow Simulations: Implications for Carbonate Reservoir Characterization*. Geofluids 2019, 1–19.

THE POST-SEISMIC EFFECTS OF THE FIANDACA PENNISI-PENNISI SHEAR ZONE, DECEMBER 26TH 2018 (MT. ETNA VOLCANO)

G. De Guidi[1,2], G. Barreca[1,2], D. Bella[6], F. Brighenti[1,2], V. Bruno[5], F. Carnemolla[1,2], A. Figlioli[1], M. Mattia[5], M. Menichetti[3,4], R. Pettinato[6], M. Roccheggiani[3,4], L. Scarfì[5], G. Tringali[6], C. Monaco[1,2]

[1] Department of Biological, Geological and Environmental Sciences, University of Catania, Catania, Italy
[2] CRUST, UR-UniCT, Catania, Italy
[3] Department of Pure and Applied Sciences (DiSPeA), University of Urbino Carlo Bo, Urbino, Italy
[4] CRUST, UR-Chieti, Italy
[5] INGV Etna Observatory, Catania, Italy
[6] Freelance geologist

Introduction. On 26th December 2018 the eastern slope of the Mt. Etna volcano was affected by a seismic sequence with maximum magnitude of 4.8 with epicenter located at about 4 km NE from the village of Viagrande at a depth of about 0.3 km (Gruppo Analisi Dati Sismici; 2019) (Fig. 1). The earthquake was preceded by a seismic swarm on the upper south-western sector of the volcano and by an eruptive event in the summit area, occurred on 24th December 2018 (Gruppo Analisi Dati Sismici; 2019). and the crustal deformation related to the active intrusion of a dike, triggered the seismic reactivation of tectonic structures of Mt.Etna's eastern flank.. The Fiandaca Pennisi- fault, one of the most seismically active shear zones belonging to the upslope extension of the Timpe fault system was reactivated, indeed, few hours after that intrusion in the SE flank of Mount Etna. This fault extends for about 8 km long with a NNW-SSE trending, the southern tip of the fault is located in the city of Acireale whereas the northern tip reaching the village of Fleri (Fig. 1).

In this work, we focus on a re-analysis of data collected during this seismic crisis and we show some results of a multidisciplinary dataset on: i) analysis of historical and instrumental seismicity, ii) mapping of historical and last coseismic fracturing, iii) analysis of geodetic (GPS and InSAR) data.

Analysis of historical and instrumental seismicity. We analysed the seismicity occurred in the southeastern sector of the volcano, within few kilometers from the Fiandaca Pennisi fault, during the period November 2018 - February 2019. The events recorded by the INGV seismic network (http://sismoweb.ct.ingv.it/index.php; Gruppo Analisi Dati Sismici, 2019) were located by using the code TomoDDPS (Zhang *et al*., 2009) and the 3D velocity model by

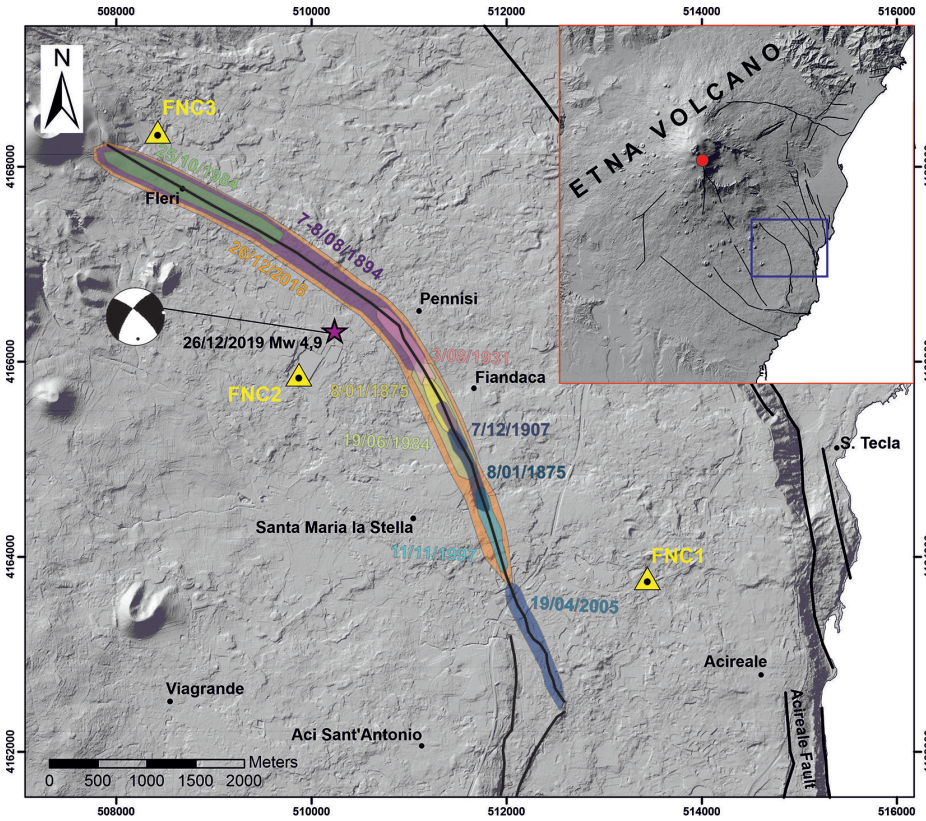

Fig. 1 - DEM of the area affected by the fault. Coloured areas show the coseismic ground fractures of historical earthquakes of Fiandaca Pennisi fault. Yellow triangles indicate the benchmarks of GNSS positioning UNICT_NET framework; the star indicate the epicentre of 26th December 2019 earthquake with relative focal mechanism.

Alparone *et al*. (2012), results denote formal location uncertainties in the order of 200 m both in horizontal and vertical directions.

Locations and event time-occurrence point out that the activity of that fault during the considered period is substantially related to the strongest earthquake (MW 4.9), on December 26th. The hypocenter of this event is very close to the cosismic fractures identified at the surface and his focal mechanism (Fig. 1) (http://sismoweb.ct.ingv.it/focal/; see Scarfì *et al*., 2013) indicates a dextral strike slip movement on a sub-vertical NW-SE oriented plane. After that shock, most of the seismicity in the sector moves at about 1 km east of the northern tip of the Fiandaca Pennisi fault with hypocentres 1-3 km deep. The focal solution of a ML 2.5 event, indicating normal movement on a NE-SW plane, would suggest the activation of neighboring structures (Monaco *et al*., 2019).

Coseismic fractures. The fracture zone extends for about 8 km through the village centres and rural countryside with average direction changing from N150° E to N130° E from southeaster to the north western sector of the shear zone (Fig. 1). The damage mainly consists of shallow and deep cracks affecting the soil surface, walls of buildings (both infilling and bearing walls), fractures and rotations of retaining walls, sidewalks, curbs and pavings. Fractures and cracks are usually aligned along bands with variable width ranging from 2 to more than 40 m. The width is highly variable ranged between 10 and 110 mt. Fractures are systematically arranged and their orientation provides important information to infer the kinematics of the main fault zone. Fractures measured have been interpreted as Riedel's R or T type fractures in a right lateral shear zone (Riedel, 1929; Mercier and Vergely, 1996). The average direction of T-type cracks

changing from N140° E to N30°÷40° E from southeaster to northwestern sector of the shear zone (Fig. 2). We analyzed the historical seismicity of the Fiandaca Pennisi fault during the last 150 years, finding 15 earthquakes occurred in different segments of the fault line, the major ones in: 7th and 8th August 1894, 19th June and 25th October 1984. The coseismic effects related to the 26 December 2018 and August 1894 earthquakes show similarities (Fig. 1).

Geodetic data. The day after the seismic event, the GEOdynamic and GEOmatic Lab. group of the University of Catania, started the survey of ground deformation related to the earthquake of December, 26 2018 following the method already shown in De Guidi *et al*. (2017).We realized 3 geodetic benchmarks along the shear zone, extending the UNICT_NET network (De Guidi et., 2018), The posteismic slip of the Fiandaca Pennisi fault resulted in a mainly horizontal movement of more than 12 cm towards WNW and 10 cm towards ESE directions (Fig. 3) (Fig. 2).

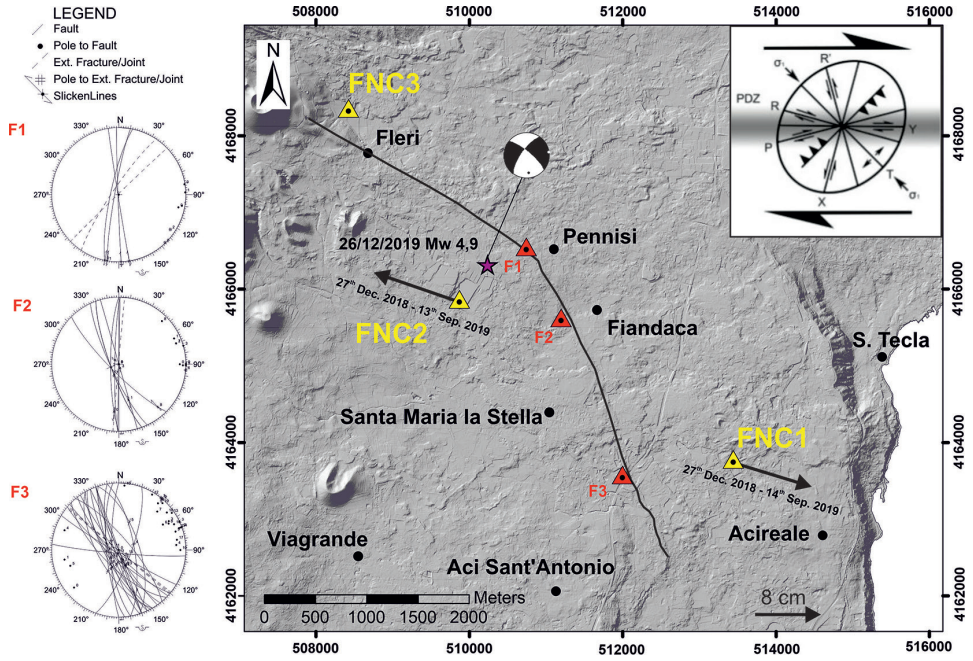

Fig. 2 - DEM of the area affected by the fault. F1, F2 and F3 are the location where the structural surveys were carried out. The movements of FNC2 and FNC1 benchmarks (UNICT-NET) are shown.

The INGV GNSS network collected data from 34 permanent stations located all around the volcano, showing intense deformative effects also to relatively low heights. These data clearly demonstrate that the active intrusion is related to a tensile effect of an intruded dike at sea level or few hundreds of meters below (Mattia *et al*., submitted). GNSS data, recorded from one year before the eruptive event since after the intense intrusive phase, indicate three distinct phase: i) volcanic inflation, ii) high deformation sequence associated with the intrusion of the dyke, iii) increasing and extension overtime of velocity field along eastern volcano slope.

Interferometric data (InSAR) were further used to support previous investigations and to better define geometric and the associated developed deformation zone. The high-resolution interferograms were obtained by Observation of Progressive Scans (TOPS) mode from the Sentinel-1 satellite, which provide high-quality Synthetic Aperture Radar images illuminating the shear zone in a time range straddling the seismic event (Fig. 3).

We have investigated the surface earthquake effects by means of SAR interferometry using the European Space Agency (ESA) Sentinel-1 A&B satellites acquisitions (C-band). For the

differential synthetic aperture radar interferometry (D-InSAR) processing we used the open source Sentinel Application Platform (SNAP) toolbox.

The coseismic slip of the Fiandaca Pennisi fault resulted in a mainly horizontal movement of more than 15 cm towards W and 20 cm towards E directions in the LOS direction (Fig. 3). Small-scale deformations patterns are detected also along the other faults of the eastern and southern side of the volcano, where aseismic slip occurred inside the timespan of the interferogram. Many discontinuities are easy detectable even from the wrapped phase thanks to the high final coherence achieved. With Sentinel-1 data along the Fiandaca Pennisi fault we have produced the differential interferograms (DESCENDING geometry). This wrapped interferogram is overlaid on the result of a filter that enhances the visibility of linear discontinuities, corresponding to faults and ground ruptures. This filter has been applied to the unwrapped interferogram. Along the main fault, the strong coseismic displacement is responsible for the decorrelated signal. However, the southern branches of the fault are clearly visible. The SAR results can be useful as a field mapping guide.

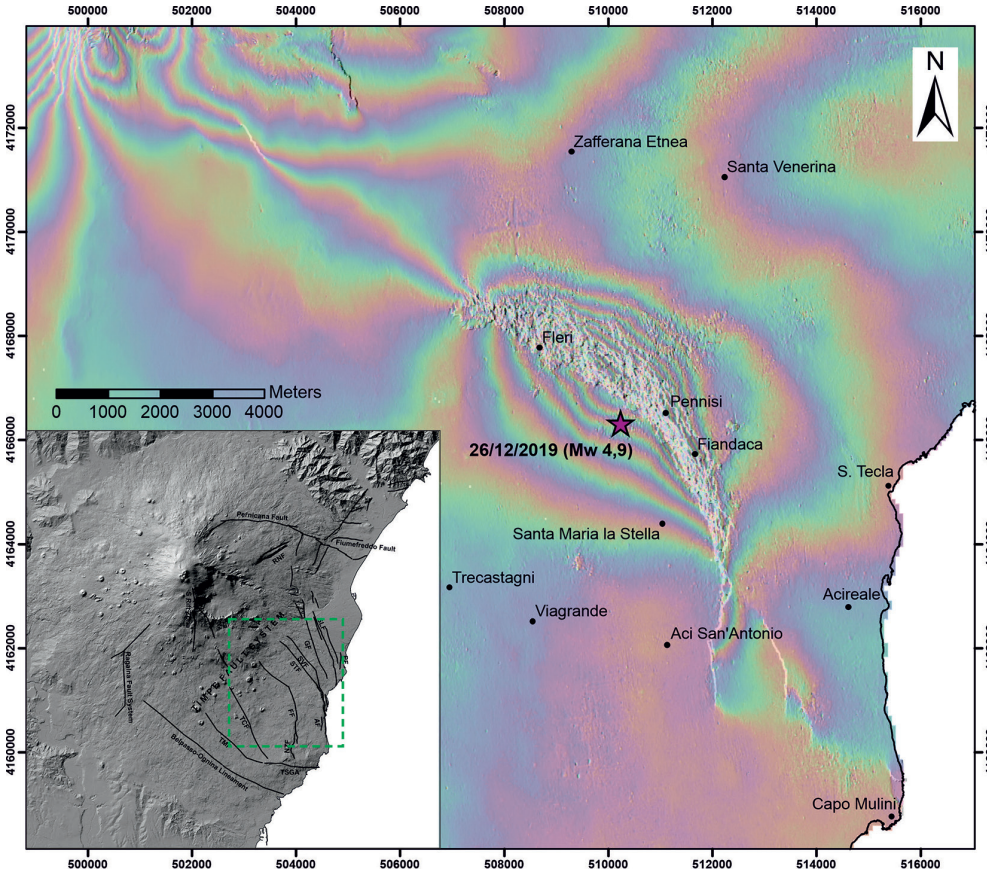

Fig. 3 - Differential interferograms (DESCENDING geometry) with on transparency the unwrapped interferogram where the jumpes of fringe are highlighted by a filter. Each colour cycle (red-blue-yellow) represents approximately 3 cm of motion in the radar line of sight.

Conclusion. Our data suggest that a dike intruded at sea level and the consequent widespread deformation the eastern slope of Mt. Etna Volcano has perturbed and concentrate local stress field along the margin of major tectonic discontinuities (Griffith 1921; Tsuchida and Nakahara, 1970; Soutas-Little, 1973; Boresi and Sidebottom 1985) triggering coseismic and

aseismic deformation of the Fiandaca Pennisi shear zone on 26 December 2018, M = 4.9 and Pernicana Fault on 9th January 2019 M = 4.1). The remote survey allowed us to better define the geometry of the Fiandaca Pennisi Fault, characterised by trending N130° E in the north-western portion and N160° E in the southern part. Morphostructural analysis data coupled with satellite interferometric information indicate very detailed distribution of surface deformations with structures interpreted as Riedel's R or T type fractures in a right lateral shear zone. From the kinematic point of view, both morphostructural and seismological data, accompanied by geodetic information, indicate a dextral strike slip movement with WNW-ESE extensional component. The developed Co-seismic rupture length (Gudmundsson *et al*., 2013), corresponds to modelled seismogenic thickness with maximum rupture lengths of about 6–6.5 km (De Guidi *et al*., 2012).

The analysis of the results highlighted the relationships between the behaviour of thinned seismogenic layer and surface field deformation along well-known fault systems. Future objectives will be to characterise slow damage effect induced by anomalous long-term post seismic surface deformation.

References

Alparone S., Barberi G., Cocina O., Giampiccolo E., Musumeci C. and Patanè D.; 2012: *Intrusive mechanism of the 2008-2009 Mt. Etna eruption: constraints by tomographic images and stress tensor analysis*. Journal Volcanology Geothermal Research, 229, 50-63. https://doi.org/10.1016/j.jvolgeores.2012.04.001.

Boresi A. P., Schmidt R. J. and Sidebottom, O. M.; 1985: *Advanced mechanics of materials (Vol. 6)*. New York *et al*.: Wiley.

De Guidi G., Scudero S. and Gresta S.; 2012: *New insights into the local crust structure of Mt. Etna volcano from seismological and morphotectonic data*. Journal of Volcanology and Geothermal Research, 223, 83-92.

De Guidi G., Vecchio A., Brighenti F., Caputo R., Carnemolla F., Di Pietro A., Lupo M., Maggini M., Marchese S., Messina D., Monaco M. and Naso S.; 2017: *Brief communication: Co-seismic displacement on 26 and 30 October 2016 (M w= 5: 9 and 6.5) - earthquakes in central Italy from the analysis of a local GNSS network*. Natural Hazards and Earth System Sciences, 17(11).

De Guidi G., Brighenti B., Carnemolla F., Imposa S., Marchese S. A., Palano M., Scudero S. and Vecchio A.; 2018: *The unstable eastern flank of Mt. Etna volcano (Italy): First results of a GNSS-based network at its southeastern edge*. Journal of Volcanology and Geothermal Research, 357, 418-424.

Griffith A. A; 1921: *VI. The phenomena of rupture and flow in solids*. Philosophical transactions of the royal society of london. Series A, containing papers of a mathematical or physical character, 221(582-593), 163-198.

Gruppo Analisi Dati Sismici; 2019: *Catalogo dei terremoti della Sicilia Orientale - Calabria Meridionale (1999-2019)*. INGV, Catania

Mercier J., and Vergely P.; 1995: *Tettonica: lezioni di geologia strutturale*. Pitagora.

Monaco C., Barreca G., Brighenti F., De Guidi G., Carnemolla F., Mattia M., Menichetti M., Roccheggiani M. and Scarfi L.; 2019: *Multidisciplinary survey methods of the Fiandaca Pennisi-Pennisi fault zone reactivated during the 26th December 2018 coseismic and postseismic event*. Tools, Data and Models for 3D Seismotectonics: The Italian over Time Laboratory - A "CRUST" INTERDISCIPLINARY WORKSHOP IN MEMORY OF GIAMPAOLO PIALLI. Perugia, 9-10 July 2019.

Riedel W.; 1929: *Zur Mechanik geologischer Brucherscheinungen ein Beitrag zum Problem der Fiederspatten*. Zentbl. Miner. Geol. Palaont. Abt., 354-368.

Scarfì L., Messina A., Cassisi C.; 2013: *Sicily and Southern Calabria focal mechanism database: a valuable tool for the local and regional stress field determination*. Annals of Geophysics, 56, 1, https://doi: 10.4401/ag-6109.

Soutas-Little R. W; 1973: Elasticity Dover Publications Mineola.

Tsuchida E. and Nakahara I.; 1970: *Three-Dimentsional Stress Concentration around a Spherical Cavity in a Semi-Infinite Elastic Body*. Bulletin of JSME, 13(58), 499-508.

Zhang H., Thurber C. and Bedrosian P.; 2009: *Joint inversion for Vp, Vs, and Vp/Vs at SAFOD, Parkfield, California*. Geochem. Geophys. Geosyst. 10 (Q110032), https://doi.org/10.1029/2009GC002709.

GRAVITATIONAL SLOPE DEFORMATION VS. NORMAL FAULTS: DIFFERENT HAZARDS, SIMILAR MICROSTRUCTURES?

L. Del Rio[1], M. Fondriest[1], M. Moro[2], M. Saroli[3], S. Gori[2], E. Falcucci[2], E. Spagnuolo[2], G. Di Toro[1,2]
[1] Dipartimento di Geoscienze, Università degli Studi di Padova, Italy
[2] Istituto Nazionale di Geofisica e Vulcanologia (INGV), Roma, Italy
[3] Università degli Studi di Cassino, Italy

Introduction. Carbonate-built rocks of the Central Italian Apennines are cut by fault zones consisting of sharp slip surfaces bounding up to few cm thick principal slip zones (PSZs) surrounded by up to hundreds of meter-thick damage zones. Recent paleo-seismological, geological and geomorphological observations pointed out that the PSZs may accommodate either large landslides (Deep-Seated Gravitational Slope Deformation: DGSD, Galadini, 2006; Moro *et al*., 2012; Gori *et al*., 2014, Saroli *et al*., 2017) and seismic or aseismic crustal scale fault deformation (Normal Faults: NF). Clearly, the distinction between DGSDs and NFs structures based on field and microstructural observations and the individuation of the processes forming the PSZs is of outstanding relevance in geological hazard studies. Currently, most of the sharp slip surfaces exposed in the Italian Central Apennines are mapped as active normal faults, even if the presence of peculiar geomorphological structures (trenches, double crest scarps, counterscarps) would suggest a gravitational origin for some of them.

Depending on the geological process (DGSD vs. NF), the slip surfaces and associated slipping zones reach different depths along dip (100-1000 m for DGSD, 10-12 km for NF), and are formed and active over a different range of temperatures (0-30 °C for DGSD vs. 0-80°C for NF), pressures (< 20 MPa for DGSD, 0 to 100 MPa for NF) and slip rates (usually < 10^{-3} m/s for DGSD, up to ~1 m/s for NF). Such large differences in loading conditions should result in the formation of distinctive secondary fault/fracture networks in the damage zones, possibly recognizable at the outcrop scale or in the microstructures of the slipping zones. Here we discuss the fault/fracture structural networks and the microstructures associated to both DGSDs and NFs by conducting (1) extensive field structural-geology surveys and (2) high-resolution microstructural studies on the PSZs and associated wall rocks.

Geological setting and case studies. The rocks outcropping in the selected area of the Central Apennines (Fig. 1a) consist of Jurassic-Cretaceous shallow-water to basin limestones and dolostones plus Plio-Pleistocene cemented conglomerates and Quaternary fluvio-lacustrine deposits. Because of the different mechanical properties (Young modulus, friction coefficient, fracture toughness, cohesion, etc.) of these rocks, we selected scarps of faults and DGSD cutting similar rocks to reduce the role of rock composition and fabric in controlling the fracture pattern and the microstructures of the slipping zones.

Though paleo-seismological and geomorphological studies suggest that some structural features are mainly associated to DGSDs while other to seismic faulting, some scarps of active seismogenic faults were thought to accommodate also DGSD (Moro *et al*., 2012; Gori *et al*., 2014). Because of the continuum between the NF and DGSD fault/fracture structural networks, we selected the following case studies (underlined: field surveys and microstructural investigations completed; numbers refer to the boxes in Fig. 1a):

1. **Valle Force Fault (VFf)**, anthitetic normal-fault bordering a small intra-mountain basin. This ~1 km in length normal fault cuts shallow-water limestones and Pleistocene carbonate breccias.
2. **Campo Felice Fault (CFf) (length ~15 km, slip rate ~0.8-1.3 mm/yr) vs. Monte Ocre fault-DGSD (Of)**. The latter is geometrically linked to the Campo Felice Fault and was reactivated as DGSD. Similar host rocks: shallow-water wackestone carbonates.
3. **Rocca Preturo Fault (RPf) (length~10 km, slip rate ~0.23-0.34 mm/yr) vs. Sant'Erasmo (SAE) DGSD**. The latter is a small antithetic fault at the footwall of the Rocca Preturo Fault and was reactivated as DGSD. Similar host rocks: rudstones with intercalated marls.
4. **Alto di Cacchia (AC) DGSD**. This ~500 m long scarp is considered a pure DSGD (end

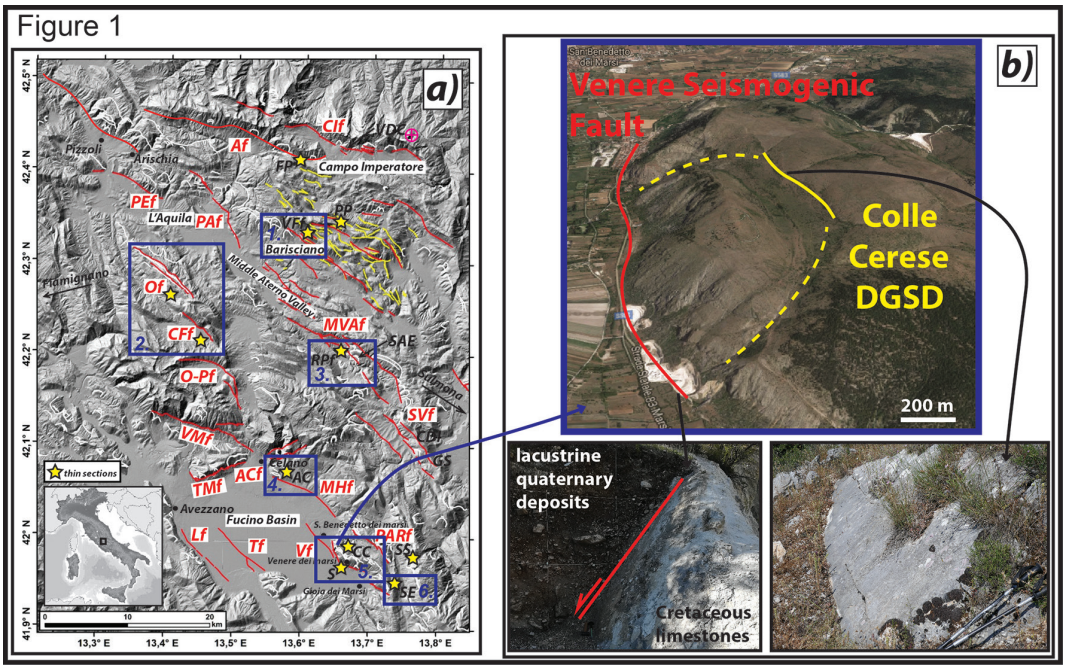

Fig. 1 - Deep-Seated Gravitational Slope Deformations (DGSDs) and Normal Faults (NFs) in the Italian Central Apennines. a) Map of the DGSDs (white in color), Normal Faults (NFs, red in color) and minor faults bordering intra-mountain basins (yellow in color). Yellow stars are the sampling sites of the studied fault rocks. The selected cases are in the blue boxes (see also list and acronyms in main text). b) Example of the case of study Venere Fault (Vf) vs. Colle Cerese (CC) DGSD. Sharp slip surfaces are present in both the Vf and in the CC.

member of the continuum between NFs and DSGD) and cuts the < 500 m thick Medium Pleistocene in-age conglomerates.

5. **Santilli (Venere) Fault (Vf) (length~10 km, slip rate ~0.4-0.5 mm/yr) vs. Colle Cerese (CC) DGSD**. The latter is a minor fault at the footwall of the Santilli Fault and reactivated as DGSD. Similar host rocks: shallow-water wackestone carbonates;
6. **Serrone (SE) DGSD.** Minor anthitetic fault at the footwall of the Gioia dei Marsi Fault and reactivated as DGSD. This ~500 m long scarp cuts Cretaceous rudstones.

The field work consisted in the collection of structural data (bedding, faults, fractures, veins, etc.) and geological mapping at 1:500 scale by exploiting aerial photos and drone images as topographic maps. Eighteen slip surfaces and slip zones from 14 main scarps were investigated with the SEM CamScan MX3000 (resolution 200-300 nm) installed at the Dipartimento di Geoscienze (Padua, Italy) and with the FESEM Merlin Zeiss (resolution 1-2 nm) installed at CERTEMA (Grosseto, Italy).

Results and discussion. Here below the main results from the field work and microstructural investigations conducted on the four selected cases underlined above so far:

Field structural data. **Alto di Cacchia («end-member» DGSD).** The scarp (main slip surface) is steeply dipping (~70°) and is discontinuous and undulated along strike and cuts sub-horizontal conglomerate strata. About one hundred joints and secondary slip surfaces were measured in the footwall and hangingwall of the main slip surface. Most of the joints are sub-vertical and opened (from 1 to 10 cm) (Fig. 2). According to the Mohr-Coulomb-Griffith's failure envelope, such a fracture distribution is consistent with low confining pressures at the time of joint formation and slip.

Valle Force Fault (minor fault bordering a small intra-mountain basin). The scarp (main slip surface) dips on average ~45°. The over 200 fractures and minor faults measured along the

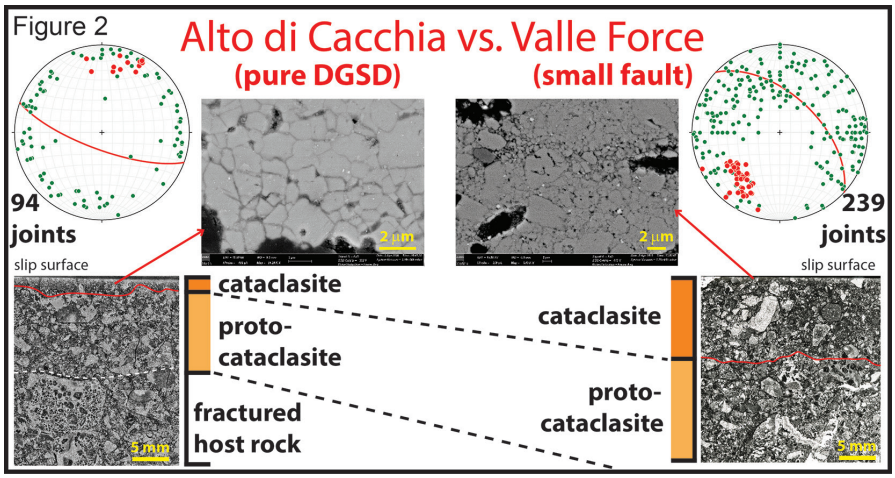

Fig. 2 - Comparison between the macro- and micro-structural observations of the Alto di Cacchia (AC) DGSD (the DGSD end-member case) and the Valle Force (VF) minor fault. The AC is characterized by opened joints dipping at high angle (>75°) and by a thin (~3 mm thick) cataclastic PSZ. Instead, the VF is characterized by a higher dispersion of the attitude of the joints in the footwall (i.e., they dip both at low and high angles), and by a thick cataclastic PSZ. At the micro- to nano-metric scale (SEM and FESEM backscatter images), the matrix of the PSZs of both the AC and the VF consist of highly packed calcite nanograins possibly resulting from sintering and solution creep processes.

footwall are often conjugated and range in dip from 80° to 45°, thus possibly associated to higher confining pressures during formation and slip with respect to the Alto di Cacchia DGSD end-member case (Fig. 2).

Sant'Erasmo (minor antithetic fault at the footwall of a main seismogenic fault and reactivated as DGSD). The about 400 m long scarp is steeply dipping (~70°) and includes secondary scarps at the hangingwall forming small trenches. The Sant'Erasmo DGSD is hosted in the footwall of the Rocca Preturo 10 km long normal fault and includes opened subvertical joints but also lower angle conjugate fractures cutting the main scarp. This fracture pattern could be related to gravitational reactivation of pre-existing secondary faults and fractures of the damage zone of the Rocca Preturo seismogenic fault.

Serrone DGSD (minor antithetic fault at the footwall of the Gioia dei Marsi Fault). The scarp is about 500 m long along stirke, discontinuous and with sinistral *en-èchelon* step-overs. The dip ranges from over 70° at the scarp tips to about 45° in the central section, where the scarp appears more polished and less karstified. As for the Sant'Erasmo DGSD, this structure is located at the footwall of a main seismogenic fault (the Venere-Gioia dei Marsi Fault) and opened sub-vertical joints (with spacing larger than 20 cm) and conjugate fractures were found.

Microstructural investigations. ***Optical microscope*** observations of the PSZs of end-member cases (i.e., shallow and small DGSD cutting Quaternary deposits like the **Alto di Cacchia DGSD)** vs. large NF producing > Mw 6.5 earthquakes like the **Venere Fault)** and intermediate cases (i.e., NF reactivated as DGSD: **Valle Force Fault**) have shown systematic differences in the deformation style and microstructural maturity (Fig. 2). The slipping zones associated to the NF are dominated by cataclastic to ultracataclastic fabric (*sensu* Sibson, 1977), including well-defined and cm-thick PSZs. Instead, the slipping zones associated to the DGSDs consist mainly of protocataclasites or crush breccias and cataclasites are extremely thin or absent.

Instead, ***Scanning Electron Microscope*** observations of the matrix of the cataclasites of the PSZs both NF and DGSD reveal that the matrix is formed by micrometer to nanometer in size highly-packed calcite grains, sometimes with foam-like fabric, and cut by stylolites (Fig. 2). These microstructures could be the result of cataclastic processes plus diffusive mass transfer (pressure solution and precipitation) and sintering processes. Sintering is a thermally-activated

densifying process mainly accommodated by diffusion mechanisms (i.e., grain boundary and volume diffusion) (Rahaman, 2003). Sintering is divided in three main stages (initial, intermediate and final), where the packing density (i.e., the ratio between the volume of solids and the total volume) increases till over 0.9 by rearranging and shrinking of initial spherical particles. Textures possibly associated to the final stage of sintering have been recognized in both Venere Seismogenic Fault and in the Alto di Cacchia DGSD. Irregular grain boundaries and indentation structures due to pressure-solution processes were identified in the slipping zones of Colle Cerese and Monte Ocre DGSDs and in the Campo Felice and Valle Force NF. Here, clay minerals and oxides, which limit the grain boundary mobility by pinning mechanisms (Olgaard and Evans, 1986), define the stylolites.

Conclusions. In the Italian Central Apennines, some of the polished and sharp slip surfaces cutting carbonate rocks may be related to both seismic faulting or deep-seated gravitational landslides. The structural data of the Alto di Cacchia DGSD (which include open fractures dipping at high angle) suggest a shallower formation depth of this structure with respect to the Valle Force Normal Fault, which, instead, includes conjugate shear fractures dipping from medium to high angles (stereograms in Fig. 2).

Under the optical microscope, the PSZs of the scarps associated to normal faults are thicker and less deformed than those associated to DGSDs. However, at the micro-metric scale, the microstructures found in the PSZs are very similar in NFs and DGSDs, suggesting the activation of grain-size dependent and diffusive-type processes.

According to the dataset presented here, we conclude that the structural and microstructural features relative to the analyzed DGSDs represent important factors in their characterization when integrated with geomorphological and paleoseismological observations.

References

Galadini, F., 2006. Quaternary tectonics and large-scale gravitational deformations with evidence of rock-slide displacements in the Central Apennines (central Italy). *Geomorphology* 82, 201–228.

Gori, S., Falcucci E., Dramis F., Galadini F., Galli P., Giaccio B., Messina P., Pizzi A., Sposato A., Cosentino D., 2014. Deep-seated gravitational slope deformation, large-scale rock failure, and active normal faulting along Mt. Morrone (Sulmona basin, Central Italy): Geomorphological and paleoseismological analyses. *Geomorphology* 208, 88–101.

Moro, M., Saroli, M., Gori, S., Falcucci, E., Galadini, F., Messina, P., 2012. The interaction between active normal faulting and large scale gravitational mass movements revealed by paleoseismological techniques: a case study from central Italy. *Geomorphology* 151 (152), 164–174.

Olgaard, D., Evans, B., 1986. Effect of Second-Phase Particles on Grain Growth in Calcite. *J Am Ceram Soc* 69, 272-277.

Rahaman. M., 2003. Ceramic processing and Sintering, 2nd edition

Sibson, R., 1977. Fault rocks and fault mechanisms. Journal of the Geological Society 133, 191-213.

Saroli M., Lancia M., Moro M., Falcucci E. Gori S., 2017. Individuazione e rappresentazione delle Deformazioni Gravitative Profonde di Versante della Regione Abruzzo. Convenzione di Ricerca tra DICeM e INGV, Progetto MIUR-FIRB "Abruzzo", Prot. N. 12281/04-07-2017.

BEFORE, DURING AND AFTER THE AMATRICE EARTHQUAKE (24 AUGUST 2016): A RECORD OF CHANGES IN THE GRAN SASSO GROUNDWATER

G. De Luca[1], G. Di Carlo[2], M. Tallini[3]

[1] Istituto Nazionale di Geofisica e Vulcanologia – Osservatorio Nazionale Terremoti, L'Aquila
[2] Istituto Nazionale di Fisica Nucleare – Laboratori Nazionali del Gran Sasso, L'Aquila
[3] Università degli Studi dell'Aquila – Dipartimento di Ingegneria Civile, Edile-Architettura e Ambientale, L'Aquila

Chemical and physical groundwater parameters are monitored in seismogenic areas worldwide, principally by measuring and analysing water level and hydrochemistry changes in wells, springs and streams to find possible correlations with local and regional seismicity and between their spatial and temporal variations and strain processes (Manga and Wang, 2015 and references therein). Moreover, in the past few decades many studies have suggested a connection between fault mechanics and underground fluid dynamics, and a large quantity of experimental results and models have appeared in the literature (Barnhoorn *et al*., 2010; Di Toro *et al*., 2011; Violay *et al*., 2013; Hirth and Beeler, 2015; Sibson, 2000; Scuderia *et al*., 2017). In this framework, starting from May 2015, we have performed continuous recording of the hydraulic pressure, of deep groundwater in the 190 m-long horizontal S13 borehole drilled next to the underground *INFN* laboratories (*LNGS*), located in the core of the Gran Sasso carbonate aquifer below a 1,400 m-thickness of rock. The aquifer is located in a seismically active area, as demonstrated by the 6 April 2009, Mw 6.3 L'Aquila earthquake and by the recent 24 August 2016, Mw 6.0 Amatrice earthquake. The distance of Amatrice earthquake location from our S13 borehole is about 39 km.

A seismographic station of the national seismic network of Istituto Nazionale di Geofisica e Vulcanologia (INGV) is located about 250 m from the S13 borehole inside the national underground laboratory of Gran Sasso (LNGS-INFN). The station (international code: GIGS) was deployed in the framework of the GINGER experiment and is equipped with a Nanometrics Trillium 240 s (see http://cnt.rm.ingv.it/en/instruments/station/GIGS for further details). The area is also monitored by a dense regional seismic network (De Luca, 2011).

Our experimental equipment includes a 3-channels 24-bit ADC (mod. SL06 by Sara Electronic Instruments – http://www.sara.pg.it/) set up in continuous local recording. We started data acquisition on 1 May 2015 by continuous high-frequency sampling (10-50 Hz) of hydraulic pressure (De Luca *et al*., 2016; De Luca *et al*., 2018). This experimental system is still in acquisition. During these last 4 years of continuous recording (May 2015 – September 2019) the hydraulic pressure signal showed the annual cycle of charge and discharge of the aquifer and follows the sun/moon tides, as expected (De Luca *et al*., 2018). Furthermorer during

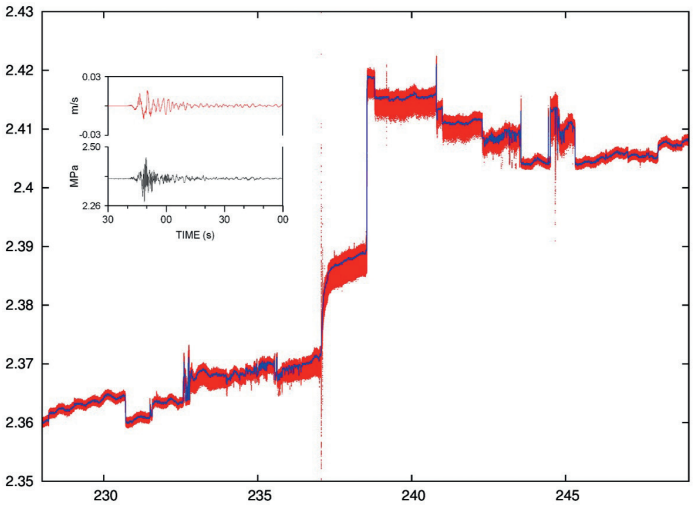

Fig. 1 - Plot of the hydraulic pressure (in MPa) at 20 Hz sampling rate (15 August, 228 doy to 4 September, 248 doy, 2016). The blue line represents the 60 s moving average. The box shows the enlargement of the signal corresponding to the Amatrice earthquake, 24 August, 01:36:32 UT, 237 doy, (Mw 6.0); the red line represents the vertical component of broadband seismic station (*GIGS*) equipped with a Trillium 240 s seismometer; the black line is the hydraulic pressure expressed in MPa. The time scale starts from 01:36:30 (UT) of 24 August 2016.

this underground groundwater monitoring the data has revealed the existence of an aquifer behaviour characterized by very high dynamics. The data collected during these 4 years turned out to be quite a useful tool to a) characterize the background in the groundwater monitoring, and b) identify more clearly the observed anomalies and the possible link with deformation phenomena of tectonic interest. In this respect, the anomalies observed in the hydraulic pressure before the 24 August 2016, Amatrice earthquake are definitely impressive (De Luca *et al*., 2018). Fig. 1 shows unprocessed data (at a 20 Hz sampling rate) of the hydraulic pressure from 19 August to 5 September 2016 with a 60 s moving average (blue line). The presence of average information emphasizes the structural change of the signal (asymmetry). The novelty coming from our time series of hydraulic pressure concerns the presence of unambiguous signals starting about 5 days before the main shock of 24 August (De Luca *et al*., 2018). To investigate in a quantitative fashion these rather unexpected phenomena we performed an elementary statistical analysis of the pressure time series looking at the first moments of full time-series. More specifically, after subtracting the (60 s) moving average we evaluated the variance (m2), the skewness m3/(m2)3/2 and the kurtosis (m4/m22 – 3) of the resulting distribution, see Fig. 2 (De Luca *et al*., 2018).

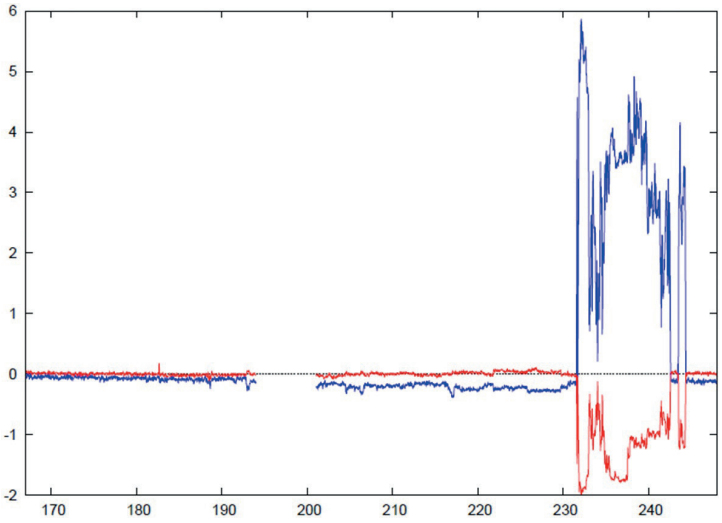

Fig. 2 - Statistical analysis: Kurtosis (blue) and Skewness (red) values from 15 June 2016 (167 doy) to 4 September 2016 from hydraulic pressure data. The statistical indicators are evaluated each 60 s. The plotted values are one hour averages. Data missing (194-201 doy) is due to instrumentation maintenance. The Amatrice earthquake (M_w 6.0): 24 August (doy 237), 01:36:32 UT.

The evidence of a signal change is already very clear about five days before the main shock. We have checked the relevance of this signal looking at the kurtosis of the full dataset (1 May 2015 to 5 September 2016) and found no significant deviation from the zero value until 40 days before the main shock (De Luca *et al*., 2018).

Further investigations on the relationships between earthquakes and groundwater variations in the vicinity of a large seismogenic faults are needed for a full understanding of the distribution of pre-seismic, coseismic and post-seismic variations and of their driving mechanisms.

References

Barnhoorn A., Cox S. F., Robinson D. J. and Senden T. Stress- and fluid-driven failure during fracture array growth: Implications for coupled deformation and fluid flow in the crust. *Geology* 38, 779-782; doi: 10.1130/G31010.1 (2010).

De Luca G. La Rete Sismica regionale d'Abruzzo e sua integrazione con la RSN. Da Miscellanea INGV, Riassunti estesi del I° Workshop Tecnico: *Monitoraggio sismico del territorio nazionale: stato dell'arte e sviluppo delle reti di monitoraggio sismico* – Roma 20-21 Dicembre 2010, pp. 22-23 (2011).

De Luca G., Di Carlo G. and Tallini M. Hydraulic pressure variations of groundwater in the Gran Sasso underground laboratory during the Amatrice earthquake of August 24, 2016. *Annals of Geophysics* 59, Fast Track 5; doi: 10.4401/AG-7200 (2016).

De Luca G., Di Carlo G. and Tallini M. A record of changes in the Gran Sasso groundwater before, during and after the 2016 Amatrice earthquake, central Italy. *Scientific Reports*, doi: 10.1038/s41598-018-34444-1 (2018).

Di Toro G. *et al*. Fault lubrication during earthquakes. *Nature* 471, 494–499; doi: 10.1038/nature09838 (2011).

Hirth, G. and Beeler, N. M. The role of fluid pressure on frictional behaviour at the base of the seismogenic zone. *Geology* 43, 223–226; doi: 10.1130/G36361.1 (2015).

Manga M. and Wang C. -Y. Earthquake Hydrology. In: *Gerald Schubert (editor-in-chief), Treatise on Geophysics*, 2nd edition, Vol 4. Oxford: Elsevier, 305-328; doi: 10.1016/B978-0-444-53802-4.00082-8 (2015).

Scuderia, M. M., Collettinia, C. and Marone, C. Frictional stability and earthquake triggering during fluid pressure stimulation of an experimental fault. *Earth Planetary Science Letters* 477, 84–96; doi: 10.1016/j.epsl.2017.08.009 (2017).

Sibson, R. H. Fluid involvement in normal faulting. *J. Geodynamics* 29, 469–499 (2000).

Violay, M. *et al*. Effect of water on the frictional behaviour of cohesive rocks during earthquakes. *Geology* 42, 27-30; doi: 10.1130/G34916.1 (2013).

TECTONIC EARTHQUAKE SWARMS (TES) IN DIFFERENT SEISMOGENIC DOMAINS: COMPRESSIONAL AND EXTENSIONAL CASES FROM CENTRAL ITALY

R. de Nardis[1], L. Carbone[1], C. Pandolfi[1], F. Pietrolungo[1], D. Talone[1], G. Monachesi[2], M. Cattaneo[2], S. Marzorati[2], G. Lavecchia[1]

[1] CRUST, DiSPUTer, Università "G. d'Annunzio", Chieti Scalo 66013, Italy

[2] Istituto Nazionale di Geofisica e Vulcanologia, Ancona, Italy

Earthquakes sequences without a clear triggering mainshock, referred to as earthquake swarms, have been observed in volcanic and hydrothermal areas for decades. Tectonic Earthquake Swarms (TES) is another category of swarms linked to active tectonic regions.

In a seismic sequence, aftershocks are associated with a mainshock and their rate of occurrence can be generally described by the modified Omori law; their spatial distribution is observed to correlate with the static stress field changes of the main shock, suggesting that stress triggering plays an important role (Stein 1999). On the contrary, earthquake swarms are not characterized by a dominant earthquake and their temporal evolution cannot be described by any simple law comparable to the Omori law (Hainzl, 2004).

The physical mechanisms proposed for the TES origin and evolution include: (1) rupture patches migrating or expanding due to the diffusion of pore-pressure lowering the effective normal stress on the rupture plane (Hainzl 2004); (2) slow-slip events or aseismic creep (themselves possibly driven by pressurised fluids) redistributing elastic stress along a large fault area (Passarelli *et al*., 2015).

TES show different style of energy release with respect to classic main shock-aftershock sequence, being characterised by the presence of numerous events with more or less the same size for the entire period of activity. Their seismic rate may increase and decrease in time with a variable velocity not following any theoretical model (Passarelli *et al*., 2015).

Studying TES offers the possibility to understand the nature and main features of the seismic activity linked to local stress condition with implications for the hazard and deformation of an area.

TES were observed in several active tectonic locations in Italy, some of the most interesting cases are those released in the Pollino range (Brozzetti *et al*., 2017) from 2010 to 2014, and in the proximity of the Alto Tiberina Fault, northern Italian Apennines, (Marzorati *et al*., 2014) in two episodes in 2010 and 2013-14. In this second case the mechanism driving the seismicity was poorly understood and the hypothesis of aseismic transient and the role of fluids was discussed.

The present work is aimed to compare the characteristics and features of clustered seismicity

in two different Italian seismogenic domains: the extensional intra-Apennine belt of Central Italy and the compressional domain of the Marche-Adriatic region, in order to find common points and differences in the characteristic of the TES activity.

The Central Apennines are an upper crust high seismic risk zone, that experienced destructive earthquakes both in historical and in instrumental time. In particular, we focus on the axial zone extending between the Irpinia 1980 (Mw 6.9) and the Accumoli-Visso-Norcia 2016 (Mw 6.5) epicentral areas, that was struck by eleven events among the largest historical-early instrumental earthquakes (Mw ≥ 6.5) of the Italian territory since 1349. On the contrary, in instrumental times, if we exclude the Barrea 1984 seismic sequence (Mw 5.9), this area is predominantly characterized by a low level of seismicity, relatively stable in the size and time domains, and by low energy seismic clustering.

The eastern Marche-Adriatic region represents a typical active fold-and-thrust belt system; the active structures are mainly buried and their geometric complexity makes the region one of the most intriguing areas of the central Mediterranean. The compressional domain shows three major layers of seismogenic activity (upper crust, middle crust, upper mantle) controlled by the presence of lithospheric shear zones reaching maximum depths of about 70 km (Lavecchia *et al*., 2003).

To identify TES in the two study areas, we applied the declustering method and the cluster analysis, starting from the ISIDe instrumental databases in the time interval 2005- 2018 (ISIDe, working group 2016) for the extensional area and from the ReSIICO high-quality dataset recorded from 2009 to 2017, for the compressional area.

The identified TES were analysed in terms of temporal and spatial evolution, at the light of their location with respect to known active individual seismogenic structures. Extensional TES are mainly located at the tip of the principal individual structures, with recurrence in the same place by the time. Compressional TES appear to be controlled in their specific features by the depth of the seismogenic layer.

A principal difference between the extensional and compressional areas consists in the characteristic TES duration, which is shorter in the compressional area than in the extensional one, with a duration of few days in the first case and up to few weeks in the second case. The study is in progress.

References

Brozzetti F., Cirillo D., de Nardis R., Cardinali M., Lavecchia G., Orecchio B., Presti D. and Totaro C.; 2017: Newly identified active faults in the Pollino seismic gap, southern Italy, and their seismotectonic significance. J. Struct. Geol., 94, 13-31.

Hainzl, S., 2004. Seismicity patterns of earthquake swarms due to fluid intrusion and stress triggering, Geophys. J. Int., 159, 1090–1096.

ISIDe working group (2016) version 1.0, DOI: 10.13127/ISIDe.4

Lavecchia G., Boncio P. and Creati N. (2003) A lithospheric-scale seismogenic thrust in central Italy. J. of Geodynamics, vol. 36, 79–94.

Marzorati, S., M. Massa, M. Cattaneo, G. Monachesi, and M. Frapiccini (2014), Very detailed seismic pattern and migration inferred from the April 2010 Pietralunga (northern Italian Apennines) micro-earthquake sequence, Tectonophysics, 610, 91–109.

Passarelli, L., S. Hainzl, S. Cesca, F. Maccaferri, M. Mucciarelli, D. Roessler, F. Corbi, T. Dahm, and E.Rivalta (2015). Aseismic transient driving the swarm-like seismic sequence in the Pollino range, Southern Italy. Geophysical Journal International, 201(3), 1553-1567.

Stein, R.S., 1999. The role of stress transfer in earthquake occurrence, Nature,402, 605–609.

RECENT AND ACTIVE TECTONICS IN THE CAMPANIAN PLAIN BASED ON INTEGRATION OF FAULT KINEMATICS AND SEISMOLOGICAL DATA: PRELIMINARY RESULTS

S. Forlano[1], L. Ferranti[1], G. Milano[2]
[1] Dipartimento di Scienze della Terra, delle Risorse e dell'Ambiente, Università Federico II, Napoli, Italy
[2] Istituto Nazionale di Geofisica e Vulcanologia, Osservatorio Vesuviano, Napoli, Italy

The Campanian Plain is a sector of Quaternary extension and subsidence on the Tyrrhenian margin of the Southern Apennines characterized by a complex evolutionary framework. From Pleistocene times extension was chiefly accommodated by E-W to NE-SW striking, listric-shaped normal faults, which caused domino-block faulting and growth of up to ~3.5 km deep extensional basins segmented by buried ridges (Milia *et al*., 2003).

Jointly with this articulated subsurface architecture, the Plain exhibits a low-energy historical and instrumental seismicity. The background seismicity in the Plain, with the exception of the local seismicity of Vesuvio and Campi Flegrei volcanic areas, is characterized prevalently by isolated events with magnitudes generally less than 3.0 even if seismic clusters are located close to the Massico Mountain and along the Avella Mountain (Gaudiosi *et al*., 2012).

So far, very few fault structural data were available to unravel the kinematic evolution of the plain. Similarly, no complete and detailed assessment of the instrumental seismicity and fault plane solutions outside the Neapolitan volcanic area are at present available.

The aim of this study is to understand and reconstruct the structural setting and the kinematics evolution of the Campanian Plain and how active and seismogenic deformation is expressed in it. The choice of a multidisciplinary approach sees integration of geological-structural data and instrumental seismicity to link the long-term kinematics evolution and the present day seismogenic deformation. The study is focused on the tectonic borders of the Plain where the footwall of faults is exposed, and tectonic seismicity is present.

We studied the geometry and kinematics of major and minor faults in the footwall of the primary faults buried in the subsurface (Bruno *et al*. 1998), as indicative of the extensional strain recorded on the latter faults. To characterize these structures at the border between the margin of the Plain and the Apennine chain, structural and fault-slip data have been acquired and collected on ~280 fault planes at more than 80 sites along the flanks of the Plain. In particular, the analysis was concentrated along three of the main border ridges (Caserta, Avella and Sarno ridges) which extend along the western flank of the Apennines into the central portion of the plain.

The ridges are dissected by faults with orientation from NW-SE to E-W. In each of these sectors, we observed superposition of two sets of slip lineations (S1, S2) on the major and minor fault surfaces. S1 and S2 slip lineations have both a moderate (~40° an average) and high (~80° on average) rake angle that indicate transtensional (left or right depending on fault orientation) or dip-slip motion, respectively. The existence of two sets of differently oriented slip lineations on the fault surfaces reveals two different kinematics regimes and related deformation events. The first set S1 is associated to normal and right-transtensional slip on NE-SW faults and minor left-transtensional slip on NW-SE and E-W striking faults.

This lineation set defines an extensional T axis whose trend progressively switch from NNE-SSW (Sarno, Avella and in the southern portion of the Caserta ridge) to NNW-SSE (Caserta ridge) (Fig. 1). Based on morphostructural criteria, this first displacement is regarded as the major episode of slip recorded on the studied faults and it is responsible for the shape of the relief.

A second set S2 of lineations developed primarily on NW-SE striking faults that had a normal to right-transtensional slip with a T axis that trends from ~NE-SW (central portion of the Caserta ridge) to ~E-W (Sarno and Avella ridges) (Fig. 1). Although this lineation set is subordinate relative to the first set, it is locally observed as the only kinematics as in the western

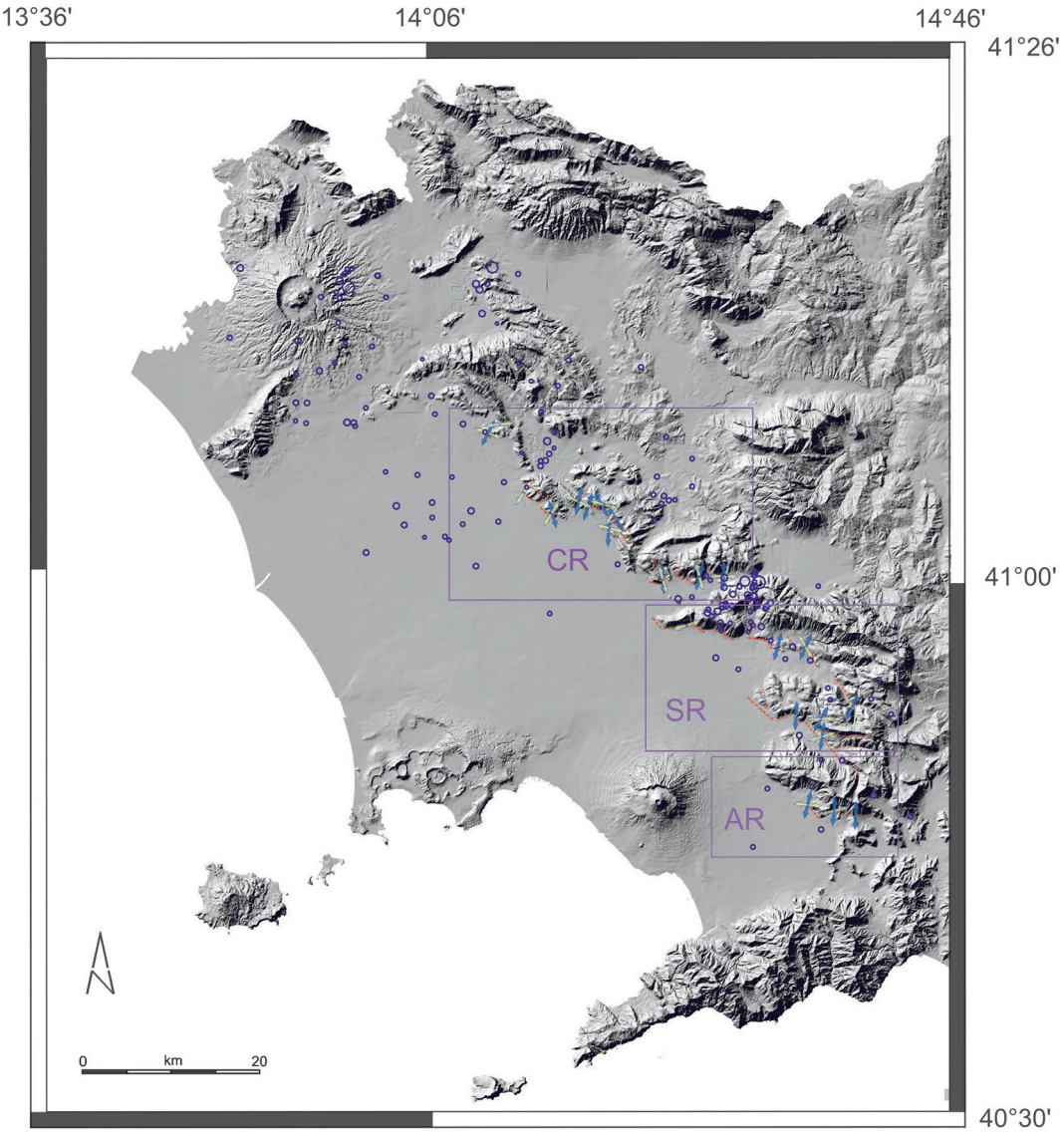

Fig. 1 - DEM of the northern Campania region showing a measured and supposed faults. Blu arrow indicate the extensional T axis defined by S1 slip lineation; yellow arrow, T axis defined by S2 slip lineation. Purple circles represent the epicentral distribution of the relocated seismicity between 2005 and 2017 in the study of area. Coloured boxes indicates the three ridges (CR-Caserta Ridge, AR-Avella Ridge, SR-Sarno Ridge) analyzed in this work.

portion of the Avella ridge. The first results deriving from structural observations indicate that: 1) the major border faults have a multiphase kinematics; 2) the second determined extension axis (NE-SW) is in agreement with the active strain axis in the Apennines (e.g., Montone and Mariucci, 2016); 3) the first extension axis is not consistent with the Apennines active strain axis.

To investigate in detail the background seismicity and, in particular, to identify active seismogenic volumes, the seismic events that occurred between 2005 and 2017 in and around the Campanian Plain has been analyzed. Starting from the INGV instrumental catalogue, we selected the seismic events with M_L>1.5 occurred in the study area. In order to perform a relocation of the seismicity, the waveforms of the selected events have been collected to carry

out a manual re-picking of the P- and S-wave arrival times, to correct any miss interpretation present in the catalogue, focusing our attention on S-phase for the reliability of the focal depth. This data-set has also been integrated with the waveforms recorded by the seismic stations of the local Osservatorio Vesuviano -INGV seismic networks operating in the volcanic areas. Preliminary relocation show that the detected seismicity in the study area, excluding that related to the volcanic areas of Vesuvio and Campi Flegrei, is characterized prevalently by temporally and spatially isolated events with magnitude less than 2.5. This seismicity is located mainly along the border between the Plain and the foothills of the Apennines. The few events with epicenter inside the Plain are located in the north-western sector, near the Mt. Massico, and along the Avella ridge. The concentration of events along this ridge is due to both low magnitude single events ($M_L \leq 2.0$), and by a low magnitude seismic swarm ($M_{Lmax} < 3.5$) that occurred in 2005. The fault plane solutions of few low magnitude events ($M < 2.5$) localized beneath the eastern flank of the plain in correspondence of the three major border ridges (Caserta, Avella and Sarno ridges) at depth between 7 and 11 km, show kinematics that changes from normal to slightly transtensional moving from north to south. These events have a trend of the T axis similar to that associated to the second set of fault-slip lineations (from ~NE-SW to ~E-W), and both are consistent with the current extension axis documented by geological data and large-magnitude seismicity along the Apennines.

References

Bruno P.G., Cippitelli G., Rapolla A.; 1998: Seismic study of the Mesozoic carbonate basement around Mt.Somma–Vesuvius, Italy. Journal of Volcanology and Geothermal Research, 84, 311–322.

Gaudiosi G., Alessio G., Cella F., Fedi M., Florio G., Nappi R.; 2012: Multiparametric data analysis from seismic source identification in the Campanian area: merging seismological, structural and gravimetric data. Bollettino di Geofisica Teorica ed Applicata, 53 (3), 283-298, doi: 10.4430/bgta0050.

Milia A., Torrente M.M., Russo M., Zuppetta A.; 2003: Tectonics and crustal structure of the Campania continental margin: relationships with volcanism. Mineral. Petrol., 79(1–2), 33–47.

Montone P. and Mariucci M.T.; 2016: The new release of the Italian contemporary stress map. Geophys. J. Int., 205(3), 1525–1531.

UN NUOVO DATABASE INTEGRATO DI DATI SISMICI PER L'APPENNINO CENTRALE (2009-2019)

A. Frepoli[1], G. De Luca[1], P. De Gori[1], B. Trionfera[2], A. Marchetti[1], C. Doglioni[1]

[1] Istituto Nazionale di Geofisica e Vulcanologia – Osservatorio Nazionale Terremoti

[2] Università La Sapienza - Roma

Negli ultimi dieci anni l'incremento del numero di stazioni della Rete Sismica Nazionale dell'INGV ha consentito di rilevare un gran numero di terremoti di bassa magnitudo. La magnitudo di completezza, al momento, per Bollettino Sismico dell'INGV è di 1.5 nel settore dell'Appennino Centrale. In questo lavoro presentiamo un nuovo database integrato di dati sismici relativi a circa 18.000 eventi del periodo 2009-2019 (Figura 1) rilocalizzati usando non solo i dati della Rete Nazionale, ma anche quelli di tutte le reti regionali e temporanee attive in questo settore appenninico (De Luca, 2011, Frepoli *et al*., 2017). Sono stati letti i tempi di arrivo su più di 200 stazioni. Inoltre, per gli eventi di magnitudo superiore a 3.0, sono stati usati anche i dati delle stazioni accelerometriche della RAN (Rete Accelerometrica Nazionale). Grazie a questa grande raccolta di forme d'onda il nostro database integrato presenta un incremento in numero di eventi rispetto al Bollettino Sismico INGV di circa il 38%. E' necessario sottolineare che questa banca dati non comprende le sequenze de L'Aquila 2009 e di Amatrice-Norcia

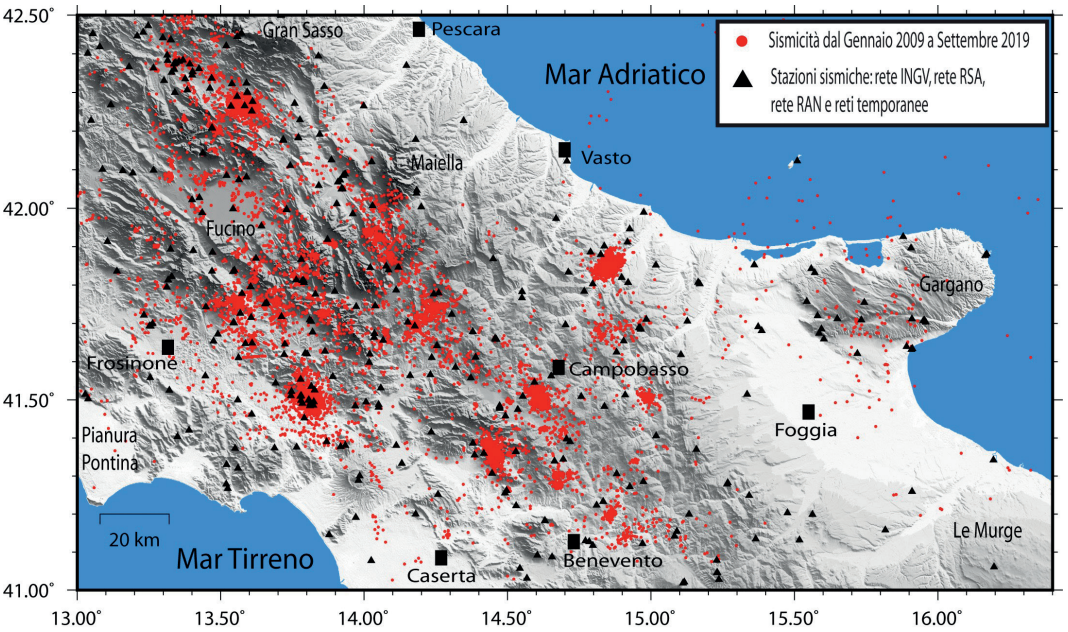

Fig. 1 - Eventi del database integrato 2009-2019 rilocalizzati con tutti i dati disponibili (reti permanenti, temporanee e stazioni accelerometriche).

del 2016-2018. Infatti, l'area appenninica interessata da questo studio si estende dal settore aquilano immediatamente a sud della sequenza del 2009 fino al Beneventano, e dal settore romano dei Colli Albani fino al Gargano. Questa è un'area che comprende l'intera regione del Molise ed ampi settori delle regioni Lazio, Abruzzo, Puglia e Campania. I dati del periodo 2009-2013 sono stati già pubblicati in un lavoro nell'ambito di un progetto di studio della sismicità appenninica (Progetto SLAM, Frepoli *et al*., 2017). Questo primo database comprende circa 6.800 eventi. A partire dalla fine del 2013 abbiamo voluto estendere l'area di studio più ad est e a sud per includere alcune importanti sequenze avvenute negli ultimi anni [sequenza del Matese 2013-2014, 900 eventi con *mainshock* di M_w 5.0; sequenza di Baranello-Vinchiaturo (CB), 600 eventi con *mainshock* di M_w 4.3; sequenza di Montecilfone-Larino (CB) del 2018, più di 1000 eventi con *mainshock* di M_w 5.1].

Il modello di velocità 1D per questo settore appenninico (modello SLAM, Frepoli *et al*., 2017), ottenuto con un algoritmo genetico a partire dal vasto database sismico del periodo 2009-2013, ci ha consentito di rilocalizzare con maggiore precisione tutti gli eventi di questo studio. In particolare, per la sequenza del Matese 2013-2014 abbiamo notato che sia il *mainshock* che le repliche ricadono nelle profondità ipocentrali classiche per tutta la sismicità situata lungo l'asse della catena appenninica (6-16 km), a differenza di alcuni lavori precedenti (Ferranti *et al*., 2015; Di Luccio *et al*., 2018; nei quali sono stati analizzati un numero minore di dati) che pongono questa sismicità a profondità maggiori ipotizzando addirittura l'esistenza di intrusioni magmatiche profonde sotto il Matese (Di Luccio *et al*., 2018). Solo la porzione adriatica dell'area in studio presenta eventi con profondità ipocentrali più grandi, comprese tra i 20 ed i 30 km. In questo settore, a differenza di quello che copre la fascia appenninica caratterizzato da eventi con meccanismi estensionali, è presente un regime di stress trascorrente destro. Molti meccanismi focali calcolati in questo lavoro arricchiscono le conoscenze su questo regime di stress già acquisite in passato con le sequenze di Potenza (1990-1991; Ekstrom, 1994) e di San Giuliano di Puglia (2002; Di Luccio *et al*., 2005).

Come sviluppi futuri, a partire da questo database integrato, ci proponiamo di calcolare un gran numero di meccanismi focali con la lettura delle polarità dei primi arrivi per poter

compiere analisi dettagliate sul campo di stress locale e le sue variazioni nello spazio. Inoltre, tramite una analisi tomografica, si vuole procedere per il calcolo di un modello di velocità 3D valido per questo settore appenninico e fruibile per il servizio di sorveglianza sismica della sala operativa INGV.

Tutta l'area in studio è stata interessata in passato da importanti eventi sismici. Riteniamo che questo lavoro potrà dare importanti risultati sia per l'interpretazione geodinamica che per la valutazione dell'*hazard* sismico.

Bibliografia

De Luca G.; 2011: *La Rete Sismica regionale d'Abruzzo e sua integrazione con la RSN*. Da Miscellanea INGV, Riassunti estesi del I° Workshop Tecnico Monitoraggio sismico del territorio nazionale: stato dell'arte e sviluppo delle reti di monitoraggio sismico - Roma 20-21 Dicembre 2010, pp. 22-23.

Di Luccio F, Fukuyama E., Pino N.A.; 2005: *The 2002 Molise earthquake sequence: What can we learn about the tectonics of southern Italy?* Tectonophysics, 405(1-4), 141-154.

Di Luccio F., Chiodini G., Caliro S., Cardellini C., Convertito V., Pino N.A., Tolomei C., Ventura G.; 2018: *Seismic signature of active intrusions in mountain chains*. Science Advances, 4.1.

Ekstrom G.; 1994: *Teleseismic analysis of the 1990 and 1991 earthquakes near Potenza*. Annals of Geophysics, 37.6.

Ferranti L., Milano G., Burrato P., Palano M., Cannavò F.; 2015: *The seismogenic structure of the 2013-2014 Matese seismic sequences, Souhern Italy: implication for the geometry of the Apennines active extensional belt*. Geophysical Journal International, 201 (2), 823-837.

Frepoli A., Cimini G.B., De Gori P., De Luca G., Marchetti A., Monna S., Montuori C., Pagliuca N.M.; 2017: *Seismic sequences and swarms in the Latium-Abruzzo-Molise Apennines (Central Italy): new observations and analysis from a dense monitoring of the recent activity*. Tectonophysics, 712-713, 312-329.

VARIAZIONE DELLO STRESS DI COULOMB A SEGUITO DEL TERREMOTO DEL 30 OTTOBRE 2016: INTERAZIONE TRA LE FAGLIE DI NORCIA E DEL MONTE VETTORE

A. Galderisi[1,2], P. Galli[3,1], O. Trotta[4]

[1] CNR-IGAG, Roma, Italia

[2] Università degli studi di Chieti-Pescara, dipartimento INGEO, Italia

[3] Dipartimento Protezione Civile, Roma, Italia

[4] Università di Roma, La Sapienza, Italia

Introduzione. In questo lavoro abbiamo applicato diverse metodologie analitiche al fine di esplorare le modalità del trasferimento frontale dello *stress* statico di Coulomb tra due sistemi di faglie sismogeniche. Lo spunto è stato offerto dalla formazione di una serie di rotture di superficie osservate lungo i piani di faglia del sistema di Norcia (NFS) a seguito dell'evento sismico del 30 ottobre 2016. Quest'ultimo, come ben noto, non è stato generato dal NFS, ma dal sistema di faglie del Monte Vettore (MVFS).

Dal momento che i dati sismologici relativi alla sequenza sismica del centro-Italia (Chiaraluce *et al*., 2017; Improta *et al*., 2019) non hanno evidenziato alcun evento di elevata magnitudo associabile al NFS, ci si è interrogati sulla natura di queste rotture e sulla possibile interazione tra questi due sistemi di faglie parallele.

Inizialmente è stato condotto un rilevamento geologico-strutturale lungo tutto il NFS, cartografando le rotture cosismiche e calcolandone lo *slip-vector*. Laddove la rottura cosismica si presentava associata ad un piano di faglia abbiamo anche misurato i *rake* delle *slickenlines* e i vari indicatori cinematici.

L'elaborazione di immagini satellitari provenienti da Sentinel-1 e di Alos-2 ha consentito di individuare, nel bacino di Norcia, un sollevamento cosismico di circa 15 cm. È stato quindi calcolata la variazione dello *stress* di Coulomb prodotta dal MVFS a seguito dell'evento del 30

ottobre. Ne è risultato che parte dello stress statico di Coulomb è stato trasferito dal MVFS al NFS.

Inquadramento geologico-strutturale. Il MVFS e il NFS sono due sistemi di faglie normali sismogeniche che si estendono parallelamente per oltre 30 km in direzione N160°, ad una distanza di circa 10 km l'una dall'altra. Entrambi risultano attivi in tempi storici, con evidenze di rotture superficiali almeno durante tutto l'Olocene (Galli *et al*., 2018; Galli *et al*., 2019). I tempi di ritorno calcolati a partire dagli studi paleosismologici sono di circa ~1.8 kyr per entrambi i sistemi (Galli *et al*., 2018; 2019), con uno slip rate di 1.3 mm/yr e 1.2 mm/yr per il MVFS e NFS, rispettivamente. Dalla raccolta dei dati strutturali sui piani di faglia principali si evince che questi sistemi di faglie sono caratterizzati da una cinematica estensionale, che in superficie si esprime prevalentemente con una componente obliqua sinistra.

Rotture cosismiche nel bacino di Norcia. Le rotture cosismiche osservate nel bacino di Norcia ribattono l'emergenza della *master fault* e degli *splay* sintetici ed antitetici già noti e riconosciuti attivi in Galli *et al*. (2005; 2018). Tenendo a mente che di tutte le faglie del NFS che ricadono nel bacino di Norcia, solo quella bordiera affiora con un piano in roccia, a seguito del terremoto del 30 Ottobre 2016, in totale, sono stati misurati oltre 2 km di rotture cosismiche con offset verticale medio di ~12 cm (Fig. 1). In dettaglio, la *master fault* in roccia (NF) ha registrato ~10 cm di offset verticale per un estensione di ~ 300 m (Galli *et al*., 2018) (Fig. 1C), lo *splay* sintetico di Patino (SFP) un offset verticale di ~ 15cm per un'estensione di ~ 500 m, mentre quello antitetico (AFP) presentava rotture cosismiche in più punti (Fig. 1b). Cumulativamente, la lunghezza di questa rottura è di ~600 m, con offset verticale medio di ~12 cm. Sullo *splay*

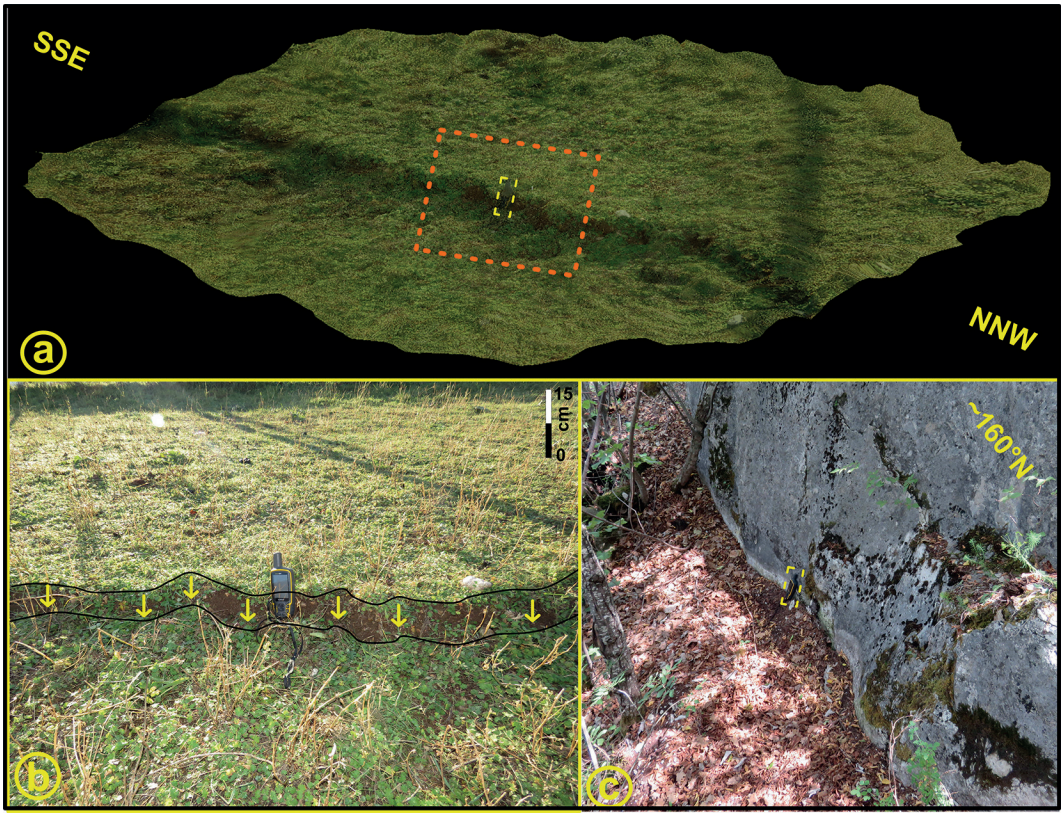

Fig. 1 - a) Vista 3D della rottura cosismica ricostruita con tecniche di fotogrammetria (il riquadro indica la foto b). b) Rottura cosismica osservata sul AFP. Le frecce gialle indicano il *coseismic slip-vector*. c) Rottura cosismica lungo il piano di faglia bordiera in roccia.

sintetico di Poggio Valaccone (PVF), l'estensione osservata è ~400 m, con offset verticale di pochi centimetri o beanze. Infine, lungo lo *splay* sintetico Wall Norcia Fault (WNF), l'offset verticale massimo osservato è di ~18 cm per ~300 metri. Lo *slip vector* mostrato dalle rotture cosismiche lungo questi *splay* indica una cinematica dip-slip.

Nel dicembre 2017, Galli *et al*. (2018) hanno scavato una trincea per studi paleosismologici lungo la rottura cosismica del SFP ove si è riscontrato che detta rottura è avvenuta in corrispondenza dell'espressione superficiale dello *splay* principale osservato sulle pareti della trincea.

Analisi InSar. È stata utilizzata la tecnica di interferometria satellitare (InSAR) per misurare le deformazioni relative a un'area di ~4700 km^2. Sono state utilizzate due immagini satellitari del 26 ottobre e 1 novembre 2016, provenienti dal satellite *Sentinel-1* (1A – 1B) in geometria *ascending*.

Le immagini sono state processate tramite il free software SNAP (http://www.esa.it) grazie alla tecnica TOPSAR *Interferometry* (http://www.sentinel.esa.int). È stato così ottenuto un primo interferogramma dell'area, ossia la mappa di deformazione del suolo misurata lungo la LoS (Line of Sight) del sensore, in termini di fase (Prati *et al*., 1990) che mostra chiaramente un'area di sollevamento nell'hanging wall della faglia di Norcia (Fig. 2a). Di fatto, analizzando la mappa della deformazione verticale ottenuta dal satellite ALOS-2 con il radar PALSAR-2 si può osservare una fluttuazione verticale di oltre 70 cm, con un massimo di abbassamento nel bacino di Castelluccio e un *uplift* di ~15 cm nel bacino di Norcia (Fig. 2b).

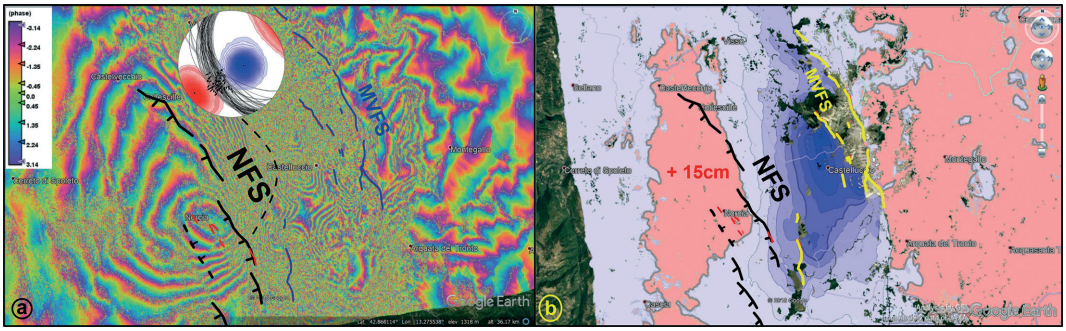

Fig. 2 - a) Interferogramma in bande dell'area di studio. In blu lungo il MVFS, in nero il NFS. I tratti rossi sul NFS sono le evidenze di rotture cosismiche. Lo steroplot è relativo ai dati di faglia strutturali misurati lungo la faglia bordiera di Norcia. b) Mappa della deformazione prodotta dall'evento del 30 ottobre (estratta da https://www.eorc.jaxa.jp/ALOS-2/img_up/jdis_pal2_ita-eq_20160825.htm#20161111_add). In giallo il MVFS, in nero il NFS.

Trasferimento dello *stress* statico di Coulomb. Secondo la teoria del cambiamento di *stress* di Coulomb, a seguito di un evento sismico parte dello *stress* statico può essere trasferito a sistemi di faglie vicini (King *et al*., 1994). Già alcuni autori hanno analizzato la variazione dello *stress* statico di Coulomb prodotto dall'evento del 30 ottobre (Improta *et al*., 2019 e bibliografia), con particolare riferimento alle interazioni laterali che intercorrono tra i sistemi sismogenetici limitrofi (Mildon *et al*., 2019). Nel nostro caso, invece, si osserva che parte dello *stress* di Coulomb è trasferito frontalmente dal MVFS al NFS. Abbiamo quindi calcolato le variazioni di *stress* di Coulomb generate il 30 ottobre dal MVFS utilizzando il software Coulomb 3.3 (Toda *et al*., 2011). Per definire la variazione dello stress di Coulomb il software si avvale di questa equazione:

$\Delta CSC = \Delta\tau s + \mu\Delta\sigma_n$

dove ΔCST è la variazione dello *stress* di Coulomb (Coulomb Stress Change – CSC), $\Delta\tau s$ è la variazione dello *shear stress*, μ è il coefficiente di frizione e $\Delta\sigma_n$ è la variazione dello *stress* normale. I parametri di faglia immessi nel software sono:

- strike N160°; dip 55°; rake -90° (http://www.eas.slu.edu); cinematica dip-slip; Mw 6.6; slip massimo -2.5 m (INGV, 2016); coefficiente di frizione μ=0.6 (tipico delle rocce carbonatiche).

Sono state condotte due simulazioni, una attivando la faglia del MVFS (S1), l'altra quella di NFS (S2), assumendo gli stessi parametri, anche se è possibile che la NFS generi magnitudo superiori (Galli *et al*., 2018).

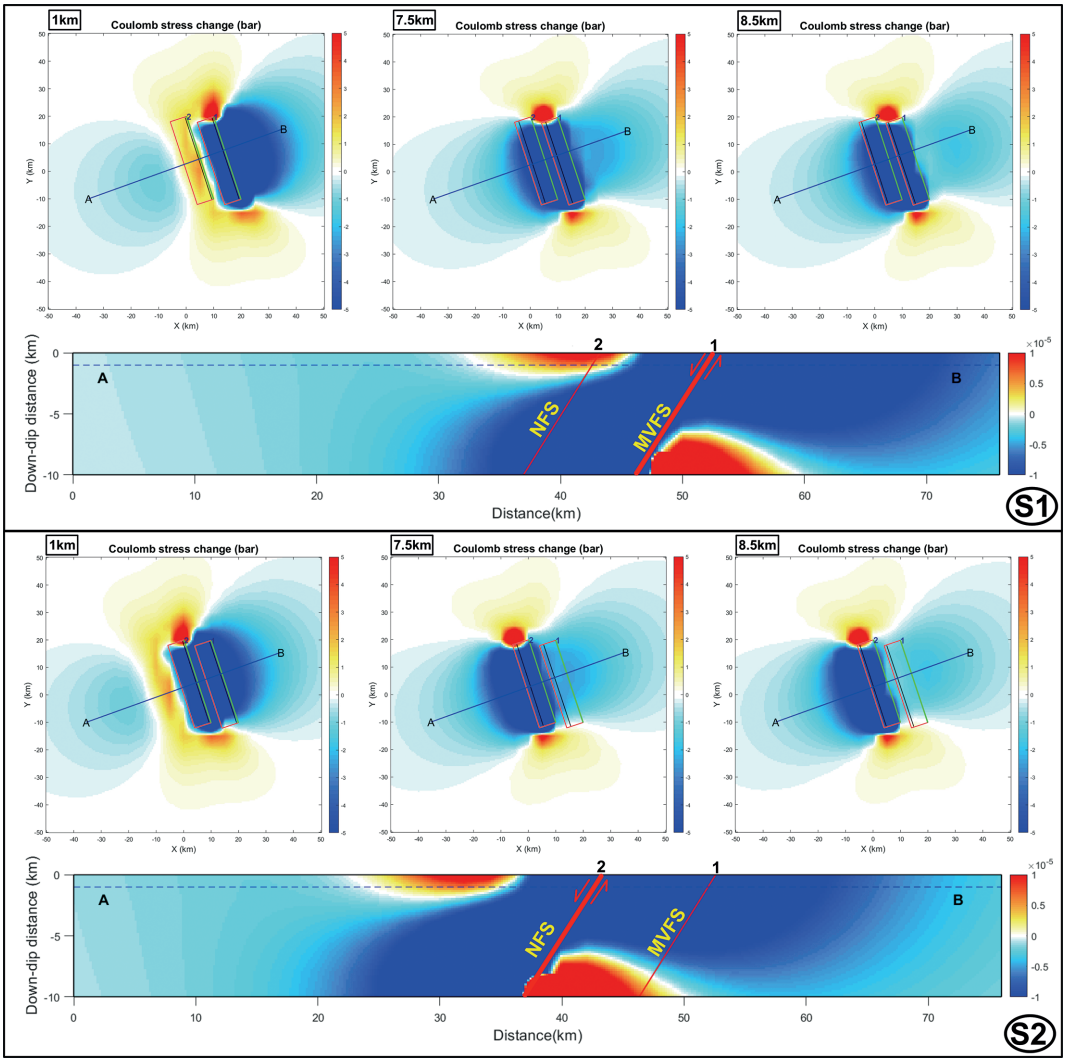

Fig. 3 - S1) Simulazione del calcolo della variazione dello *stress* di Coulomb relativo all'evento del 30 ottobre. Visione in mappa a diverse profondità e relativa sezione. MVFS – faglia 1, NFS – faglia 2. S2) Simulazione della variazione dello *stress* di Coulomb calcolato per la NFS.

Discussioni e conclusioni. L'insieme di tutte queste analisi ci ha consentito di ipotizzare il motivo per cui la NFS si sia attivata in superficie e come interagisca con la MVFS. I risultati ottenuti dalle simulazioni per il calcolo della variazione dello *stress* statico di Coulomb mostrano che, nella simulazione S1 si osserva la formazione di un lobo di accrescimento dello *stress* nei primi 2 km nell'hanging-wall del MVFS, corrispondente alla parte superficiale del NFS (Fig. 3). Nella simulazione S2, invece, si osserva un lobo di accrescimento dello *stress* di Coulomb

a circa 6.5 km di profondità nel *footwall* del NFS, in corrispondenza della parte profonda del MVFS. In altre parole, questo suggerisce che quando il MVFS si attiva, viene aumentato lo *stress* statico di Coulomb solamente nella porzione più superficiale di crosta attraversato dal NFS, mentre quando si attiva la NFS è lo *stress* statico nella porzione profonda attraversato dal MVFS che aumenta.

Considerando che gli *slip vector* osservati lungo le rotture cosismiche indicano una cinematica *dip-slip* pura, mentre le *slickenlines* misurate sui piani di faglia bordiera, indicano una cinematica obliqua sinistra (i.e., con direzione d'estensione appenninica), compatibile con il campo di *stress* attuale, è possibile che l'attivazione sul NFS a seguito dell'evento del 30 Ottobre non sia imputabile a dinamiche di deformazione indotte dal rilascio dello stress tettonico appenninico. Escludendo fenomeni di compattazione differenziale o movimenti di versante indotti dallo scuotimento cosismico – impossibili, peraltro, negli *splay* della piana - possiamo dunque ipotizzare che l'improvviso aumento dello *stress* di Coulomb indotto dalla rottura di MVFS, accoppiato al sollevamento cosismico del blocco di Norcia, abbiano indotto un *gravity-slip* passivo lungo i piani di faglia preesistenti, ossia gli *splay* del NFS.

Come ipotesi finale, ancora tutta da esplorare, considerando la lunga storia paleosismica dei due sistemi di faglie (Galli *et al*., 2018; 2019), è possibile che il MVFS e il NFS interagiscono da migliaia di anni, inducendo vicendevolmente variazioni dello *stress* di Coulomb l'uno nell'hanging wall dell'altro. Ma mentre l'attivazione del MVFS sembra favorire solamente la formazione di rotture passive superficiali lungo il NFS, l'attivazione del NFS, che sembra precedere di 100-500 anni quella del MVFS, potrebbe agire da *triggering* per la rottura completa di quest'ultimo.

Bibliografia

Chiaraluce L., Di Stefano R., Tinti E., Scognamiglio L., Michele M., Casarotti E., Cattaneo M., De Gori P., Chiarabba C., Monachesi G., Lombardi A., Valoroso L., Latorre D., Marzorati S., 2017. *The 2016 Central Italy seismic sequence: a first look at the mainshocks, aftershocks, and source models*. Seism. Res. Lett., 88, 757-771.

Galli P., Galadini F., Calzoni F., 2005. *Surface faulting in Norcia (central Italy): a "paleoseismological perspective"*. Tectonophysics, 403, 117–130.

Galli P., Galderisi A., Ilardo I., Piscitelli S., Scionti V., Bellanova J., Calzoni F., 2018. *Holocene paleoseismology of the Norcia fault system (Central Italy)*. Tectonophysics, 745, pp. 154–169.

Galli P., Galderisi A., Peronace E., Giaccio B., Hajdas I., Messina P., Pileggi D., Polpetta F., 2019. *The awakening of the dormant Mt Vettore fault (2016 central Italy earthquake, Mw 6.6). Paleoseismic clues on its millennial silences*. Tectonics, 38, 687-705.

King, G.C.P., R.S. Stein, J. Lin. 1994. *Static stress changes and the triggering of earthquakes*. Bull. Seismol. Soc. Amer., 84 (3), 935-953.

Improta L., Latorre D., Margheriti L., Nardi A., Marchetti A., Lombardi A., Castello B., Villani F., Ciaccio M., Mele F., Moretti M., The Bollettino Sismico Italiano Working Group, 2019. *Multi-segment rupture of the 2016 Amatrice-Visso-Norcia seismic sequence (central Italy) constrained by the first high-quality catalog of Early Aftershocks*. Scientific Reports, 9:6921.

INGV Working Group "Terremoto in centro Italia". *Summary report on the October 30, 2016 earthquake in central Italy Mw 6.5. (2016)*.

Mildon Z.K., Roberts G.P., Faure Walker J.P., Toda S., 2019. *Coulomb pre-stress and fault bends are ignored yet vital factors for earthquake triggering and hazard*. Nature Communications, 10:2744

Prati C., Rocca F., Monti Guarnieri A., Damonti E., 1990. *Seismic migration for SAR focusing: Interferometrical applications*. IEEE Transactions on Geoscience and Remote Sensing, Vol.28, N.4, pp.627-640.

Toda, S. and Enescu, B., 2011. *Rate/state Coulomb stress transfer model for the CSEP Japan seismicity forecast*. Earth Planets Space, 63(3), 171–185.

Sitografia

http://www.esa.it
http://www.sentinel.esa.int
https://www.eorc.jaxa.jp
http://www.eas.slu.edu

RILIEVO MACROSISMICO SPEDITIVO SUGLI EFFETTI DEL TERREMOTO IN AREA ETNEA DEL 6 OTTOBRE 2018

P. Galli, A. De Sortis
Dipartimento Protezione Civile, Rome, Italy

Introduzione. L'evento della notte del 6 ottobre 2018 (Mw 4.6; Ml 4.8), in provincia di Catania, è avvenuto nella fascia pedemontana sudoccidentale dell'Etna (Figura 1), sede di modesta sismicità storica. L'epicentro è molto prossimo a quello di altri due eventi di minore magnitudo (Mw 4.3 e 4.0) avvenuti il 1 Gennaio 1850 e il 14 Maggio 1898, che ebbero effetti decisamente più alti (Io 7 MCS e 7-8 MCS, rispettivamente) rispetto a quello odierno, forse a causa di una minor profondità. Gli effetti macrosismici storici più elevati nelle località della zona epicentrale sono tuttavia legati ai grandi terremoti della Sicilia orientale, quale quello del 1693 o del 1908 dello Stretto, mentre in genere non superano il 6-7 grado MCS per terremoti locali.

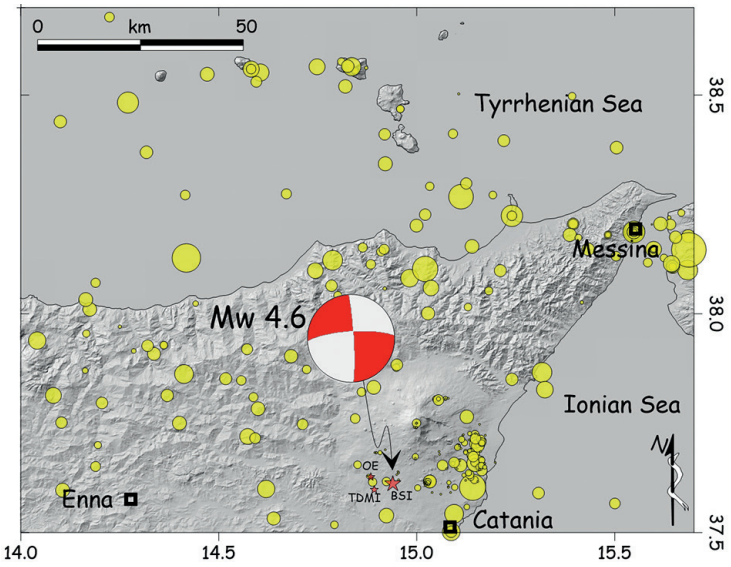

Fig. 1 - Ubicazione del terremoto del 6 ottobre 2018 in confronto alla sismicità storica della Sicilia nordorientale.

L'evento, generato da una faglia verticale a cinematica pura strike-slip (piani nodali N-S ed E-W), non è associabile ad una particolare struttura tettonica, considerato anche che le faglie note in superficie sono in genere connesse a processi vulcano-tettonici più superficiali rispetto alla profondità alla quale il terremoto in questione è avvenuto (~6 km).

L'evento principale è stato seguito da una sismicità di bassa magnitudo distribuita prevalentemente sotto l'abitato di Biancavilla.

Osservazioni macrosismiche speditive. Al fine di verificare la distribuzione degli effetti macrosismici del terremoto del 6 ottobre 2018, è stato effettuato un rilievo macrosismico speditivo nelle località intorno all'epicentro fornito da INGV.

Il rilievo è stato svolto applicando la scala MCS (Mercalli-Cancani-Sieberg, Sieberg, 1930), utilizzando le progressioni di danno percentuale calcolate da Molin (2009), così come in tutti i rilievi macrosismici condotti e pubblicati da DPC nei terremoti passati.

È opportuno ricordare che il rilievo macrosismico viene condotto esclusivamente all'esterno degli edifici, a meno di situazioni particolari, quali la verifica di edifici monumentali che, in ogni caso, non pesano poi nell'attribuzione del grado. Considerando l'entità del terremoto in oggetto, si ricorda che l'attribuzione del VI grado MCS prevede che il 50% degli edifici abbia subito danni di livello 1, il 25% dei quali abbia subito danni di livello 2, con un 5% di danni

di livello 3 (i.e., danno grave, ovvero strutturale). Per l'assegnazione del grado V-VI MCS, è previso che il 25% degli edifici abbia subito danni di livello 1 e il 5% di livello 2.

La prima località visitata è stata **Santa Maria di Licodia**, costituita da 2400 edifici secondo ISTAT (2011). All'interno dell'abitato sono state riscontrate rarissime lesioni di livello 2 a vecchi edifici in muratura, molte delle quali riaperture di lesioni pregresse. Molte altre vecchie lesioni non mostrano segni di ringiovanimento a seguito del terremoto in oggetto. Solo Palazzo Ardizzone, dimora storica del paese e sede della biblioteca, presenta il distacco esteso dell'intonaco del paramento superiore della facciata. Altri edifici vetusti o in pessime condizioni di manutenzione non presentano particolari situazioni di aggravamento del quadro fessurativo pregresso. Anche tenendo conto della decina di inagibilità assegnate dai tecnici regionali, la percentuale di danno di livello 2, associata agli effetti sulla popolazione, conduce all'assegnazione del V grado MCS.

A **Biancavilla**, costituita da 8500 edifici, sono state riscontrate diverse lesioni di livello 2 pregresse in edifici vetusti o in stato di abbandono, oltre a rarissime filature tra edifici dovuto a martellamento tra gli stessi. La chiesa di Santa Maria dell'Idria, in pessime condizioni di manutenzione, ha subito il crollo del pinnacolo sinistro della facciata. La chiesa madre ha riportato danni ai cupolini e alle volte. Un danno di livello 3, consistente nel crollo parziale di un cantonale e del sottotetto di una casa in abbandono, è stato osservato in un edificio in prossimità della chiesa di Sant'Antonio di Padova, anch'essa con lesioni lievi in facciata e sul fianco sinistro. Sul fondovalle del Simeto, in C.da Schettino, alcuni ruderi hanno subito il crollo del tetto e di parte delle murature). In C.da Giardinello, un edificio isolato in cemento armato ha subito lesioni di distacco delle tamponature del piano terra, con espulsione e caduta limitata ad un breve tratto.

Considerando il livello e la diffusione dei danni rilevati e che gli edifici dichiarati inagibili corrispondono ad una percentuale inferiore al 1%, tenuto anche conto che il terremoto è stato avvertito da tutti con paura, il grado assegnabile è pari al V MCS.

Ad **Adrano**, costituita da 10500 edifici, non è stata riscontrata nessuna lesione recente negli edifici. Gli stessi, in genere, sono in migliori condizioni di manutenzione rispetto a quelli di Santa Maria di Licodia e Biancavilla. È stata osservata una lieve lesione sull'arco della Cappella Palatina all'interno della Torre Normanna e la riapertuna di una vecchia lesione nella volta della chiesa madre. Considerando il livello bassissimo di danno e la circostanza che l'evento sia stato avvertito da tutti con apprensione, il grado assegnabile è V MCS.

A **Ragalna**, località sparsa composta da 2500 edifici, non è stata osservata alcuna lesione evidente negli edifici. Solo le due chiese risultano chiuse per inagibilità. Quella ubicata nella porzione alta del paese (S. Maria del Carmelo) mostra distacchi di intonaco e di elementi decorativi del campanile. Anche in questo caso, considerata anche il forte risentimento avvertito con paura dalla popolazione, il grado assegnabile è V MCS.

A **Paternò**, composto da 10600 edifici, sono state riscontrate rarissime lesioni di livello 2 in alcuni edifici del centro storico e rarissime lesioni in edifici in cemento armato, limitatamente al contatto tra le travi e le tamponature. La Torre Normanna non ha subito alcun danno, eccetto una leggera riapertura di una lesione pregressa nella volta del primo piano. La vicina chiesa del Cristo al monte presenta leggere riaperture di lesioni pregresse sul muro maestro di destra. Gli unici danni significativi sono stati rinvenuti nella C.da Schettino, dove edifici vetusti in pietrame misto presentano riapertura di vecchie lesioni. Sempre in zona, sono stati rinvenuti tre crolli parziali di vecchie case abbandonate (Fig. 2). Tenuto conto della diffusione e livello del danno e del numero di edifici censiti a Paternò, il grado macrosismico assegnabile è pari al V MCS.

Figura 2 – Svuotamento di un muro a sacco di un vecchio edificio in valle del Simeto.

Nel complesso, il terremoto ha indotto solo danni di livello 2 ad un limitato numero di

Fig. 2 - Svuotamento di un muro a sacco di un vecchio edificio in valle del Simeto.

edifici delle località visitate, quasi tutti osservati in edifici in muratura e pietrame in cattivo stato di manutenzione, ad eccetto di rarissime lesioni in edifici in cemento armato e sempre confinate al contatto tra il telaio e le tamponature. I casi di crollo parziale censiti riguardano solo case in abbandono ed elevatissima vulnerabilità pregressa, situate quasi tutte nella Valle del Simeto e fondate su depositi argillosi. Tenuto conto delle Intensità assegnate alle singole località, l'intensità macrosismica epicentrale (Io) è V grado MCS.

Considerazioni finali. Nel complesso, il terremoto ha indotto solo danni lievi ad un limitato numero di edifici delle località epicentrali (S. Maria di Licodia, Biancavilla, Adrano, Ragalna e Paternò), quasi tutti osservati in edifici in muratura e pietrame in cattivo stato di manutenzione, ad eccezione di rarissime lesioni in edifici in cemento armato e sempre confinate al contatto tra il telaio e le tamponature. I casi di crollo parziale osservati riguardano solo case in abbandono ed elevatissima vulnerabilità pregressa, situate quasi tutte nella Valle del Simeto e fondate su depositi argillosi. L'intensità macrosismica epicentrale (Io) è pari al V grado nella scala MCS. Anche nelle predette località l'intensità macrosismica attribuita (Is) è stata V grado MCS.

Tabella 1 - Piano quotato delle località visitate. Is, intensità al sito.

COMUNE	LOC - 2011	LOCALITÀ	Pop.Res.Tot	Edif.Tot	Long	Lat	Is MCS
Adrano	8700610001	Adrano	34446	10468	14.839	37.663	5
Biancavilla	8700810001	Biancavilla	23188	8479	14.867	37.644	5
Paternò	8703310001	Paternò	46030	10632	14.903	37.567	5
Ragalna	8705810001	Ragalna	3302	2344	14.956	37.640	5
Santa Maria di Licodia	8704720002	Cavaliere-Bosco	28	42	14.920	37.654	5
Santa Maria di Licodia	8704710001	Santa Maria di Licodia	6810	2401	14.898	37.613	5

NUOVI DATI SUL TERREMOTO DEL 1599 A CASCIA E SULLA POSSIBILE SORGENTE SISMOGENICA

P. Galli[1,2], A. Galderisi[2,3], R. Marinelli[4], P. Messina[2], E. Peronace[2], F. Polpetta[2,5]
[1] Dipartimento Protezione Civile, Rome, Italy
[2] CNR-IGAG, Rome, Italy
[3] University Chieti-Pescara, Italy
[4] free lance researcher, Cascia, Italy
[5] DST Sapienza University, Rome, Italy

Introduzione. La regione colpita dalla sequenza distruttiva del 2016, nei secoli passati, è stata l'area epicentrale di frequenti terremoti di elevata energia, alcuni catastrofici, come quello avvenuto il 14 Gennaio 1703 (Mw 6.9, XI grado MCS). In particolare, il settore nursino di questa regione vanta il poco invidiabile primato di essere zona sorgente di almeno 7 terremoti con vasti effetti macrosismici di intensità ≥ VIII-IX MCS e magnitudo tra 5.8 e 6.9, avvenuti a partire dal 1328, uno di media ogni secolo. Ad eccezione della sequenza del 2016 - in gran parte generata dal sistema di faglie del Monte Vettore, ivi compreso il *mainshock* del 30 Ottobre (Mw 6.6) – gli eventi dei secoli scorsi, e specificatamente quelli del 1328 (Mw 6.5), 1599 (Mw~6.0), 1703 (Mw 6.9), 1730 (Mw 6.0), 1859 (Mw 5.7) e 1979 (Mw 5.8), sono stati tentativamente associati all'attivazione parziale o completa del complesso e segmentato sistema di faglie normali di Norcia, esteso NNW-SSE per oltre 30 km da Preci al Monte Alvagnano (Galadini *et al*., 1999; Galli e Galadini, 1999; Galli *et al*., 2005; 2017; 2018).

L'associazione tra i singoli terremoti e i diversi segmenti di faglia del sistema di Norcia si basa in gran parte sulla coincidenza spaziale tra le aree di massima intensità di ciascun evento e l'*hanging wall* dei segmenti. Questa assunzione, almeno per il terremoto del 1703, è geologicamente provata grazie ai risultati di una vasta campagna paleosismologica condotta sugli *splays* sintetici ed antitetici nella piana di Norcia ove, nelle 10 trincee aperte, è stata riconosciuta e datata la fagliazione del 1703 (Galli *et al*., 2005; 2018).

Dal momento che il terremoto del 1703 - insieme ai diversi altri paleoeventi individuati nelle trincee - è l'unico con una magnitudo compatibile ad una estesa ed importante rottura di faglia (p.e., gli oltre 30 km del sistema di Norcia), l'attribuzione degli altri eventi storici minori (Mw~6) alle singole sorgenti dell'area è difficilmente comprovabile geologicamente e quindi fortemente vincolata alla quantità e qualità dei dati macrosismici, oltre che alla loro distribuzione.

Tra gli eventi più problematici vi è quello del Novembre 1599, studiato da Baratta (1901) che scoprì, nella Biblioteca Apostolica Vaticana, una copia dell'unica relazione coeva dalla quale fino ad oggi, in grandissima parte, discendeva la conoscenza del terremoto e la sua parametrizzazione.

In questo nuovo lavoro, oltre allo studio archivistico di numerose fonti inedite sul terremoto, i rilievi che abbiamo condotto sulle faglie affioranti nella risultante area mesosismica hanno consentito di estendere le conoscenze sull'attività del sistema di Norcia e sulla possibile sorgente del 1599.

La riscoperta del terremoto del 1599. Considerando la scarsità delle fonti primarie di questo evento e l'esiguo numero di località per le quali fosse possibile valutarne gli effetti in termini di intensità macrosismica (13 in area mesosismica e altri 7 "*felt*"), è stata effettuata un'approfondita ricerca negli archivi e biblioteche pubblici, religiosi e privati di Cascia e di altre località, oltre che nell'archivio di Stato di Perugia (e sezioni), nella Biblioteca Apostolica Vaticana, in quella Nazionale Centrale di Roma. In aggiunta a decine di atti pubblici, sono stati rinvenuti i manoscritti originali della relazione sul terremoto conservata in copia in Vaticano, altre relazioni manoscritte coeve sul terremoto e numerose copie di atti e manoscritti coevi andati poi perduti nei successivi terremoti. Tra le altre è stata rinvenuta la relazione originale sul terremoto del 1703, contenente informazioni inedite anche su quello del 1599, spedita al Commissario Apostolico nelle settimane seguenti ed utilizzata *tout court* dallo stesso nella sua Relazione generale (De Carolis, 1703).

Grazie alle nuove fonti reperite, è stato possibile raddoppiare le osservazioni macrosismiche, portando il numero di località a 43, di cui ben 36 in area mesosismica. In breve, a parte Cascia, per la quale si hanno le percentuali di vittime e di crolli (Is 8.5 MCS), si è deciso di attribuire un valore corrispondente ad una distruzione quasi totale alle numerose località abbandonate e mai più ricostruite (Is 9.5 MCS), un valore pari a Is 9.0 MCS a quelle nelle quali "*solo pochissime case*" erano rimaste in piedi e, a scalare, Is 7.0 MCS per quelle con danni gravi estesi, ma senza distruzioni e crolli, come Norcia, Fogliano, Montesanto ed altre minori. Il *mainshock* del 5 Novembre fu avvertito in una vasta area dell'Italia centrale, a Perugia, Spoleto, L'Aquila, Ancona, Pesaro, e nell'intero Piceno e in Romagna, mentre la sua eco giunse persino tra le pagine delle cronache coeve d'oltralpe. A Roma, per esempio, fu inteso distintamente, ma senza provocare danno alcuno (Fig. 1).

Applicando l'algoritmo Boxer4 (Gasperini *et al*., 2010), la magnitudo equivalente è risultata Mw 5.98±0.42 con un'intensità epicentrale e massima di IX-X MCS. La box sismogenetica di 12x8 km ha una direzione N135°±9° (Fig. 1).

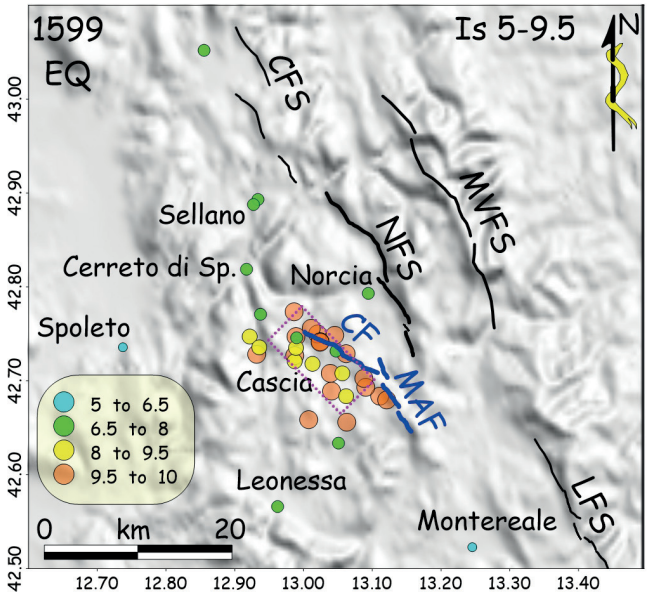

Fig. 1 - Distribuzione delle intensità macrosismiche rivalutate per il terremoto del 5 Novembre 1599. In viola, punteggiata, la box sismogenetica calcolata tramite Boxer4. Sistemi di faglie attive: CFS, Colfiorito; MVFS, Monte Vettore; NFS, Norcia (di cui Cascia e Monte Alvagnano in blu: CF, MAF); LFS, Monti della Laga. Notare come le massime intensità del 1599 ricadano tutte nell'*hanging wall* delle faglie di Cascia e del Monte Alvagnano.

Evidenze di tettonica attiva. L'area di distribuzione delle massime intensità e la box sismogenetica del terremoto del 1599 ricadono interamente nell'*hanging wall* delle faglie di Cascia e del Monte Alvagnano, già in passato considerate potenzialmente attive (Calamita *et al*., 1982; Blumetti, 1995; Galadini e Galli, 2000).

I conseguenti rilievi geologici, focalizzati nell'area mesosismica del terremoto, hanno consentito di individuare e cartografare in dettaglio l'espressione in superficie delle *master faults* del sistema di Cascia e del Monte Alvagnano. Entrambe dislocano di diverse centinaia di metri una coppia di paleosuperfici di erosione di età incerta (Pleistocene inferiore? Gentili e Panbianchi, 1999), oltre che i depositi lacustri di riempimento del bacino di Cascia (0.4 Ma). Alla base delle rispettive scarpate di faglia, la prima presenta con discontinuità uno specchio di faglia alto anche diversi metri, in genere alterato e con rari indicatori cinematici, mentre nella seconda lo stesso affiora con discreta continuità e in buono stato di conservazione, suggerendo una sua recente esumazione.

Entrambe le faglie mostrano evidenze geologiche di attività molto recente. Quella di Cascia, nella sua estremità orientale, ove evidentemente interagisce con quella del Monte Alvagnano (Fig. 1), presenta evidenze di ripetute rotture in superficie che coinvolgono depositi datati con

metodi radiometrici dall'Ultimo Massimo Glaciale all'epoca Moderna (Fig. 2). Quella del Monte Alvagnano mostra effetti di fagliazione databili sicuramente ad un periodo successivo al Neolitico (datazioni ^{14}C; Fig. 3), in accordo anche alle notizie storiche che riportano estese rotture in occasione del terremoto del 1703 (si veda in Galli *et al*., 2018).

Fig. 2 - Fagliazione di depositi di versante tardo-glaciali e storici lungo uno *splay* antitetico della faglia di Cascia. Il suolo sottostante i depositi detritico-colluviali ha un'età ^{14}C di ~22 ka.

Fig. 3 - Monte Alvagnano: fagliazione dei depositi di versante tardo olocenici. Ai piedi della persona a sinistra si trova un livello ricco in carboni, datato al Neolitico (età ^{14}C).

Conclusioni. Il ritrovamento di materiale archivistico coevo ed inedito ha consentito di approfondire le conoscenze sugli effetti e sull'estensione del poco studiato terremoto del 1599, indirizzando anche la successiva ricerca geologica della possibile struttura responsabile di questo e degli altri forti eventi della zona.

La distribuzione degli oltre 40 punti di intensità ricalcolati hanno indicato, come area sorgente del 1599, il bacino intermontano di Cascia l.s., del quale sono state rilevate in dettaglio le faglie bordiere (faglia di Cascia), e la loro prosecuzione verso sud (faglia del Monte Alvagnano). Entrambe mostrano, in diversa misura, evidenze geologiche di fagliazione di superficie nel corso della parte terminale del Pleistocene Superiore, sino al Presente.

Considerando l'area epicentrale del terremoto del 1599, è quindi altamente probabile che la genesi dello stesso vada ascritta, in toto o in parte, a queste due faglie. È invece certo che la faglia del Monte Alvagnano, e parte di quella di Cascia, si siano attivate in occasione del terremoto del 1703, insieme al resto dei segmenti che compongono il sistema di Norcia, così come d'altronde testimoniato da fonti coeve.

I risultati di questo lavoro, oltre a provare per la prima volta l'attività delle faglie di Cascia e dell'Alvagnano, sembrano confermare l'idea che il sistema di faglie di Norcia si possa rompere sia nella sua interezza, generando eventi di elevata magnitudo (Mw 6.9), che per segmenti singoli o raggruppati, dando origine ad eventi di magnitudo prossima o superiore a 6, questi ultimi, verosimilmente, non accompagnati da fagliazione di superficie. .

Bibliografia

Baratta M.; 1901: *I terremoti d'Italia; saggio di storia geografia e bibliografia sismica italiana*, pp. 950. Torino.

Blumetti A.M.; 1995: *Neotectonic investigation and evidence of paleoseismicity in the epicentral area of the January–February 1703, central Italy, earthquakes*. In: Serva, L., Slemmons, B. (Eds.), Perspectives in Paleoseismology. Special Publication-Association of Engineering Geologists, vol. 6. pp. 83–100.

Calamita F., Coltorti M., Deiana G., Dramis F., Pambianchi G.; 1982: *Neotectonic evolution and geomorphology of the Cascia and Norcia depression (Umbria–Marche Apennine)*. Geogr. Fis. Din. Quat. 5, 263–276.

De Carolis P.; 1703: *Relazione generale delle ruine, e mortalità cagionate dalle scosse del Terremoto de' 14. Gennaro e 2. Febbraro 1703 in Norcia, e Cascia, e loro contadi* (omissis). In: Chracas, L.A., (Roma. 27 pp.)

Galadini F., Galli P., Leschiutta I., Monachesi G., Stucchi M.; 1999: *Active tectonics and seismicity in the area of the 1997 earthquake sequence in Central Italy: A short review*. Journal of Seismology, 2, 1–9.

Galadini F., Galli P.; 2000: *Active tectonics in the central Apennines (Italy)—Input data for seismic hazard assessment*. Natural Hazards, 22, 202–223.

Galli P., Galadini F.; 1999: *Seismotectonic framework of the 1997-98 Umbria-Marche (Central Italy) earthquakes*. Seismological Research Letters, 70, 404–414.

Galli P., Galadini F., Calzoni F.; 2005: *Surface faulting in Norcia (central Italy): A "paleoseismological perspective"*. Tectonophysics, 403, 117–130.

Galli P., Castenetto S., Peronace E.; 2017: *The macroseismic intensity distribution of the 30 October 2016 earthquake in Central Italy (Mw 6.6): Seismotectonic implications*. Tectonics 36, 1–13. https://doi.org/10.1002/2017tc00458.

Galli P., Galderisi A., Ilardo I., Piscitelli S., Scionti V., Bellanova J., Calzoni F.; 2018: *Holocene paleoseismology of the Norcia fault system (central Italy)*. Tectonophysics, 745, 154–169. https://doi.org/10.1016/j.tecto.2018.08.008.

Gasperini P., Vannucci G., Tripone D., Boschi E.; 2010: *The location and sizing of historical earthquakes using the attenuation of macroseismic intensity with distance*. Bull. Seismol. Soc. Am. 100, 2035–2066. https://doi.org/10.1785/0120090330.

Gentili B., Pambianchi G.; 1999: *Contributo alla ricostruzione dell'evoluzione geomorfologica del versante adriatico dell'Appennino umbro-marchigiano (Italia centrale)*. In: Orombelli G. Studi geografici e geologici in onore di Severino Belloni, Glauco Briganti Genova, 391-403.

ACROSS-STRIKE VARIATIONS OF FAULT SLIP-RATES CONSTRAINED USING IN-SITU COSMOGENIC ^{36}CL CONCENTRATIONS

F. Iezzi[1], G. Roberts[1], J. Faure Walker[2], I. Papanikolaou[3], A. Ganas[4]

[1] Department of Earth and Planetary Sciences, Birkbeck, University of London, London, UK

[2] Institute for Risk and Disaster Reduction, University College London, London, UK

[3] Mineralogy-Geology Laboratory, Department of Natural Resources Development and Agricultural Engineering, Agricultural University of Athens, Greece

[4] National Observatory of Athens, Institute of Geodynamics, Athens, Greece

The identification of slip-rates on active faults is vital in order to quantify earthquake recurrence intervals for probabilistic seismic hazard analysis. It has been already shown that the interaction between adjacent faults within dense fault systems influences the slip-rate of single faults (e.g. Cowie and Roberts, 2001; Bennett *et al*., 2004; Roberts and Michetti, 2004). To better understand the dynamics of normal fault systems, it is important to improve the knowledge on the relationships between faults distributed across the strike of a fault system. Recent findings suggest that adjacent faults arranged across the strike of a narrow fault system in Central Italy, with faults spaced ~5 km across strike or less, works together to accommodate the regional deformation (Iezzi *et al*., 2019). However, less is known about the interaction between more distant across-strike faults.

Cowie *et al*. (2013; 2017) suggested that parallel sets of faults interact through time, with activity switching back and forth across-strike yet maintaining the regional strain-rate. This is supported by observation of post 1349 AD historical seismicity localized on specific sets of faults on the NE flank of the Apennines, yet earlier Holocene strains, constrained by observations of

offsets across post-Last Glacial Maximum (LGM) scarps, are distributed across the entire width of the orogen, including earthquakes in 1349 AD and earlier times that were clearly located on the SW flank of the orogen causing severe damage in Rome (Cowie *et al*., 2017; Beck *et al*., 2018). However, at the time of writing there are no direct observations of the switching activity between faults arranged across strike, on a timescale less than the age of the LGM.

The fault system in Attica, central Greece, provides an ideal opportunity to study the temporal relationships between activity on parallel sets of faults, over the required timescale, in order to provide observations of the characteristics of across-strike switching of activity. The Attica region contains sets of parallel active faults with across-strike fault spacing larger than 5 km (between 5-16 km). These faults have already revealed themselves as highly dangerous, for example during the 7th September 1999 Mw 6.0 earthquake, which caused severe damage in the northwest part of Athens and 143 deaths due to building collapse (Pavlides *et al*., 2002; Ganas *et al*., 2004). Thus, studying the evolution of the slip histories for faults in Attica could provide key information on the dynamics of fault systems with parallel faults, such as the Central Apennines, and on the mitigation of the seismic hazard of the city of Athens.

To do so, we present measurements of the exposure ages of three faults arranged parallel across the strike in the Attica fault system using *in-situ* ^{36}Cl cosmogenic exposure dating of fault planes tectonically-exhumed since the demise of the LGM. Detailed site characterization helped to ensure that the fault surface is exposed only through tectonic exhumation during repeated earthquakes, and it is not disturbed by geomorphological processes.

The concentrations of cosmogenic ^{36}Cl have been modelled using a Bayesian reversible-jump Markov chain Monte Carlo approach, which iterates the slip history many tens of thousands of times, forward modelling expected ^{36}Cl concentrations each time, to search for the best-fit to measured ^{36}Cl concentrations. This allows reconstruction of the slip histories of faults to define the Holocene activity rates by constraining (1) the slip-rate on active faults, (2) the timing of the last earthquake (Telap), (3) the mean recurrence interval for maximum magnitude earthquakes (Tmean) and (4) the variability in recurrence (CV), that is the standard deviation of recurrence intervals divided by the mean recurrence interval (Pace *et al*., 2016).

Our modelling shows that faults have episodic behaviour, with a non-systematic alternance of periods of rapid slip accumulation (i.e. earthquake clustering) and periods of quiescence (i.e. earthquake anti-clustering). The comparison between the modelled slip histories on the different faults shows that the activity switches between faults, with earthquake clusters alternating on the different faults: earthquake clustering on one specific fault is accompanied by low rates of activity on the other faults. These results show that parallel faults spaced > 5 km interact in terms of sharing the regional strain-rate, with switching activity between faults that affects the slip-rate on a single fault. The clustered behaviour of parallel faults implies that the definition of key parameters for seismic hazard assessments (Tmean, Telap and CV) is complicated in fault systems with across-strike distributed faults. Moreover, the retrieved slip histories also highlight a difference in the ages since the three fault scarps started to be preserved. The modelling performed in Attica, located at lower latitudes compared to Central Italy, shows that for these faults exist a correlation between the age since the fault scarp started to be preserved and the elevation of the fault scarp: the lower the elevation of the fault scarp, the older is the age since the scarp started to be preserved. This implies that, at these latitudes, the elevation above the sea level seems to play a role in the dynamics of the erosion processes associated with the LGM (e.g. freeze-thaw erosion and frost-shattering).

Overall, the measurements and modelling of cosmogenic ^{36}Cl concentrations on fault planes on three faults arranged across the strike of a fault system in Central Greece provides fundamental insights on the dynamics of normal fault systems, and on the interplay between the LGM-related erosion processes and elevation on the preservation of fault scarps. These results also imply important insights for the dynamics of faults in Central Italy, where multiple faults are arranged parallel across the strike of the fault system. We suggest that parallel faults within

the Central Apennines are likely to interact through time, with switching activity between faults distributed across the strike of the fault system. This can lead to the alternance of phases of earthquake clustering and anti-clustering on single faults located on different flanks of the fault system. Moreover, the results herein presented suggest that more work is needed to understand whether fault scarps in Southern Italy have started to be preserved for time periods older than 15 ± 3 ka.

References

Beck, J., S. Wolfers, and G. P. Roberts (2018): Bayesian earthquake dating and seismic hazard assessment using chlorine-36 measurements (BED v1), Geosci. Model Dev., 11 (2018), pp. 4383-4397.

Bennett, R. A., A. M. Friedrich and K. P. Furlong (2004): Codependent histories of the San Andreas and San Jacinto fault zones from inversion of fault displacement rates. Geology, 32(11), 961-964.

Cowie, P.A. and G.P. Roberts (2001): Constraining slip rates and spacings for active normal faults. Journal of Structural Geology, 23(12), pp.1901-1915 https://doi.org/10.1016/S0191-8141(01)00036-0.

Cowie P. A., R. J. Phillips, G. P. Roberts, K. McCaffrey, L. J. J. Zijerveld, L. C. Gregory, J. Faure Walker, L. N. J. Wedmore, T. J. Dunai, S. A. Binnie, S.P. H. T. Freeman, K. Wilcken, R. P. Shanks, R. S. Huismans, I. Papanikolaou, A. M. Michetti and M. Wilkinson (2017): Orogen-scale uplift in the central Italian Apennines drives episodic ehavior of earthquake faults, Nature Sci. Rep. 7., 44858; doi:10.1038/srep44858.

Iezzi, F., G. Roberts, J. F. Walker and I. Papanikolaou (2019): Occurrence of partial and total coseismic ruptures of segmented normal fault systems: Insights from the Central Apennines, Italy, Journal of Structural Geology, 126, 83-99. https://doi.org/10.1016/j.jsg.2019.05.003.

Pace, B., L. Peruzza, G. Lavecchia, and P. Boncio (2006): Layered seismogenic source model and probabilistic seismic-hazard analyses in central Italy. Bulletin of the Seismological Society of America, 96(1), pp.107-132.

Roberts, G. P., and A. M. Michetti (2004): Spatial and temporal variations in growth rates along active normal fault systems: an example from The Lazio–Abruzzo Apennines, central Italy. Journal of Structural Geology, 26(2), 339-376. http://dx.doi.org/10.1016/S0191-8141(03)00103-2.

THE SHALLOW STRUCTURE OF A SURFACE FAULT OF THE 30 OCTOBER 2016 MW 6.5 CENTRAL ITALY EARTHQUAKE FROM MULTIDISCIPLINARY GEOPHYSICAL APPROACH

S. Maraio[1], F. Villani[2], L. Serri[1], P.P.G. Bruno[3], L. Improta[2]

[1] Centro di Geotecnologie, Università di Siena, Italy

[2] Istituto Nazionale di Geofisica e Vulcanologia, Italy

[3] Dipartimento di Scienze della Terra, dell'Ambiente e delle Risorse, Università di Napoli Federico II

Introduction. The Pian Grande di Castelluccio is ~20 km^2 wide intermontane basin developed in the hangingwall of the Mt. Vettore normal fault-system (Fig. 1; Calamita and Pizzi, 1992, 1994; Calamita *et al*. 1992). The almost flat-bottomed plain (1300 m a.sl. average elevation) is surrounded by high and steep slopes on the western side and particularly on the eastern border, where Mt. Vettore (2476 m) represent the culmination of a > 1100 m high cumulative fault scarp. The substratum is made of Jurassic to Paleogene shallow-to-deep marly-calcareous deposits, and the plain is filled with sequences of lacustrine, alluvial fan and fluvio-glacial deposits (Coltorti and Farabollini, 1995; Pierantoni *et al*. 2013). The 30 October 2016 Mw 6.5 earthquake caused surface ruptures along this mountainside and within the plain (Villani *et al*., 2018): here, coseismic breaks closely follow the trend of a subtle fault scarp affecting Late Pleistocene to Holocene alluvial fan deposits, and which we label Valle delle Fonti fault (VF fault). On 30 October 2016, the average coseismic throw along this fault was about 0.05 m, and the overall rupture length is about 1.8 km. The paleoseismic history of the VF fault was first studied by Galadini and Galli (2003) and later revised by Galli *et al*., (2019) and Cinti *et al*., (2019). Villani and Sapia (2017) suggest syn-depositional fault activity producing

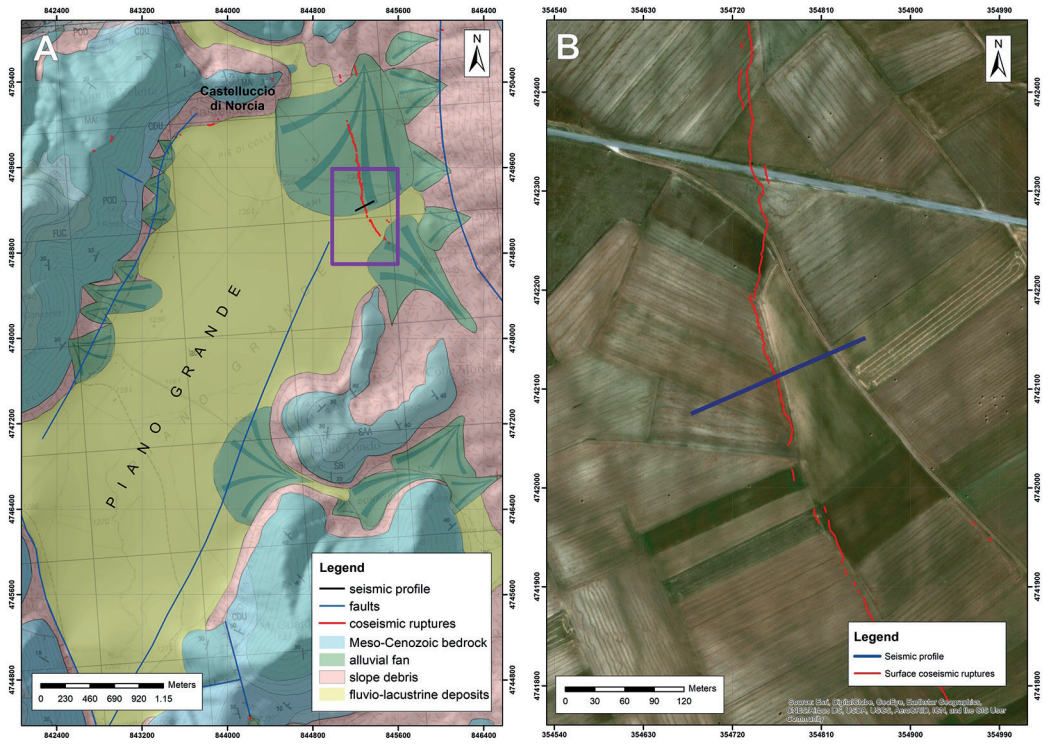

Fig. 1 - A) geological sketch map of the Pian Grande di Castelluccio basin (modified after Pierantoni *et al*. 2013). The violet rectangle encloses the survey area showed in figure 1B. B) Detail of the seismic survey.

>30 m total vertical displacement achieved since the Middle Pleistocene, based on the offset of electrical units across the VF fault trace, whereas a 2.3-2.8 m-high fault scarp at the surface was generated in the last ~12 kyr. Subsequent geophysical investigations by Villani *et al*., (2019) point out a high structural complexity of the VF shallow subsurface and evaluate 100-120 m total throw accrued by the VF fault in the last 0.4 Myr. In this study, we investigate in detail the ultra-shallow structure of the VF fault, combining reflection seismology, seismic refraction tomography and multichannel analysis of surface waves (MASW) with the available electrical resistivity data from Villani and Sapia (2017).

The seismic survey. The seismic profile was acquired across the coseismic surface rupture of the VF fault and coincides with the ERT profile acquired by Villani and Sapia (2017). The profile was acquired using a 5 kg hammer source; at each shot point we stacked 2 blows and source move-up was 2 m. The seismic data were recorded by fixed array of 96 vertical geophones with a 4.5 Hz eigen-frequency, placed at 2 m intervals along the 190-m-long dense, wide-aperture seismic profile.

Seismic data analysis and inversion. After a pre-processing flow, aimed at improving resolution and signal/noise ratio of seismic reflection data, the picking of the maximum of semblance on Common Mid Point (CMP) super-gathers was used in our attempt to define a velocity model (VNMO) for CMP ensemble stack. The final stack velocity macro-model (VNMO) from the CMP processing was smoothed and used for post-stack depth conversion.

Two different seismic refraction analysis was performed. The input data consists of 8640 first arrival travel-times handpicked on 90 Common Shot Gathers (CSG) and checked for consistency according to reciprocity rules. We applied a non-linear multi-scale tomography that does not require a starting reference model and is able to cope with very heterogeneous media as fault zones and tectonic basins (Improta *et al*., 2002, 2003, 2010; Improta and Bruno, 2007;

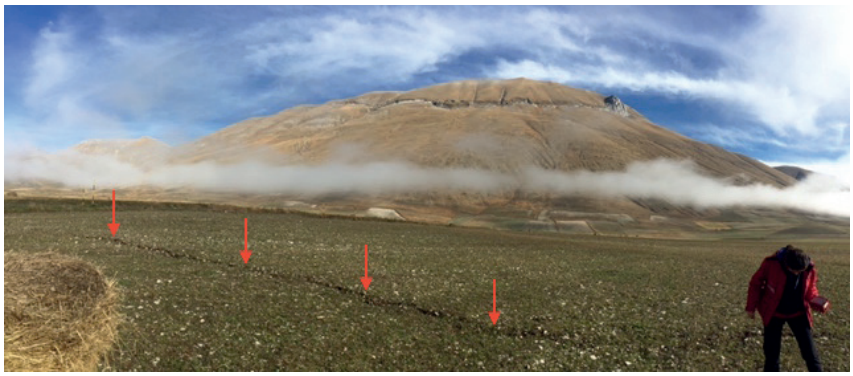

Fig. 2 - acquisition site. The red arrows indicate the 30 October 2016 coseismic rupture.

Bruno *et al*., 2010 b, 2013; Villani *et al*., 2015a, b, 2017, 2018b). Models are parameterized through velocity grid nodes and traveltimes are computed by a finite-difference technique, which accounts for transmitted, diffracted and head waves. The best-fit P-wave velocity model is searched by a Monte Carlo inversion method. We performed a second refraction tomography based on a linear inversion approach and on the SIRT image reconstruction technique (Gilbert, 1972). The theoretical travel times are computed via ray-tracing method, using a starting velocity model that is iteratively upgraded to minimize the misfit between observed and compute travel times.

The data for MASW analysis were extrapolated from acquired dataset using common receiver configurations with 24 geophones and a minimum offset of 1 m. Each common shot data was analyzed generating a frequency-phase velocity spectrum and picking the fundamental mode. The dispersion curve was successively inverted to generate a S-wave 1-D vertical profile. To constrain the space of the model-search, a range of parameters are defined *a-priori*. At last, a pseudo-2D shear-velocity section was made by the interpolation on aligning 1D models at the midpoint of each CSG (Yinhe *et al*., 2009).

By using the Vs pseudo-section and the Vp tomographic model, we computed the Vp/Vs ratios and the Poisson coefficient to infer the degree of saturation of the soils and in the fault zone and to facilitate comparison of velocity and stack sections with the electrical resistivity data. Seismic and resistivity models were also processed through the k-means algorithm, that performs a cluster analysis for the bivariate data set to individuate relationships between the two sets of variables (Bernardinetti *et al*. 2017). The result is an integrated model with a finite number of homogeneous clusters, which therefore helps to distinguish and interpret different geophysical facies.

Results. Both reflection image and velocity models clearly show a WSW-dipping normal fault zone, located at 40-80 m that matches the VF fault surface rupture. Analyzing the depth converted reflection section, the VF fault is clearly detected by an abrupt reflection truncation in the 5-80 m depth range, while synsedimentary activity is inferred by shallow reflectors that show back-tilt increasing with depth in the fault hangingwall. Reflection truncations indicate a cumulative fault throw, within the fan deposits, of about 30 m, which agrees with the cumulative throw since Middle-Late Pleistocene calculated by Villani *et al*. (2017). Furthermore, an unknown NW-dipping normal fault is detected in the eastern part of the profile, located at 120-150 m. The reflection image clearly points out the occurrence of alternating high-amplitude reflections that we interpret as sandy-gravels layers related to different phases of alluvial fan accretion. Those layers show variable dip and incremental steepening at depth due to recent fault activity.

The two Vp tomographic sections (i.e. linear and non-linear) have a resolution depth of about 50 m, show comparable features, but the non-linear velocity model better describes

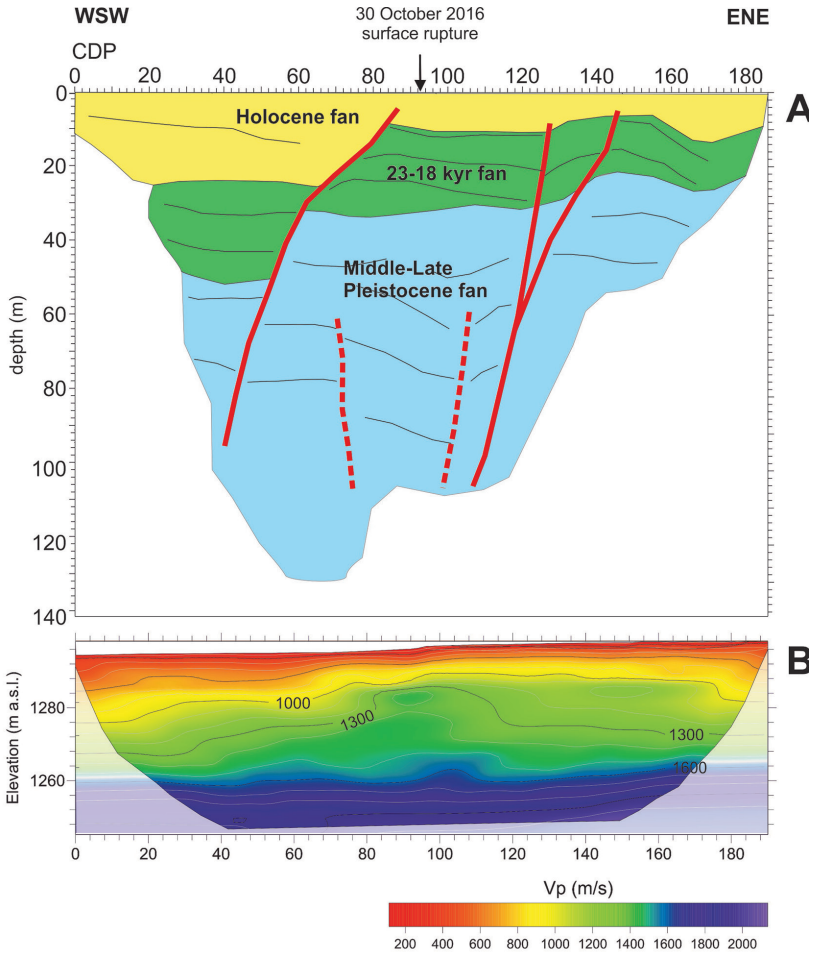

Fig. 3 - A) Line drawing and geological interpretation of depth converted reflection section; B) Vp tomographic model from SIRT algorithm.

the complexity of the fault zone. Vp and Vs models exhibit a lateral velocity variation in correspondence of the fault. Near-surface soils (Vp < 400 m/s) thicken just ahead the fault scarp and a low-velocity wedge (Vp < 700 m/s) is imaged in the shallow portion of the hanging wall. On the Vp models, the fault zone is characterized by a relatively high-velocity (1400-1500 m/s) body that dips SW. High Vp/Vs ratios (> 3) and the derived Poisson's coefficient indicate that this region represents a nearly-saturated medium, probably related to the increase of permeability within the fault zone due to fracturing and shearing. This appears in agreement with the low-resistivity signature in the ERT surveys by Villani *et al*. (2017), which hypothesized a fluid-filled fault zone made of fine granular sediments. Conversely, the low-velocity (Vp < 700 m/s) shallow wedge imaged down to 10-15 m to the west of the fault-zone is associated to low Vp/Vs ratios (around 2) and high resistivity values. We relate this low-Vp, low-Vp/Vs zone to loose/compact sand and gravel with low saturation degree that fill the fault hanging-wall. The results from the K-means cluster analysis also identify a homogeneous cluster in correspondence of the saturated fault zone.

Acknowledgements. We thank Vincenzo Sapia for the ERT data processing and Stefano Bernardinetti for his precious comments during the cluster analysis processing. This survey was financially supported by the INGV Project MIUR-FISR 2016-2017 4-D - *Structure of Central Italy and active geodynamics process* - Task1: *3-D Structure of Central Italy*.

References

Bernardinetti S., Maraio S., Bruno P. P. G., Cicala V., Minucci S., Giannuzzi M.,*et al*.; 2017: *Potential shallow aquifers characterization through an integrated geophysical method: multivariate approach by means of k-means algorithms*. Acque Sotterranee-Italian Journal of Groundwater, 6(2).

Bruno P.P.G., Castiello A., Improta L.; 2010b: *Ultrashallow seismic imaging of the causative fault of the 1980, M6.9, southern Italy earthquake by pre-stack depth migration of dense wide-aperture data*. Geophys. Res. Lett., 37, L19302, doi:10.1029/2010GL044721.

Bruno P.P.G., Castiello A., Villani F., Improta L.; 2013: *High-resolution densely spaced wide-aperture seismic profiling as a tool to aid seismic hazard assessment of fault-bounded intramontane basins: application to Vallo di Diano, Southern Italy*. B. Seismol. Soc. Am., 103, n. 3, 1969-1980, doi: 10.1785/0120120071.

Calamita F., Pizzi A.; 1992: *Tettonica quaternaria nella dorsale appenninica umbromarchigiana e bacini intrappenninici associati*. Studi Geol. Camerti 1992 (1), 17–25.

Calamita F., Pizzi A.; 1994: *Recent and active extensional tectonics in the southern Umbro-Marchean Apennines (central Italy)*. Mem. Soc, Geol. Ital. 48, 541–548.

Calamita F., Pizzi A., Roscioni M.; 1992: *I fasci di faglie recenti ed attive di M. Vettore – M. Bove e di M. Castello – M. Cardosa (appennino Umbro-Marchigiano)*. Studi Geologici Camerti, 1992/1, 81-95.

Cinti F. R., De Martini P. M., Pantosti D., Baize S., Smedile A., Villani F., *et al*.; 2019:. *22-kyr-Long Record of Surface Faulting Along the Source of the 30 October 2016 Earthquake (Central Apennines, Italy), from Integrated Paleoseismic Data Sets*. Journal of Geophysical Research: Solid Earth, 124, https://doi.org/10.1029/2019JB017757

Coltorti M., Farabollini P.; 1995: *Quaternary evolution of the Castelluccio di Norcia Basin*. Il Quaternario 8, 149–166.

Galadini F., Galli P.; 2003: *Paleoseismology of silent faults in the Central Apennines (Italy): the Mt. Vettore and Laga Mts. Faults*. Annals of Geophysics, 46(5), 815-836, https://doi.org/10.4401/ag-3457

Galli P., Galderisi A., Peronace E., Giaccio B., Hajdas I., Messina P., *et al*.; 2019:. *The Awakening of the Dormant Mount Vettore Fault (2016 Central Italy Earthquake, Mw 6.6): Paleoseismic Clues on Its Millennial Silences*. Tectonics, 38(2), 687-705.

Gilbert P.; 1972: *Iterative methods for the three-dimensional reconstruction of an object from projections*. Journal of Theorical Biology, 36(1), 105-117.

Improta L., Zollo A., Herrero A., Frattini M. Virieux J. Dell'Aversana P.; 2002: *Seismic imaging of complex structures by non-linear traveltime inversion of dense wide-angle data: Application to a thrust belt*. Geophys. J. Int., 151, 264–278, doi: 10.1046/j.1365-246X.2002.01768.x.

Improta L., Zollo A., Bruno P. P., Herrero A., Villani F.; 2003: *High resolution seismic tomography across the 1980 (Ms 6.9) Southern Italy earthquake fault scarp*. Geophys. Res. Lett., 30(10), 1494, doi: 10.1029/2003GL017077.

Improta L., Bruno P. P.; 2007: *Combining seismic reflection with multifold wide-aperture profiling: An effective strategy for high-resolution shallow imaging of active faults*. Geophys. Res. Lett., 34, L20310, doi:10.1029/2007GL031893.

Improta L., Ferranti L., De Martini P. M., Piscitelli S., Bruno P. P., Burrato P., Civico R., Giocoli A., Iorio M., D'Addezio G., Maschio L.; 2010: *Detecting young, slow-slipping active faults by geologic and multidisciplinary high-resolution geophysical investigations: A case study from the Apennine seismic belt, Italy*. J. Geophys. Res., 115, B11307.

Yinhe L. *et al*.; 2009: *Research on the middle-of-receiver-spread assumption of the MASW method. Soil Dynamics and Earthquake Engineering*, 29.1 (2009): 71-79.

Pierantoni P.P., Deiana G., Galdenzi S.; 2013: *Geological map of the Sibillini Mountains (Umbria-Marche Apennines, Italy)*. Ital. J. Geosci. 132 (3), 497–520.

Villani F., Pucci S., Civico R., De Martini P.M., Nicolosi I., D'Ajello Caracciolo F., Carluccio R., Di Giulio G., Vassallo M., Smedile A., Pantosti D.; 2015a: *Imaging the structural style of an active normal fault through multi-disciplinary geophysical investigation: a case study from the Mw 6.1, 2009 L'Aquila earthquake region (central Italy)*. Geophys. J. Int., 200 (3), 1676-1691, doi: 10.1093/gji/ggu462.

Villani F., Tulliani V., Sapia V., Fierro E., Civico R., Pantosti D.; 2015b:. *Shallow subsurface imaging of the Piano di Pezza active normal fault (central Italy) by high-resolution refraction and electrical resistivity tomography coupled with time-domain electromagnetic data*. Geophys. J. Int., 203 (3), 1482-1494, doi: 10.1093/gji/ggv399.

Villani F., Sapia V.; 2017: *The shallow structure of a surface-rupturing fault in unconsolidated deposits from multi-scale electrical resistivity data: the 30 October 2016 Mw 6.5 central Italy earthquake case study*. Tectonophysics, 717(16), 628-644, doi: 10.1016/j.tecto.2017.08.00.

Villani F., Improta L., Pucci S., Civico R., Bruno P.P., Pantosti, D.; 2017:. *Investigating the architecture of the Paganica Fault (2009 Mw 6.1 earthquake, central Italy) by integrating high-resolution multiscale refraction tomography and detailed geological mapping*. Geophys. J. Int., 208(1), 403-423, doi:10.1093/gji/ggw407.

Villani F., Pucci S., Civico R., De Martini P.M., Cinti F.R., Pantosti D.; 2018: *Surface faulting of the 30 October 2016 Mw 6.5 central Italy earthquake: Detailed analysis of a complex coseismic rupture*. Tectonics, 37, 10, 3378-3410, https://doi.org/10.1029/2018TC005175.

Villani F., D'Amico S., Panzera F., Vassallo M., Bozionelos G., Farrugia D., Galea P.; 2018b: *Shallow high-resolution geophysical investigation along the western segment of the Victoria Lines Fault (island of Malta)*. Tectonophysics, 724, 220-233, 10.1016/j.tecto.2018.01.010.

Villani F., Sapia V., Baccheschi P., Civico R., Di Giulio G., Vassallo M., Marchetti M., Pantosti D.; 2019: *Geometry and structure of a fault-bounded extensional basin by integrating geophysical surveys and seismic anisotropy across the 30 October 2016 Mw 6.5 earthquake fault (central Italy): the Pian Grande di Castelluccio basin*. Tectonics, 38, 1, 26-28, doi: 10.1029/2018TC005205.

STRUCTURAL ANALYSIS OF THE 2016 EARTHQUAKE RUPTURES GEOMETRIES IN THE NORTHERN SECTOR OF THE SIBILLINI MOUNTAINS

M. Menichetti, E. Tirincanti, M. Roccheggiani
Dipartimento di Scienze Pure e Applicate, Università di Urbino, 61029, Urbino (PU)

A complete and detailed survey of the geometries of coseismic ruptures is central to define the kinematic and the dynamic relationships of active faults and the regional seismic hazard. Earthquakes producing coseismic surface deformation generate offsets in the landforms that are linked to the kinematics and the magnitude of the seismic events. Even though their importance in the seismic hazard assessment and their utility in the developing hazard reduction procedure, the ground ruptures accurate morphologies and their structural geometries remain uncertain. In many cases, the relevant extension of the coseismic ruptures and the morphologically complex landscape made it necessary to do a long-time fieldwork to recognize and survey each strand of the fractures. During the earthquakes sequence occurred in the Sibillini Mountains in Central Italy from August to October 2016, several ground ruptures have been generated over a large area. These ruptures, that reactivated pre-existing normal faults, extend from the Tronto river valley in the south to the Chienti river valley in the north, over a distance of about 40 km. On August 24th, a Mw 6.1 earthquake struck the southernmost area between the town of Amatrice and Arquata del Tronto. Several ground ruptures along different strands of SW dipping extensional faults developed for more than 20 km in the M.Vettore area. The October 26th Mw 6.0 earthquake was centred in the Visso area, approximately 30 km northwest of the previous event. In this case, only few coseismic fractures have been surveying because, on October 30th, a new seismic event of Mw 6.5 occurred in the area near Norcia. This event, occurred between the epicenters of the former earthquakes. It reactivated existing ground fractures and produced further ruptures over a larger area, including the northernmost sector of the Sibillini Mountains (Fig. 1). Despite many authors published preliminary maps of the ruptures for the central part of the epicentral area, especially for the M.Vettore sector, the structural and kinematic features of the northernmost sector have been poorly investigated. A highly detailed map of the coseismic surface ruptures is proposed for the area between M. Bove, Visso and Pieve Torina integrating a classical geo-structural field survey with low altitude aerial photos and remote sensing data interpretation. Images with centimeter resolution obtained via SfM (Structure From Motion) photogrammetry permitted to map in 3D the details of the vertical and horizontal displacements, constraining the spatial geometrical characteristics of the active faults. The spatial pattern of fracture distribution, ruptures offsets, and links between geometries along the fault strands are fundamental in order to extrapolate and constrain the depth of the fault planes from a seismotectonic point of view. The surveyed ruptures seem to be the result of the cumulative effects of several events during the 2016 earthquake sequence. In the M. Bove area at least three subparallel rupture strands run in the NW-SE direction for about 5 km on the whole western slope of M. Bicco and M. Bove Sud (Fig. 1). Other fractures strands, of many tens of meters of

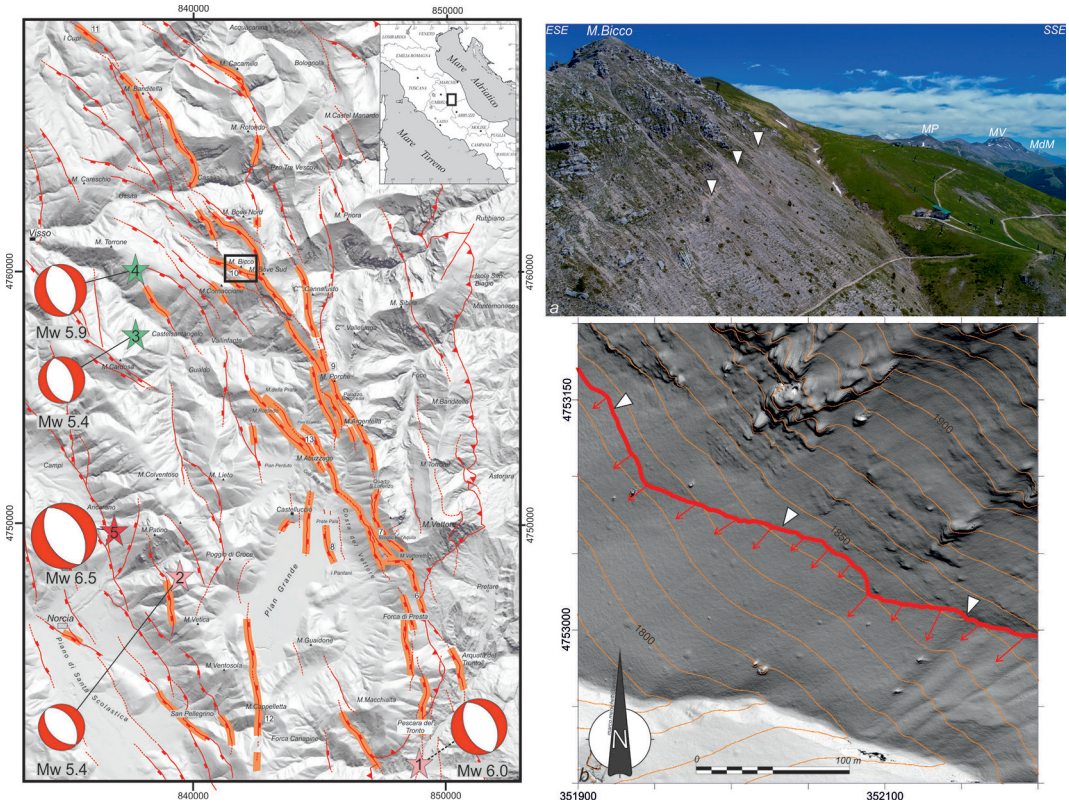

Fig. 1 - left - structural map of the main Plio-Quaternary normal faults (barbs in the hw) and the Mio-Pliocenico Sibillini thrust (triangle in the hw). The seismic ruptures are highlighted and the stars are the epicenters of the main earthquakes. The enclose frame indicate the location of images a) and b). In the right - a) oblique aerial view of SW slope of M. Bicco; in the background M. delle Porche (MP), M. Vettore (MV) and M. Macera della Morte (MdM); b) DSM of the same area of M.Bicco with indicate the coseismic ruptures.

length, are present in the summit sector of M. Bove North faces. Some of these ruptures, with a displacement of a few centimeters, had been detected after the October 26th event and then reactivated by the October 30th earthquake. In this area, all the ruptures are located along the SW dipping normal faults that run down through the axial part of the M. Bove anticline. The geological offset of these extensional structures is several hundred meters, with the footwall in Jurassic carbonate bank and the hanging wall in the Upper Jurassic to Lower Cretaceous limestone formations. The main rupture, of a length just over km, is composed of at least three sectors arranged in a right staircase with an average vertical offset of 0.3 m and an average opening of 0.15 m. Another rupture of few hundred meters in length, with a displacement of about 0.15 m, is located along the same NW-SE lineament, in the south-western slope of M. Cornaccione. Northward, other coseismic fractures are mapped in the area of Ussita village, and in the western slope of M. Rotondo, until the M. Banditella. These ruptures are arranged with sectors of many hundred meters of length subdivided into strands of tents meters. The geometry of these later, in the stepped slope, is controlled by gravitational processes affecting the debris and soil cover. The main ruptures are located in the Upper Cretaceous-Eocene limestone and marly-limestone, with a vertical displacement reaching up the meter, with an average of 0.35 m. In the area of Cupi, other coseismic fractures develop in correspondence of an SW dipping normal fault with a geological offset of hundred meters. The coseismic fractures have an average vertical offset of 0.18 m and a horizontal displacement of 0.1 m. It is not clear if these ruptures are connected to the seismic event of 26th or 30th October, because the area was surveyed

only during 2017 springtime. Other alignments of relevant superficial coseismic fractures, with centimeters displacement and connected to the SW dipping normal fault, are mapped along the Nottoria - Preci alignment. They run from the Norcia area through the Nera river valley up to the north. Geometrical analysis of these displacements versus distance of the fault planes and ground ruptures was analyzed along several cross-sections orthogonal to the fault strikes. The cross-sections highlight slip accommodation through linkage, which shows to be a common fault growth mechanism. Moreover, the analysis of coseismic ruptures shows that about 40% of the total surface displacement occurred as off-fault deformation, over a mean deformation zone width of a hundred meters. The rupture zone fabric and the off-fault deformation is mostly controlled by the structural complexity of the fault system, with a weaker correlation with the rheology of the ruptures materials.

HOW DEFINING A QUALITY FACTOR TO CLASSIFY EARTHQUAKE LOCATIONS

M. Michele[1], A. Emolo[2], D. Latorre[1]
[1] Istituto Nazionale di Geofisica e Vulcanologia, Rome, Italy
[2] Dipartimento di Fisica 'E. Pancini', Università Federico II, Naples, Italy

After computing an earthquake location, it is necessary to define the uncertainties related to the obtained estimate. Generally, despite of the method used to locate a hypocenter, the solution is validated *a posteriori* considering different reasonable range of the uncertainty estimators derived after the inversion, like the root mean square (RMS), the number of phases used (NPHS), the azimuthal gap (GAP) and so on. Although this is the standard way to classify the goodness of a seismic location, it is still an unsolved problem to establish an exhaustive and quantitative criterion that provides a simple and accessible classification of earthquake location.

Aiming at giving an objective estimate of a seismic location's quality, we analyze the behavior of different uncertainty estimators, founding that they are dependent on each other (Fig. 1), implying the need to evaluate all the estimators together. For this reason, we combined in an empirical formula the different uncertainty estimator of an earthquake location with the goal of determining a unique value depicting the reliability of the solution. The formula is applied after estimators normalization (so to legitimate the summation of different physical measurements) and a cleaning procedure based on the Chauvenet criterion application for outliers removal. The formula provides a value that we named q_f (quality factor), ranging from 0 to 1. The smaller is the q_f value, the more constrained the location is. By computing this value, a simple classification of the location's quality can be done. We defined 4 evenly spaced goodness intervals for q_f, corresponding to four quality classes, from A (best class) to D (worst class).

To verify the efficiency of the described approach, we applied it to different case studies, sequence and no-sequence seismicity, located by means of different method (linearized and global). Our results confirm a reasonable quality classification for the statistical distribution of parameters, allowing to highlight, just using best quality classes locations, the active seismic structures. The uncertainty estimators used, common for both the cases study, are the root mean square (RMS), the number of phases (NPHS), the azimuthal gap (GAP), the formal errors of horizontal (ERH) and vertical (ERZ) component. Only for the locations derived with the global method, where the hypocenters are provided with a probability density function, additional parameters can be used for adding information about the uncertainty of the location. We added the distance between the pdf expected value and its maximum likelihood (LOCDIST) that

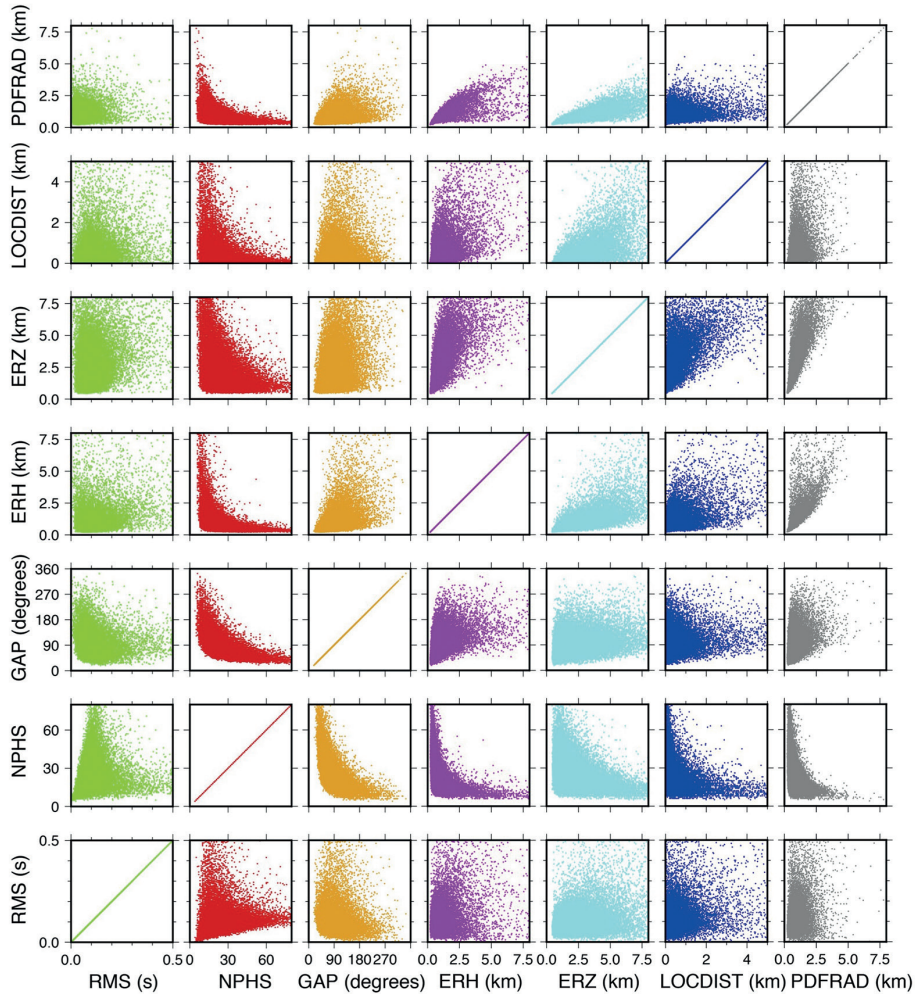

Fig. 1 - Correlation matrix for different uncertainty estimators.

provides information about the symmetry of the pdf distribution and the PDFRAD, representing the radius of a sphere having volume equivalent to that recovered by the scatter points (i.e., samples of the pdf distribution). The formula is:

$$q_f(i) = \left(\frac{w_1 RMS_n(i)^2 + w_2 NPHS_n(i)^2 + w_3 GAP_n(i)^2 + w_4 ERH(i)^2 + w_5 ERZ_n(i)^2 + w_6 DISTLOC_n(i)^2 + w_7 PDFRAD(i)^2}{N_{est}} \right)^{\frac{1}{2}}$$

where N_{est} is the number of used estimators and w_i are the weights that could be eventually associated with each of them.

We show the application of our criterion to two cases study. First of all, we used the 32,773 crustal earthquakes of the 2016-2017 Central Italy seismic sequence (Chiaraluce *et al*., 2017), located by means the NonLinloc code (Lomax *et al*., 2000), based on a global approach. The sequence was recorded by Italian National Seismic Network (Rete Sismica Nazionale, RSN) and 100 stations, in an 100x100 km^2 area around the first mainshock, were used for the relocation.

Then, we used a 3-year long subset (2013-2015) of the Italian Seismicity Catalog available in the database ISIDe (ISIDe Working Group, 2016; see Data and Resources), composed by 68,151 earthquakes located by mean of IpoP code, based on a linearized approach. In this case, we used crustal and lithospheric earthquakes (down to 600 km) occurred on the whole Italy

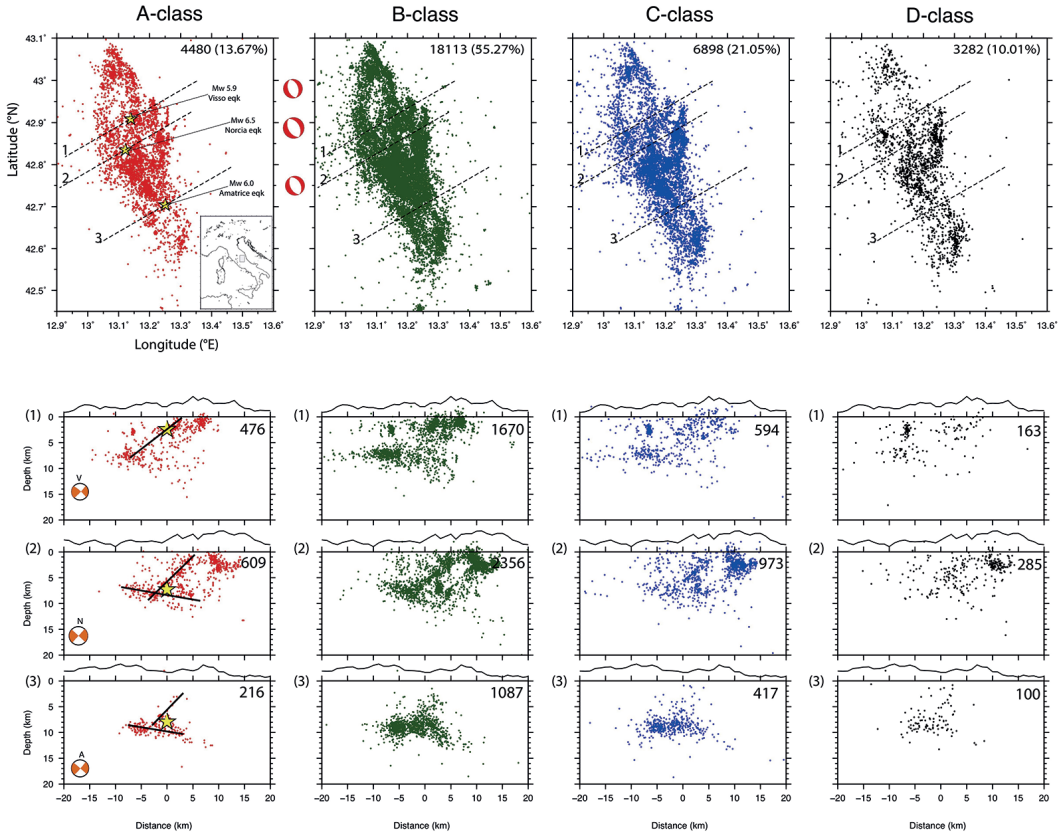

Fig. 2 - Map-view and cross-sections, distinct by the quality class. Starting from left, the first, the second, the third and the fourth panel are the A-, B-, C- and D-class locations, respectively. The stars are the Mw >= 5.9 earthquakes occurred during the sequence. Related focal mechanisms are reported. Cross-sections are oriented N60E (dashed lines in map-view) and show +/-2.5 km seismicity projected. Thick lines in A-class cross-sections underline the main faults. Number of pertaining earthquake locations is reported (after Michele *et al*., 2019 in press).

(about 1200x1200 km^2 area), located by the whole Italian National Seismic Network (RSN) (about 350 stations). No relevant seismic sequence occurred in the analyzed period.

We show the classification of locations for the first case study, in Fig. 2.

We demonstrate the usefulness, the feasibility and the flexibility of this innovative method, that can help also for routinely monitoring location computation.

Here we illustrated the application of the method to two catalogs, related to two different case studies. We found that the approach works with different location method and different number of uncertainty estimators used. We have to understand how to ensure the steady-state of uncertainty estimators with time as when a long-in-time catalog is used, theoretically you have to consider that the q_f computed could vary during different stations-hypocenters configuration periods.

References

Chiaraluce L., Di Stefano R., Tinti E., Scognamiglio L., Michele M., Casarotti E., *et al*.; 2017: The 2016 central Italy seismic sequence: A first look at the mainshocks, aftershocks, and source models. Seism. Res. Let., 88 757-771.

Lomax A., Virieux J., Volant P., Berge C.; 2000: Probabilistic earthquake location in 3D and layered models: Introduction of a Metropolis-Gibbs method and comparison with linear locations, in Advances in Seismic Event Location Thurber, C.H., and N. Rabinowitz (eds.), Kluwer, Amsterdam, 101-134.

Michele M., Latorre D., Emolo A.; 2019: An Empirical Formula to Classify the Quality of Earthquake Locations. Seism. Soc. Am., in press.

THE 2016-2017 CENTRAL ITALY SEISMIC SEQUENCE: FROM A REAL-TIME ANALYSISTS DATA TO AN AUTOMATIC AND NEARLY REAL TIME CATALOG

M. Michele, L. Chiaraluce, R. Di Stefano
INGV (National institute of Geophysics and Volcanology), Rome

Within few months after the first mainshock (Mw 6.0, Amatrice 2016/08/24) of the Central Italy seismic sequence, a quasi-automatic procedure was developed to locate the aftershocks occurring in the epicentral area, by using the data collected in monitoring environment at INGV (National Institute of Geophysics and Volcanology). The location code implemented in the procedure was NonLinLoc (Lomax *et al*., 2001), based on a probabilistic approach in determining the hypocenter location, that allows to retrieve information about the probability density function related to it. For this reason, it gives very exhaustive estimates of the location uncertainty and robustness. We used a 1D velocity model and we included in the relocation process the stations corrections to balance the lack of information about shallow depth layers. With this setting, we produced the first absolute locations catalog for the seismic sequence (Chiaraluce *et al*., 2017), covering the period 2016/08/24 – 2016/11/30.

We built an automatic procedure to update in near-real time the locations occurring during the sequence, up to January 2018.

Considering that we reached more than 90,000 locations, we tried to improve the retrieved locations, by using the double-difference method, implemented in the HypoDD code (Waldhauser *et al*., 2001) extending the catalogue in time up to 2018/01/18. Since our goal was to highlight active structures, building a fast procedure, able to produce in a short time refined pictures of structures, we selected the earthquakes locations' qualities (RMS £ 0.5 s, horizontal and vertical formal errors £ 1.5 km and £ 3.0 km, respectively, at least 10 P- and S-phases, and an azimuthal gap £ 180°) and the earthquakes magnitudes (M_w ³ 1.5). The selected dataset, including ~34,000 events, consists of 612,207 P and 465,693 S travel times recorded by the INGV monitoring room personnel and ~4.4 millions of P and ~1.1 millions of S times computed by means of cross-correlation procedure.

The obtained relocations allow us to describe the fault system structure, achieving improved locations resolution, that highlight minor anti- and synthetic structures not visible before and that give insights about the basal layer (Michele *et al*., submitted to JGR). In particular, we focused on the space-time evolution of the sequence, on the system geometry description, exploring details in map view and in cross-sections. The resulting complex fault system is 80 km long and NW-SE trending, composed of SW-dipping normal faults segments (15-30 km long). The dip of the entire fault system is variable and ranges from 38° to 55° moving from South to the North, while the strike is pretty constant. The updated locations clearly underline the shear-zone, whose depth ranges from 6 to 9 km, presenting diverse undulations and a step probably corresponding to the intersection between the main and the secondary faults of the Norcia earthquake (2016/10/30).

Seismicity alignments seem to correspond to geological faults at depth, looking at the comparison between the geological profiles and cross-sections.

Another focus regards the comparison of the relocated 2016-2017 sequence with the two previous Central Apennines sequences: Colfiorito 10997 and L'Aquila 2009. Looking at the structures activated during the sequence and before, we see that to the North, the faults described by the seismicity are parallel to the Colfiorito fault, while to the South seismicity aligns on the Campotosto fault, already activated during the 2009 sequence, and extends its lengths at depth.

The approach used, able to recover the uncertainties on the travel times recorded by mean of cross-correlation procedure and to achieve accurate scientific results starting from a real-time analysists data, suggested to adopt this work flow in near real time, aiming to determine

a rapid image of the activated structures during a sequence. This could represent the first step toward the integration in the INGV monitoring room of the DDRT (double-difference in near-real-time).

References

Lomax A., Zollo A., Capuano P., Virieux J.; 2001: *Precise, absolute earthquake location under Somma-Vesuvius volcano using a new 3D velocity model*. Gephys. J. Int., 146, 313-331.

Waldhauser F.; 2001: HypoDD: *A program to compute double-difference hypocenter locations*. U.S. Geol. Surv. Open File Rep., 01–113.

Chiaraluce L., Di Stefano R., Tinti E., Scognamiglio L., Michele M., Casarotti E., et. al.; 2017a:

The 2016 central Italy seismic sequence: A first look at the mainshocks, aftershocks, and source models. Seismological Research Letters, 88(3), 757-771.

Michele M., Chiaraluce L., Di Stefano R., Waldhauser F.; 2019: *From data recorded at the Italian National Network to fine-scale fault geometry of the 2016-2017 Central Italy Seismic Sequence*. Submitted to JGR.

STIMA RAPIDA DELLA MW PER LA MICROSISMICITÀ REGISTRATA NELL'AREA DI COLLALTO (TV)

L. Moratto[1], A. Lanzoni[1,2], E. Priolo[1], M.A. Romano[1]

[1] Istituto Nazionale di Oceanografia e di Geofisica Sperimentale - OGS, Trieste, Italy

[2] Università di Trieste, Trieste, Italy

L'iniezione e l'estrazione di fluidi nel sottosuolo può far variare la pressione dei fluidi in profondità rendendo instabili eventuali faglie e aumentando la possibilità di innescare terremoti. Lo studio della sismicità locale, e in particolare della microsismicità, nelle aree in cui tali attività sono sviluppate, sono elementi essenziali per discriminare tra eventi naturali e terremoti eventualmente indotti. In questo contesto, la magnitudo da momento (M_W) è un parametro chiave sia per valutare il bilancio energetico e gli sforzi coinvolti nel processo di rottura del terremoto, sia per valutare accuratamente il rischio sismico correlato. Disporre di procedure rapide per la stima della M_W è estremamente importante, dato che questa grandezza fornisce una stima accurata dell'energia sismica effettiva rilasciata durante un terremoto, anche in caso di piccoli eventi (Moratto *et al*., 2017).

In questo studio abbiamo stimato la M_W per la microsismicità registrata in oltre sei anni attorno al sito di stoccaggio sotterraneo di gas presente nell'area di Collalto (Italia nord-orientale) che è monitorata da una rete sismica dedicata - RSC (Priolo *et al*., 2015). L'area di Montello-Collalto, dove viene svolta questa attività industriale, è densamente popolata e caratterizzata da un rilevante rischio sismico (Romano *et al*., 2019).

In questo studio abbiamo applicato l'approccio proposto da Atkinson *et al*. (2014) basato sull'uso di spettri di risposta per i quali è stato proposto un rapporto di scalatura con M_W pari a 3/2. In questo lavoro, abbiamo innanzitutto verificato sperimentalmente che questa relazione è valida analizzando i segnali verticali registrati da una specifica stazione per una sequenza sismica avvenuta nel 2015 nell'area di studio. Poi, abbiamo esteso la procedura originariamente proposta da Moratto *et al*. (2017) per l'Italia nord-orientale al fine di rendere più efficace la stima di M_W per la microsismicità ($M_W < 1.5$) utilizzando lo spettro di risposta calcolato a un periodo più corto, cioè a 0.1 s (SA01). Nonostante la stima di M_W derivata da SA01 sia caratterizzata da una maggiore incertezza, questo sviluppo ci consente di stimare il momento sismico fino a un valore minimo di magnitudo di 0.4. Inoltre, abbiamo introdotto all'interno della procedura la correzione relativa alla risposta di sito per eliminare gli effetti di amplificazione locale e la distorsione spettrale dovuta all'installazione in profondità dei velocimetri del pozzo. Questa

ulteriore correzione migliora significativamente i risultati finali, come evidenziato dal confronto con la magnitudo da momento stimata da Moratto *et al*. (2019) per un sottoinsieme di eventi.

Utilizzando questo nuovo approccio, abbiamo stimato M_W per 1659 dei 1773 terremoti presenti nel catalogo originale, con una percentuale di successo del 94%. L'intervallo di magnitudo stimata varia dall'originale $-1.8 \leq M_L \leq 3.8$ a $0.4 \leq M_W \leq 3.5$.

La regressione ortogonale evidenzia che M_W e M_L sono correlate linearmente con un coefficiente angolare di 2/3, analogamente a quanto osservato in altre aree, ma con un valore di intercetta sull'asse M_L pari a 0.82, che è un valore leggermente maggiore rispetto a quello calcolato da Moratto *et al*. (2017) per l'Italia nord-orientale. Questa modesta variazione può essere correlata o alle diverse proprietà di attenuazione del mezzo di propagazione tra le due aree di interesse, considerando la banda di frequenza più elevata e l'intervallo di distanza più breve intrinseche adottate in questo studio, o ad alcune differenze nelle procedure utilizzate per stimare M_L dalle reti sismiche della RSC e dell'OGS per l'Italia nord-orientale. In ogni caso, il fattore di scala di 2/3 è in accordo con il valore previsto dai modelli teorici e con quanto osservato negli studi precedenti, e conferma l'efficacia della procedura proposta nello stimare M_W dai valori di SA anche per i microterremoti. I residui di magnitudo in funzione della distanza rimangono perlopiù costanti, tranne a distanza ipocentrale minore di 10 km, dove gli effetti di near-field (non considerati in questo studio) possono avere un impatto importante.

Abbiamo infine stimato, per il nuovo dataset, la relazione frequenza-magnitudo per valutare la magnitudo di completezza (M_C) e i parametri della Gutenberg-Richter (valori *a* e *b*) utilizzando M_W, e confrontato i risultati ottenuti con quelli basati su M_L. La differenza riscontrata nella stima di tutti i parametri, ma soprattutto del valore *b*, ci spinge ad evidenziare le possibili conseguenze che possono derivare dall'uso di M_W anziché M_L, o, peggio, dal mescolare i due tipi di magnitudo, nella valutazione della pericolosità sismica (Deichmann, 2017). Poiché M_L porta a stimare la dimensione della porzione di faglia soggetta a rottura in maniera non consistente se applicata alla microsismicità o a terremoti più forti (Deichmann, 2018), ne consegue che è preferibile stimare i parametri della relazione Gutenberg-Richter (*a* e *b*), nonché la magnitudo di completezza, esclusivamente sulla base della relazione frequenza-M_W. Ricordiamo che disporre di una stima affidabile del valore del coefficiente *b* è importante anche per discriminare la sismicità indotta da quella naturale (Stabile *et al*., 2014; Goebel *et al*., 2016).

Sottolineiamo, infine, che la nostra procedura può entrare a far parte delle analisi standard effettuate in tempo reale nell'ambito del monitoraggio di attività industriali in grado di innescare sismicità, soprattutto quando svolte in regioni tettonicamente attive; tale procedura infatti potrebbe essere un fondamentale aiuto nell'interpretare l'origine della microsismicità, supportando più efficacemente eventuali processi decisionali (come ad esempio i protocolli a semaforo).

Bibliografia

Atkinson G.M., Greig W.D. and Yenier E.; 2014: Estimation of moment magnitude (M) for small events (M<4) on local networks. Seismol. Res. Lett., **85**, 1116 -1124.

Deichmann N.; 2017: Theoretical basis for the observed break in ML/Mw scaling between small and large earthquakes. Bull. Seism. Soc. Am., **107**, 505-520.

Deichmann N.; 2018: The relation between ME, ML and Mw in theory and numerical simulations for small to moderate earthquakes. J. Seismol., **22**, 1645-1668.

Goebel T.H.W., Hosseini S.M., Cappa F., Hauksson E., Ampuero J.P., Aminzadeh F. and Saleeby J.B.; 2016: Wastewater disposal and earthquake swarm activity at the southern end of the Central Valley, California. Geophys. Res. Lett., **43**, 1092–1099.

Moratto L., Saraò A. and Priolo E.; 2017: Moment magnitude (M_W) estimation of weak seismicity in Northeastern Italy. Seism. Res. Lett., **88**, 1455-1464.

Moratto L., Romano M.A., Laurenzano G., Colombelli S., Priolo E., Zollo A., Saraò A. and Picozzi M.; 2019: Source parameter analysis of microearthquakes recorded around the underground gas storage in the Montello-Collalto Area (Southeastern Alps, Italy). Tectonophysics, **762**, 159-168.

Priolo E., Romanelli M., Plasencia Linares M.P., Garbin M., Peruzza L., Romano M.A., Marotta P., Bernardi P., Moratto L., Zuliani D. and Fabris P.; 2015: Seismic monitoring of an underground natural gas storage facility: The Collalto Seismic Network. Seism. Res. Lett., **86**, 109–123.

Romano M.A., Peruzza L., Garbin M., Priolo E. and Picotti V.; 2019: Microseismic Portrait of the Montello Thrust (Southeastern Alps, Italy) from a Dense, High-Quality Seismic Network. Seism. Res. Lett., **90**, 1502-1517.

Stabile T.A., Giocoli A., Lapenna V., Perrone A., Piscitelli S. and Telesca L.; 2014: Evidence of Low-Magnitude Continued Reservoir-Induced Seismicity Associated with the Pertusillo Artificial Lake (Southern Italy). Bull. Seism. Soc. Am., **104**, 1820–1828.

DETAILED STUDY OF THE 2010-2014 POLLINO SWARM-LIKE SEQUENCE (ITALY) AND IMAGING OF SURROUNDING AREA

F. Napolitano[1], A. Gervasi[2,3], D. Galluzzo[2], L. De Siena[4], R. Scarpa[1], M. La Rocca[3]

[1] Università degli Studi di Salerno, Fisciano (SA), Italy

[2] INGV, Roma, Italy

[3] Università della Calabria, Arcavacata di Rende (CS), Italy

[4] JGU, Mainz, Germany

Introduction. A sequence of almost 10.000 small-to-medium size ($M \leq 5$) earthquakes occurred between 2010 and 2014 in the western sector of the Pollino Range, Southern Italy. The seismic events were distributed in time as a swarm-like sequence rather than a classic mainshock-aftershock succession (Passarelli *et al*., 2015, Totaro *et al*., 2015). This behaviour is typical of slow strain areas like Mt.Pollino (Cheloni *et al*., 2017). The abundance of earthquakes and the high number of seismic stations available during some periods of the sequence allowed for many detailed analyses of the local seismicity and geological structure. Here we describe the results of two different analyses: 1) a detailed imaging of the main seismogenic fault responsible for the 2010-2014 Pollino sequence; 2) a 2D attenuation and absorption tomography of the area. Some earthquakes of the sequence and seismic noise were also analyzed to assess site effects (Napolitano *et al*., 2018). Here we focus our attention on the results obtained from relative location and attenuation analysis in the Pollino area in order to thoroughly image the source responsible for the swarm and confirm a physical evidence of the role that fluids may have had in driving the earthquake swarm. We also propose to apply the same analysis to other natural or induced swarm-like sequences to give new insights about the physical processes behind the swarms, still not fully understood. Such kind of applications would be useful to increase the interpretation of seismicity, especially in areas of exploitation of geo-resources.

Relative location analysis. The idea is that detailed analysis of small earthquakes is the best way to image active faults. However, even in well instrumented regions the absolute hypocenter location is affected by errors from some hundreds of meters to kilometers, giving only a vague picture of the fault geometry. We applied a simple method of relative location based on the *master-slave approach* (Got *et al*., 1994) to earthquakes of similar waveforms in order to reduce the error on the hypocenter relative location. This analysis allows for a high resolution imaging of some faults very active during the 2010-2014 Pollino seismic swarm. Applying an automatic picking algorithm to continuous recordings at a reference station (MMN, Fig.1), we selected 6261 events occurred during two periods of the seismic swarm: November 2011-April 2012 and September 2012–June 2013 (Fig.1A and 1B). During these time periods the number of seismic stations installed in the area was sufficient to perform the relative location. We performed the normalized cross-correlation for each pair of band-pass filtered waveforms, then we retained those couples whose cross-correlation was equal or higher than 0.8 and with an average $RMS \geq 1500$ counts (roughly $M>0.6$). From this selection we collected 27 clusters (432

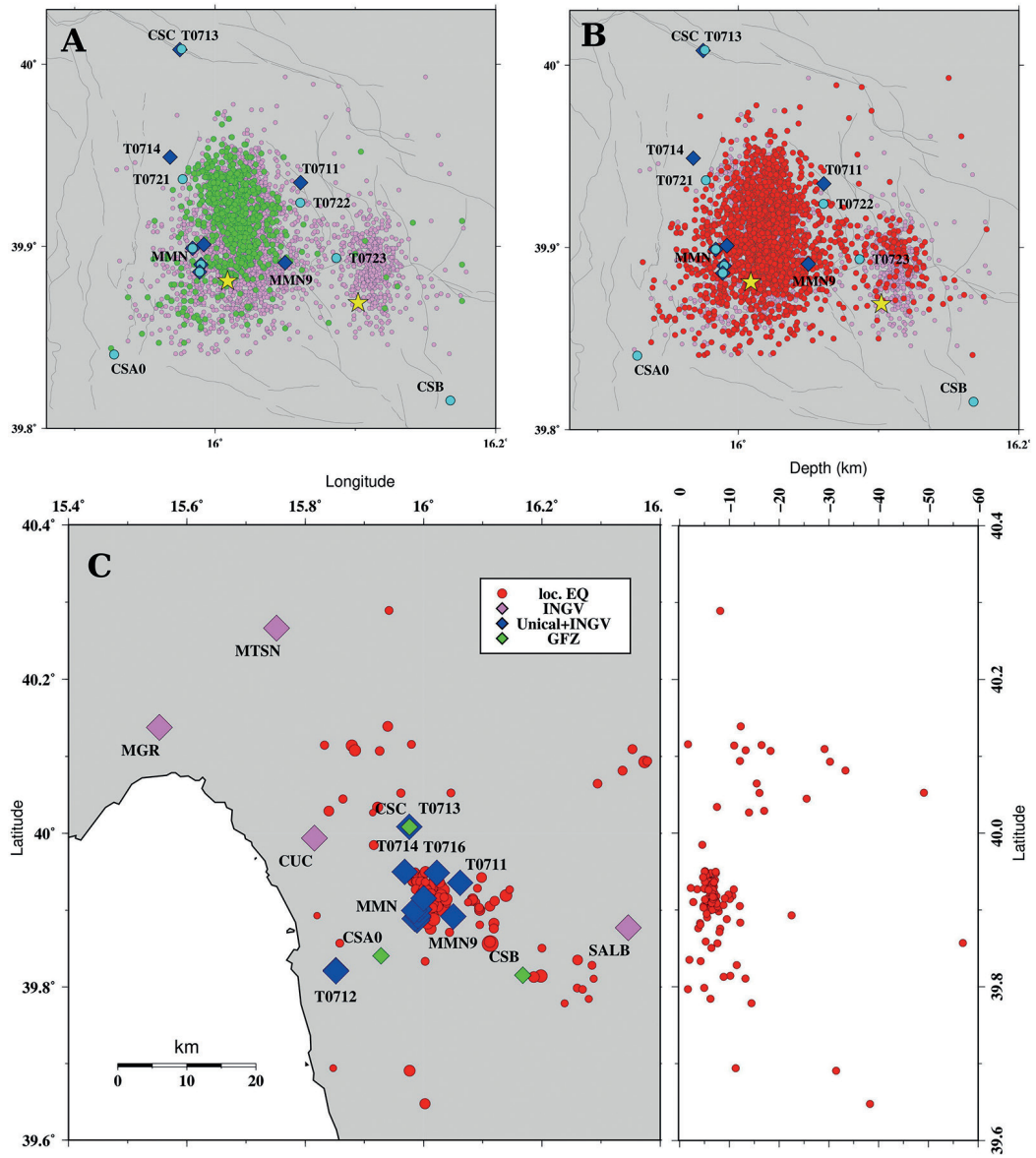

Fig. 1 - Data selected for the relative location analysis (panels A and B) and attenuation estimation (panel C). In panels A and B magenta circles represent the whole sequence epicenters. In panel A green circles represent the events selected from November 2011 to April 2012, in panel B the red circles represent the events from September 2012 to June 2013. The locations are taken from the ISIDE catalogue. The two yellow stars represent the two mainshocks: the M5.0 (west) and the M4.3 (east). Blue diamonds and cyan circles represent the seismic stations installed in the first and second period selected in this work. The faults are taken from Brozzetti *et al*., 2017. In panel C, the red circles represent the events selected for the attenuation estimation, blue, magenta and red diamonds are the stations used for this analysis. On the right side of panel C we also show a vertical cross-section of the area.

earthquakes): 18 in the first period; 9 in the second period.

The master-slave method by Got *et al*. (1994) is based on the computation of the time differences between the current event and the *master event*, for each cluster of similar waveforms, at each station. The method relies on the assumption that the distance between the two hypocenters is much smaller than the source-receiver distance. Under this hypothesis

the velocity around the source position is assumed to be constant, thus the relative time delay between nearly identical waveforms allows for an estimation of the slightly different location in space of the two events. Calling the relative hypocenter coordinates ($\Delta x, \Delta y, \Delta z, \Delta T_0$), positive to the E, N and up, of an event related to the master event and ϕ and θ the azimuth and take-off angles at the k-th seismic station, respectively, the time delays Δt_N are used to compute the inversion for the hypocentral coordinates of the current event with respect to the master event as follows:

$$\frac{1}{v}\begin{pmatrix} sin\theta_1 sin\phi_1 & sin\theta_1 cos\phi_1 & -cos\theta_1 & v \\ sin\theta_2 sin\phi_2 & sin\theta_2 cos\phi_2 & -cos\theta_2 & v \\ \vdots & \vdots & \vdots & \vdots \\ sin\theta_N sin\phi_N & sin\theta_N cos\phi_N & -cos\theta_N & v \end{pmatrix}\begin{pmatrix} \Delta x \\ \Delta y \\ \Delta z \\ \Delta T_0 \end{pmatrix} = \begin{pmatrix} \Delta t_1 \\ \Delta t_2 \\ \vdots \\ \Delta t_N \end{pmatrix} \quad (1)$$

Equation (1) may be written in matrix form as $\mathbf{Gm = d}$, which is a standard mathematical problem whose solution is given by $\mathbf{m = [G^T G]^{-1} G^T d}$. We estimated the relative time delays from the cross-correlation of filtered waveforms. We adopted different bandpass filtering and window length of analysis to check the stability of the results. For each cluster the distribution of source positions obtained from the relative location was fitted by a plane. The orientation of the best fit plane was compared with that of both fault and auxiliary planes obtained from the focal mechanism of the master event, estimated through the software FOCMEC (Snoke *et al*., 1984; Snoke, 1989). The high number of seismic stations available in the area allowed for the estimation of focal mechanisms of earthquakes characterized by very low magnitude, down to M_L 1.2. Taking into account the focal mechanism, we computed the synthetic seismograms at all stations that recorded the events (*Computer programs in seismology*, Herrmann R.B., 2013), and compared the polarity of P wave with that of the recorded signals in order to be sure about the reliability of the estimated source kinematics. We finally applied the relative location technique to the fault patches obtained from the single cluster re-locations to enhance the imaging of the seismogenic volume. Since the master events do not have similar waveforms among them to estimate the time delay through the cross-correlation, we a slightly different procedure. Seismograms were bandpass filtered in a high frequency band (10 Hz - 20 Hz), then they were manually cut retaining only the first 3 pulses, and those starting with a negative impulse were multiplied by -1. The cross-correlation of these signals gave an estimate of the time differences to be used for the relative location applying the same method previously used for any clusters. We also performed the absolute location of all the events of the clusters using a self-made code, for comparison with the relative locations (Fig. 2).

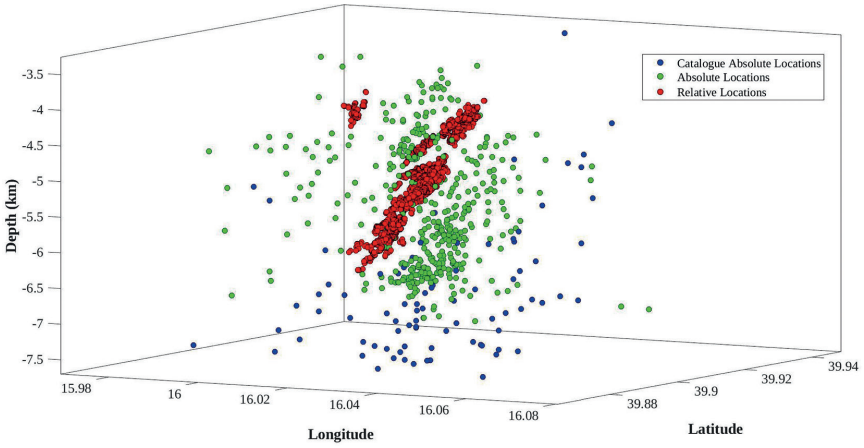

Fig. 2 - The 432 earthquakes of the 27 clusters. Different colors show the catalog location (blue), absolute location performed in this work (green) and relative location of all the events of the clusters (red).

Scattering and absorption tomography. The aim of this analysis is to use earthquakes occurred in and around the area of the 2010-2014 Pollino seismic swarm to separate scattering and absorption contribution to the total attenuation. The choice of this technique is related to its higher sensitivity to heterogeneity and fluid variation if compared with velocity tomography. We mainly propose a physical validation of the presence of fluids and of the role that fluids may have had in driving the Pollino swarm (Passarelli *et al*., 2015). We used 117 earthquakes selected among the events of the swarm and nearby, characterized by magnitude range between 1.8 and 4.3 and depth between 1 and 56 km (Fig.1C). We used all stations installed in the area between 2010 and 2014 to obtain a suitable ray coverage. Then we applied two techniques: the *peak delay* method to measure the scattering, and the *Q-coda method* to measure the absorption. The peak-delay, defined as the time lag from the direct-wave onset to the maximum amplitude of the signal envelope, is a direct measure of the multiple forward scattering (Calvet and Margerin, 2013). The greater the lag, the higher the scattering, that means presence of a significant amount of heterogeneities. We mapped the variation of the scattering in the medium using the regionalization approach.

The Q-coda method is based on the equation by Aki and Chouet, 1975:

$$E(r,t) = S(t)t^{-\alpha}exp\left(-2\pi f t Q_C^{-1}\right) \quad (2)$$

that describes the coda waves envelope. Q_c^{-1} is the inverse coda quality factor and, in diffusive regime and in absence of leakage, represents the absorption quality factor Q_i^{-1}. High Q_c^{-1} is representative of high absorption, that usually corresponds to the presence of fluids. Assigning a Q_i^{-1} value to each waveform, using the diffusive kernels by Del Pezzo *et al*. (2016) we inverted for the 2D spatial distribution of the variations of absorption in the area.

Results and discussion. We performed the relative location of clusters of similar waveforms to obtain a detailed image some faults responsible for the 2010-2014 Pollino seismic swarm. One of the main results of the relative location analysis is an improved imaging of the fault size, position, direction and dipping. Relocated hypocenters depict a clear fault plane that we could only guess from the absolute locations. Fitting the hypocenter distribution obtained from the relative location we find a fault characterized by strike around 150°, dip 48°, and an overall normal fault kinematics. The seismogenic volume involved in the swarm is inferred to be 5x2x2 km^3, at a depth between 4.5 and 6.5 km b.s.l., and its orientation in space is in agreement with the focal mechanism of the mainshock of M5.0 (s=166°, d=47°, r=–84°), that likely occurred at the southern end of the same structure. The high precision locations allows also to follow the evolution in time of the swarm, that nucleated from the central part of the seismogenic volume and migrated northward. Then, after few months, during which the seismicity migrated on the eastern fault the most of earthquakes occurred again in the main western fault filling the edges of the seismogenic volume. The lack of seismic stations during some periods is a serious issue because we could only have an incomplete picture of the swarm evolution.

We mapped scattering and absorption taking into account part of the events of the swarm and surrounding area. The attenuation analysis highlights that the Pollino area is characterized by relative high scattering-high absorption at high frequency (12 Hz). We interpret this result as a fluid-filled connected fault network, mainly composed by medium size young structures that include the 2010-2014 volume imaged from the relative location (Fig.3). The results are in agreement with the slow strain regime highlighted by Cheloni *et al*. (2017), with the high v_p/v_s found by Piana Agostinetti and Amato (2009) and with the role the fluids that drove the sequence as suggested by Passarelli *et al*. (2015).

In conclusion, the 2010-2014 Pollino seismicity was a swarm-like sequence occurred in an area of slow strain, filled by fluids that may have driven the sequence that started from the central portion of the main fault. The application of the techniques described here to other tectonic areas may contribute to better understand the physical mechanisms behind the nucleation and evolution of swarms. The investigation of areas where the exploitation of geo-

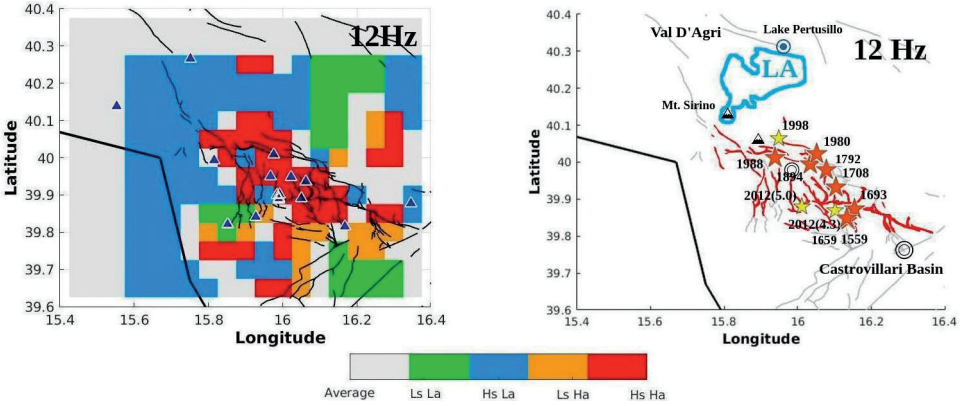

Fig. 3 - Relative scattering and absorption map of the Pollino area at frequency 12 Hz. High Scattering-High Absorption pattern (red) spreads all around the fault system. Historical and recent earthquakes are shown by orange and yellow stars, respectively. The blue pattern (High Scattering-Low Absorption) represents the Lucanian Apennines.

resources is ongoing would be particularly useful, since a detailed image of the faults together with maps of scattering and absorption to detect presence of heterogeneities and fluids becomes crucial in such cases.

References

Aki K. and Chouet B.; 1975: *Origin of coda waves: Source, attenuation, and scattering effects*. J. Geoph. Res. 80, 3322–3342.

Brozzetti F., Cirillo D., de Nardis R., Cardinali M., Lavecchia G., Orecchio B., Presti D., and Totaro C.; 2017: *Newly identified active faults in the Pollino seismic gap, Southern Italy, and their seismotectonic significance*. J. Struct. Geol, 94, 13–31.

Calvet M. and Margerin L.; 2013: *Lapse-time dependence of coda Q: Anisotropic multiple-scattering models and application to the Pyrenees*. Bull. Seism. Soc. Am. 103, 1993–2010.

Cheloni D., D'Agostino N., Selvaggi G., Avallone A., Fornaro G., Giuliani R., Reale D., Sansosti E., and Tizzani P.; 2017: *Aseismic transient during the 2010–2014 seismic swarm: evidence for longer recurrence of m 6.5 earthquakes in the Pollino gap (Southern Italy)?*. Scientific Reports, 7(1), 576.

Del Pezzo E., Ibanez J., Prudencio J., Bianco F., De Siena L.; 2016: *Absorption and scattering 2-D volcano images from numerically calculated space-weighting functions*. Geoph. J. Int. 206, 742– 756.

Got J.-L., Fréchet J. and Klein F.W.;1994: *Deep fault plane geometry inferred from multiplet relative relocation beneath the south flank of Kilauea*. J. Geoph Res.: Solid Earth, 99(B8), 15,375–15,386.

Herrmann R. B.;2013 *Computer programs in seismology: An evolving tool for instruction and research*.Seism. Res. Lett., 84(6), 1081–1088.

Napolitano F., Gervasi A., La Rocca M., Guerra I., and Scarpa R.,2018: *Site effects in the Pollino region from the hvsr and polarization of seismic noise and earthquakes*. Bull. Seism. Soc. Am., 108(1), 309–321.

Napolitano F., De Siena L., Gervasi A., Guerra I., Scarpa R., and La Rocca M.; *Scattering and absorption imaging of a highly fractured fluid-filled seismogenetic volume in a region of slow deformation*. accepted for publication on Geoscience Frontiers (Ms.Ref.No.:GSF-D-19-00069R2)

Passarelli L., Hainzl S., Cesca S., Maccaferri F., Mucciarelli M., Roessler D., Corbi F., Dahm T., and Rivalta E.; 2015: *Aseismic transient driving the swarm-like seismic sequence in the Pollino range, Southern Italy*. Geoph. J. Int., 201(3), 1553–1567.

Piana Agostinetti N., and Amato A.;2009: *Moho depth and V_p/V_s ratio in peninsular Italy from teleseismic receiver functions*. J. Geoph. Res. 114, B06303.

Snoke J.;1984: *A program for focal mechanism determination by combined use of polarity and Sv-P amplitude ratio data*. Earthquake notes, 55, 15.

Snoke J.; 1989: *Earthquake mechanisms*. Encyclopedia of Geophysics (de James, ed.).

Totaro C., Seeber L., Waldhauser F., Steckler M., Gervasi A., Guerra I., Orecchio B., and Presti D.; 2015: *An intense earthquake swarm in the southernmost apennines: Fault architecture from high-resolution hypocenters and focal mechanisms*. Bull. Seism. Soc. Am., 105(6), 3121–3128.

TEST OF SOURCE-PARAMETRES INVERSION OF THE 11 JANUARY 1693 CATANIA EARTHQUAKE IN A NEW CONTEST

F. Pettenati, D. Sandron
Istituto Nazionale di Oceanografia e di Geofisica Sperimentale OGS, Trieste, Italy

Introduction. The preliminary results of the 11 January 1693 Catania earthquake, after the the new inversions of macroseismic intensity data, using the KF technique, are shown. The inversions are constrained on four source hypotheses, formulated by other studies, including those related to the inversions of some of the four sources indicated. The choice of constrained inversions is also due to the large extension of the area investigated (between teh hinterland of south-eastern Sicily and the Ionian Sea). Four source hypotheses have been taken, including a new one, compared to those already investigated.

At first, a macroseismic dataset from the CFTI (Boschi *et al*., 1997) catalog was selected within a squared area with a side of 200 km, and centre the macroseismic epicentre. Subsequently a reduced dataset was used, keeping only the data of the January 11 event outside the zone of damage (intensity greater than V) of the previous shock of January 9 in the same area. The results always confirm the ground hypothesis compatible with the Scicli-Ragusa-Monte Lauro structure.

Modelling. The Mw 7.3 (CPTI15) earthquake in south-eastern Sicily of 11 January 1693, historically has been associated to the large offshore structure Ibleo Maltese. Sirovich and Pettenati (1999, 2001), led to the formulation of a hypothesis in the Catania hinterland, denying the source at sea. The method used is the macroseismic data inversion of the KF kinematic function (Pettenati and Sirovich, 2007), driven by genetic algorithms. The question of the great tsunami, that accompanied the earthquake, remains and this makes the ground source hypothesis falsifiable. We must also bear in mind the event of January 9th, an earthquake of Mw 6.5 occurred 40 hours before. Although the macroseismic catalogs distinguish the two earthquakes, for the hazard estimates, it is possible that the effects of this shock have in part influenced the damage estimates of the following event. Furthermore, we need consider five sites along the coast (Brucoli, Augusta, Belvedere, Siracusa and ancient Avola, Fig. 1), with an intensity decidedly lower than the XI estimates immediately placed in the hinterland.

Starting from the work of 2001 (Sirovich and Pettenati, 2001), to have a comparison, we started from the CFTI database (Boschi *et al*., 1997), taking the data inside a window of side of 200 km, with centre the macroseismic epicentre. The three hypotheses considered in the 2001 work, were then tested: Scarpata Ibleo Maltese (IBLMAL); the Graben Scordia Lentini (SCOLEN) and the Scicli-Ragusa-Monte Lauro structure (SCICLI) (Fig. 1). A new hypothesis at sea was tested, identified in a portion to the north of the tear fault recognized in the western Jonio (Del Ben *et al*., 2008), also

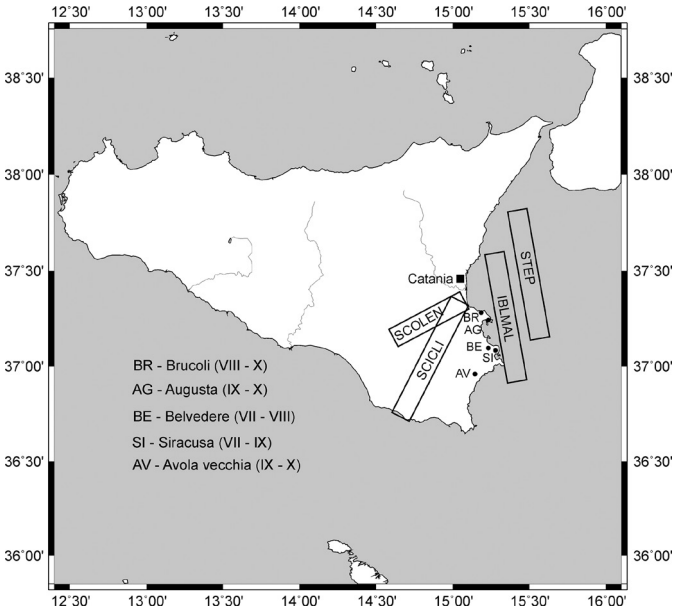

Fig. 1 - Area of the study. In legend the name of the five sites interested of a fall of intensities respect the hinterland. The two intensities reported in the brackets are refferd to 9 – 11 January event.

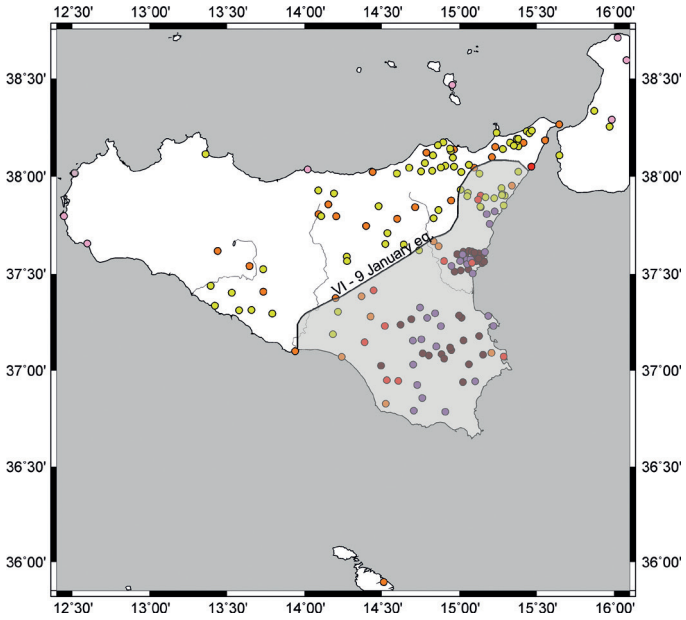

Fig. 2 - Distribution of intensities of CFTI (Boschi *et al*., 1995) of the Mw 7.3 earthquake in south-eastern Sicily of 11 January 1693. The gray shaded area is the zone of damage (intensity greater than V) of the earthquake of January 9. The data inside this area were not taken into account in the second phase of inversions.

defined as STEP sensu Govern and Wortel (2005).

In this work the grid-search inversion technique was used, constrained on the four hypotheses. Furthermore, constraints have been placed on the five sites mentioned, with a tolerance of ± one degree of intensity. Then we switched the CFTI dataset with intensities outside the damage zone (intensities greater than V) of the shock of 9 January (Fig. 2), avoiding any doubt about the possible influence on the macroseismic estimates of the 11 January event.

Results. The results using the complete data set of 11 January are shown in Table 1. The lowest fit is always obtained for the hinterland solution relative to the Scicli-Ragusa-Monte Lauro fault system (SCICLI).

In general the results are comparable with the study of Sirovich and Pettenati (2001). Table 2 shows the results obtained using the reduced dataset, considering the influence of the earthquake of 9 January as a foreschock. The SCICLI model is always the best solution and the The STEP hypothesis is better than IBLMAL. But, by this reduced dataset if we don't put the constrains for the five sites, the best solution became the IBLMAL model. However, in the forward modelling, for IBLMAL we achieve intensity XI for all the five sites, that for the 11 January earthquake don't justify the best solution.

Table 1 - Dataset CFTI full, with constrain of the five sites on the shore (178 site data).

Parametres	IBLMAL	SCOLEN	SCICLI	STEP
Longitude E	15.3	15.09	14.88	15.5
Latitude N	37.3	37.34	37.19	37.25
FPL, s, d, r [°] **	350, 76, 310 &	242, 58, 300 &	27, 82, 224 &	349, 82, 310 &
Depth [km]	7	6	5	14
Length [km] #	+36, -40	+36, -40	+29, -32	+34, -30
Mach numb $	+0.56, -0.59	+0.7, -0.58	+0.51, -0.50	+0.52, -0.66
Vs [km/s]	3.61	3.64	3.6	3.82
S mom [N m] 10^{20}	4.65	4.76	4.67	8.89
FIT	348	150	127	300

** Fault Plane Solution: strike, dip, rake. & By intensities KF inversion cannot distinguish the polarity. We assume normal faults by tectonic informations.
# The length are + in the strike verse; - in antistrike verse.
$ The mach number are + in the strike verse; - in antistrike verse.

Table 2 - Dataset CFTI reduced, with constrain of the five sites on the shore (80 site data).

Parametres	IBLMAL	SCOLEN	SCICLI	STEP
Longitude E	15.31	15.06	14.88	15.48
Latitude N	37.29	37.33	37.03	37.27
FPL, s, d, r [°] **	352, 75, 303 &	242, 58, 301 &	29, 81, 219 &	351, 79, 304 &
Depth [km]	7	5	3	10
Length + [km] #	+31, -38	+47, -39	+43, -23	+39, -22
Mach numb $	+0.55, -0.70	+0.60, -0.56	+0.51, -0.50	+0.51, -0.64
Vs [km/s]	3.5	3.52	3.5	3.73
S mom [N m] 10^{20}	4.89	4.74	4.7	8.92
FIT	43	51	37	39

References

Boschi E., Guidoboni E.,. Ferrari G, Valensise G., and Gasperini P.; 1997: *Catalogo dei forti terremoti in Italia dal 461 a. C. al 1990, no. 2*, Istituto Nazionale di Geofisica, Storia Geofisica Ambientale (SGA), Rome, Italy, CD and paper versions (in Italian).

CPTI15 Group: *Catalogo Parametrico dei Terremoti Italiani. Release v1.5*, https://emidius.mi.ingv.it/CPTI15-DBMI15/description_CPTI15.htm

Del Ben A., Barnaba C., Taboga A.; 2008: *Strike-slip systems as the main tectonic features in the Plio-Quaternary kinematics of the Calabrian Arc*. Mar Geophys Res (2008) **29**,1–12, doi 10.1007/s11001-007-9041-6.

Govers R., Wortel M. J. R.; 2005: *Lithosphere tearing at STEP faults: Response to edges of subduction zones*. Earth Planet. Sci. Lett., **236**, 505–523, doi:10.1016/j.epsl.2005.03.022.

Pettenati F., Sirovich L.; 2007: V*alidation of the Intensity-Based Source Inversions of Three Destructive California Earthquakes*. Bull. Seism. Soc. Am., **97**, 5, 1587-1606, doi: 10.1785/0120060169.

Sirovich, L. &. Pettenati F; 1999: *Seismotectonic outline of South-Eastern Sicily: an evaluation of available options for the scenario earthquake fault rupture*. Journal of Seismology, **3**, 213-233.

Sirovich, L. & Pettenati F;. 2001. *Test of Source-Parameter Inversion of the Intensities of a 54,000-Deaths Shock of the Seventeeth Century in Southeast Sicily*. Bull. Seism. Soc. Am., **91**, 4, 792-811.

GEOLOGICAL SETTING AND FIRST PALEOSEISMOLOGICAL DATA OF THE MULAZZO FAULT (LUNIGIANA BASIN, NORTHERN TUSCANY)

L. Piccardi[1], G. Nirta[1], D. Montanari[1], G. Moratti[1], A.M. Blumetti[2], P. Di Manna[2], E. Vittori[2], M. Baglione[3], P. Fabbroni[3]

[1] CNR, Istituto di Geoscienze e Georisorse, Firenze, Italy
[2] ISPRA, Dipartimento per il Servizio Geologico d'Italia, Roma, Italy
[3] Regione Toscana, Settore Sismica, Firenze, Italy

The Lunigiana depression is the northernmost intermontane basin of the Northern Apennines, bounded by ca. NW-SE-trending normal fault systems on the northeastern and southwestern margins (Bernini & Papani, 2002, Di Naccio *et al*., 2013, Bonini *et al*., 2016, Molli *et al*., 2018) (Fig. 1a). Southward it passes to the narrower Garfagnana basin and here, at the transition between the two basins, occurred the most destructive seismic event ever recorded in the Northern Apennines (i.e., the 1920 Mw 6.5 Garfagnana earthquake). Other moderate but still damaging seismic events hit the Lunigiana historically, particularly in 1834 (Mw~6.0), 1837 (Mw~5.9) and 1481 (Mw~5.6).

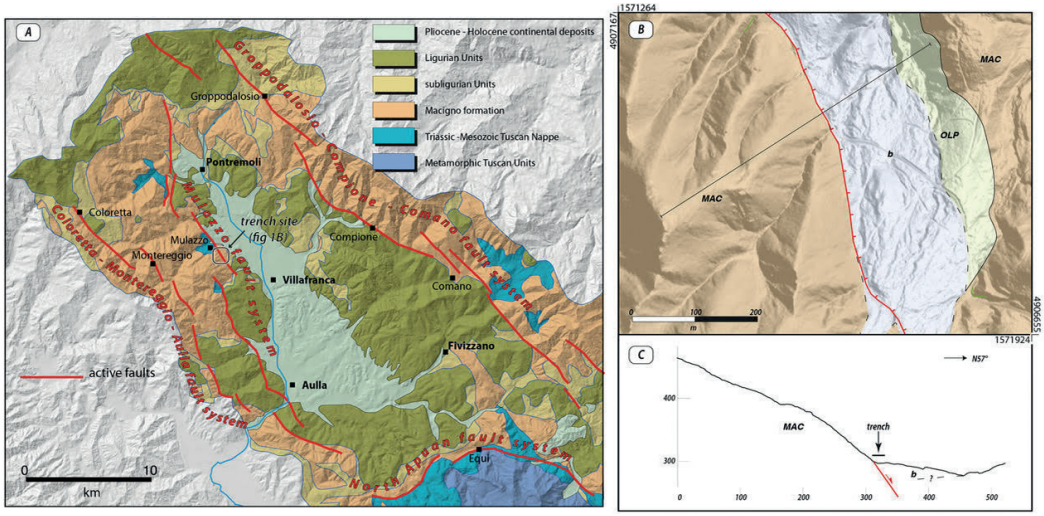

Fig. 1 - Left: A) Tectonic sketch-map of the Lunigiana basin. Main fault systems and the site of the paleoseismic trench across the Mulazzo fault are marked. Right: B) geological map of the central sector of the Mulazzo fault wrapped on LiDAR bare-earth image. MAC: Macigno Formation, upper Oligocene-early Miocene; OLP: Olivola conglomerate, lower Pleistocene; b: alluvial deposits, ?upper Pleistocene-?Holocene. C) Topographic cross section across the fault scarp of the Mulazzo fault; the location of the paleoseismic trench is shown.

In this northernmost sector of the inner Apennines, extensional fault activity followed, and possibly accompanied, the Apuan Alps exhumation to the south since early Pliocene. Despite some peculiar characteristics, the Quaternary sediments of the Lunigiana and Garfagnana basins describe a common general evolution. The basins are filled with continental deposits that generally show an evolution from low-energy fluvial environment, lake and marsh (lower Pliocene-lower Pleistocene) to coarse-grained fluvial deposits (lower Pleistocene) and finally alluvial deposits organized in terraces and fans (middle Pleistocene-Holocene) (Federici, 1978; Puccinelli, 1987; Bernini *et al*., 1991; Bertoldi, 1997; Bernini and Papani, 2002; Landi *et al*., 2003; Perilli *et al*., 2004; Coltorti *et al*., 2008).

Historical and recent seismicity (i.e. the 2013, June 21, Mw 5.1 event) confirm that the transfer zone between Lunigiana and Garfagnana graben is seismically active and is considered the most hazardous area of the Northern Apennines (Pezzo *et al*., 2014). Moreover, the actual seismic hazard posed by the Lunigiana rather long fault systems (> 30 km) is not completely resolved, especially for the lack of field data focused on the characterization of fault capability. This note is a first contribution to fill this knowledge gap for the southwestern fault-bound edge of the Lunigiana: the Mulazzo Fault.

As a contribution to the project on active faults prompted by the Tuscany Region, a detailed structural and geological investigation was carried out across the whole Lunigiana basin (covering an area of about 1000 km^2), resulting in a new map of the active tectonic structures in the area (Fig. 1a).

Moreover, along the most prominent fault systems a geomorphic analysis was performed with the aim to estimate their cumulative throw and variations along strike, the segmentation pattern within each system and any possible interaction between faults. Footwall relief was measured through the topographic analysis of 44 swath profiles built on 5x5 DEM along the Mulazzo (MUL, 34 km long) and the Coloretta-Montereggio-Aulla (CMA, 22 km long) systems on the western border of the basin and along the Groppodalosio-Compione-Comano (GCC, 38 km long) on the eastern border. The cumulative throw and footwall profiles along fault strike were compared with prominent knickpoints detected along river profiles crossing the fault systems. Knickpoint heights scale with footwall relief and documented fault throw.

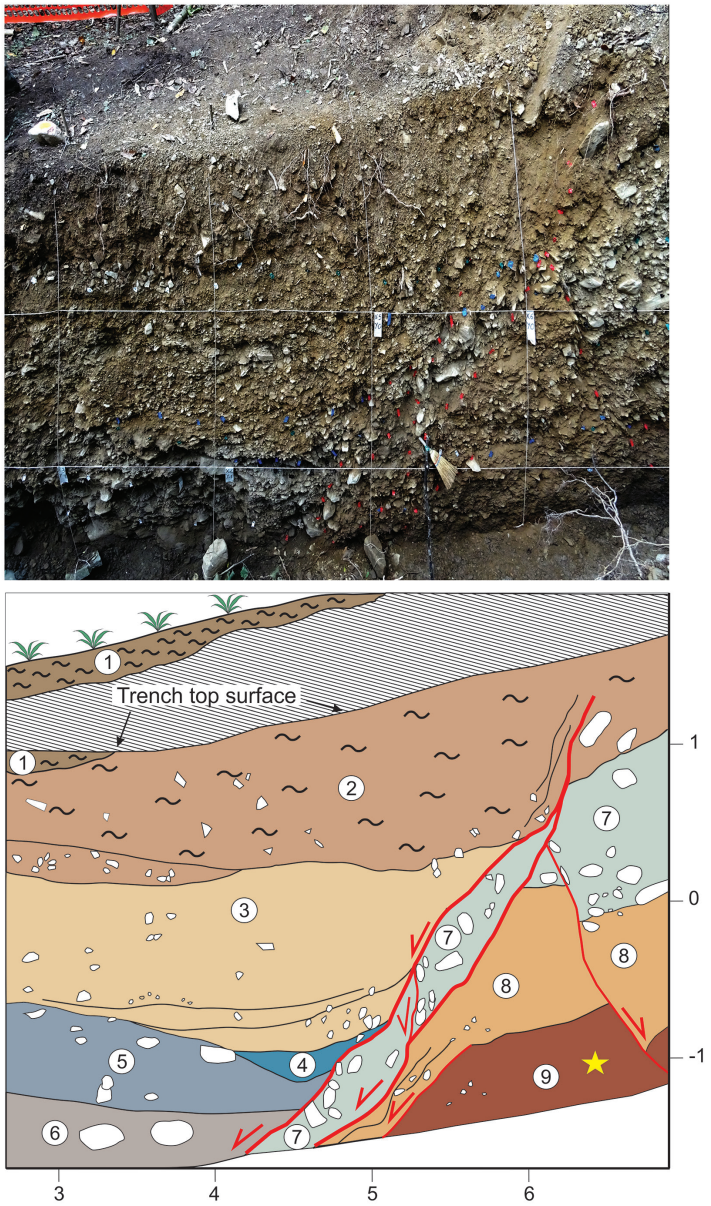

Fig. 2 - Above: view of the downslope fault zone exposed in the southern trench wall. Below: preliminary log from photograph of the downslope fault zone. Legend: 1) Dark brown present soil; 2) brown gravelly colluvium; 3) very immature fan deposit with sub-angular centimetric clasts; 4) coarse sub-rounded gravelly body with a roughly triangular shape 5) Sub-rounded to rounded alluvial gravel, centimetric to decimetric in size, (northward paleocurrents, i.e. parallel to the fault slope); 6) rounded alluvial boulders; 7) sub-rounded to rounded alluvial fan gravel, centimetric to decimetric in size; 8) very immature fan deposit with subangular centimetric clasts; 9) cemented debris with small angular clasts in brown sandy matrix including a level with small charcoal fragments (yellow star).

Moreover, the knickpoint heights distribution suggests that fault segments of CMA and MUL that are far away from each other could be linked at depth with important implication on the seismogenic potential of the faults in the area.

All the investigation listed above allowed to locate the fault segments with the most conspicuous evidence of activity during the late Pleistocene and Holocene and to select some

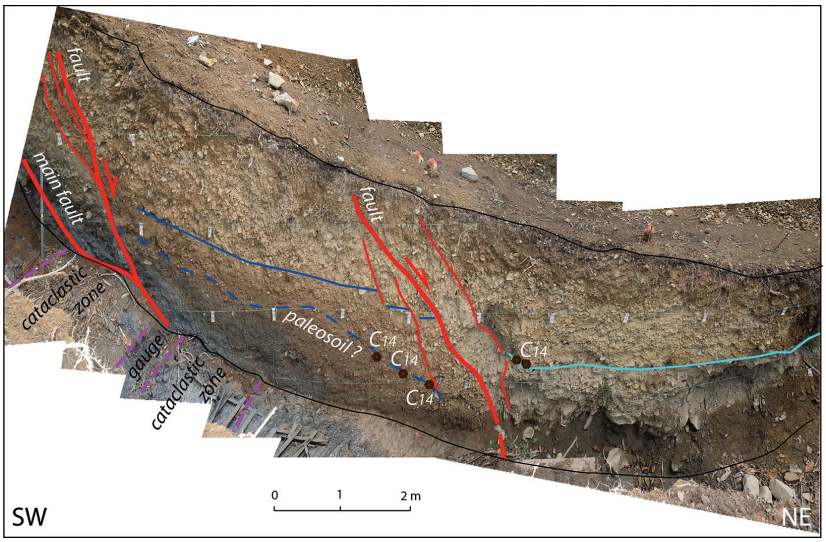

Fig. 3 - Preliminary draft line-drawing exemplifying the structures in the north wall of the trench. Location of samples for C14 dating is shown.

promising sites for paleoseismological investigations. The first of such investigations was performed by means of a trench excavated across the central portion of the Mulazzo Fault, just 500 m west of the Mulazzo village (Fig. 1a). In spite of the thick wood cover, the considered fault segment is here made well evident by prominent triangular facets and a composite fault scarp (Figs. 1b,c). The survey along the streams incisions nearby had already revealed a steep tectonic contact between the bedrock (Macigno Fm.) and Late Quaternary gravel deposits.

The trench was dug orthogonal (N50E) to the morphological scarp for a length of about 20 meters and a maximum depth of more than 3 m (Figs. 2, 3). Both wall exposures were logged and samples (charcoal and bulk sediments) were gathered for radiocarbon age determinations. Both trench walls show the footwall made of unaltered, grey, highly fractured sandstone (Macigno Fm) put in sharp contact with Late Pleistocene-Holocene clastic slope and fan deposits through a narrow fault zone, marked by fault breccia and clayey gouge. The striations on the fault plane indicate an almost pure dip-slip kinematics. The shear zone penetrates in the recent deposits resting above, which are cut and deformed (subvertical clasts) up to the bottom of the thin soil top cover. The fault zone plunges underneath the trench floor and the geometry of the top surface of the bedrock is being investigated by geophysics (a 30 m long reflection seismic profile). A couple of meters downslope, within the hangingwall, a second fault zone cuts through mostly stratified fine to coarse fan deposits with some contribution from the slope. The throw here might be in excess of one meter, but further investigation and the results of absolute dating are needed to correlate the cut sediments and properly estimate the actual offset and number of events (Figs. 2, 3).

References

Bernini M., Papani G.; 2002: *La distensione della fossa tettonica della Lunigiana nord-occidentale (con carta geologica alla scala 1:50,000)*. Bollettino della Società Geologica Italiana, **121**, 313–341.

Bernini M., Papani G., Dall'Asta M., Lasagna S., Haida P.; 1991: *The Upper Magra Valley extensional basin: a cross section between Orsaro Mt. and Zeri (Massa Province)*. Bollettino della Società Geologica Italiana, **110**, 451-458.

Bertoldi R.; 1997: *Lineamenti palinostratigrafici di depositi continentali del Pliocene-Pleistocene inferiore iniziale dell'Italia nord-occidentale*. Boll. Soc. Paleont. It., **36**, 63-73.

Bonini M., Corti G., Delle Donne D., Sani F., Piccardi L., Vannucci G., Genco R., Martelli L., Ripepe M.; 2016: *Seismic sources and stress transfer interaction among axial normal faults and external thrust fronts in the Northern Apennines (Italy): A working hypothesis based on the 1916–1920 time–space cluster of earthquakes*. Tectonophysics, **680**, 67-89.

Coltorti M., Pieruccini P., Rustioni M.; 2008: *The Barga Basin (Tuscany): a record of Plio-Pleistocene mountain building of the Northern Apennines, Italy*. Quat. Int., **189**: 56–70.

Di Naccio D., Boncio P., Brozzetti F., Pazzaglia F.J., Lavecchia G.; 2013; *Morphotectonic analysis of the Lunigiana and Garfagnana grabens (northern Apennines, Italy): Implications for active normal faulting*. Geomorphology, **201**, 293–311.

Federici P.R.; 1978: *La tettonica recente dell'Appennino. 2. Il bacino fluvio-lacustre di Pontremoli (alta Val di Magra) e le sue implicazioni neotettoniche*. Gruppo St. Quat. Pad. Quaderno, **4**, 121-131.

Landi E., Ravani S., Sarti G., Sodini M.; 2003: *The Villafranchian deposits of the Castelnuovo Garfagnana and Barga Basins (Lucca, Tuscany, Italy): facies analysis and paleoenvironmental reconstruction*. Atti della Societa` Toscana di Scienze Naturali, Memorie, Serie A, **108**, 81–93.

Molli G., Carlini M., Vescovi P., Artoni A., Balsamo F., Camurri F., Clemenzi L., Storti F., Torelli L.; 2018: *Neogene 3-D structural architecture of the north-west Apennines: The role of the low-angle normal faults and basement thrusts*. Tectonics, **37**. https://doi. org/10.1029/2018TC005057

Perilli N., Puccinelli A., Sarti G., D'Amato Avanzi G.; 2004: *Lithostratigraphy of the Plio-Pleistocene continental deposits of the Barga and Castelnuovo Garfagnana (Tuscany, Italy) tectonic depressions*. In: Morini, D., Bruni, P. (Eds.), The Regione Toscana project of geological mapping. Regione Toscana, Firenze, 121-132.

Pezzo G., Boncori J.P.M, Atzori S., Piccinini D., Antonioli A., Salvi S.; 2014. *The 2013 Lunigiana (Central Italy) earthquake: Seismic source analysis from DInSAR and seismological data, and geodynamical implications for the northern Apennines*. Tectonophysics, **636**, 315-324. http://dx.doi.org/10.1016/j.tecto.2014.09.005

Puccinelli A.; 1987: *Un esempio di tettonica recente nella Val di Serchio: il sollevamento di Monte Perpoli*. Atti Soc. Tosc. Sc. Nat. Mem., Serie B, **94**, 105-117.

CASSANO IRPINO: ESEMPIO DI RICOSTRUZIONE DOPO IL TERREMOTO DEL 1980

M. Pizza[1], A.M. Michetti[1], R. Nappi[2], S. Porfido[2,3]

[1] Università degli Studi Insubria-Como

[2] INGV- sez. Osservatorio vesuviano, Napoli

[3] CNR- I.S.A., Avellino

Introduzione. L'impatto dei forti eventi sismici sull'ambiente fisico e antropico è un tema di cruciale interesse in un territorio densamente popolato e con un patrimonio artistico, storico e culturale di inestimabile valore come quello italiano. Investigare le complesse interazioni uomo-ambiente in un contesto specifico di grande vulnerabilità come quello delle aree interne dell'Appennino meridionale costituisce un'operazione interessante fornendo molti spunti di riflessione sia dal punto di vista scientifico sia dal punto di vista sociale. Per questa ricerca è stato scelto come caso di studio il paese di Cassano Irpino (AV) che offre caratteristiche uniche, a causa della ricchezza di dati disponibili, che attraverso un intervallo temporale di quasi quaranta anni dal terremoto dell'Irpinia e Basilicata del 23 Novembre 1980, consentono di descrivere il processo di ricostruzione e adattamento, e quindi di resilienza, di un'intera comunità rispetto al sisma (Pizza, 2019).

Il terremoto del 23 Novembre 1980. Il terremoto del 23 novembre 1980, più comunemente noto come il terremoto dell'Irpinia-Basilicata, è stato il più forte evento sismico che ha colpito l'Appenino meridionale negli ultimi 100 anni, caratterizzato da una M_w=6,9 ed una Io=X MCS (Postpischl *et al*., 1985; CFTI15).

Le regioni più colpite furono la Campania e la Basilicata, ma fu avvertito in quasi tutta la penisola, dalla Sicilia a Sud, all'Emilia Romagna e Liguria a Nord. Causò gravi danni in oltre 800 località; furono distrutte complessivamente 75.000 abitazioni e 275.000 furono gravemente danneggiate. Le vittime furono circa 3000, i feriti 10.000. Castelnuovo di Conza, Conza della Campania, Lioni, Santomenna, Sant'Angelo dei Lombardi, Caposele, Calabritto, San Mango sul Calore, San Michele di Serino, Pescopagano, Guardia dei Lombardi, Laviano, Sant'Andrea

di Conza, Senerchia e Teora furono i comuni quasi totalmente distrutti con intensità I ≥IX MCS/MSK.

Numerosi e devastanti furono anche gli effetti sull'ambiente naturale, intesi come effetti primari, quali fenomeni di fagliazione superficiale (Westaway and Jackson, 1984; Pantosti and Valensise, 1990; Blumetti *et al*., 2002) o come effetti secondari, quali frane (oltre 200 frane sismoindotte), fratture nel suolo, variazioni idrologiche e fenomeni di liquefazione (21 casi) e variazioni idrologiche delle sorgenti (Porfido *et al*., 2007; Serva *et al*., 2007). Anche l'intensità epicentrale, stimata, sulla base della nuova scala macrosismica ESI-2007 (Michetti *et al*., 2007), risulta essere pari al X grado (Serva *et al*., 2007).

Nell'ottica di esaminare lo stato della ricostruzione a quasi 40 anni di distanza dal terremoto, sono stati eseguiti diversi studi di dettaglio relativi alla resilienza connessa agli sviluppi urbanistici di alcuni paesi tra quelli maggiormente colpiti, come Conza della Campania, Calitri, San Mango sul Calore, Balvano (Porfido *et al*. 2017a; 2017b; Porfido and Spiga, 2018) e ci è sembrato interessante proseguire l'indagine anche attraverso l'esame di alcuni comuni, come ad esempio quello di Cassano Irpino con un livello di danneggiamento lievemente inferiore. Il punto di partenza è costituito dalle relazioni tecniche effettuate immediatamente dopo il sisma per la ricostruzione, sono state, infatti, esaminate le microzonazioni sismiche preliminari eseguite nell'ambito del PFG-CNR (AAVV, 1983), che realizzò un intervento urgente in 39 centri abitati dell'area epicentrale della Campania e Basilicata colpiti dal terremoto.

Il caso di studio di Cassano Irpino (AV). Cassano Irpino è un piccolo comune della provincia di Avellino, con circa 1.000 abitanti, posizionato a 34 km da Avellino e a 90 km da Napoli (Fig. 1). Il suo territorio, ricco di acque, è compreso tra gli oltre 900 m s.l.m. dei Monti Toppo Capitino e Serra Nocelleta e i 450 m s.l.m. nel fondovalle del Fiume Calore Irpino. Il centro abitato situato su sperone roccioso dei Monti Picentini, è caratterizzato da un

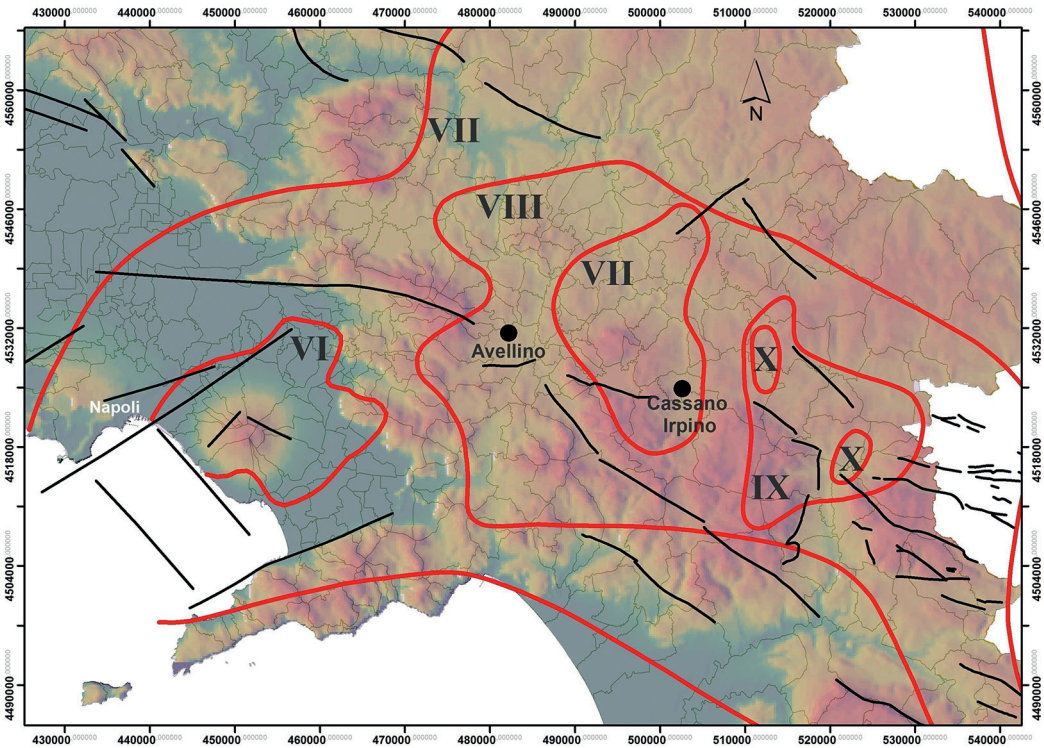

Fig. 1 - Ubicazione dell'area: in rosso le isosiste del terremoto dell'Irpinia del 23 novembre 1980 (Postpischl *et al*., 1985); in nero le faglie capaci estratte dal catalogo ITHACA (Michetti *et al*., 2000).

gruppo sorgentizio (Pollentina, Peschiera, Acqua del Prete e Bagno della Regina), ubicato a valle dell'abitato, che alimentano l'Acquedotto Pugliese e quello dell'Alto Calore, rifornendo acqua a numerosi comuni della Puglia, della Campania e della Basilicata.

A seguito del sisma del 23 Novembre 1980 Cassano Irpino risultò mediamente danneggiato raggiungendo un'intensità pari a VII-VIII MCS e VIII ESI (Postpischl *et al*., 1985 ; CPTI15, Serva *et al*., 2007), stessa intensità registratasi anche per gli eventi storici avvenuti nel 1694 e nel 1732, attualmente è classificato nella II categoria sismica (DGR Campania n. 5447, del 2002).

Il danneggiamento al tessuto urbano. Cassano Irpino pur distando poco meno di trenta chilometri dall'epicentro del terremoto del 1980 subì un danneggiamento relativamente grave (Fig. 2), infatti le unità edilizie distrutte o danneggiate più o meno gravemente a seguito del sisma furono 684, le persone rimaste senzatetto furono 111 (11,5%) su un totale di 983 abitanti, vi furono 5 morti e 11 feriti (Proietti, 1985-89). Subì gravissimi danni la Chiesa Matrice di San Bartolomeo Apostolo, in cui crollarono quasi totalmente la copertura della navata e parzialmente le volte e la cupola, con lesioni profonde e diffuse nelle murature. Subì gravi danni la struttura portante del campanile, che dovette essere abbattuto. Gravi danni subì anche la chiesa di Santa Maria delle Grazie, che già dagli anni '70 versava in precarie condizioni statiche ed era chiusa al culto, crollarono le coperture e risultarono lesionate e sconnesse le strutture portanti. Danneggiamenti più o meno importanti furono riscontrati anche nelle chiese di Santa Maria la Longa, con il crollo dell'annessa casa canonica, e di San Rocco. Subirono importanti danni anche il Municipio, successivamente abbattuto e il Palazzo Baronale. In quest'ultimo edificio, si verificarono 4 vittime, i danni furono particolarmente diffusi sia alla struttura portante sia alla copertura, tanto che dovette essere quasi totalmente riedificato.

Come si evince dalla Carta di microzonazione sismica preliminare (PFG-CNR, C.N.R., 1983), e dal successivo studio di Nicotera (1987), il differente grado di danneggiamento nei settori Nord e Sud del centro abitato è imputabile al diverso assetto lito-stratigrafico e morfologico delle due aree. Infatti, il settore meridionale dell'abitato, dove i danneggiamenti maggiori si riscontrano nei pressi della chiesa di San Rocco e di via Pretarello, è situato su "roccia compatta

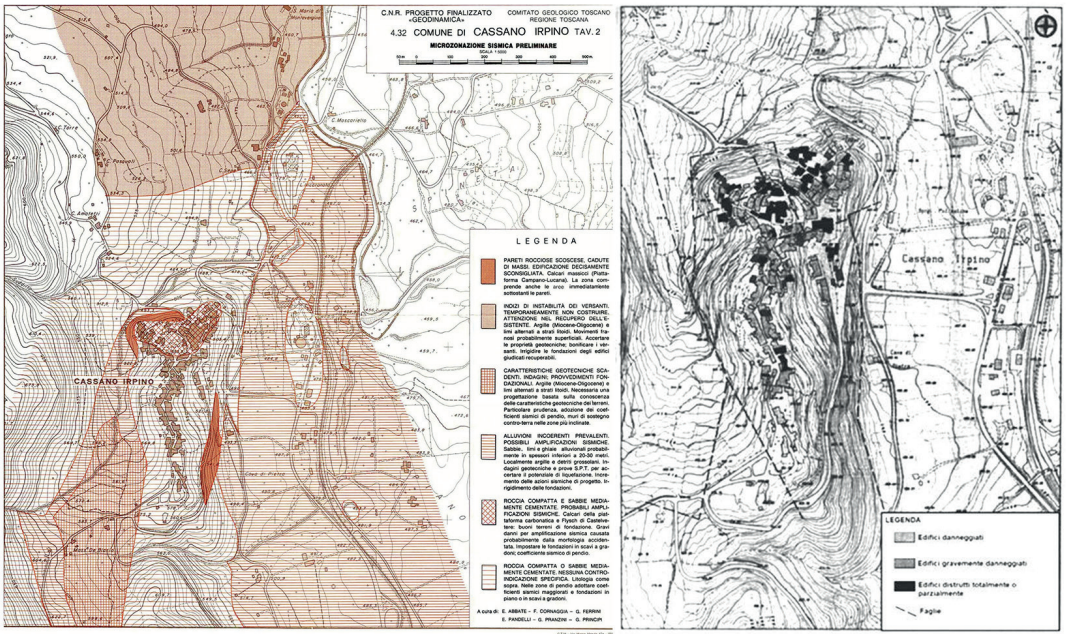

Fig. 2 - Cassano Irpino. A sinistra Carta di microzonazione sismica preliminare (a cura di PFG-CNR, C.N.R., 1983); a destra Carta del danno (da P.R.G., a cura del Prof. Nicotera, 1987).

(calcari) con nessuna controindicazione specifica su possibili amplificazioni sismiche" (C.N.R., 1983), mentre il settore settentrionale con più ampi e diffusi danneggiamenti (Palazzo Baronale e chiese di San Bartolomeo Apostolo e di Santa Maria delle Grazie; gravi danneggiamenti nelle vie Municipio, Barbuti, Ripa e Revota e rione Fondaco) è dovuto a un substrato composto oltre che da calcari anche da sabbie mediamente cementate, con amplificazioni sismiche, causate probabilmente dalla morfologia accidentata (C.N.R., 1983).

Effetti sull'ambiente naturale. Il terremoto indusse effetti anche sull'ambiente naturale (Fig. 3), alcuni dei quali di notevole rilievo, quali l'importante variazione di portata delle acque del gruppo sorgentizio comprendenti le sorgenti Bagno della Regina e Pollentina, con l'intorbidamento delle acque, quest'ultimo fenomeno durato solo poche ore (Cotecchia and Salvemini, 1981; Coppola *et al*., 1989; Esposito *et al*., 1998; 2001; Serva *et al*., 2007).

Relativamente alla sorgente Pollentina, un primo significativo aumento della portata fu riscontrato già a partire nei giorni 10-12 Novembre 1980, da una portata media di 2.900 l/s del 1° Novembre si giunse ai 3.010 l/s del 10 Novembre. A questo primo incremento se ne sovrappose un secondo, il 23 Novembre quando la portata raggiunse ben 4.600 l/s, con un aumento giornaliero, a partire dal giorno 10, di ben 80-100 l/s. Nei primi giorni di Dicembre venne raggiunta e superata la portata eccezionale di 5.000 l/s, registrando un valore medio mensile di 5.558 l/s (Coppola *et al*., 1989; Esposito *et al*., 2001), valore massimo mai registrato in passato.

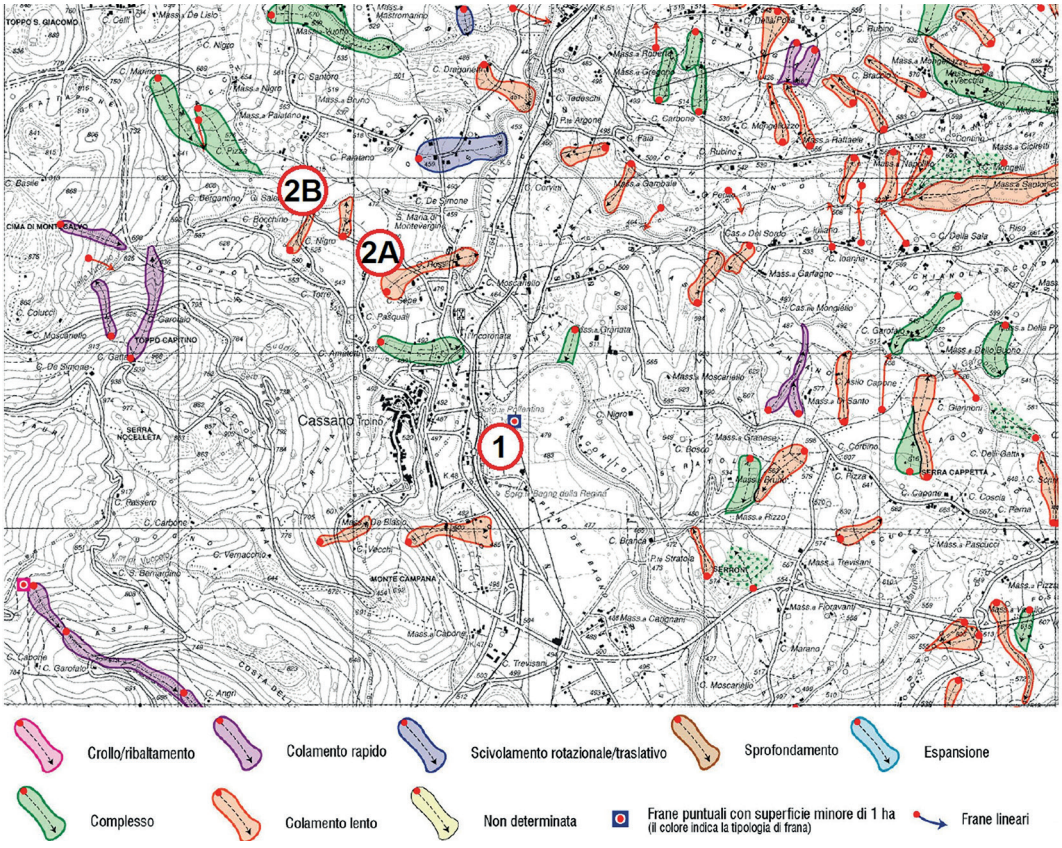

Fig. 3 - Localizzazione dei fenomeni franosi nel territorio di Cassano Irpino *(da Carta inventario dei fenomeni franosi in Campania, Progetto IFFI, 2007)*, a cui sono stati aggiunti i fenomeni sismoindotti osservati, a seguito del terremoto del 1980: 1 - Incremento della portata presso il gruppo sorgentizio; 2A cedimento strada presso C. da Campora e 2B cedimento strada presso C. da Airile.

Furono riscontrati inoltre, anche alcuni fenomeni gravitativi di modesta entità in Contrada Campora e in Contrada Airile, dove si verificò un cedimento ed una lieve deformazione della sede stradale (Pizza, 2019).

I tempi della ricostruzione. Agli studi di microzonazione sismica preliminare del PFG-CNR del 1981-83, fecero seguito studi di dettaglio per la realizzazione del Piano Regolatore Generale nel 1987 ad opere del Prof. Nicotera, dell'Università di Napoli Federico II. La ricostruzione degli edifici pubblici e privati fu effettuata, tenendo in debito conto i tempi burocratici, soprattutto nel periodo che va dal 1985 al 2000.

Buona parte dello sviluppo urbano post-sisma fu realizzato a Nord dell'abitato storico, in contrada Torre, in quest' area, preferita alla contrada Rena per maggior stabilità geologica (Nicotera, 1987), fu localizzato il Piano di Zona, divenuto successivamente il nucleo urbano in cui si è insediata una fetta consistente di popolazione.

Le opere di urbanizzazione dell'area furono eseguite tra il 1986 e il 1990, gli edifici furono invece completati e consegnati agli abitanti nella seconda metà degli anni '90.

Attualmente la ricostruzione può dirsi pressoché conclusa, infatti negli ultimi anni è stato dapprima completato il Palazzo Baronale e poi nel 2016, è stato completato il ripristino degli edifici lesionati, situati nelle vie Ripa e Revota.

Un paese ricostruito, che vede da un lato la rinascita del vecchio nucleo urbano vicino all'originale impianto medievale, e dall'altro la parte moderna di espansione, costruita nel Piano di Zona concettualmente distante dall'impianto originale del "paese".

Un percorso, a ben vedere, estremamente lungo, complesso ed articolato, conclusosi nell'arco di più di un trentennio, per una località con un livello di danneggiamento valutato del VII-VIII MCS. Un percorso, che offre più di uno spunto di riflessione per quello che potrebbe essere la programmazione futura per i centri antichi in zona sismica, in considerazione non solo di scenari che prevedono il riscontro nel tessuto urbano ma anche nell'ambiente fisico.

Bibliografia

AA.VV.; 1983: *Indagini di microzonazione sismica*. CNR-Progetto Finalizzato Geodinamica, CNR pubbl. n. 492.

Blumetti A.M., Esposito E., Ferreli L., Michetti A.M., Porfido S., Serva L., and Vittori E.; 2002: *New data and reinterpretation of November 23, 1980, M 6.9 Irpinia – Lucania earthquake (Southern Apennines) coseismic surface effects*. In Dramis F., Farabollini P., and Molin P. (eds), Large-scale vertical movements and related gravitational processes, Studi Geol. Camerti, special issue 2002, 19-27.

Coppola L., Cotecchia V., Lattanzio M., Salvemini A., Tadolini T., and Ventrella N.A.; 1989: *Il gruppo di sorgenti di Cassano Irpino (Avellino - Italia meridionale): regime idrologico ed analisi strutturale del bacino di alimentazione*. Geol. Appl. e Idrogeologia, 24, 227-260.

Cotecchia V. and Salvemini A.; 1981: *Correlazione tra eventi sismici e variazioni di portate alle sorgenti di Caposele e Cassano Irpino, con particolare riferimento al sisma del 23 novembre 1980*. Geol. Appl. e Idrogeologia, Vol. XVI, pagg. 167-192.

Esposito E., Pece R., Porfido S. and Tranfaglia G.; 2001: *Hydrological anomalies precursory of earthquakes in Southern Apennines (Italy)*. Natural Hazards and Earth System Sciences, 1, 137–144.

Michetti A.M., Serva L. and Vittori E.; 2000: *ITHACA (Italy hazard from Capable Faulting), a database of active capable faults of the Italian onshore territory*. Report of ANPA-Agenzia Nazionale Protezione Ambiente, Roma; http://sgi2.isprambiente.it/ithacaweb/viewer/

Michetti A.M., Esposito E., Guerrieri L., Porfido S., Serva L., Tatevossian R., Vittori E., Audemard F., Azuma T., Claque J., Comerci V., Gurpinar A., Mc Calpin J., Mohammadioun B., Morner N.A., Ota Y. and Roghozin E.; 2007: *Environmental Seismic Intensity Scale 2007 - ESI 2007*. Mem. Descr. Carta Geol. d'Italia, 74, 1-56.

Pantosti D. and Valensise G.; 1990: *Faulting mechanism and complexity of the 23 November 1980, Campania-Lucania earthquake, inferred from surface observations*. J. of Geophys. Res., 95, 15319-15341.

Pizza M.; 2019: *Cassano Irpino (AV) Dal 1980 al 2019: un percorso di resilienza dopo il terremoto*. Tesi in Scienze dell'ambiente e della natura, Università degli Studi dell'Insubria. Relatore Michetti A.M., Correlatore Porfido S.

Porfido S., Esposito E., Guerrieri L., Vittori E., Tranfaglia G. and Pece R., 2007: *Seismically induced ground effects of the 1805, 1930 and 1980 earthquakes in the Southern Apennines, Italy*. Boll. Soc. Geol. It., n. 126, 333-346.

Porfido S., Alessio G., Gaudiosi G., Nappi R. and Spiga E.; 2017: *The Resilience of Some Villages 36 Years After the Irpinia-Basilicata (Southern Italy) 1980 Earthquake*. In: Mikoš M., Vilímek V., Yin Y., Sassa K. (eds) Advancing Culture of Living with Landslides. WLF 2017. Springer ed. DOI: 10.1007/978-3-319-53483-1_15.

Porfido S., Alessio G., Gaudiosi G., Nappi R. and Spiga E.; 2017: *Effetti ambientali indotti dai terremoti: il caso di studio di alcune località colpite dal sisma del 1980*. Conf. Naz. ASITA,. ISBN 978-88-941232-8-9.

Porfido S. and Spiga E.; 2018: *Il terremoto del 23 novembre 1980: ricostruzioni e abbandoni di alcuni paesi nell'Appennino meridionale*. In Capano F., Pascariello M.I., and Visone M. (eds), La Città Altra. Storia e immagine della diversità urbana: luoghi e paesaggi dei privilegi e del benessere, dell'isolamento, del disagio, della multiculturalità. 2018 by CIRICE ISBN 978-88-99930-03-5.

Postpischl D., Branno A., Esposito E., Ferrari G., Marturano A., Porfido S., Rinaldis V. and Stucchi M.; 1985: *The Irpinia earthquake of 23 november 1980*. In Atlas of Isoseismal Maps of Italian Earthquakes, CNR-PFG, n.114, vol.2A, 152-159.

Proietti G. (a cura di); 1985-89: *"Dopo la polvere". Rilevazione degli interventi di recupero post-sismico del patrimonio archeologico, architettonico ed artistico delle regioni Campania e Basilicata danneggiato dal terremoto del 23 novembre 1980 e del 14 febbraio 1981*. Ministero per i Beni Culturali e Ambientali, Soprintendenza generale agli interventi post-sismici in Campania e Basilicata, 5 voll. Roma.

Rovida A., Locati M., Camassi R., Lolli B. and Gasperini P. (eds); 2016: *Catalogo Parametrico dei Terremoti Italiani* (CPTI15). Istituto Nazionale di Geofisica e Vulcanologia (INGV), https://doi.org/10.6092/INGV.IT-CPTI15

Serva L., Esposito E., Guerrieri L., Porfido S., Vittori E. and Comerci V.; 2007: *Environmental effects from five historical earthquakes in Southern Apennines (Italy) and macroseismic intensity assessment: Contribution to INQUA EEE Scale Project*. Quaternary Int., 173-174, 30-44.

Westaway R. and Jackson J. A.; 1984: *Surface faulting in the southern Italian Campania-Basilicata earthquake of 23 November 1980*. Nature, 312, 436-438.

EVIDENZE DI ATTIVITÀ TETTONICA RECENTE LUNGO IL RETROSCORRIMENTO DI CRESPANO DEL GRAPPA (PREALPI VENETE, TV)

M.E Poli[1], G. Patricelli[1], G. Paiero[1], G. Monegato[2], F. Marinoni[3], M. Olivotto[3], A. Marchesini[1], N. Abu Zeid[4], E. Unterpertinger[1], A. Zanferrari[1]

[1] Università di Udine
[2] CNR - Padova
[3] Liberi professionisti – ODG Veneto
[4] Università di Ferrara

Nell'ambito della Microzonazione di terzo livello del Comune di Crespano del Grappa/ Pieve del Grappa (TV), sono state eseguite tre trincee paleosismologiche lungo la traccia del retroscorrimento di Crespano del Grappa al fine di definirne attività e capacità secondo le Linee guida Faglie Attive e Capaci – FAC (2015).

L'area fa parte delle Prealpi venete, dove il fronte Pliocenico-Quaternario delle Alpi Meridionali orientali (Castellarin e Cantelli, 2000) si propaga attualmente con una velocità di circa 2-3 mm/anno verso meridione (Serpelloni *et al*., 2016). Le strutture più esterne sono organizzate in una serie di archi fra loro *en echelon*, a direzione media WSW-ENE e vergenza meridionale (Galadini *et al*., 2005). L'attività sismica è testimoniata da una sismicità medio/ bassa all'interno della quale si registra un solo evento con M>6 (terremoto di Asolo, 1695: Mw 6.45 – DBMI15).

Da un punto di vista strutturale, l'area di studio è compresa fra il sovrascorrimento Bassano-Valdobbiadene a Nord e il s. Bassano-Cornuda a Sud (Fig. 1). La faglia in oggetto, tradizionalmente considerata un retroscorrimento legato al sistema Bassano-Cornuda, ha un andamento circa WSW-ENE e una vergenza settentrionale. Passando da Est a Ovest, essa affiora estesamente a monte dell'abitato di Castelcucco dove da origine ad un rigetto di circa un centinaio di metri della Molassa miocenica affiorante (Braga, 1970). Nei pressi del centro abitato di Crespano il retroscorrimento disloca di alcune decine di metri i conglomerati quaternari del T. Lastego, mettendoli a contatto con le siltiti micacee della Molassa (Parinetto, 1987). Nel centro abitato sono presenti ulteriori indizi del passaggio della struttura, anche se la forte urbanizzazione ne

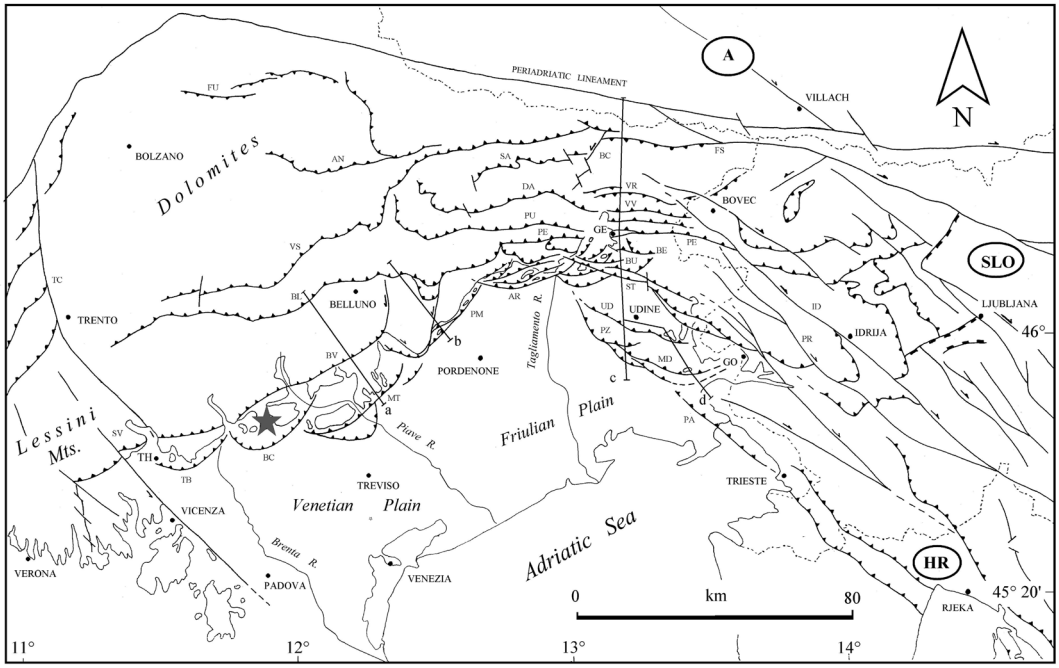

Fig. 1 - Inquadramento strutturale del Sudalpino orientale. La stella in grigio indica Crespano del Grappa. BC: sovrascorrimento Bassano-Cornuda; BV: s. Bassano – Valdobbiadene; MT: s. del Montello; TB: s. Thiene-Bassano; SV: faglia Schio-Vicenza.

Fig. 2 - Parete orientale della trincea paleosismologica eseguita a Crespano del Grappa in località Col Canil. I filoni sabbiosi, suturati dal suolo agrario, sono legati a fenomeni di paleoliquefazioni e sono spesso polifasici. I quadrati sono di 1 m di lato.

impedisce lo studio di dettaglio. Per questo motivo le trincee paleosismologiche sono state scavate ai margini orientali (Col Canil) e occidentali (San Vito) dell'abitato. Nel primo caso la trincea ha attraversato una spessa coltre di colluvi depostisi probabilmente entro una bassura (probabilmente una valle sepolta), mentre le altre due trincee hanno interessato l'esteso conoide coalescente di età Ultimo Massimo glaciale (LGM) che caratterizza tutta la zona pedemontana alla base del massiccio carbonatico del Grappa.

I risultati ottenuti indicano una intensa attività deformativa riferibile all'azione del retroscorrimento di Crespano del Grappa. Tale attività ha generato in particolare: i) il basculamento dei colluvi olocenici verso monte (i colluvi provenienti dal massiccio del Grappa immergono infatti di circa 35° verso Nord); ii) intensi fenomeni polifasici di liquefazione che hanno originato dicchi di dimensioni anche metriche e talora completamente obliterato la struttura sedimentaria dei depositi colluviali (Fig. 2); iii) una ampia zona di fratturazione che accompagna la scarpata morfologica e si associa ad un picco di polarizzazione indotta. Tale osservazione suggerisce che la faglia di Crespano ha raggiunto la superfice topografica probabilmente durante uno o più eventi che hanno generato gli importanti effetti di paleo-liquefazione; iv) il rigetto di circa 3-4 m dei depositi che formano il conoide LGM.

Per quanto riguarda l'età della deformazione, le datazioni effettuate sui terreni coinvolti (^{14}C_metodo AMS, Beta Analytic) suggeriscono una attivazione della struttura probabilmente anche in epoca assai recente (storica ?) e comunque sicuramente post-LGM.

Bibliografia

Braga G.P. (1970) – L'assetto tettonico dei dintorni di Possagno (trevigiano occidentale). Lincei. Rendiconti Sc. Fis., Mat. e Nat. vol. XLVIII, aprile 1970.

Castellarin A. e Cantelli L. (2000) - Neo-Alpine evolution of the Southern Eastern Alps. J. Geodyn., 30, 251-274.

Linee guida per la gestione del territorio in aree interessate da Faglie Attive e Capaci (FAC), versione 1.0 Commissione tecnica per la microzonazione sismica, Conferenza delle Regioni e delle Province Autonome – Dipartimento della protezione civile, Roma, 2015.

Galadini F., Poli M.E. e Zanferrari A. (2005) - Seismogenic sources potentially responsible for earthquakes with M≥6 in the eastern Southern Alps (Thiene-Udine sector, NE Italy). Geophys. J. Int., 161, 739-762.

Locati M., Camassi R., Rovida A., Ercolani E., Bernardini F., Castelli V., Caracciolo C.H., Tertulliani A., Rossi A., Azzaro R., D'Amico S., Conte S., Rocchetti E. (2016) - DBMI15, the 2015 version of the Italian Macroseismic Database. Istituto Nazionale di Geofisica e Vulcanologia. doi:http://doi.org/10.6092/INGV.IT-DBMI15

Parinetto, A. (1987) - Aspetti morfotettonici del versante meridionale del Grappa e delle colline antistanti, Unpublished Degree Thesis, University of Padova, Italy, 160 pp.

Serpelloni E., Vannucci G., Anderlini L. e Bennett R.A. (2016) - Kinematics, seismotectonics and seismic potential of the eastern sector of the European Alps from GPS and seismic deformation data. Tectonophysics, 688, 157-181.

WEB-BASED MACROSEISMIC DATA USED AS A "ROSETTA STONE" TO INTERPRET THE DEPTH OF HISTORICAL EARTHQUAKES

P. Sbarra, P. Burrato, P. Tosi, P. Vannoli, V. De Rubeis, G. Valensise
Istituto Nazionale di Geofisica e Vulcanologia

The knowledge of the parameters of damaging earthquakes of pre-instrumental era is a crucial information for the seismotectonic characterization of slow deforming active regions and for the evaluation of the associated hazard. The indication of the hypocentral depth of the historical events may help to constrain their causative source, especially where active faults are spatially overlapped and occur with a wide range of different depths. As a matter of fact, the determination of the depth of pre-instrumental earthquakes is a long-standing geophysical

issue that still awaits to be completely elucidated (e.g. Mallet 1862; Jánosi 1907; Kövesligethy 1907; Blake 1941; Sponheuer 1960; Ambraseys 1985; Burton *et al*., 1985; Levret *et al*.,1996; Musson 1996). To this aim, we analysed the seismicity of an area that includes the NE-verging Northern Apennines fold-and-thrust belt and its foredeep/foreland basin in the southern Po Plain, where earthquakes exhibit largely variable depth, ranging from very shallow (< 10 km) to deep (< 100 km). In the study region, the potential seismogenic sources belongs to one of seven genetically and geodynamically independent fault types (DISS Working Group, 2019; Vannoli *et al*., 2015). In the Po Plain, besides the most external Northern Apennines thrust fronts, that are shallow blind thrusts associated for example to the 2012 seismic sequence (e.g. Maesano *et al*., 2015), the foreland crust is cut by a set of deeper inherited faults that formed during the Mesozoic extensional phases and are located below the Northern Apennines basal detachment (Scardia *et al*., 2015). Moving backward, the Northern Apennines thrusts continue with a ramp-flat geometry and are characterised by both shallow, along the mountain front, and deep seismogenic segments up to several tens of km of depth. At the back of the compressional domain, the ongoing extension is taken up by a regional, NE-dipping, low angle normal fault system (e.g. Boncio *et al*., 2000). Further potential seismogenic sources are deep intraslab compressional faults and transverse fault systems related to the differential slab retreat.

We used as input web-based macroseismic data from the HSIT database (http://www.haisentitoilterremoto.it/; Sbarra *et al*., 2010; Tosi *et al*., 2015), relating to instrumental earthquakes that occurred in the study area during the past 12 years and are characterised by a wide range of hypocentral depth.

Thanks to this citizen-science system it is possible to gather a large amount of information from the population and to carry out detailed studies that due to the wealth of closely spaced data points may highlight amplification and attenuation areas also at urban scale (Sbarra *et al*. 2012). The direct correlation between the statistically analyzed web-based observation and the local seismic effects was recently highlighted using as comparison peak ground acceleration and velocity values (PGA and PGV; Molinari *et al*., 2015; Sbarra *et al*., 2017). Molinari *et al*. (2015) showed that peaks of ground shaking (PGV) predicted by the 3D MAMBo geological model for two moderate earthquakes occurred in the Po Plain matched the positive anomalies of the corresponding macroseismic intensity pattern as shown by the HSIT maps. At a more regional scale, Sbarra *et al*. (2017) studying the effects of both regional earthquakes and local shallow and deep earthquakes found that high attenuation zones were highlighted by low PGA values and *vice versa*.

We started our analysis from three instrumental earthquakes that occurred in 2012 in our study area: the 20 May 2012, Mw 5.8 Emilia earthquake, with an hypocentral depth of 6.3 km; the 25 January 2012, Mw 4.9 event, with a depth of 29 km; and the 27 January 2012, Mw 4.9 event, having a depth of 72.4 km (Fig. 1).

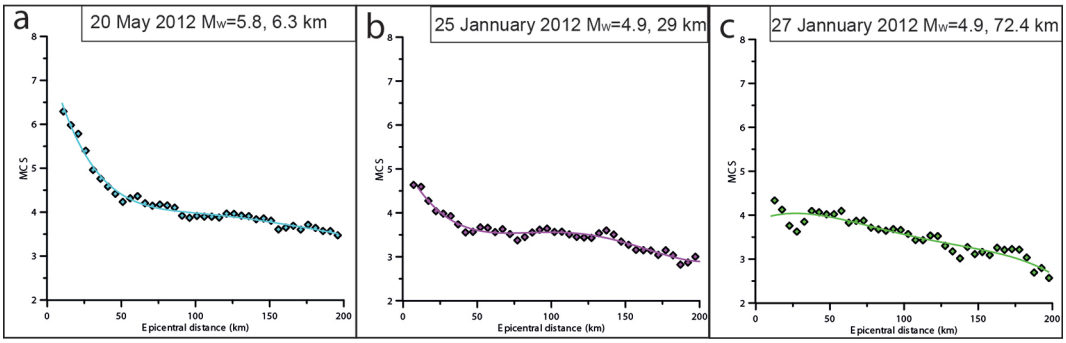

Fig. 1 - attenuation curves of the three events occurred in 2012 used as starting observation and characterised by different hypocentral depth.

The attenuation curves describing the decay of macroseismic intensity of these three events, elaborated by using a distance-binning approach similar to that used by Gasperini 2001, showed a marked difference in the near-field, which seemed to be due to their different hypocentral depth. Analyzing other earthquakes included in the HSIT database, occurred in the same region, we found a correlation between the depth of the earthquakes, and the slope of the attenuation curve within 50 km of the epicenter, regardless of their magnitude.

We used a straight line to fit the intensity data within the first 50 km from the epicenter because, as already noted by Gasperini 2001, the attenuation curves of Italian earthquakes can be approximated by a bilinear function showing a change in slope between 40 and 50 km. An abrupt change in the slope of the attenuation curve was also evidenced at about the same epicentral distance by using a numerical simulation of the attenuation of the PGA (Fah and Panza, 1994). Our experimental observations arising from the analysis of the attenuation curves of the HSIT dataset shows that generally the change in slope is closer to 50 km.

We calculated the absolute value of the slope of the best-fitting straight lines for a total of 20 earthquakes and plotted each one against its hypocentral depth. The resulting distribution of data points is well fitted by a logarithmic function. The trend of slope of the lines, fitting intensity attenuation with distance versus depth, agrees with both an Intensity Prediction Equation (IPE) and a Ground Motion Prediction Equation (GMPE), thus confirming the reliability of experimental behaviour. In particular we show that the values of slope computed through the IPE elaborated with HSIT intensity data and those obtained by the transformation of PGA in MCS (Faenza and Michelini, 2010), the former predicted by using the GMPE of Bindi *et al*. (2014), are consistent with our experimental function. We then used such function as a modern "Rosetta Stone" to uncover the hypocentral depth range of 20 selected pre-instrumental earthquakes ranging in age from the 1570 "Ferrara" to the 1972 "Appennino settentrionale" events, and with a magnitude range of 4.9 to 6.5.

Our statistics show that the entire approach is independent of the magnitude of the earthquake being considered but depends only on its focal depth (Fig. 2), and as such it is ideal for application to pre-instrumental earthquakes. Besides, knowing the focal depth of these earthquakes also allows for recalculating their equivalent magnitude by inverting for the magnitude the IPE proposed by Tosi *et al*., 2015. By applying this formula, we obtain M_L magnitude values, which we converted into M_W using the equation proposed by Grünthal and Wahlström (2003). The resulting equivalent magnitudes are consistently larger for deeper events (i.e. depth larger than 30 km) than those calculated using traditional methods based on intensity alone.

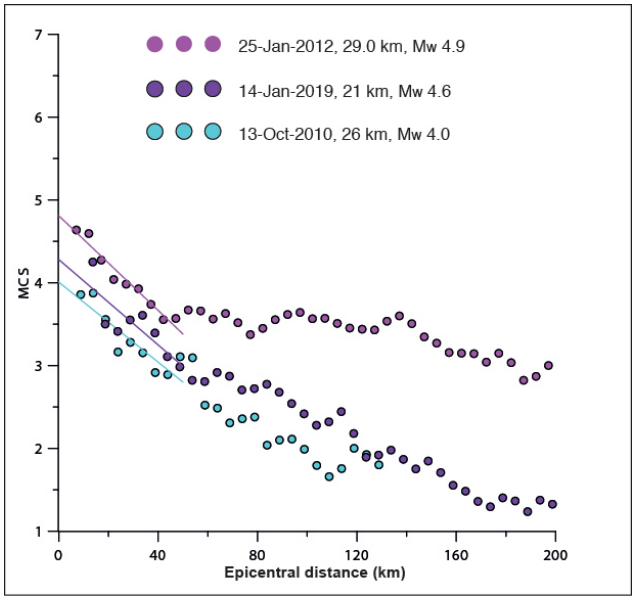

Fig. 2 - attenuation curves of three events occurred at similar hypocentral depth but having different magnitude. The slope of the best-fitting line in the first 50 km is similar among the three, attesting its independence from the magnitude.

We present case histories referred to selected events and discuss the seismotectonic implication. As an example, our study showed the occurrence of several earthquakes in the Po Plain having hypocentral depths larger

than the local depth of the basal thrust, that for this reason can be attributed to a class of seismogenic sources rooted in the lower plate. The existence and seismic potential of this class of deeper and less known seismogenic sources may have an impact on the calculation of the annual earthquake rates, particularly in areas of low strain rates and infrequent seismicity such as the Po Plain.

We tested our approach in the Northern Apennines of Italy, but the method can be extended to any other seismogenic area of the world following a re-calibration based on local data.

Acknowledgements This work was partially financed by the INGV-DPC 2019-2021 agreement (Allegato A, WP7).

References

Ambraseys N.; 1985: *Intensity-attenuation and magnitude-intensity relationships for northwest European earthquakes*. Earthq. Eng. Struct. Dyn., **13**, 6, 733-778.

Bindi D., Massa M., Luzi L., Ameri G., Pacor F., Puglia R. and Augliera P.; 2014: *Pan-European ground-motion prediction equations for the average horizontal component of PGA, PGV, and 5%-damped PSA at spectral periods up to 3.0 s using the RESORCE dataset*. Bulletin of Earthquake Engineering, **12**, 391-430.

Blake A.; 1941: *On the estimation of focal depth from macroseismic data*. Bull. Seismol. Soc. Am., **31**, 225-231.

Boncio P., Brozzetti F. and Lavecchia G.; 2000: *Architecture and seismotectonics of a regional low-angle normal fault zone in central Italy*. Tectonics, **19**, 6, 1038-1055.

Burton P. W., McGonigle R., Neilson G. and Musson R. M. W.; 1985: *Macroseismic focal depth and intensity attenuation for British earthquakes*, in Earthquake engineering in Britain, Telford, London, pp. 91-110.

DISS Working Group; 2018: Database of Individual Seismogenic Sources (DISS), Version 3.2.1: *A compilation of potential sources for earthquakes larger than M 5.5 in Italy and surrounding areas*. <http://diss.rm.ingv.it/diss/>, Istituto Nazionale di Geofisica e Vulcanologia; doi:10.6092/INGV.IT-DISS3.2.1.

Faenza L. and Michelini, A.; 2010: *Regression analysis of MCS intensity and ground motion parameters in Italy and its application in ShakeMap*. Geophysical Journal International, **180**, 1138-1152.

Fah D. and Panza G.F.; 1994: *Realistic modelling of observed seismic motion in complex sedimentary basins*. Ann. Geofis., **37**, 6, 1771-1797.

Gasperini P.; 2001: *The attenuation of seismic intensity in Italy: a bilinear shape indicates the dominance of deep phases at epicentral distances longer than 45 km*. Bull. Seismol. Soc. Am., **91**, 4, 826-841.

Grünthal G. and Wahlstrom R.; 2003: *An Mw based earthquake catalogue for central, northern and northwestern Europe using a hierarchy of magnitude conversions*. J. Seismol., **7**, 4, 507-531.

Jánosi I.; 1907: *Makroszeizmikus rengések feldolgozása a Cancani-féle egyenlet alapján, in A. Réthly* (ed.), Az 1906 évi Magyarországi Földrengések, A. M. Kir. Orsz. Met. Föld. Int., Budapest, pp. 77- 82.

Kövesligethy R. V.; 1907: *Seismischer Stärkegrad und Intensität der Beben*. Gerlands Beitr. Geophys., **8**, 363-366.

Maesano F. E., Ambrogi C., Burrato P. and & Toscani G.; 2015: *Slip-rates of blind thrusts in slow deforming areas: examples from the Po Plain (Italy)*. Tectonophysics **643**, 8-25, doi:10.1016/j.tecto.2014.12.007.

Mallet R.; 1862: *The first principles of observational Seismology as developed in the Report to the Royal Society of London of the Expedition made by command of the Society into the interior of the Kingdom of Naples to investigate the circumstances of the great earthquake of December, 1857,* 5-160 (Chapman and Hall, 1862).

Molinari I., Argnani A., Morell A. and Basini P; 2015: *Development and testing of a 3D seismic velocity model of the Po Plain sedimentary basin, Italy*.Bulletin of the Seismological Society of America, **105** (2A), 753764.

Musson R. M.; 1996: *Determination of parameters for historicaI British earthquakes*. Ann. Geofis., **39**, 1041-1047.

Levret A., Cushing M. and Peyridieu G.; 1996: *Etude des caractéristiques de séismes historiques en France: Atlas de 140 cartes macroseismiques*, IPSN, Fontenay-Aux-Roses.

Sbarra P., Tosi P. and De Rubeis V.; 2010: *Web-based macroseismic survey in Italy: method validation and results*. Nat. Hazards, **54**, 563-581, doi:10.1007/s11069-009- 9488-7.

Sbarra P., Tosi P. and De Rubeis V.; 2017: *Role of African–Eurasian plate setting in the felt areas of intermediate-depth earthquakes: an investigation using crowdsourced data*. Terra nova, **29**(1), 36-43, doi: 10.1111/ter.12245.

Scardia G. *et al*.; 2015: *Evidence for late Alpine tectonics in the Lake Garda area (northern Italy) and seismogenic implications*. Geol. Soc. Am. Bull., **127**, 113-130, doi:10.1130/b30990.1.

Sponheuer W.; 1960: *Methoden zur Herdtiefenbestimmung in der Makroseismik, Freiberger Forschungshefte*, C88, Berlin Akademie Verlag, Germany 120 pp.

Tosi P., Sbarra P., De Rubeis V. and Ferrari C.; 2015: *Macroseismic intensity assessment method for web questionnaires*. Seismol. Res. Lett., **86**, 985-990, doi:10.1785/0220140229.

Vannoli P., Burrato P. and Valensise G.; 2015: *The Seismotectonics of the Po Plain (Northern Italy): Tectonic Diversity in a Blind Faulting Domain*. Pure Appl. Geophys., **172**, 1105-1142, doi:10.1007/s00024-014-0873-0.

INSIGHT ON SEISMIC HAZARD OF THE IBERO-MAGHREBIAN REGION FROM SEISMIC AND GEODETIC MOMENT-RATES COMPARISON

F. Sparacino[1], M. Palano[1], J.A. Peláez[2]
[1] *Istituto Nazionale di Geofisica e Vulcanologia, Osservatorio Etneo - Sezione di Catania, Catania, Italy*
[2] *Department of Physics, University of Jaén, Jaén, Spain*

Introduction. Seismic and geodetic moment-rates comparison can reveal regions with unexpected potential seismic hazard. Their ratio, expressed as a percentage, is called Seismic Coupling Coefficient (SCC) and allows to differentiate crustal deformation modality (seismic versus aseismic), as well as to highlight regions showing gaps in seismic cycle. We performed such a comparison for Southeastern Iberia - Maghreb region which (Fig. 1), located at the western Mediterranean border along the Eurasian-Nubian plate convergence, has been marked by the occurrence of large earthquakes in the last millennium. To this aim, on the basis of available geological, tectonic and seismological data, we divided the study area in twenty-five seismogenic source zones.

Data and methodology. For each seismogenic source zone, the seismic moment-rate was computed according to the Hyndman and Weichert (1983) formulation, obtained by integrating the cumulative truncated Gutenberg-Richter distribution up to a maximum magnitude value, i.e., the magnitude of the largest earthquake that could occur within a specified region. These values and associated uncertainties have been estimated by adopting different approaches. Regarding the Spanish seismogenic source zones, maximum values have been primarily estimated on the dimensions of known active faults and considerations of the maximum dimension of other mapped faults and structures recognized on field by adopting the empirical laws reported in Wells and Coppersmith (1994). For the zones characterized by a lack tectonic data, maximum values have been estimated directly from the seismic catalog by adopting a cumulative exponential-truncated Gutenberg-Richter recurrence relationship. Regarding the seismic source zones located along the African margin, maximum values have been estimated from the seismic

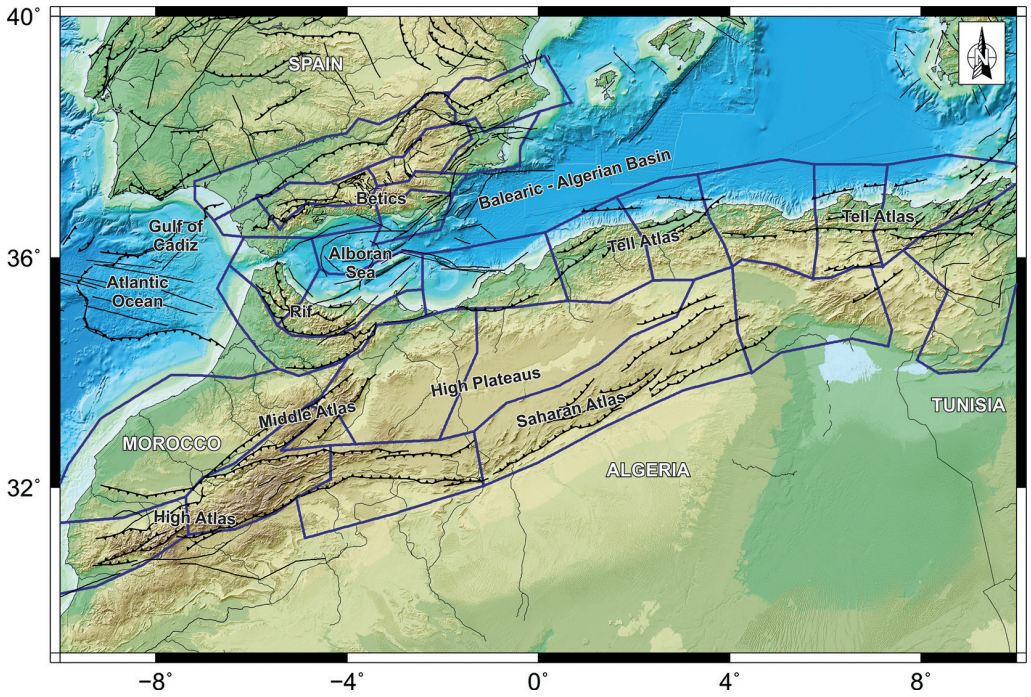

Fig. 1 - Simplified tectonic map of the Southeastern Iberia - Maghreb region. Seismogenic sources are also reported.

catalog by adopting the Kijko-Sellevoll approach (Kijko and Singh, 2011), a method usually applied on regions where only a limited number of the largest magnitudes are available.

Regarding data processing, we analysed an extensive GNSS dataset which, covering 20 years of observations (from 1999 up to 2019), includes more than 300 continuous GNSS sites and various networks developed on the Iberian Peninsula by local institutions and agencies mainly for mapping, engineering and cadastral purposes. In addition, we also included data from 25 episodic GNSS sites located in Morocco (Koulali *et al*., 2011). The GNSS phase observations were processed by using the GAMIT/GLOBK 10.7 software (http://www-gpsg.mit.edu), following the strategy described in Palano (2015). As a final processing step, a consistent set of positions and velocities into a fixed Nubian reference frame has been computed. In a next step, the horizontal strain-rates have been estimated on a regular 0.5° x 0.5° grid over the investigated area by adopting the method reported in Shen *et al*. (2015). Finally, the geodetic moment-rate (and its standard error) was estimated for each seismic source zone by adopting the Savage and Simpson (1997) formulation. The moment-rate estimate from geodetic strain-rates is proportional to the chosen seismogenic thickness. In order to choose appropriate values, the depth distributions of earthquakes with magnitude M≥1 are analyzed for each seismic source zone. After some preliminary estimations, all the seismic source zones have been merged into 3 main regions, defining approximate seismogenic thicknesses of 15, 18 and 25 km for Betics, Rif-western Atlas and Tell Atlas, respectively.

Results. The geodetic moment-rate is a measure of both elastic and anelastic loading rates while the seismic moment-rate is a measure of the elastic unloading rate. The SCC values usually lie between 0% and 100%: the more the value close to 100, the more the larger part of the deformation is released by brittle deformation (earthquakes). A low ratio instead suggests an apparent deficit of seismic moment-rate. This may be due to regions characterized by the presence of faults with aseismic behavior or seismic gaps. Another cause can be attributed to an incomplete seismic catalog or to a seismic catalog covering a very short time interval if compared with the seismic cycle of the investigated region. Moreover, value larger than 100% can be also observed, although less frequently. Such a case would occur if the estimation of the seismic moment-rate has been computed soon after a large earthquake, especially if the time interval covered by geodetic data appears to be insufficient to capture the spectrum of seismic and aseismic components. Another explanation can be attributed to a bad geometry of the geodetic network due to a highly heterogeneous distribution of GPS stations.

Taking into account the considerations above, achieved results highlight as most of the studied area is characterized by an apparent seismic moment-rate deficit, in according to previous estimations. A large number of these seismogenic source zones (western Betics, western Rif, High, Middle and Saharan Atlas) is characterized by SCC values lower than 23%, evidencing its prevailing aseismic behaviour. Intermediate SCC values (between 30% and 60%) are also obtained in some seismogenic sources, where well-known faults have hosted moderate earthquakes (eastern Betics, central Rif and Middle Atlas), indicating as crustal seismicity accounts only for a moderate fraction of the total deformation-rate budget. Finally, high SCC values (>95%) are observed along most of the Tell Atlas, suggesting that crustal deformation is mostly released through earthquakes, but also depicting a potential seismic gap in the Eastern Tellian Atlas.

It must be considered that the comparison between seismic and geodetic moment-rates involves a large number of assumptions and simplifications. Nonetheless, it provides significant insights into the seismic hazard of regions subjected to relevant tectonic deformation, essentially for time-dependent seismic hazard assessments.

References

Hyndman R. D., Weichert D. H.; 1983: *Seismicity and rates of relative plate motion on the plate boundaries of western North America*. Geophys. J. R. Astron. Soc., **72**, 59–82, DOI 10.1111/j.1365-246X.1983.tb02804.x.

Kijko A., Singh M.; 2011: *Statistical tools for maximum possible earthquake magnitude estimation*. Acta Geophysica, **59**, 674-700, DOI 10.2478/s11600-011-0012-6.

Koulali A., Ouazar D., Tahayt A., King R.W., Vernant P., Reilinger R. E., McClusky S., Mourabit T., Davila J. M., Amraoui N.; 2011: *New GPS constrains on active deformation along the Africa-Iberia plate boundary*. Earth Planet. Sci. Lett. 308(1), 211-217, DOI 10.1016/j.epsl.2011.05.048.

Palano M.; 2015: *On the present-day crustal stress, strain-rate fields and mantle anisotropy pattern of Italy*. Geophys. J. Int., 200 (2), 969-985, DOI 10.1093/gji/ggu451.

Savage J. C., Simpson R. W.; 1997: *Surface strain accumulation and the seismic moment tensor*. Bull. Seismol. Soc. Am., **87**, 1345-1353.

Shen Z.-K., Wang M., Zeng Y., Wang F.; 2015: *Optimal interpolation of spatially discretized geodetic data*. Bull. Seismol. Soc. Am., **105**, 2117-2127, DOI 10.1785/0120140247.

Wells D. L., Coppersmith K. J.; 1994: *New empirical relationship among magnitude, rupture length, rupture width, rupture area, and surface displacement*. Bull. Seismol. Soc. Am., **84**, 974-1002.

THE CAMPOTOSTO LINKAGE FAULT ZONE IN BETWEEN THE 2009 AND 2016–2017 SEISMIC SEQUENCES OF CENTRAL ITALY: IMPLICATIONS FOR SEISMIC HAZARD ANALYSIS

E. Tondi[1], D. Jablonská[1], T. Volatili[1], M. Zambrano[1], M. Michele[2], S. Mazzoli[3], P.P. Pierantoni[1]

[1] School of Science and Technology - Geology Division, University of Camerino, Italy

[2] Istituto Nazionale di Geofisica e Vulcanologia, Roma, Italy

[3] Department of Earth, Environmental and Resources Sciences- University of Napoli Federico II, Italy

The Central Italy has been struck by severe earthquakes along the Apennine chain, as documented in the historical sources (Rovida *et al*., Eds., 2015). The most significant earthquakes, clustered along the Central Apennines Fault System (CAFS in Cello *et al*., 1997), have been documented in 3 periods over the last millennium: in the 13th-14th and 17th-18th centuries; and the recent events from the 1970s till present (Tondi and Cello, 2003). The last decades witnessed several devastating earthquakes resulting in hundreds of casualties (i.e. 1997 Colfiorito-Sellano Mw=6.0; 2009 L'Aquila Mw=6.3 and 2016 Amatrice-Visso-Norcia Mw max=6.5). These events were caused by the reactivation of NW-SE striking normal faults dipping SW (Fig. 1; Tondi *et al*., Eds., 2009, Pantosti and Boncio, Eds. 2012, Civico *et al*., 2018; Villani *et al*., 2019).

The Fig. 1 shows the seismogenic faults related to the mainshocks of the 1997 Umbria-Marche, 2009 L'Aquila and the 2016 Amatrice-Visso-Norcia seismic sequences.

The three south-west dipping seismogenic faults have been modelled on the base of the available focal mechanisms and the seismic moment detected during the following mainshocks: 1. CSF - 26th September 1997 Umbria-Marche earthquake (Mw=6.0); 2. PF - 6th April 2009 L'Aquila earthquake (Mw=6.3); 3. MVF - Cumulative of 24th August 2016 Amatrice earthquake (Mw=6.0), 26th October 2016 Visso earthquake (Mw=5.9), 30th October 2016 Norcia earthquake (Mw=6.5). The Campotosto area represents a step in between the PF and MVF. This area has been affected by seismic swarms with magnitude ranging from 5.0 to 5.5 during both the 2009 and the 2017 seismic sequences, as shown in Fig. 1 (Valoroso *et al*., 2013; Chiaraluce *et al*., 2017). The hypocentre clusters of the 2009 and 2017 seismic sequences in the Campotosto area occurred at a depth of more than 5km, which suggests the presence of a deep structure, that can be interpreted as a relay-growing fault zone in between the seismogenic PGF and MVF.

According to this interpretation, the seismogenic potential of the relay zone, on the base of its dimension, is in the order of Mw=6.0 (even if all the faults belonging to the relay zone activate simultaneously). Moreover, for the same reason, the Campotosto area does not represent a seismic gap, as suggested by Falcucci *et al*. (2018).

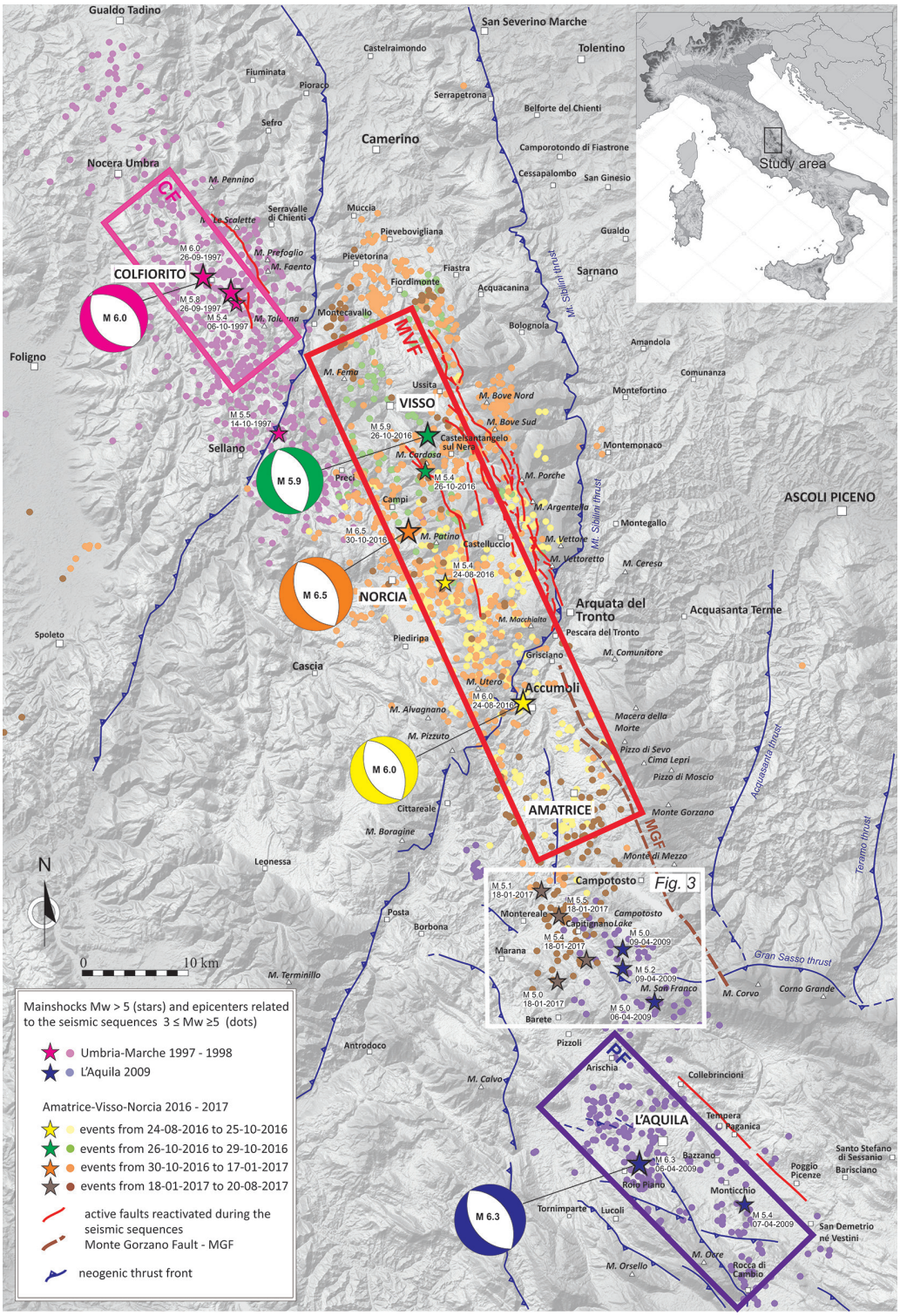

Fig. 1 - Map of the recent seismic events, capable faults and seismogenic sources in -Central Italy. The focal mechamism for the mainshocks of each sequence are shown. CSF = Colfiorito-Sellano Fault; PF = Paganica Fault, MVF = Monte Vettore Fault.

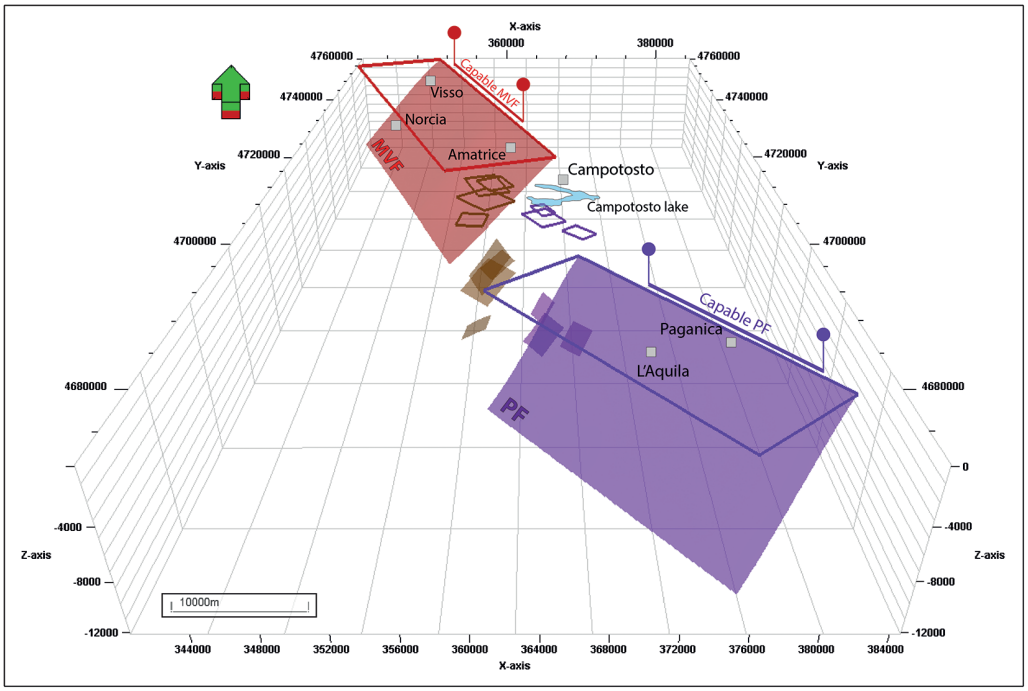

Fig. 2 - 3D model of the Campotosto linkage fault zone in between the Paganica and Monte Vettore seismogenic faults. The seven south-west dipping seismogenic faults belonging to the relay has been modelled on the base of the available focal mechanisms and the released seismic moment.

This observation has relevant implications for seismic hazard assessment in Central Italy, since this area host the NW-SE striking Monte Gorzano Fault, interpreted by several authors as active and able to generate an earthquake with maximum magnitude Mw 6.5-6.7 (Barchi *et al*., 2000; Boncio *et al*., 2004; Galadini and Galli, 2003).

In order to deepen the knowledge of the area and therefore to better understand the timing of the activity of the Monte Gorzano normal Fault, we carried out an integrated structural and stratigraphic field analysis. The displacement-length ratio (see also Boncio *et al*., 2004) for the whole Monte Gorzano Fault is significantly larger with respect to commonly described values from normal faults worldwide. From a stratigraphic point of view, the Monte Gorzano fault cuts Mesozoic carbonate succession and Upper Miocene siliciclastic formations (the Laga Formation, Marini *et al*., 2015). The Laga basin has a triangular shape and is surrounded by main tectonic elements: the Monti Sibillini thrust from West and East, and the Gran Sasso thrust from South. The activity of the aforementioned thrusts is coeval to the deposition of the Laga Formation. Lateral variation of the stratigraphy is given by passage from channelized deposits in the western and southern part to the lobe deposits to the east and south-east (Marini *et al*., 2015). The interpretation of available well data in Campotosto area, and correlation with field-based outcomes helped to select several marker beds, such as turbiditic marker beds, arenaceous-pelitic levels. The thickness was evaluated between two recognized stratigraphic levels: top of Orbulina formation and turbiditic marker beds recognizable both in the field and from the well. From the field mapping, this thickness corresponds to 750 - 780 m within the footwall. Meanwhile the estimation of the thickness of this package in the hanging wall (measured from the well and field mapping) corresponds to ~ 900-1050 m. This portion of the Laga Formation results 150 – 300 m thicker in the hanging-wall than in the footwall. These features and field evidences of buttressing of the hanging-wall succession against the fault (Calamita *et al*., 2018), are consistent with the pre-thrusting syn-sedimentary Upper Miocene

activity of the faults. Moreover, Bigi *et al*. (2013) pointed out that the 2009 hypocenters of earthquakes in the Campotosto area does not have any superficial expression nor connection with Monte Gorzano Fault.

Accordingly, the Campotosto linkage fault zone represent a deep seismogenic structure, that rules the seismic hazard in the area between the L'Aquila 2009 and Amatrice-Visso-Norcia 2016 earthquakes, and it is not necessarily connected with the superficial Monte Gorzano fault.

References

Barchi, M., Galadini, F., Lavecchia, G., Messina, P., Michetti, A.M., Peruzza, L., Pizzi, A., Tondi, E., Vittori, E. (2000). Sintesi delle conoscenze sulle faglie attive in Italia Centrale: parametrizzazione ai fini della caratterizzazione della pericolosità sismica, CNR-Gruppo Nazionale per la Difesa dai Terremoti, Roma. 62 pp.

Bigi, S., Casero, P., Chiarabba, C., Di Bucci, D. (2013). Contrasting surface active faults and deep seismogenic sources unveiled by the 2009L'Aquila earthquake sequence (Italy). *Terra Nova*, *25*(1), 21–29.

Boncio, P., Lavecchia, G., Milana, G., Rozzi, B. (2004). Seismogenesis in Central Apennines, Italy: An integrated analysis of minor earthquake sequences and structural data in the Amatrice-Campotosto area. Annals of Geophysics, 47(6), 1723–1742.

Calamita, F., Di Domenica, A., Pace, P. (2018). Macro- and meso-scale structural criteria for identifying pre-thrusting normal faults within foreland fold-and-thrust belts: Insights from the Central-Northern Apennines (Italy). *Terra Nova*, *30*(1), 50–62.

Cello G., Mazzoli S., Tondi E., Turco E. 1997. Active tectonics in the central Apennines and possible implications for seismic hazard analysis in peninsular Italy. Tectonophysics 1997; 272: 43-68.

Civico, R., Pucci, S., Villani, F., Pizzimenti, L., De Martini, P.M., Nappi, R., & the Open EMERGEO Working Group 2018. Surface ruptures following the 30 October 2016 Mw 6.5 Norcia earthquake, central Italy. Journal of Maps, 14, 151-160.

Falcucci, E., Gori, S., Bignami, C., Pietrantonio, G., Melini, D., Moro, M., … Galadini, F. (2018). The Campotosto Seismic Gap in Between the 2009 and 2016–2017 Seismic Sequences of Central Italy and the Role of Inherited Lithospheric Faults in Regional Seismotectonic Settings. *Tectonics*, *37*(8), 2425–2445.

Galadini, F., Galli, P. 2003. Paleoseismology of silent faults in the Central Apennines (Italy): The Mt. Vettore and Laga Mts. faults. *Annals of Geophysics*, *46*(5), 815–836.

Marini, M., Milli, S., Moscatelli, M. 2011. Facies and architecture of the Lower Messinian turbidite lobe complexes from the Laga Basin (central Apennines, Italy). Journal of Mediterranean Earth Sciences, 3, 45–72. 27th IAS Meeting of Sedimentology Alghero, September 20-23, 2009: 279-297

Pantosti, D., Boncio, P. (Eds.) 2012. Understanding the April 6th, 2009 L'Aquila earthquake - the geological contribution: an introductory note to the special issue. Italian Journal of Geosciences, 131, f.3.

Rovida A., Locati M., Camassi R., Lolli B. and Gasperini P. (eds) 2016. CPTI15, the 2015 version of the Parametric Catalogue of Italian Earthquakes. Istituto Nazionale di Geofisica e Vulcanologia. doi.org/10.6092/INGV.IT-CPTI15.

Tondi E., Chiaraluce L. and Roberts G. (Eds.) 2009. "Ten years after the Umbria-Marche earthquake". Tectonophysics, Vol. 476, Issue 1-2.

Villani F., Civico, R., Pucci, S., Pizzimenti, L., Nappi, R., De Martini, P.M. and the Open EMERGEO Working Group 2018. A database of the coseismic effects following the 30 October 2016 Norcia earthquake in Central Italy. Sci. Data 5:180049.

HIGH-RESOLUTION SEISMIC PROFILING OF THE CASTELLUCCIO BASIN: NEW CONSTRAINTS ON THE SHALLOW SUBSURFACE OF THE 30 OCTOBER 2016 MW 6.5 NORCIA EARTHQUAKE FAULT (CENTRAL ITALY)

F. Villani[1], S. Maraio[2], P.P. Bruno[3], L. Improta[1], K. Wood[4], R. Civico[1], Pa. Baccheschi[1], V. Sapia[1], S. Pucci[1], C.A. Brunori[1], P.M. De Martini[1], D. Pantosti[1], P. Conti[2], C. Doglioni[1]

[1] Istituto Nazionale di Geofisica e Vulcanologia, Italy
[2] Centro di Geotecnologie, Università di Siena, Italy
[3] Università degli Studi di Napoli Federico II, Italy
[4] Universitè Montpellier, France

In the past twenty years, the central Apennines (Italy) were hit by three important seismic sequences affecting a region >100 km-long parallel to the chain axis, causing heavy damage, economic losses and >600 deaths (Colfiorito, 1997, M_w 6.0; L'Aquila, 2009, M_w 6.1; Amatrice-Visso-Norcia, 2016, M_w 6.1, 5.9 and 6.5). The mainshocks of those sequences were generated by the in-cascade activation of segmented normal fault-systems (Chiaraluce *et al*., 2017; Improta *et al*., 2019), which at places bound Quaternary extensional basins. The Pian Grande di Castelluccio basin (PGC) is located in the hangingwall of the Mt. Vettore - Mt. Bove normal fault-system (VBFS; Calamita *et al*., 1992; Pizzi *et al*., 2002), responsible for the 30 October 2016 M_w 6.5 Norcia earthquake (Fig. 1). The widespread coseismic surface faulting following this earthquake (Civico *et al*., 2018; Villani *et al*., 2018b) affected also part of this basin, confirming the occurrence of active fault splays able to rupture up to the surface during large earthquakes (Galadini and Galli, 2003) and linked to the seismogenic fault at depth. Moreover, the basin position matches the locus of the largest long-term displacement of the VBFS, where the width of the coseismic deformation zone attains about 3 km and cumulative coseismic throws locally exceed 2 m (Villani *et al*., 2018b). Therefore, unveiling the subsurface structure of the PGC basin provide hints for the long-term behavior of the VBFS.

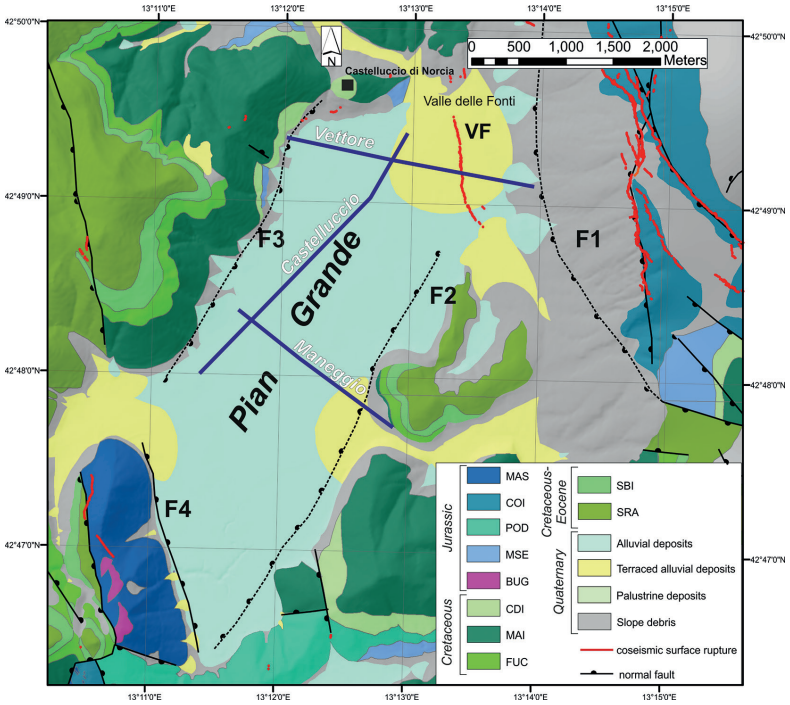

Fig. 1 - The Pian Grande di Castelluccio (geology simplified after Pierantoni *et al*., 2013) with the location of the seismic profiles (thick blue lines) and the coseismic surface ruptures following the 30 October 2016 Norcia earthquake (modified after Civico *et al*., 2018).

Recently, through the integration of shallow electrical resistivity profiles, electromagnetic soundings, ambient noise recordings and seismic anisotropy data, Villani *et al*., (2019) proposed an interpretation of two cross-sections within the PGC basin. However, high-resolution information on location, geometry and throw of buried fault splays, as well as fine details of the continental infill architecture, are still lacking. Active-source seismic profiling is crucial to fill this gap of knowledge.

To improve the subsurface basin imaging, on September-October 2017 we acquired three high-resolution seismic profiles within the PGC with a multi-fold wide-aperture acquisition geometry that allows collecting simultaneously reflection and refraction dense data in a wide offset range. The first profile (labelled *Vettore*) is 2635 m-long, trends WNW, and crosses nearly orthogonal the 2016 surface ruptures as well as an important splay of the VBFS. The second profile (labelled *Maneggio*) is 2035 m-long, trends WNW, and intercepts one of the basin-bounding faults to the south. The third profile (labelled *Castelluccio*) is 3355 m-long, trends NNE, and connects the first two profiles. All profiles were collected by deploying a 1195 m-long linear array of 240 vertical geophones 5-m spaced that was shifted using a roll-along technique to cover the overall profiles length. The geophones were connected to ten 24-bit seismometers. We used a 6-tons vibroseis (Minivib of IVI©) as a powerful yet safe energy source, with average 5-m spacing.

A total number of 1212 shot-gathers (consisting of 290880 seismic traces) were collected.

We calibrated our geophysical data with the nearby available shallow boreholes (Ge.Mi.Na., 1963), some of which reach the pre-Quaternary limestone bedrock, and geological data (by updating the map of Pierantoni *et al*., 2013, in particular regarding the PGC deposits). Our imaging strategy combines reflection data processing and non-linear refraction tomography.

Fig. 2 - The Minivib used for the acquisition of seismic data in the Pian Grande di Castelluccio basin.

For each profile, we handpicked first-arrival traveltimes in order to perform a non-linear tomographic inversion of a dense dataset (94320 readings for profile *Vettore*, 47520 for line *Maneggio* and 37920 for line *Castelluccio*). We use a multi-scale imaging strategy, successfully applied for imaging complex thrust-structures, fault-controlled basins and shallow fault zones (Improta *et al*., 2002, 2003; Improta and Bruno, 2007; Villani *et al*., 2015, 2017). Seismic tomography is fundamental for inferring the large-scale geometry of the basin. The obtained P-wave velocity models illuminate the PGC structure down to 350-500 m depth along the three key sections. The limestone bedrock is imaged as a high-velocity region (Vp ~4000-5500 m/s) showing a complex geometry due to the presence of a large number of subsurface faults defined by abrupt lateral Vp changes.

We apply an advanced processing flow to the reflection data taking advantage of the high fold and large offset range of the Common-Mid-Point (CMP) gathers that show reflections with an overall good signal-to-noise ratio and coherency (see methodological details in Bruno *et al*., 2019). The obtained migrated and depth-converted stack sections show details of the depositional architecture down to about 700-800 m depth. Within the continental infill, we observe clear and continuous high-amplitude reflections, corresponding to low-Vp regions in the tomographic models (Vp < 2500 m/s), define alternating fine and coarse sediments (silty sands and sandy gravels), which may be related to distal alluvial fan or to lacustrine deposits

(as suggested by borehole data and electrical resistivity profiles by Villani *et al*., 2019). Steeply dipping reflections coupled with relatively high Vp (> 3000 m/s) indicate alluvial fan bodies from the basin borders. These data put additional constraints on the location and geometry of several subsurface faults, which are detected by reflection truncations or disrupted zones.

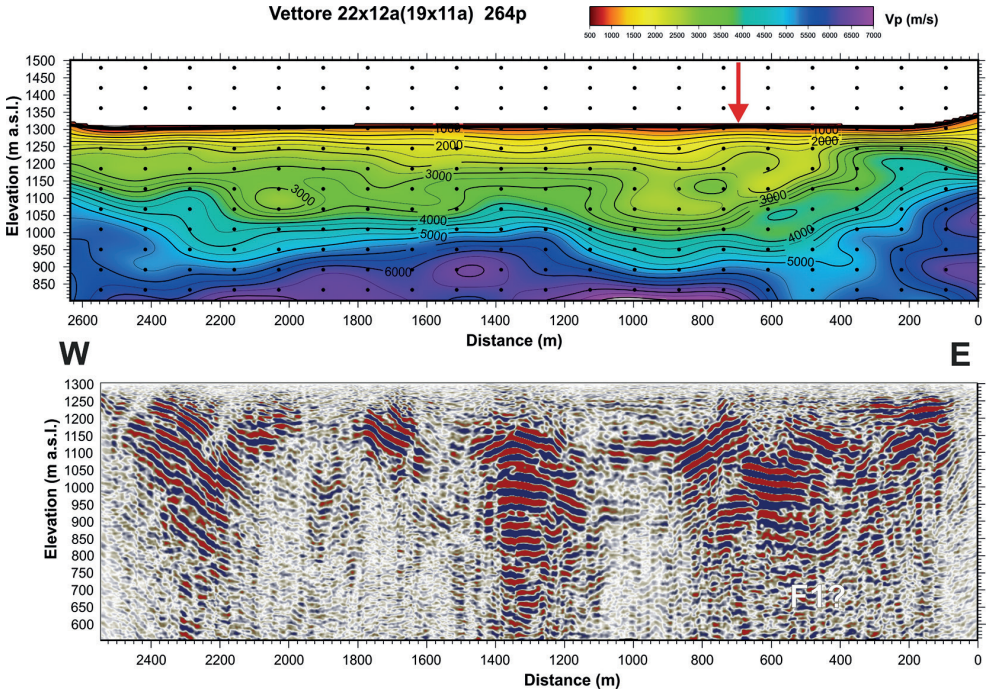

Fig. 3 - Seismic profile Vettore (looking to the north). Top panel: high-resolution Vp tomographic model (the red arrows points to the Valle delle Fonti – Prate Pala fault, that ruptured the surface during the Norcia earthquake). Bottom panel: migrated depth-converted reflection section.

As an example, we show preliminary results from seismic profile *Vettore* (Fig. 3). The high-resolution tomographic model (Fig. 3 upper panel) indicates a complex velocity field with several lateral variations that we relate to the occurrence of subsurface faults. The limestone basement corresponds to the deep high-Vp region (Vp > 4000-4500 m/s). The reflection section (Fig. 3 lower panel) shows a complex continental infill with variable dip and the occurrence of different seismic facies related to interfingering coarse and fine-grained deposits, likely representing different generations of alluvial fans. The red arrow points to the surface rupture trace of the Norcia earthquake, in correspondence of the Valle delle Fonti - Prate Pala active splay (VF), characterized by a surface fault scarp ~2.3-2.8 m high, likely related to the last ~12 kyr of activity (Galadini and Galli, 2003). Previous investigations (Villani and Sapia, 2017; Villani *et al*., 2019) suggest that this fault has total throw of ~100 m. Our new tomographic image shows that the VF fault zone is characterized by a wide low velocity zone (Vp < 2500 m/s) deepening down to ~300 m below the surface. Moreover, the reflection image highlights the internal complexity of the VF fault zone, characterized by at least three shallow and closely spaced sub-vertical splays. Therefore, the 2016 ruptures are the surface expression of a normal fault with complex architecture and being responsible for ~200 m throw affecting the limestone basement.

We hypothesize that the PGC basin structure is characterized by several fault splays distributed in a >3 km-wide deformation zone. In addition, our tomographic and reflection images point out the occurrence of other splays with different orientations with respect to the N150° general trend of the VBFS. In most cases, a 50 m to 100-m thick cover of deposits seals

the upper termination of such transversal faults. This suggests that the extensional activity in the PGC basin involved several fault systems characterized by different timings of activity. The shallowest active splays of the VBFS imaged by our profiles probably represent the most recent phase of extension. With regard to the oldest faults imaged by our seismic profiles, we suggest they may have ceased their activity by the Middle Pleistocene.

References

Bruno P.P.G., Berti C., Pazzaglia F.J.; 2019: *Accommodation, slip inversion and segmentation in a province-scale shear zone from high-resolution, densely spaced, wide-aperture seismic profiling, Centennial Valley, MT, USA*. Scientific Reports, 9:9214, https://doi.org/10.1038/s41598-019-45497-1.

Calamita F., Pizzi A., Roscioni M.; 1992: *I fasci di faglie recenti ed attive di M. Vettore – M. Bove e di M. Castello – M. Cardosa (appennino Umbro-Marchigiano)*. Studi Geologici Camerti, 1992/1, 81-95.

Chiaraluce L., Di Stefano R., Tinti, E., Scognamiglio L., Michele M., Casarotti, E., Cattaneo M., De Gori P., Chiarabba C., Monachesi G., Lombardi A., Valoroso L., Latorre D., Marzorati S.; 2017: *The 2016 Central Italy seismic sequence: a first look at the mainshocks, aftershocks and source models*. Seismol. Res. Lett., 88(3), 757–771, https://doi.org/10.1785/0220160221.

Civico R., Pucci S., Villani F., Pizzimenti L., De Martini P.M., Nappi R., and the Open EMERGEO Working Group; 2018: *Surface ruptures following the 30 October 2016 Mw 6.5 Norcia earthquake, central Italy*, Journal of Maps, https://doi.org/10.1080/17445647.2018.1441756.

Galadini F., Galli P.; 2003: *Paleoseismology of silent faults in the Central Apennines (Italy): the Mt. Vettore and Laga Mts. Faults*. Annals of Geophysics, 46(5), 815-836, https://doi.org/10.4401/ag-3457.

Ge.Mi.Na (Geomineraria Nazionale); 1963: *Il bacino di Castelluccio di Norcia*, in: Ligniti e Torbe dell'Italia continentale, 207-210, Industria Libraria Tipografica Editrice (ILTE), Torino.

Improta L., Zollo A., Herrero A., Frattini M., Virieux J., Dell'Aversana P.; 2002: S*eismic imaging of complex structures by non-linear traveltime inversion of dense wide-angle data: Application to a thrust belt*. Geophys. J. Int., 151, 264–278, doi: 10.1046/j.1365-246X.2002.01768.x.

Improta L., Zollo A., Bruno P. P., Herrero A., Villani F.; 2003: *High resolution seismic tomography across the 1980 (Ms 6.9) Southern Italy earthquake fault scarp*. Geophys. Res. Lett., 30(10), 1494, doi: 10.1029/2003GL017077.

Improta L., Bruno P. P.; 2007: *Combining seismic reflection with multifold wide-aperture profiling: An effective strategy for high-resolution shallow imaging of active faults*. Geophys. Res. Lett., 34, L20310, doi:10.1029/2007GL031893.

Improta L., Latorre D., Margheriti L., Nardi A., Marchetti A., Lombardi A.M., Castello B., Villani F., Ciaccio M.G., Mele F.M., Morett, M., and Bollettino Sismico Working Group; 2019: *Multi-segment rupture of the 2016 Amatrice-Visso-Norcia seismic sequence (central Italy) constrained by the first high-quality catalog of Early Aftershocks*, Scientific Reports, 9:6921, https://doi.org/10.1038/s41598-019-43393-2.

Pierantoni P.P., Deiana G., . Galdenzi S.; 2013: *Geological map of the Sibillini Mountains (Umbria-Marche Apennines, Italy)*, Italian J. Geosci., 132(3), 497-520.

Pizzi A., Calamita F., Coltorti M., Pieruccini P.; 2002: *Quaternary normal faults, intramontane basins and seismicity in the Umbria-Marche-Abruzzi Apennine Ridge (Italy): contribution of neotectonic analysis to seismic hazard assessment*, Boll. Soc. Geol. It. Spec. Issue 1, 923-929.

Villani F., Tulliani V., Sapia V., Fierro E., Civico R., Pantosti D.; 2015: *Shallow subsurface imaging of the Piano di Pezza active normal fault (central Italy) by high-resolution refraction and electrical resistivity tomography coupled with time-domain electromagnetic data*. Geophys. J. Int., 203 (3), 1482-1494, doi: 10.1093/gji/ggv399.

Villani F., Sapia V.; 2017: *The shallow structure of a surface-rupturing fault in unconsolidated deposits from multi-scale electrical resistivity data: the 30 October 2016 Mw 6.5 central Italy earthquake case study*, Tectonophysics, 717(16), 628-644, doi: 10.1016/j.tecto.2017.08.00.

Villani F., Improta L., Pucci S., Civico R., Bruno P.P., Pantosti D.; 2017: *Investigating the architecture of the Paganica Fault (2009 Mw 6.1 earthquake, central Italy) by integrating high-resolution multi-scale refraction tomography and detailed geological mapping*, Geophysical Journal International, 208, 403-423, doi: 10.1093/gji/ggw407.

Villani F., Civico R., Pucci S., Pizzimenti L., Nappi R., De Martini P.M., and the Open EMERGEO Working Group; 2018a: *A database of the coseismic effects following the 30 October 2016 Norcia earthquake in Central Italy*, Scientific Data, doi: 10.1038/sdata.2018.49.

Villani F., Pucci S., Civico R., De Martini P.M., Cinti F.R., and Pantosti D.; 2018b: *Surface faulting of the 30 October 2016 Mw 6.5 central Italy earthquake: detailed analysis of a complex coseismic rupture*, Tectonics, 37, 10, 3378-3410, doi: 10.1029/2018TC005175.

Villani F., Sapia V., Baccheschi P., Civico, R. Di Giulio G., Vassallo M., Marchetti M., Pantosti D.; 2019: "*Geometry and structure of a fault-bounded extensional basin by integrating geophysical surveys and seismic anisotropy across the 30 October 2016 Mw 6.5 earthquake fault (central Italy): the Pian Grande di Castelluccio basin*", Tectonics, 38, 1, 26-48, doi: 10.1029/2018TC005205.